The mobility of charge-carriers in dielectric liquids

A. S. Bloor

The Mobility of Charge-carriers in Dielectric Liquids

A Thesis submitted to the University of Durham for the Degree of Doctor of Philosophy

by

A.S. Bloor

ABSTRACT

This thesis describes work carried out in the Department of Applied Physics, Durham University, from October 1964 to September 1967. The work was a continuation of investigations, under the supervision of Dr. M.J. Morant, into the electrical properties of dielectric liquids.

The work of Sletten in 1959 and that of Morant and Kahan in 1964 has shown that dissolved oxygen has a marked effect on the breakdown strength and the conductivity of a typical dielectric liquid, n-hexane. The present investigation shows that the reduced breakdown strength and increased conductivity observed on de-gassing hexane may not be explained in terms of an increase in carrier mobility. The mobility of photo-injected carriers in highly de-gassed hexane is found to be no greater than the mobility of the same carriers in air-saturated liquid. Further, no increase of mobility with applied field is observed in the de-gassed liquid for fields up to 140 KV/cm; nor is there any indication, under these conditions, of the existence of an additional 'fast' carrier. The variation of the injected current with both the applied field and the degree of oxidation of the cathode, however, indicates that the 'oxygen effect' referred to above is an electrode surface phenomenon and not a property of the liquid itself.

The current transients from which the mobility determinations were made are not exactly of the form predicted by simple theory. This and other anomalous observations indicate a strong interaction between

the charge-carriers and the neutral liquid molecules. Such an interaction is consistent with self-trapping of the injected carriers by polarization of the surrounding medium.

Suggestions for further work on the identification of the charge-carriers in dielectric liquids and on the factors affecting breakdown and conductivity are made in the text.

CONTENTS

APPENDIX C : 'PROBE AND CHARGE TRANSIT STUDIES OF THE POTENTIAL DISTRIBUTION IN DIELECTRIC LIQUIDS'

(A copy of the paper presented by A.S. Bloor and M.J. Morant at the Conference 'Phénomènes de conduction dans les liquides isolants', Grenoble, 17 - 19 September 1968).

CHAPTER 1

INTRODUCTION

Although investigations into the effects of electric stress on materials in the gaseous, liquid and solid states have been carried out for a similar period of time, there appears to be a great disparity between the rates of progress in these three domains. Certainly the present states of knowledge of the electrical behaviour of solids and gases are comparable, but this statement would have been more than open to question twenty years ago. As regards the corresponding comparison with the liquid state one must first allow that the theories of conduction in electrolytes have been well developed for almost a century. However, as recently as 1958 it was generally recognized that electrical transport phenomena in both liquid metals and liquid insulators were in need of considerable experimental and theoretical examination (1, 2). Since then a great deal of systematic investigation has been carried out in these fields, resulting in many improvements and innovations in experimental technique and theoretical analysis, together with a substantial increase in the amount of associated literature, particularly on the subject of insulating or dielectric liquids.

The fact remains that the mechanisms of electrical conduction and breakdown in these liquids are still unknown, although hypotheses and experimental data relating to them are numerous. Sections (1) and (2) of this chapter provide a brief resume of such data and hypotheses which are relevant to the subject of the thesis, and illustrate the line of reasoning which has led to the inception of the present investigation.

1.1 EXPERIMENTAL MATERIALS

Early interest in the electrical properties of insulating liquids was concerned with the measurement and improvement of the breakdown strength of transformer oils and allied materials. The importance of these investigations to electrical engineering is evident. However the complex and often variable composition of this type of liquid, not to mention the wide variety of possible contaminants and trace impurities, (some of which may be unstable), have rendered the control of experimental variables very difficult, if not impossible. As a result, the data obtained from these measurements was not amenable to systematic analysis, and very few general deductions could be made as to the possible mechanisms of breakdown, or even of an accurate and reproducible electrical strength for a particular oil or type of oil.

In order to conduct a more reliable and fundamental investigation into the breakdown phenomenon in insulating liquids it became evident

that experiments must be carried out on pure, stable liquids of good insulating properties, having as simple a structure as possible. Several materials possessing these properties immediately suggest themselves. They may be divided into the following groups:

1.1.1 Inorganic liquids

The liquefied elemental gases fulfil all the requirements mentioned above, but suffer from two disadvantages as far as experimental suitability is concerned. First, they are only liquid at low temperatures for atmospheric pressures, which immediately raises a number of technical problems. Secondly, as far as relevance to the parent problem is concerned, they do not bear any particular structural or chemical resemblance to commonly used insulating liquids. However, their simplicity of structure is advantageous to the study of the liquid state itself, and a considerable amount of work has been carried out on the electrical properties of such materials (1,3,4,11,12).

1.1.2 The paraffin hydrocarbons

These compounds from a homologous series of general formula C_nH_{2n+2}, where n = 1,2,3.. in the case of the straight-chain members of the series. A series of cyclic paraffins also exists, in which the two ends of the chain are joined by the elimination of two hydrogen atoms. The general formula of the cyclic series is C_nH_{2n}, where n = 3,4,5.... Table (1.1) lists some of the members of

Table (1.1) Temperature range of the liquid phase at atmospheric pressure for some paraffin hydrocarbons

Name	Formula	Liquid range, °C.	
methane	CH_4	-182	-162
ethane	C_2H_6	-183	-89
propane	C_3H_8	-188	-42
butane	C_4H_{10}	-138	-1
n-pentane	C_5H_{12}	-130	+36
n-hexane	C_6H_{14}	-95	+69
n-octane	C_8H_{18}	-57	+126
n-decane	$C_{10}H_{22}$	-31	+174
cyclopropane	C_3H_6	-127	-34
cyclobutane	C_4H_8	-50	+13
cyclopentane	C_5H_{10}	-93	+50
cyclohexane	C_6H_{12}	+7	+81

both series, together with their melting and boiling points. The saturated nature of the carbon-hydrogen and carbon-carbon bonds in the paraffin hydrocarbons ensures that its members are remarkably stable and chemically inert. They have the additional advantage of low dielectric constants which inhibit the solution of ionic impurities, and their structure, though reasonably simple, provides the basis for many of the compounds of which commercial insulating oils are composed.

Pentane is the simplest of the straight-chain paraffins which is a liquid at room temperature and atmospheric pressure. The next higher homologue, n-hexane, has a similar temperature range of the liquid phase, displaced towards higher temperatures by about 30°C. Hexane has in fact been chosen as an experimental material by a considerable number of workers.

1.1.3. The aromatic hydrocarbons

Benzene and its derivatives provide an often used alternative to the paraffins. However, the range of conductivity values of these materials are generally several orders of magnitude greater than those of the paraffins. This property has been ascribed (5) to the nature of the de-localised π-orbitals, which are also responsible for the lower degree of chemical inertness of the aromatics.

Breakdown measurements have been made by many workers using, for the most part, simple hydrocarbon liquids. These

investigations, however, have not in general produced the accurate and unambiguous results that might have been expected. The values of electric strength and the degree of associated scatter were found to depend on one or more of the following factors:

i) the number of previous breakdowns in the sample - "conditioning".

ii) the use of pulsed - or continuously applied - stress.

iii) the electrical history of the liquid - "pre-stressing".

iv) the composition and cleanliness of the electrodes.

v) the purity of the liquid.

An extensive description of the types of experiment performed in this line of investigation and the (often ambiguous) conclusions involved, may be found in the review articles of Lewis (1) and Sharbaugh and Watson (3).

1.2. The effects of dissolved oxygen

In 1959, A.M. Sletten was performing an investigation (6) which required the use of a liquid of high breakdown strength. Normal hexane was chosen partly because the electric strength of the pure liquid had been reasonably well established as not less than 1·2 MV/cm. under D.C. conditions. The method of purification adopted by Sletten included a de-gassing process which reduced the air pressure over the liquid to an estimated value of less than 1 torr.

It was found that the breakdown strength of hexane so treated was sensitive to the degree of de-gassing and was always less than the previously accepted value. He was able to show (7,8) that the effect was due to the amount of dissolved oxygen in the liquid and that the higher reported strengths could only be obtained by allowing the liquid to reach equilibrium with a partial oxygen pressure in excess of 100 torr. It was also noted by the same worker that, under de-gassed conditions, the current at high fields became very erratic and occurred in irregular bursts of high value. This phenomenon was not observed in air-saturated hexane.

Continuing this line of investigation, Morant, later assisted by Kahan, (9) measured the current level in n-hexane as a function of applied field for both air-saturated and de-gassed hexane. Vapour phase chromatography (V.P.C.) was employed to investigate the identity and concentration of impurities present in the liquid used. The main source of high-purity hexane in this country is B.D.H. "Special for Spectroscopy" grade, which has been used by a number of workers, including Sletten. This material was shown by Kahan (10) to contain only approximately 80% n-hexane.

Hexane of a much higher degree of purity was found to be obtainable from Koch - Light Laboratories Ltd. The use of this liquid as an experimental material yielded a substantial increase in the reproducibility of the current-voltage characteristics under

de-gassed conditions.

This investigation confirmed the findings of Sletten with regard to the reduction of breakdown strength in the absence of high partial pressures of oxygen. The partial pressure of air above the liquid in Kahan's case was estimated as 10^{-5} to 10^{-6} torr, and the lower values of electric strength obtained are attributed, in part, to the greater degree of de-gassing.

Figure (1.1) illustrates the difference in the form of the current voltage characteristics of air-saturated and well de-gassed hexane.

The main feature in the de-gassed case is the transition of the current over several orders of magnitude from a low level to a high level on increasing the applied field. Further increase in the applied field yields a relatively slight increase in current before breakdown occurs.

Several hypotheses have been put forward to explain the effect of dissolved oxygen on the breakdown strength and current level in n-hexane. Such explanations must inevitably involve the postulation of a particular mechanism of conduction in the liquid, and vice versa, any postulate concerning the nature of the charge carrier must incorporate an explanation of the effect of oxygen on that carrier.

Kahan (9) suggests that the currents associated with the de-gassed liquid are due to conduction through channels of aligned, or ordered, molecules. These channels would be expected to be of a transitory

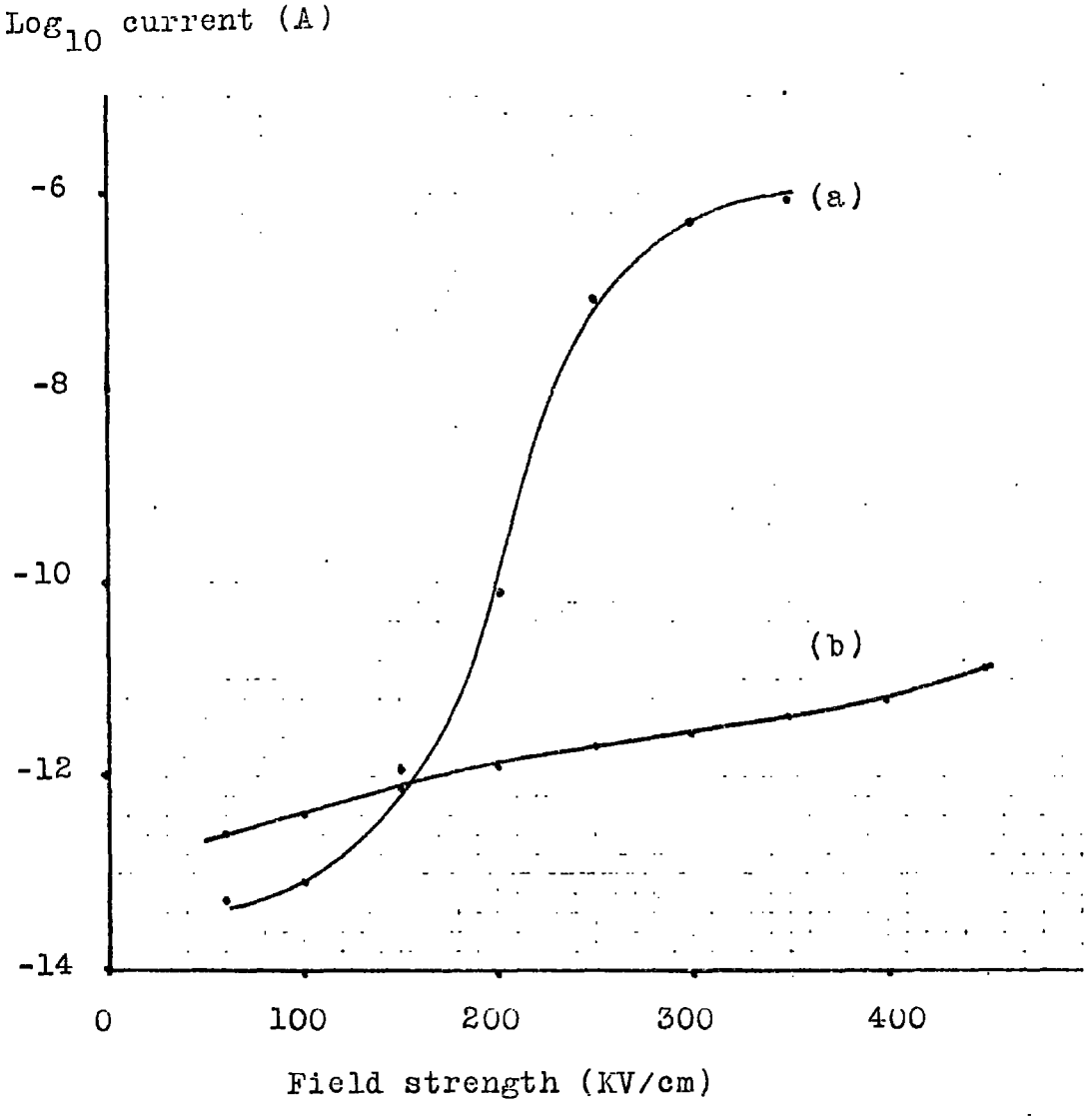

Figure (1.1). Current-voltage characteristics of hexane, after Kahan (9). Curve (a), de-gassed hexane; curve (b), air-saturated hexane.

nature, thus giving rise to the observed erratic currents at low current levels and steadier currents at higher fields. According to this hypothesis, the effect of oxygen is to reduce the probability of alignment and thus the current magnitude.

Taking a more general view, that the movement of charge-carriers through the liquid is hindered by the presence of oxygen, one may postulate three similar reasons for the effect of oxygen on the conduction level. The removal of oxygen sites from the liquid could result in:

i) a reduction in the probability of short-term trapping and hence an increase in the overall mobility of carriers.

ii) a reduction in the probability of long-term or permanent trapping and therefore an increase in the total number of available carriers.

iii) the existence of free electrons of high mobility in the liquid, by analogy with recent work on liquid argon (11,12).

It is thus of importance to the understanding of the oxygen effect in n-hexane and similar liquids, to measure both the mobility and concentration of carriers under the same conditions as those used by Kahan and Morant. Furthermore, the variation of these two quantities with applied field and oxygen concentration should provide valuable information concerning the conduction mechanism itself.

The work described in the remaining chapters of this thesis,

therefore follows directly from that of Sletten, Kahan and Morant and seeks primarily to determine the mobility of charge-carriers in highly de-gassed n-hexane.

1.4 REFERENCES

1. Lewis, T.J. Progress in Dielectrics, Volume 1. (Heywood, London 1959)
2. Cusack, N. The Electrical and Magnetic Properties of Solids, 188-189. (Longmans, London, 1958)
3. Sharbaugh, A.H. Watson, P.K. Progress in Dielectrics Volume 4. (Heywood, London, 1962)
4. Swan, D.W. Brit. J. App. Phys. 13, 208, (1962)
5. Forster, E.O. J. Chem. Phys. 37, 5, 1021-1028,(1962), ibid., 40, 1, 86-91, (1964)
6. Sletten, A.M. Ph.D. Thesis, London, 1960
7. Sletten, A.M. Nature, London, 183, 311, (1959).
8. Sletten, A.M. Brit. J. App. Phys. 14, 883-888, (1963).
9. Kahan, E. Ph.D. Thesis, Durham, 1964.
10. Kahan, E. Brit. J. App. Phys. 16, 943.945, 1965).
11. Rice, B.S., Jortner, J. Progress in Dielectrics, Volume 6. (Heywood, London, 1965).
12. Schnyders, H., Rice, B.S., Meyer, L. Phys. Rev. 150, 1, 127-145, (1966).

CHAPTER 2

METHODS OF MOBILITY MEASUREMENT

The magnitude of the natural conductivity in pure dielectric liquids is very small. In order to measure the properties of the charge carriers, it is usually necessary to enhance the carrier concentration by some means. The two most frequently used methods of producing such excess carriers in the liquid are discussed in section 2 of this Chapter. It is obviously important, when using the excess carrier technique, to identify the carriers produced and to show that they may be equated to the naturally occurring carriers. Certain methods of mobility measurement have been suggested which overcome this difficulty by using only the natural conductivity of the liquid. Section (1) of this Chapter is devoted to a brief discussion of the feasibility of three such techniques.

2.1. THE USE OF NATURALLY OCCURRING CARRIERS

2.1.1. The Hall Effect

The application of the Hall effect technique to dielectric liquids would be particularly useful, since it would enable both the mobility and sign of the carrier (or carriers) to be determined.

In the simple model of a single carrier Hall effect, the force on the moving carrier due to the magnetic field is equated to the force resulting from the Hall field. Thus the Hall voltage, V_h, across the the sample is given by:

$$V_h = E_z . d = \mu . E_x . H_y . d \quad \ldots\ldots\ldots\ldots\ldots\ldots (1)$$

where μ is the carrier mobility;

E_x is the electric field applied along the x-axis;

H_y is the magnetic field applied along the y-axis;

and d is the z-dimension of the sample.

Assuming reasonable values for H_y and d, one may compare the experimental situation in metals, semiconductors and insulators by means of the product $\mu . E_x$, the carrier velocity. Typical values of mobility may be taken as 10 - 100 $cm^2/V.$ sec for metals, and approximately 10 times these values for semiconductors. The corresponding Hall voltages range from a few microvolts to a few millivolts in normal circumstances. However when the experimental material is a liquid dielectric with a mobility in the range 10^{-3} - 10^{-4} $cm^2/V.sec.$, considerably higher electric fields than those used with non-insulators are required to produce comparable Hall voltages. The presence of a large potential gradient along the x-axis of the insulator could make the measurement of a small voltage across the z-dimension very difficult. In particular, the slightest displacement of the Hall probes from the same equipotential line would produce a potential difference between them which could be much greater than the Hall voltage itself. An additional difficulty which may be forseen is that the Hall effect relies on the establishment of a concentration gradient of the carriers in the z-direction, resulting in the Hall field. Since the

carrier concentration and mobility are both low, the time required to establish the equilibrium gradient would be long, and the effects of spurious electrostatic charging considerable.

2.1.2. Carrier Density Distribution

Silver (1) has shown that, by making certain simplifying assumptions, values for the mobilities of natural charge carriers in benzene may be deduced from Forster's measurements of the potential distribution in the liquid (2). This treatment provides an excellent illustration of the difficulty of such an analysis. Four basic assumptions must be made in order to allow a reasonably simple solution of the mathematical equations involved in the problem:

i) there is a slow and constant rate of generation of carriers of both signs;

ii) the electrodes are non-injecting;

iii) the effect of recombination is ignored for the region remote from the electrodes;

iv) the effect of carrier diffusion is neglected entirely.

Although the resulting expressions predict correctly the form of the variation of conductivity with electrode spacing in Forster's work, the mobility values deduced are approximately 100 times lower than those found by other workers (3).

The validity of the application of this procedure to conduction in n-hexane is very dubious in view of the assumptions which must be

made concerning the conduction mechanism. Quite apart from this consideration, the difficulties and ambiguities of potential profile measurement in n-hexane, referred to in section (3) of this chapter and reported in more detail in Appendix (A), are sufficient to limit the practicability of the method.

2.1.3. Breakdown Time-lag

Crowe (4) and more recently Felsenthal (5), have obtained values for mobility in n-hexane from statistical analyses of the breakdown time-lag between the application of fields in excess of the breakdown strength and the actual breakdown event. Crowe's analysis involves the postulation of certain conduction and breakdown mechanisms, and the value of mobility deduced (9.10^{-3} $cm^2/V.sec.$) is somewhat higher than that obtained by other methods. Both this result and Felsenthal's ($8 \cdot 7.10^{-2} cm^2/V.sec.$) can only be explained at present by a rapid increase of mobility at high fields. In addition to these difficulties, the exact nature of the breakdown time-lag and the very existence of a fundamental formative time for breakdown have been the subject of considerable discussion (6), (7). It seems unwise therefore to base an accurate measurement of mobility on a hypothetical conduction mechanism and a controversial experimental method.

ADDITION OPPOSITE

2.1.4. Conclusions

It is evident from the preceding examples that the use of naturally occuring carriers for mobility measurement is beset with

considerable difficulties, both of experimental technique and theoretical justification. These disadvantages are due to the very low conductivity of the liquids in question. The substantial increase in current afforded by the use of artificially created carriers, and the ease and accuracy with which such currents may usually be controlled, are factors largely responsible for the widespread use of this technique in the measurement of mobility. The procedure usually adopted is to determine the transit-time of the excess carriers between two electrodes, in a uniform electric field. The transit-time method for mobility measurement is discussed in section (3) of this chapter, while section (2) deals with the relative merits of available means of generating excess carriers in dielectric liquids.

2.2. THE USE AND GENERATION OF EXCESS CARRIERS

The methods available for the production of excess carriers fall into two categories: those which involve deliberate ionization of the liquid, and those which merely attempt to introduce low-energy electrons.

2.2.1. Ionization

The use of α, β, γ, or X-irradiation to promote increased conduction in liquid dielectrics is generally recognised as doing so by means of ionizing either the liquid itself or its impurities. There are two main objections to the use of such methods. First, the absorption of high-energy radiation by the hydrocarbon molecule

produces rupture of the carbon-carbon or carbon-hydrogen bonds. The resulting fragments are highly reactive and capable of recombining in several ways. For example:

(i) with each other to form isomers and homologues of the original compound;

(ii) with organic impurities;

(iii) with inorganic impurities, such as dissolved gas, to form organic materials based on the original hydrocarbon.

Thus an important disadvantage of ionization-induced currents is the progressive change in the composition of the liquid. Although a great deal of valuable work has been carried out using such methods, (8,9) their application to the present project would be undesirable in view of the self-imposed condition of maximum liquid purity.

The second objection to the use of ionizing radiation is that the problem of carrier identification is complicated under these conditions. Adamczewski (10), for example, reports the existence of three carrier types (two positive and one negative) in hexane and nonane ionized by X-rays.

2.2.2. Electron injection

In order to circumvent the difficulties associated with ionization-produced currents, several workers have investigated the possibility of introducing low-energy electrons into hydrocarbon liquids.

Watson and Clancy (11) and Sato, Nagao and Toriyama (12) have shown that electron injection may be achieved by directing a beam of thermionically emitted electrons towards a liquid-vapour interface. Under these conditions it is observed that electrons appear to be trapped in the liquid, forming stable carriers of low mobility. However, the operation of the electron gun in this method requires that the liquid vapour pressure be very low, thus ruling out its application to the lower hydrocarbons such as hexane, except perhaps at temperatures close to their freezing-points.

In 1959 LeBlanc (13) described a photo-emissive method of injecting electrons into liquid hexane, in order to measure their drift mobility. The technique consisted of illuminating an aluminium cathode, immersed in the liquid, with a flash of ultra-violet light, and determining the drift velocity of the carriers so formed. The instantaneous response of photo-emitters to illumination provides the method with a distinct advantage: the ease with which sharp-edged current transients may be generated in the liquid. This property is essential to the transit-time method for mobility measurement in general, since the carrier source must be switched on or off in a time which is short compared with the transit-time itself (see section (3) of this chapter). However, the injected current-level observed by LeBlanc was only about 10^{-12} A, considerably lower than the corresponding figure for photo-emission into a vacuum (13). Following the

publication of the paper, therefore, efforts were made by several workers to improve the efficiency of the photo-injection process with a view to extending the application of the method. These investigations, described in the following sub-section (2.2.3.), have lead to certain improvements in technique which render the method particularly suitable for the present project.

More recently Coe, Hughes and Secker (14) have demonstrated the possibility of producing currents of the order 10^{-6} A in air-saturated hexane by means of field-emission from an array of sharp edges. The measurement of carrier mobility using this method of carrier generation is described in a later publication (15). A disadvantage of the technique is that the high currents involved produce substantial movement of the liquid away from the emitters. The measured carrier velocity and hence the calculated mobility are therefore found to depend on the electrical power input to the system, and also on the geometry of the test-cell. The objection is likely to apply, in some degree, to other methods of carrier generation, where high continuous currents are produced.

2.2.3. The Photo-injection Process

As mentioned in the previous sub-section (2.2.2.), a number of investigations into the factors affecting the efficiency of the photo-injection process have been carried out since 1959.

Chong et al. (16) reasoned that a lower photo-electric work

function would enhance the signal, and accordingly used magnesium as the cathode material. Unfortunately their reported current transients of approximately 10^{-10} A are not directly comparable with those of LeBlanc ($\sim 10^{-12}$ A) in view of the differences between field strength and type of light source in the two cases.

Morant (17) indicated that it is apparently necessary to de-gas the liquid in order to obtain photo-injection. Using well de-gassed hexane and an aluminium cathode, photocurrents were obtained which proved to be at least 1,000 times greater than the natural current level, but between 200 and 2,000 times smaller than those observed from the same cathode in vacuo. Later work by the same author (18) however, indicated that the processes concerned are more complex than photo-injection of electrons from the cathode into the liquid. This conclusion was drawn from the observation that, although the electrode material has a marked effect on the magnitude of the currents, these may equally well be produced by illumination of the anode or the bulk of the liquid.

Terlecki and Gzowski (19) compared the merits of various surface conditions of zinc and aluminium as photo-emitters when immersed in dielectric liquids. They discovered that the most effective was a fresh, vacuum-deposited film of aluminium. Terlecki (20) used this technique to measure drift mobility in air-saturated hexane, octane and decane, but encountered some difficulty with a progressive decrease in cathode sensitivity This 'fatigue' effect, mentioned in the earlier paper (19) also caused

distortion of the current transient.

The same slow current decay was observed by Swan (21), using a semi-transparent aluminium cathode illuminated from the rear. Swan obtained current levels of up to 2.10^{-10} A at 40 KV/cm and estimated the carrier mobility by observing the current transient due to switching on the light source.

Pugh (22) following the work of Morant, investigated the conditions necessary to achieve true photo-emission into the liquid. It was confirmed that the production of carriers in the bulk of the liquid is due to the absorption of ultra-violet light. Purification of the liquid, in order to increase its transparency in the ultra-violet region, brought about a substantial reduction in the bulk-effect current. A vacuum-deposited aluminium film, immersed immediately after its formation in highly de-gassed hexane, was found to be an excellent source of photo-injected carriers. Currents of up to 10^{-8} A were obtained at fields of approximately 3 KV/cm, the light source being the same as that used by Morant (17, 18). This major improvement in efficiency was maintained for much longer periods than those reported by Terlecki and Gzowski, a fact which may be associated with the de-gassed state of the liquid.

The relevance of Pugh's findings to the present project is that the conditions of low gas-content and high liquid purity, necessary for the successful operation of the photo-injection technique, coincide with the conditions under which it was originally proposed to measure the

carrier mobility. Further, the adoption of these conditions ensures the production of reasonably large concentrations of excess carriers, the majority of which have been generated by the injection of low-energy electrons from the cathode into the liquid. In view of these considerations and those of the previous section (2.2.2.), it was decided to determine the carrier mobility in n-hexane by the transit-time method, using photo-injected electrons to provide the necessary excess carriers.

2.3. THE TRANSIT-TIME METHOD OF MOBILITY MEASUREMENT

Basically, the transit-time method of mobility measurement consists of determining the drift velocity of excess carriers in a known electric field. It will be assumed for the purposes of the following discussion that the field is uniform and equal to the ratio of applied voltage to electrode separation. The drift velocity of the carriers is determined by observing the current transient produced in the external circuit when the source of carriers is switched on or off, or pulsed. The current transient may be recorded directly or integrated to give the charge collected as a function of time. The choice between a step-wise and a pulsed variation of the carrier concentration on the one hand, and between current and charge measurement on the other, requires an analysis of the equivalent circuit associated with the method. This analysis is presented in the following sub-sections, together with a short discussion of the relative merits of the four possible combinations of technique.

2.3.1. Uniformity of the applied field

The assumption, that the applied field is uniform, requires careful justification from an experimental standpoint if the transit-time technique is to be used with any confidence. In view of this, a preliminary study was made of the effects of a non-uniform field on the measurement of mobility by this method. The study consisted of (a) a simple theoretical analysis of the errors which might result from the incorrect assumption of a uniform field and (b) a series of attempts to determine the potential profile in hexane and benzene, using a physical probe technique. The details of this preliminary investigation are reported in Appendix B, but the conclusions will be summarised here for the sake of continuity.

It is shown in Appendix B that a departure from uniformity of the applied field results in an apparent mobility which is lower than the true mobility. Physically this is due to the predominant effect of the reduced carrier velocity in the regions where the local field is less than the average value. In order to determine the true mobility it is therefore necessary to know the field distribution during the transit-time of the carriers. Under certain conditions, of course, the field distribution will be constant and independent of the presence of the excess carriers. The field distribution may then be determined at any time.

The use of a physical voltage probe to determine the potential profile (or field distribution) in n-hexane was unfortunately found to be impracticable. The basic reason for this is the very high resistance of

the material, which presents unique problems in the construction of apparatus and measuring instruments. The method was found to be applicable to benzene, having a resistivity 100 to 1,000 times less than hexane, and exhibiting a closely uniform field distribution.

In view of the failure of the voltage probe technique for hexane, and in the absence at that time of a suitable alternative, it was not strictly possible to justify the assumption of a uniform field. The results obtained for benzene were not sufficient to support the assumption. It was decided, however, to discontinue the probe measurements in hexane in favour of transit-time determinations. It was considered that local departures from uniformity of the field distribution would be revealed by anomalous behaviour of the current transients produced in the external circuit. The interpretation, in terms of the field distribution, of transient shapes obtained subsequently is discussed in Section 6.4 and also in a paper presented jointly by the author and Dr. M.J. Morant at Grenoble in September 1968. A copy of the paper appears as Appendix C. It was concluded that such an analysis of the shape of the transient provides valuable qualitative information on the extent of field distortion during the transit of the charge carriers and may be used to determine the actual potential profile, provided that other causes of transient distortion are carefully eliminated.

2.3.2. The equivalent measuring circuit

In view of the adoption of the photo-injection method as the source of carriers for the present work, the analysis of the equivalent measuring circuit will include the assumptions that the carriers are injected from one electrode and that they all move across the entire inter-electrode space. It is further assumed that the voltage applied to the electrodes remains constant during the current transient.

The source of applied voltage may be represented by an ideal D.C. voltage generator, V_{HT}, together with a source resistance, R_s, and a parallel capacitance, C_s, as shown in figure (2.1a). The electrodes between which the carriers move have a capacitance, C_e, and the recorded signal, $V(t)$, is measured across the resistance, R. The assumed constancy of the applied voltage during the transient implies that C_s is an effective short-circuit of C_e and R for that time. The movement of excess carriers between the electrodes may then be represented by a current generator, $i(t)$, in parallel with R and C_e. In practice, C_e will be supplemented by stray capacitance, the input capacitance, C_i, of the measuring circuit and, in the case of an integrating circuit, by a measuring capacitance, C_m. The total capacitance is represented in fugure (2.1b) by C, such that:

$$C = C_e + C_{stray} + C_i + C_m \quad \ldots\ldots\ldots\ldots\ldots \quad (2)$$

The differential equation governing the behaviour of the circuit is therefore:

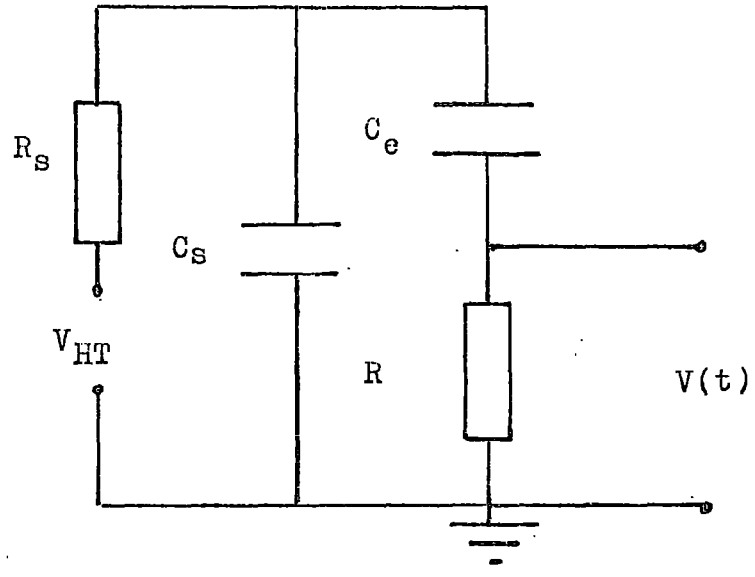

Figure (2.1a). General experimental circuit

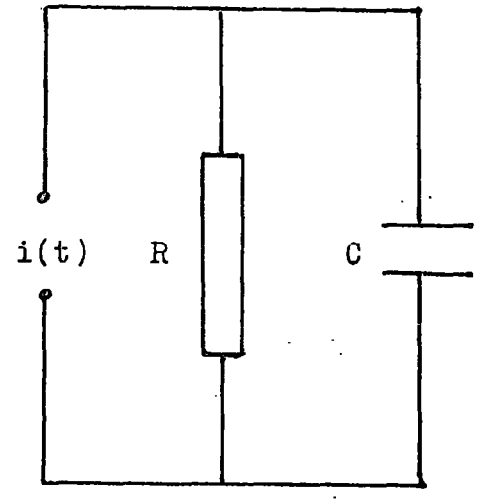

Figure (2.1b). Equivalent circuit

$$C.dV/dt + V/R = i(t) \quad \ldots\ldots\ldots\ldots\ldots\ldots (3)$$

The general solution of this equation is:

$$V(t) = 1/C.e^{-t/RC}\left[\int_o^t e^{t/RC}.i(t).dt + C.V(O)\right] \ldots\ldots\ldots (4)$$

Three particular solutions are of interest, corresponding to the carrier source being switched on, switched off, or pulsed.

2.3.2.1. Step increase in carrier concentration

Let N be the rate of generation of excess carriers at one electrode, such that:

$$N(t) = O \text{ for } t \leq O; \quad N(t) = N \text{ for } t \geq O$$

Then the boundary conditions to be applied to equation (4) are:

$$i(t) = eNt/\tau \text{ for } O < t \leq \tau \; ; \quad i(t) = eN \text{ for } t \geq \tau \ldots\ldots (5)$$

where e is the carrier charge and τ the transit-time.

Substitution of (4) into (3) yields the result:

$$V(t) = (eNR/\tau)\left[t - RC(1 - e^{-t/RC})\right] \text{ for } O < t \leq \tau$$

$$V(t) = eNR.\left[1 - (RC/\;)e^{-t/RC}\left(e^{\tau/RC} - 1\right)\right], \quad \text{for } t \geq \tau \qquad (6)$$

A simple interpretation of (6) is possible for each of the two limiting conditions $\tau/RC \rightarrow O$, and $\tau/RC \rightarrow \infty$, corresponding to charge and current-measurement respectively:

i) $\tau/RC \to 0$ ($RC \gg \tau$), charge-measurement

$$V(t) \doteq 0, \text{ for } 0 < t \leq \tau$$

$$V(\tau) \doteq 0 \qquad (7)$$

$$V(t) = eNt/C, \text{ for } \tau < t \ll RC$$

ii) $\tau/RC \to \infty$ ($RC \ll \tau$), current-Measurement

$$V(t) = eNR.t/\tau, \text{ for } 0 < t \leq \tau$$

$$V(\tau) = eNR \qquad (8)$$

$$V(t) = eNR, \text{ for } t \geq \tau$$

2.3.2.2. Step decrease in carrier concentration

In this case:

$N(t) = N$, for $t \leq 0$; $N(t) = 0$, for $t \geq 0$. The resultant boundary conditions are:

$$i(t) = eN(1 - t/\tau), \text{ for } 0 < t \leq \tau$$

$$i(t) = 0, \text{ for } t \geq \tau \qquad (9)$$

$$V(0) = eNR$$

Substitution of (9) into (3) yields the relationship:

$$V(t) = (eNR/\tau)\left[\tau - t + RC(1 - e^{-t/RC})\right] \text{ for } 0 < t \leq \tau \qquad (10)$$

$$V(t) = eNR.(RC/\tau)(e^{\tau/RC} - 1).e^{-t/RC}, \text{ for } t \geq \tau$$

In the limiting conditions this becomes:

i) $\tau/RC \to 0$ ($RC \gg \tau$), charge-measurement

$$V(t) = eNR, \text{ for } 0 < t \leq \tau$$

$$V(\tau) = eNR \qquad (11)$$

$$V(t) = eNR(1 - t/RC), \text{ for } \tau < t \ll RC$$

ii) $\tau/RC \to \infty$ ($RC \ll \tau$), current-measurement

$$V(t) = eNR(1 - t/\tau), \text{ for } 0 < t \leq \tau$$
$$V(\tau) = 0 \qquad (12)$$
$$V(t) = 0, \text{ for } t \geq \tau$$

2.3.2.3. Short pulse variation of the carrier concentration

Let a negligibly thin layer of excess carrier concentration, n, be formed instantaneously at one electrode.

The boundary conditions are:

$$i(t) = en/\tau, \text{ for } 0 < t \leq \tau$$
$$i(t) = 0, \text{ for } t \geq \tau \qquad (13)$$
$$V(0) = 0$$

The resultant solution is:

$$V(t) = (enR/\tau)(1 - e^{-t/RC}), \text{ for } 0 < t \leq \tau$$
$$V(t) = V(\tau).e^{-(t-\tau)/RC}, \text{ for } t \geq \tau \qquad (14)$$

This may be reduced to the following forms:

i) $\tau/RC \to 0$ ($RC \gg \tau$), charge-measurement

$$V(t) = (en/C).(t/\tau), \text{ for } 0 < t \leq \tau$$
$$V(t) = en/C, \text{ for } \tau < t \ll RC \qquad (15)$$

ii) $\tau/RC \to \infty$ ($RC \ll \tau$), current-measurement

$$V(t) = enR/\tau, \text{ for } 0 < t \leq \tau$$
$$V(t) = 0, \text{ for } t \geq \tau \qquad (16)$$

2.3.3. Discussion

The solutions of equation (3) for various boundary conditions are shown graphically in Figures (2.2), (2.3) and (2.4). Broken lines indicate the form of the solution for a limiting condition, corresponding to ideal charge- or current-measurement. In practice, of course, a certain amount of distortion of the trace will occur due to the necessarily finite value of the parameter τ/RC. In order to illustrate the effect of such distortion on the measurement of τ, the shapes of the transients have been calculated from equations (6), (10) and (14) for $\tau/RC = 10$, 0.1, and are plotted on Figures (2.2), (2.3) and (2.4). With the aid of these diagrams, it is possible to discuss, qualitatively, the relative merits of the four combinations of technique.

i) Step-function injection, current-measurement: Figure (2.2a) shows that, even for $\tau/RC = 10$, a substantial portion of the trace is linear. Thus, although the discontinuity of gradient at $t = \tau$ is masked by the non-infinite value of τ/RC, a reasonably accurate determination of τ is possible by extrapolation of the linear parts of the transient. One disadvantage of the technique is the conflict between the requirements of signal magnitude and degree of distortion, both being proportional to the value of the measuring resistor, R. For short transit-times it may be necessary to reduce the product RC in order to minimize distortion. This could be achieved at the expense of signal size by reducing R, or without any effect on the signal size by reducing C.

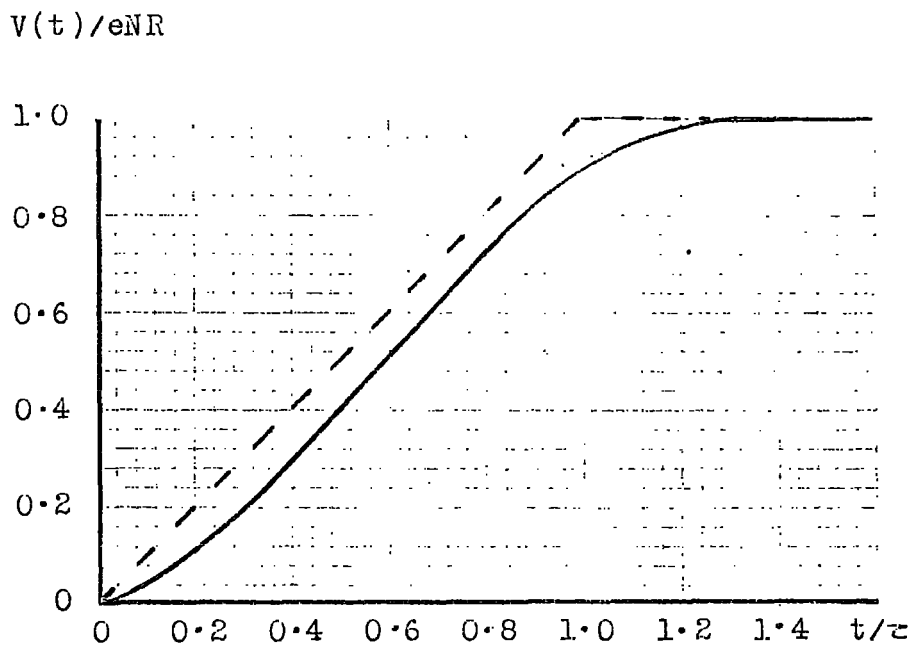

Figure (2.2a). Step increase in carrier concentration at t = 0. Full line, $\tau/RC = 10$; broken line, $\tau/RC \to \infty$

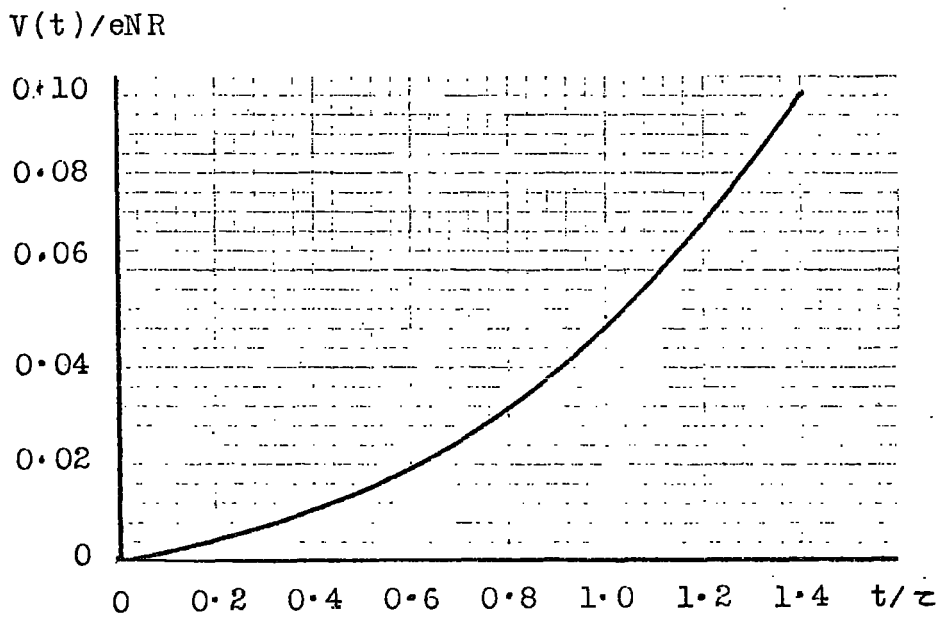

Figure (2.2b). Step increase in carrier concentration at t = 0. $\tau/RC = 0{\cdot}1$.

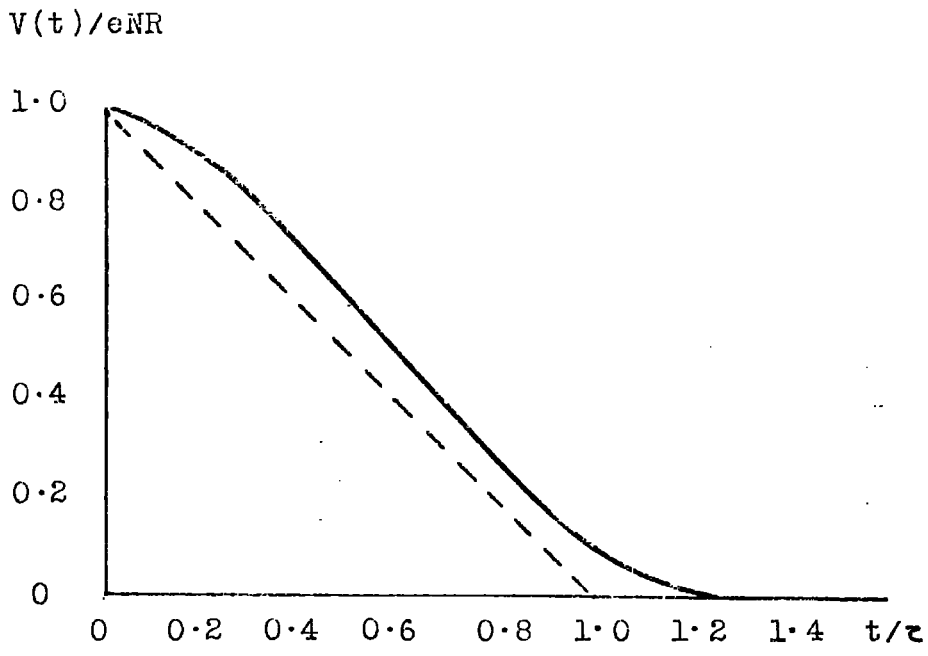

Figure (2.3a). Step decrease in carrier concentration at $t = 0$. Full line, $\tau/RC = 10$; broken line, $\tau/RC \to \infty$

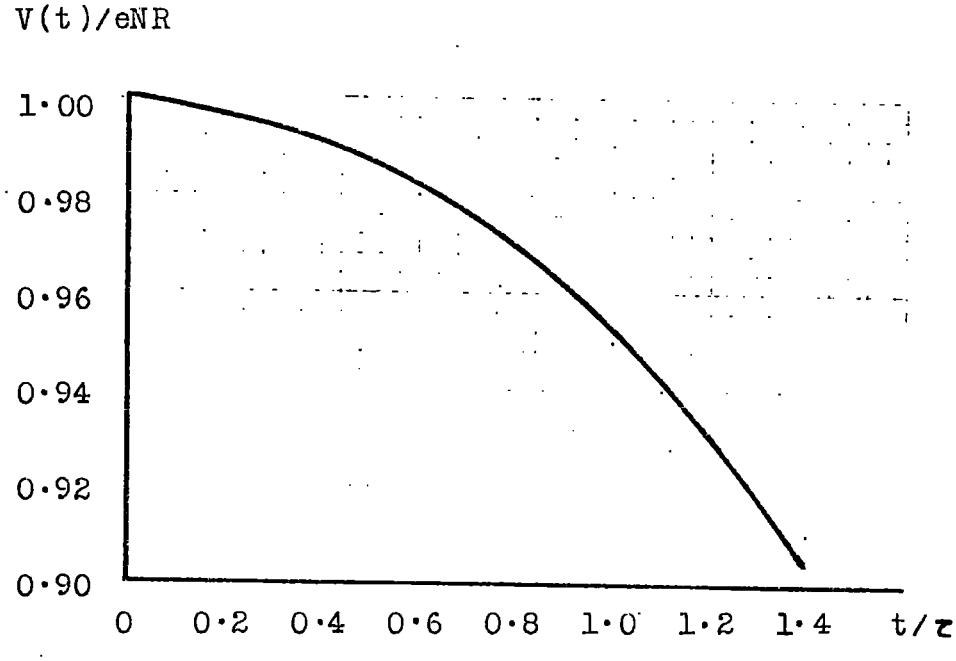

Figure (2.3b). Step decrease in carrier concentration at $t = 0$. $\tau/RC = 0{\cdot}1$.

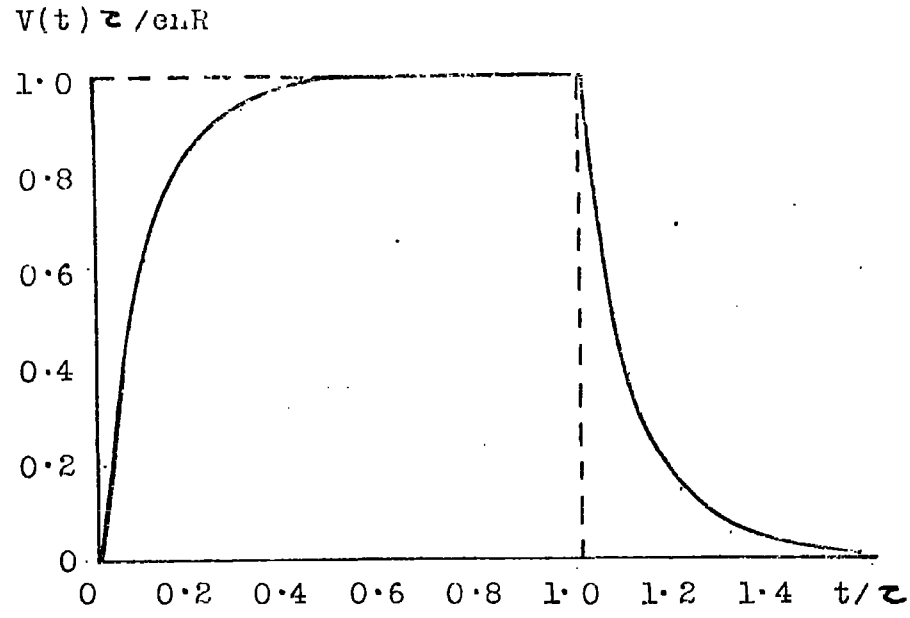

Figure (2.4a). Single pulse injection at t = 0.
Full line, $\tau/RC = 10$; broken line, $\tau/RC \rightarrow \infty$

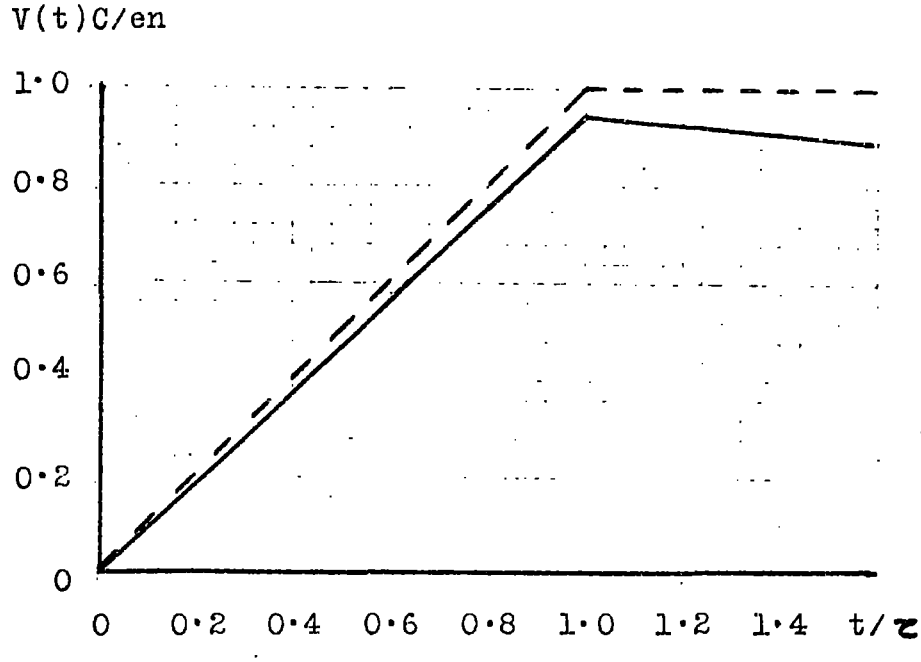

Figure (2.4b). Single pulse injection at t = 0.
Full line, $\tau/RC = 0{\cdot}1$; broken line $\tau/RC \rightarrow 0$.

Thus the lower limit on values of τ determined by this method is governed by the extent to which C may be reduced and the minimum detectable signal of the measuring instrument.

ii) Step-function injection, charge-measurement: The limited usefulness of this method is clearly demonstrated by examination of Figure (2.2b). For $\tau/RC = 0.1$, no discontinuity is detectable at $t = \tau$, nor does extrapolation of the linear part of the trace result in an intercept at $t = \tau$. If the value of τ/RC is reduced to approach the limiting form of the transient - equations (7), (11) - the signal magnitude in the region $t = \tau$ also decreases. Thus an easily detected signal must necessarily be difficult to interpret. Measurement of transit-time using this technique would in fact require a knowledge of the exact value of RC, and a complete analysis of each transient.

iii) Single pulse injection, current-measurement: In this case the distortion of the leading and trailing edges of the transient, due to a finite value of τ/RC, does not seriously affect the measurement of τ. Figure (2.4) shows that the discontinuity at $t = \tau$ is almost equally well-defined for $\tau/RC = 10$ as it is for $\tau/RC \rightarrow \infty$. The signal magnitude is given by the expression:

$$V(\tau) = enR/\tau, \text{ for } 0 < t \leq \tau \qquad (16)$$

Any major decrease in τ, therefore, serves to increase $V(\tau)$ at the expense of the trace-shape. In this event the values of both $V(\tau)$ and τ/RC may be maintained by a reduction of RC. In the limit, however,

the effective value of RC will be determined by the rise-time, t_m of the measuring instrument. The minimum transit-time which could be measured accurately by this method would then be given by: $\tau_{(min)} \gtrsim t_m$.

The signal magnitude may be compared with that obtained by step-variation of the source:

Let t_p be the duration of the pulse, which must be very short compared with the transit-time, τ. We may then substitute $N.t_p$ for n in equation (16), giving:

$$V(\tau) = eNR.t_p/\tau, \quad \text{for } 0 < t \leq \tau \qquad (17)$$

Reference to equation (8) shows that, for a given value of N, the ratio of signal magnitude for the two methods is simply t_p/τ, which must be small in comparison with unity.

iv) Single pulse injection, charge-measurement: In common with the previous method, the degree of distortion introduced by the finite value of τ/RC does not affect the determination of transit-time to any great extent - see figure (2.46). As τ becomes smaller, the degree of distortion decreases, provided that RC is constant. The peak height of the transient occurs at $t = \tau$, when:

$$V(\tau) = en/C \qquad (15)$$

The signal magnitude is therefore independent of the value of R, which may be increased or decreased in order to adjust the value of τ/RC. The technique is particularly useful when τ is small, for C may then be reduced to a minimum, resulting in a high value of $V(\tau)$.

The lower limit for the accurate measurement of τ is reached when $\tau \doteq t_m$, causing curvature of the transient and uncertainty as to the position of the discontinuity.

The maximum transit-time to which the method is applicable depends on the extent to which RC may be increased. The upper limit on R will usually be the input resistance of the measuring instrument, and C may only be increased to the point where $V(\tau)$ is still easily detectable.

The choice of one or other of the methods discussed above depends to a large extent on the ultra-violet source used to illuminate the photo-injecting cathode.

The primary consideration is whether or not the source may be operated in such a manner as to produce single pulses of light which are short compared with the minimum transit-time envisaged.

If this is possible, then the considerable advantages of method (iv) may be realized. This technique provides a large signal and the shape of the transient enables the transit-time to be measured accurately and directly, particularly when the latter is short. In view of the smaller signal involved, current-measurement of this type of transient would only be used if the transit-time were so long as to be comparable with the maximum value of RC attainable.

In the event of the light-source not being amenable to pulsed operation, the transit-time must be determined from observation of the

transient produced when the source is switched on, or off. The current transient is then best measured directly, since no useful purpose is served by integration of the signal under these conditions. The technique must, however, be regarded as less advantageous than the pulsed-source method, in view of the reduction in signal size for short transit-times, and the effect on the measurement of τ of finite values of τ/RC.

2.4 REFERENCES

1. Silver, M.; J. Chem. Phys. 42, 3, 1011-1013 (1965)
2. Forster, E.O.; J. Chem. Phys. 37, 5, 1021-1028 (1962)
3. Chong, P. and Inuishi, Y.; Tech. Rep. Osaka Univ. 10, 414, 545-551 (1960)
4. Crowe, R.W.; J. Appl. Phys. 27, 2, 156, (1956)
5. Felsenthal, P.; J. Appl. Phys. 37, 10, 3713-3715 (1966)
6. Sharbaugh, A.H. and Watson, P.K.; Progress in Dielectrics 4, 201, (Heywood, London, 1962)
7. Ward, B.W. and Lewis, T.J.; Brit. J. Appl. Phys. 14, 368-373 (1963)
8. Adamczewski, I.; Brit. J. Appl. Phys. 16, 759-769 (1965)
9. Jachym, B.; Acta Phys. Polon. 29, 1, 21-27 (1966)
10. Adamczewski, I.; Acta Phys. Polon. 6, 432, (1937)
11. Watson, P.K. and Clancy, T.M.; Rev. Sci. Instr. 36, 2, 217-222 (1965)
12. Sato, T., Nagao, S. and Toriyama, Y.; Brit. J. Appl. Phys. 7, 297 (1956)
13. LeBlanc, O.H.; J. Chem. Phys. 30, 6, 1443-1447 (1959)
14. Coe, G., Hughes, J.F. and Secker, P.E.; Brit. J. Appl. Phys. 17, 885-890 (1966)
15. Essex, V. and Secker, P.E.: Brit. J. Appl. Phys. 2, 1, 63-69 (1969)

16. Chong, P., Sugimoto, T. and Iniushi, Y. ; J. Phys. Soc. Japan 15, 1137-1138 (1960)

17. Morant, M.J.; Nature, 187, 4731, 48-49 (1960)

18. Morant, M.J. Paper presented at Durham Conference on Electronic Processes in Dielectric Liquids, April 1963. A summary of the Conference was published:
Morant, M.J.; Brit. J. Appl. Phys. 14, 469-473 (1963)

19. Terlecki, J. and Gzowski, O.; Acta Phys. Austriaca, 15, 4, 337-343 (1960)

20. Terlecki, J.; Nature 194, 4824, 172 (1962)

21. Swan, D.W.; Nature 190, 4779, 904 (1961)

22. Pugh, D.R.; Ph.D. Thesis, Durham University (1968) and by Private Communication.

23. Beddow, A.J., Brignell, J.E. and House, H., Conference proceedings "Phénomènes de conduction dans les liquides isolants", Grenoble 1968, 99 - 107.

CHAPTER 3

DESCRIPTION OF APPARATUS

The conditions under which the carrier-mobility was to be measured, and the method to be used, have been discussed in Chapters 1 and 2. In order that the following description of the necessary apparatus may be read in context, the decisions taken in these earlier chapters will now be reiterated.

The transit-time of excess carriers between two electrodes, immersed in high-purity, de-gassed n-hexane, was to be measured. The carriers were to be generated by ultra-violet photo-injection of electrons from an evaporated aluminium cathode. The ultra-violet source was to be operated in the form of single short pulses, provided that these were of sufficient intensity to produce detectable current-transients in the liquid.

As mentioned in section 1.3 pure n-hexane, containing only 0.1 % isomeric impurities, was found by Morant, Kahan (1) to be available from Koch-Light Laboratories Ltd. In view of the increased reproducibility obtained by these workers when using the liquid supplied by Koch-Light as 'Puriss' grade n-hexane, and in order to maintain continuity with their work, the same source of experimental material was used in the present investigation.

The need to ensure a high degree of transparency of the liquid

to ultra-violet radiation was established by Pugh, as recorded in section 2.2.3. Accordingly, the measurement of ultra-violet absorption in the liquid and, where necessary, its reduction by means of further purification, formed an important part of the liquid preparation process.

The distillation and de-gassing procedure to which the n-hexane was subjected was the same as that used by Morant, Kahan, and Pugh in their respective investigations.

The following sections deal with the design and development of the apparatus with the exception of the mobility-measurement cells, which are described in Chapters 4 and 5.

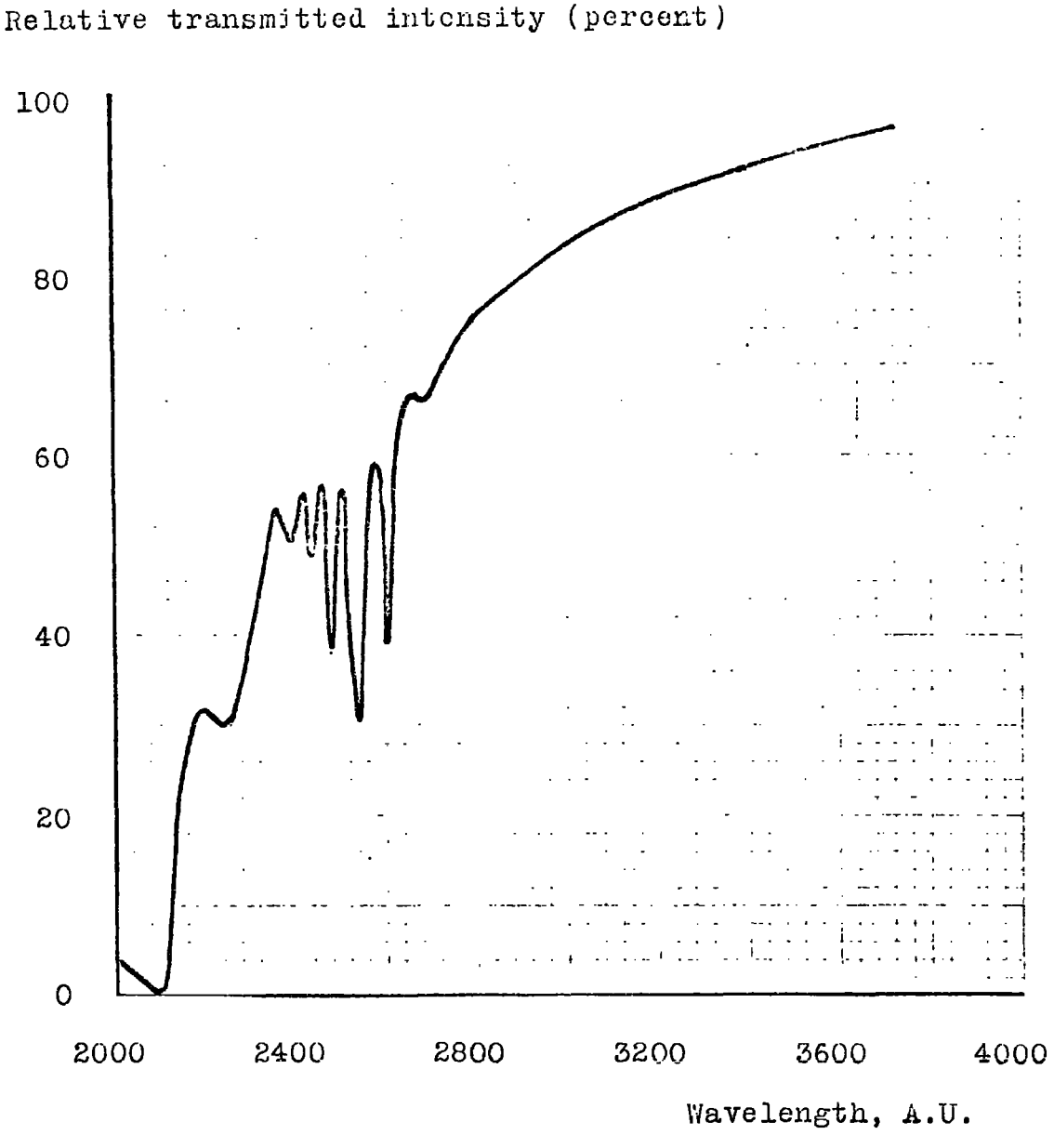

Figure (3.1). The optical absorption, in the region 2000 - 4000 A.U., of n-hexane supplied by Koch-Light Laboratories. Optical path length: 1 cm. Reference cell: air.

3.1. PREPARATION OF THE LIQUID

3.1.1. The silica-gel process

Figure (3.1) shows the optical absorption, in the region 2,000 - 4,000 Å, of n-hexane supplied by Koch-Light Laboratories. The multiple peaks between 2,400 and 2,700 Å were identified by Pugh (2) as due to a low concentration of benzene, not detected by Kahan's analysis (1). In order to minimize the possible photo-ionization or photo-excitation of this impurity by the ultra-violet source, the transparency of the liquid in this region of the spectrum must be substantially increased. Pugh achieved this by a modification of the method described by Potts (3) for the preparation of hydrocarbon solvents for ultra-violet spectroscopy. The method consists essentially of allowing the dried hydrocarbon liquid to pass through a column of silica-gel, which has been activated by the removal of absorbed water.

The activation procedure adopted by Potts was to heat the silica-gel in a glass tube for 12 hours at 350°C. The column was then allowed to cool to room-temperature in a moisture-free atmosphere, prior to use. Pugh, on the other hand, used a coarse grade of gel which was dried in an electric oven at 200°C. and then crushed to expose fresh surfaces. For the present work, activation was achieved by heating the silica-gel in a vertical zone-refining furnace. This method, described below, is similar to that of Potts and avoids the necessity for handling the gel after activation.

Figure (3.2) is a schematic diagram of the activation system. The Pyrex tube (A) was filled to a depth of about 60 cm. with coarse silica-gel, the smaller fragments and fine dust being retained in the tube by the sintered-glass filter (B). The lower outlet of the column was then sealed by the ground-glass joint (C) and the upper end connected to the pumping system at (D). With the vapour-trap (E) cooled to -80°C. by a mixture of solid carbon-dioxide and methylated spirit, the column was evacuated and the annular furnace (F) switched on. After a suitable interval to allow the furnace to reach its equilibrium temperature, the furnace drive motor was started. The furnace drive speed was 15 cm./hour and the temperature at the furnace position was between 200°C. and 300°C. The column was pumped continuously during the activation process, the desorbed water being collected in the vapour-trap, which also served to prevent contamination of the column by oil from the rotary pump (I).

When the furnace had moved beyond the upper surface of the silica-gel, both the heating current and the drive motor were switched off, but the pump remained on until the column had cooled to room-temperature. Two passes of the furnace were usually made, although the second did not remove a measurable quantity of water. On completion of the activation procedure, air was slowly admitted to the column through the phosphorus pentoxide trap (G) and the vapour-trap, by opening the valve (H). Immediately, joints (C) and (D) were

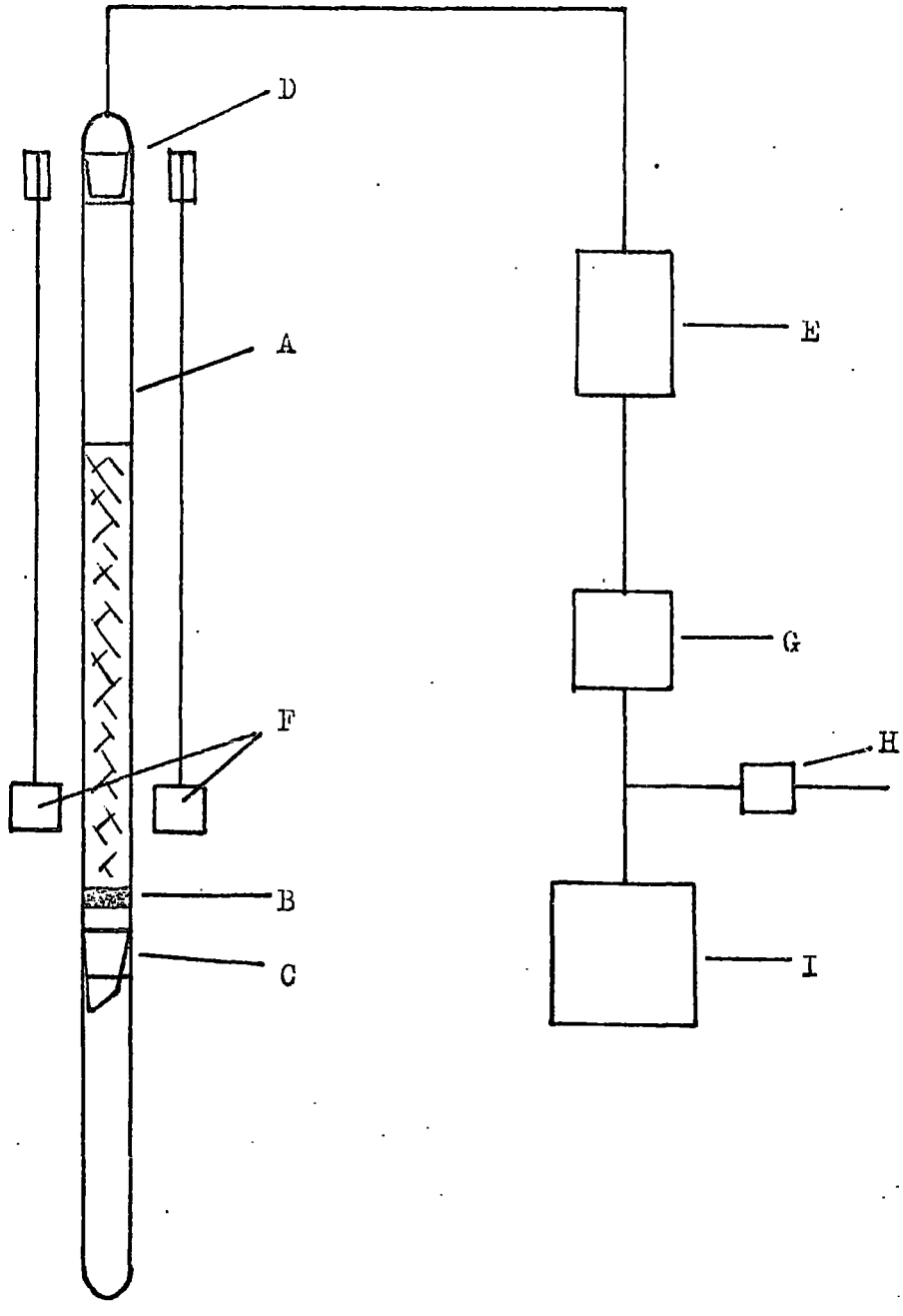

Figure (3.2). Schematic diagram of the silica gel activation system.

dismantled and the tube (A) filled to the top with hexane, which flowed slowly through the silica-gel and was collected in a clean dry bottle.

The de-hydrated and partially purified liquid so produced was used as starting material for a repetition of the entire process, using a fresh charge of silica-gel. Figure (3.3) shows the optical absorption of the liquid after the second purification. By comparison with figure (3.1) it is evident that the transparency of the liquid was substantially increased by the silica-gel process, although some absorption due to residual benzene was still detectable. Presumably a third repetition of the purification process would have reduced the absorption level still further. However, the optical quality of the hexane as depicted in figure (3.3) was judged to be satisfactory in view of the proposed use of a selective filter between the liquid and the photo-injecting light source. It was therefore decided not to attempt any additional purification by the silica-gel method, unless substantial impurity photo-conduction were found to occur under the conditions of the mobility measurement. The experimental determination of the signal magnitudes due to photo-conduction and photo-injection is described in Chapters 4 and 5.

3.1.2 The de-gassing procedure

The method of de-gassing the liquid was the same as that used by Kahan (4). The system was in fact, designed and used by Morant in earlier work (5), and modified by Kahan. Since both the apparatus and procedure have been fully described in Kahan's Ph.D. thesis (4), only a

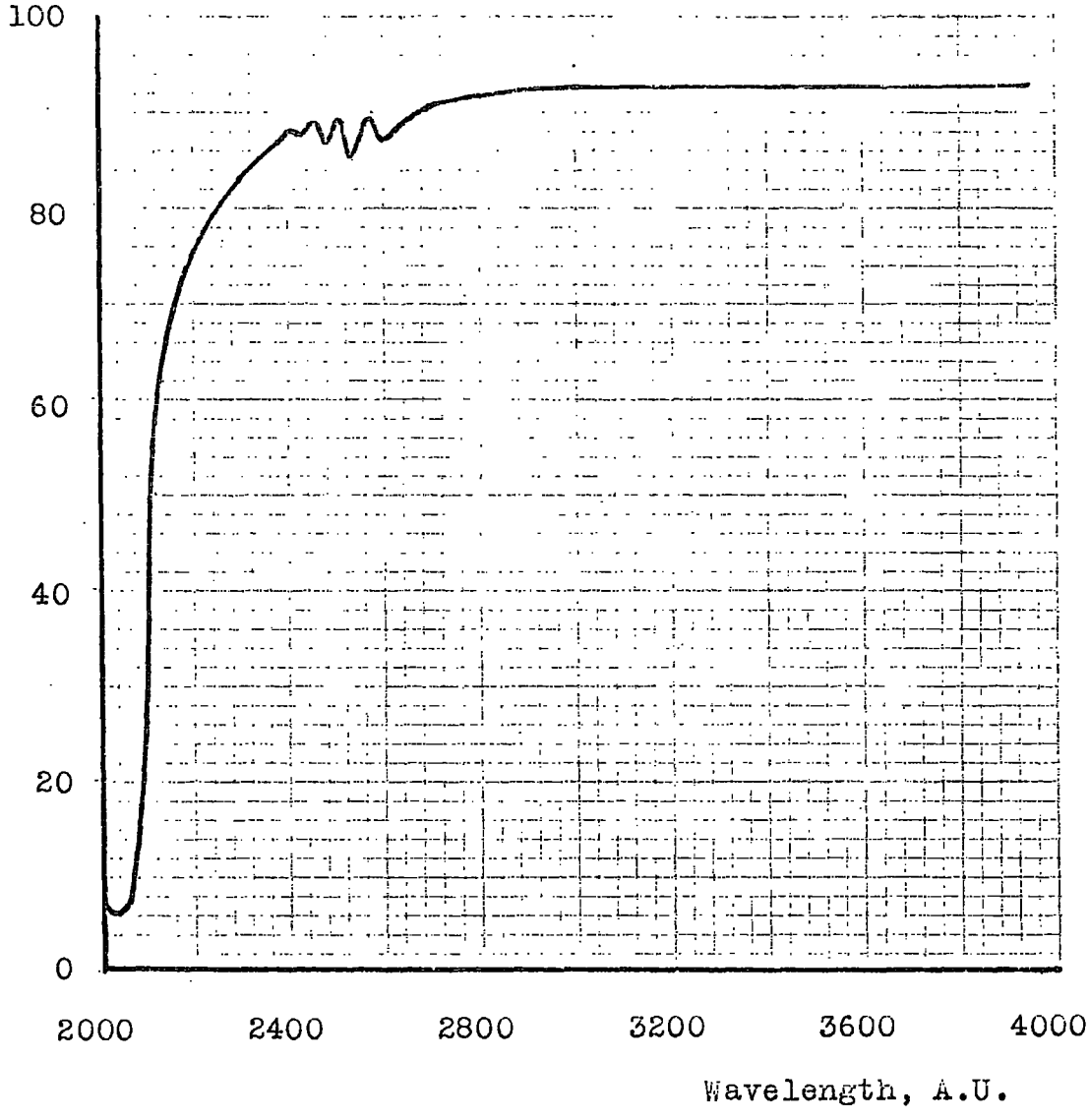

Figure (3.3). The optical absorption, in the region 2000 - 4000 A.U., of n-hexane (Koch-Light) after purification by silica gel.

Optical path length: 1 cm. Reference cell: air.

brief outline of the stages in the process will be given here.

i) preparation of the apparatus

The leak- and outgassing-rates of the apparatus must be sufficiently small not to interfere with the de-gassing procedure. Prior to admitting the hexane, therefore, the system is pumped for about 8 hours in every 24, using a mercury diffusion-pump. The pressure rise during the remaining 16 hours is recorded by means of a Pirani-gauge, and the relative contributions of gas and vapour to this rise are determined by solidification of the latter at liquid-nitrogen temperature. The pumping cycle is continued until the gas-pressure rise in the final section of the system, including the test-cell, corresponds to a leak-rate of $\sim 10^{-7}$ lusec. A vapour-pressure rise over the same period of approximately 10 times this magnitude is tolerated, since it is mainly due to adsorbed hexane from the previous batch.

ii) the removal of water and dust

The temperature of the hexane is reduced to -80°C. and the liquid is passed through a sintered-glass filter. This removes water, in the form of ice crystals, and solid particles down to 1 micron in diameter.

iii) initial de-gassing

The system is pumped continuously by a rotary oil-pump during a vacuum distillation between room-temperature and -80°C. Contamination of the hexane by pump-oil is prevented by a vapour trap,

at - 80°C., between the pump and the distillation system.

iv) solidification from the vapour

The receiving vessel of stage (iii) is evacuated at - 80°C. by means of a mercury diffusion-pump. The vessel is then isolated from the pump and allowed to regain room-temperature, while the hexane solidifies on a surface at liquid-nitrogen temperature (- 196°C.)

v) high-vacuum de-gassing

The hexane is allowed to transfer slowly between a vessel at - 80°C. and a surface at - 196°C., while the system is pumped by the diffusion pump. A liquid-nitrogen trap prevents contamination of the liquid by mercury vapour. The rate of transfer is approximately 10-15 cc. per hour. On completion of the transfer, the solid hexane is allowed to melt. The diffusion pump is only isolated from the system when the pressure recorded by a Pirani gauge rises rapidly, at the melting point.

vi) filling and isolating the test-cell

The de-gassed hexane is solidified in the test-cell, which is then isolated from the vacuum system by sealing-off the glass connection between them. This operation is carried out while pumping with the diffusion pump, so that the final gas-pressure in the test-cell is 10^{-5} - 10^{-6} torr. Particular care is taken to ensure that leak- and outgassing-rates of the test-cell are sufficiently small to maintain the hexane in a highly de-gassed state for a considerable period. The leak rate of the

test-cell is compared with that of the final section of the system, determined by Kahan as 10^{-7} lusec., by measuring the total leak rates before and after the cell is joined to the system.

3.2 THE ULTRA-VIOLET SOURCE

3.2.1. Specification

A high-intensity pulse of ultra-violet light was required, the duration of which had to be short compared with the transit-time to be measured. In order to evaluate the merits of a particular source, these properties were expressed in the following quantitative terms:

i) spectral distribution

The photoelectric threshold for injection from an aluminium cathode into hexane is approximately 3,000 Å (5). The intensity of the source must therefore remain high for wavelengths less than this value. The existence of any major reduction in intensity between 2,500 Å and 3,000 Å may be detected by comparing the transmission through the Chance-Pilkington filters OX1 and OX7.

ii) pulse length

The minimum transit-time envisaged in the present work is of the order of 1 msec., assuming a mobility of 10^{-3} cm.^{2}/V.sec. This value must therefore be regarded as the maximum permissible pulse length.

iii) intensity

It is known from Pugh's work (2) that a current of 10^{-10} A.

may be injected into de-gassed hexane, using a particular mercury discharge lamp ('Hanovia'). A standard of intensity, directly related to the photo-injection process, may therefore be established by measuring the response of a photocell to this same source. Other sources whether pulsed or continuous, may then be compared with the 'Hanovia' lamp, and an order of magnitude estimate made of the photo-injected current level they could produce.

3.2.2. Evaluation of available sources

Three types of light source were examined according to the above specification, using an ultra-violet sensitive photocell (Mullard 150 UV).

i) 'Hanovia' mercury discharge lamp

This source was known to be capable of injecting 10^{-10} A. into de-gassed hexane. At a distance of 2m. from the lamp, to which an OX1 filter had been fitted, the photocell current was 10^{-7} A. Regarding these as the standard conditions referred to in the previous section, the scaling factor between photocell and test-cell current was established as 10^{3}. A pulse of duration 10^{-3} sec. from this source would therefore be expected to produce 10^{-13} coulomb of injected charge in the test-cell.

ii) High voltage spark in air

A series of experiments was performed to determine the conditions necessary for the production of an intense spark, rich in

ultra-violet light. Several combinations of storage-capacitor size, electrode material and geometry,and breakdown voltage were examined. The discharge of a 0.02 μF paper capacitor at 8KV. between 1 cm. chromium-plated spheres, was found to be particularly satisfactory. The photocell response at 2m. was a 10 μsec. pulse of peak height 20 μA. The total charge involved was 10^{-10} coulomb, which would correspond to 10^{-13} coulomb injected into the liquid. This source had the advantage of short pulse length, but the intensity was not sufficiently high to produce a larger signal than (i) above. Other disadvantages were the statistical scatter in breakdown voltage, and hence of light intensity, and also the major problem of radiated electrical noise.

iii) Electronic flash-gun

The model investigated consisted of a 2.5 cm. arc-gap flash-tube, set in a paraboloid reflector, and powered by a 250 μF capacitor charged to 500V. The overall pulse length was 1.5 msec., and the total charge involved was 10^{-7} coulomb (10^{-10} coulomb in the liquid). There was some indication of a reduction of intensity between 2,500 A.U and 3,000 A.U., which was ascribed to the transmission properties of the flash-tube envelope. The high intensity of this source, combined with a good degree of reproducibility and low electrical noise were considered to be important advantages. It was therefore decided to construct a modified version of the device, using a quartz flash-tube

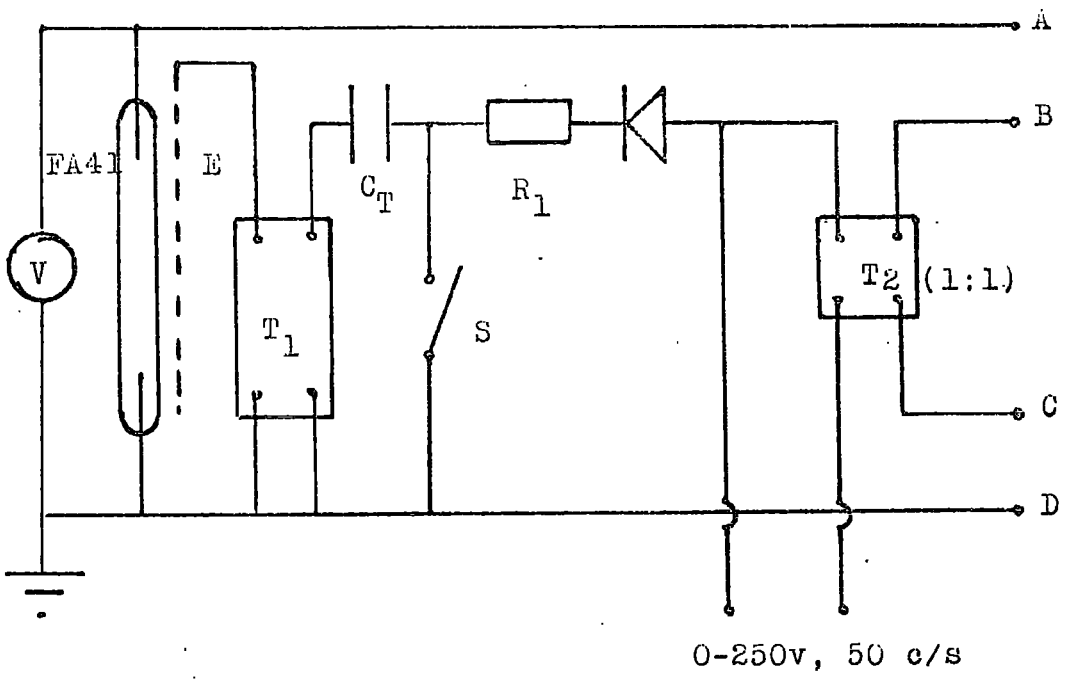

(a) The flash-tube unit

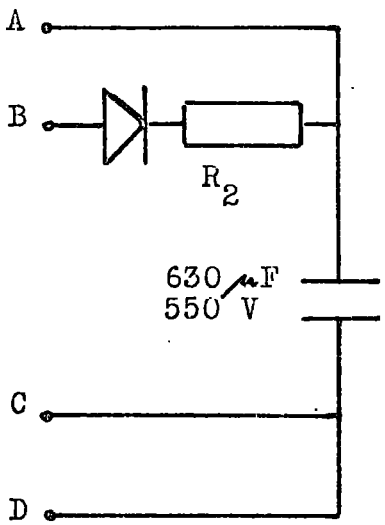

(b) The 'long' flash capacitor unit.

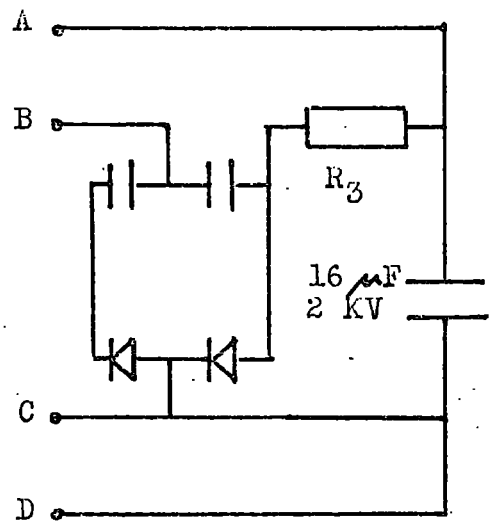

(c) The 'short' flash capacitor unit.

Figure (3.4). Circuit diagrams of the ultra-violet source.

to eliminate absorption of the shorter wavelengths and re-designing the circuit to reduce the pulse length to less than 1 msec.

3.2.3. The quartz-xenon flash-unit

The basis of the unit is a xenon-filled flash-tube, type FA 41, supplied by A.E.I. Ltd. The tube, together with the trigger-circuit, was mounted inside a metal case. Two plug-in capacitor units were constructed, allowing a choice of pulse length and intensity. Figure (3.4) shows the circuit daigrams of the unit. The flash-tube is triggered by closing the switch (S). This discharges the capacitor (C_t) through the primary of (T_1), resulting in the application of a 10KV. pulse to the external trigger electrode (E). It was found necessary during preliminary trials to situate the switch inside the flash-unit, in order to reduce interference from the trigger-circuit.

Figures (3.5a), (3.5b) illustrate the pulse shapes, referred to as the 'long' and 'short' flashes respectively, corresponding to the two capacitor units. Some basic characteristics of the pulses are listed in Table (3.1). The effective duration of the 'long' flash was less than, and the mean intensity greater than, that of the electronic flash-gun (section 3.2.2.). As a result, the estimated injected charge of 10^{-10} coulomb was maintained, while the pulse length was decreased from 1.5 msec. to 0.5 msec. Both the pulse length and the charge injected for the 'short' flash were approximately 10 times less than the corresponding values for the 'long' flash.

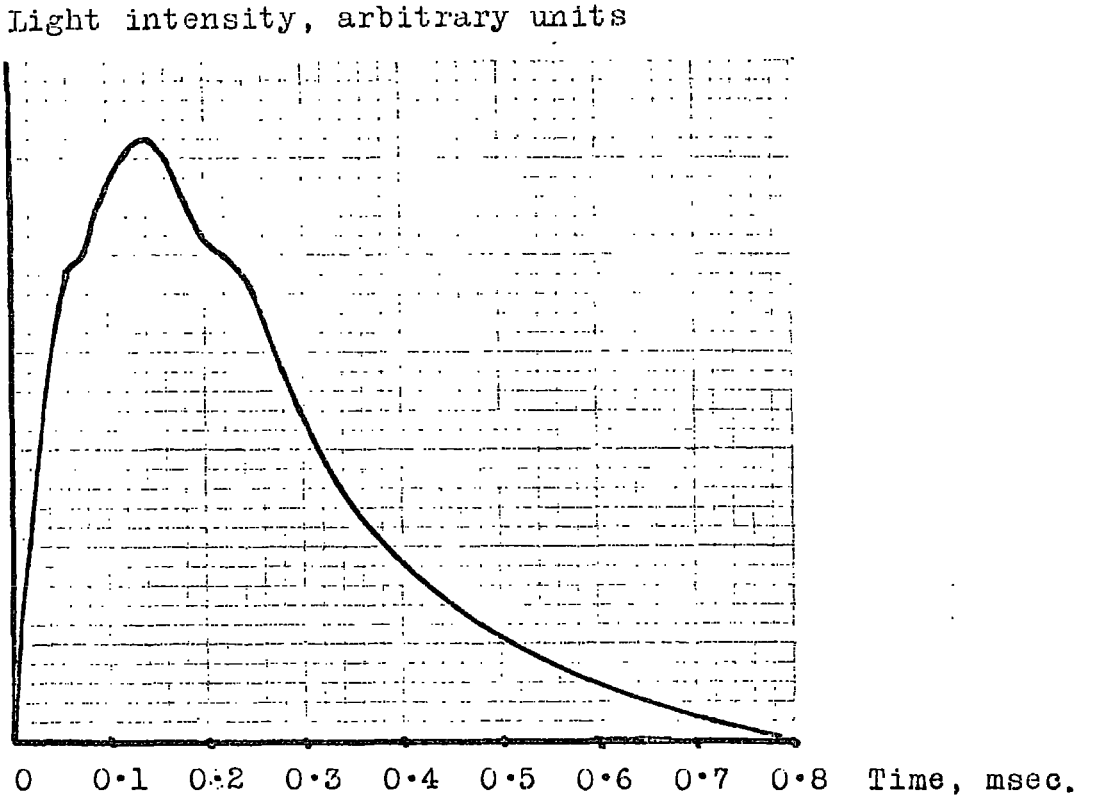

Figure (3.5a). Flash-unit output - long flash.

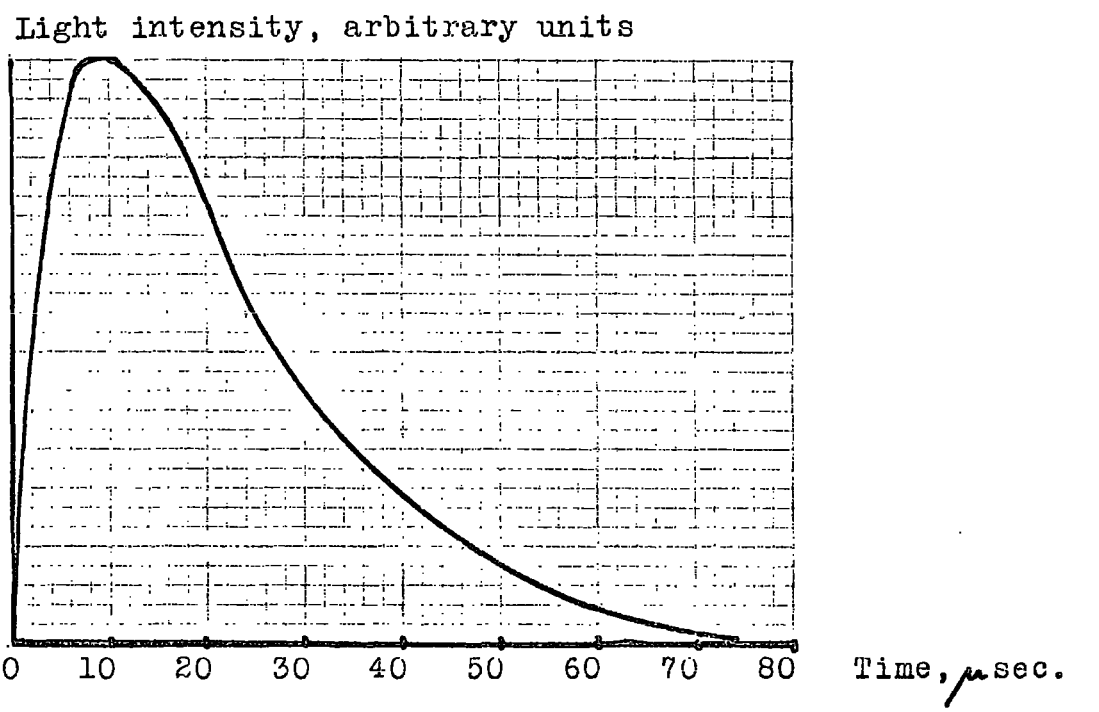

Figure (3.5b). Flash-unit output - short flash.

Capacitor unit	Long flash unit	Short flash unit
Capacitor value and type	630 μF, electrolytic	16 μF, oil-filled
Capacitor voltage	450 V	1 KV
Energy stored	64 J	8 J
Effective pulse length	500 μsec	45 μsec
Estimated injected charge	10^{-10} coulomb	10^{-11} coulomb

Table (3.1). Basic characteristics of the flash-unit

In contrast to the measurements made on the electronic flash-gun, no indication of an intensity reduction between 2,500 Å. and 3,000 Å was observed.

3.3. DETECTION OF THE CURRENT TRANSIENT

3.3.1. Requirements of the detection circuit

The development of a sufficiently intense source of ultra-violet light (section 3.2.) enabled the charge-measurement method of transit-time determination to be adopted. As explained in section 2.3.3., the condition $RC \gg \tau$ required by the method must be achieved by means of a high value of R, since the signal size is inversely proportional to C. The value of R required to produce a given signal, V_s, depends on the transit-time and the ratio RC/τ. Equation (15) of Chapter (2) may be expressed in these terms:

$$V_s = ne/C = ne(\tau/RC).(R/\tau) \qquad (1)$$

Assuming a maximum transit-time of 1 sec., an injected charge of 10^{-10} coulomb (section 3.2.3.) and a value for RC/τ of 10, the relationship between V_s and R becomes:

$$V_s = 10^{-11}.\ R \text{ volts} \qquad (2)$$

The value of R required to produce a signal suitable for measurement by a standard oscilloscope was therefore in the region of 10^9 - $10^{10}\ \Omega$. Since the input resistance of such an instrument is typically $10^6\ \Omega$, it was evident that an impedance-matching stage was necessary between the integrating RC circuit and the oscilloscope.

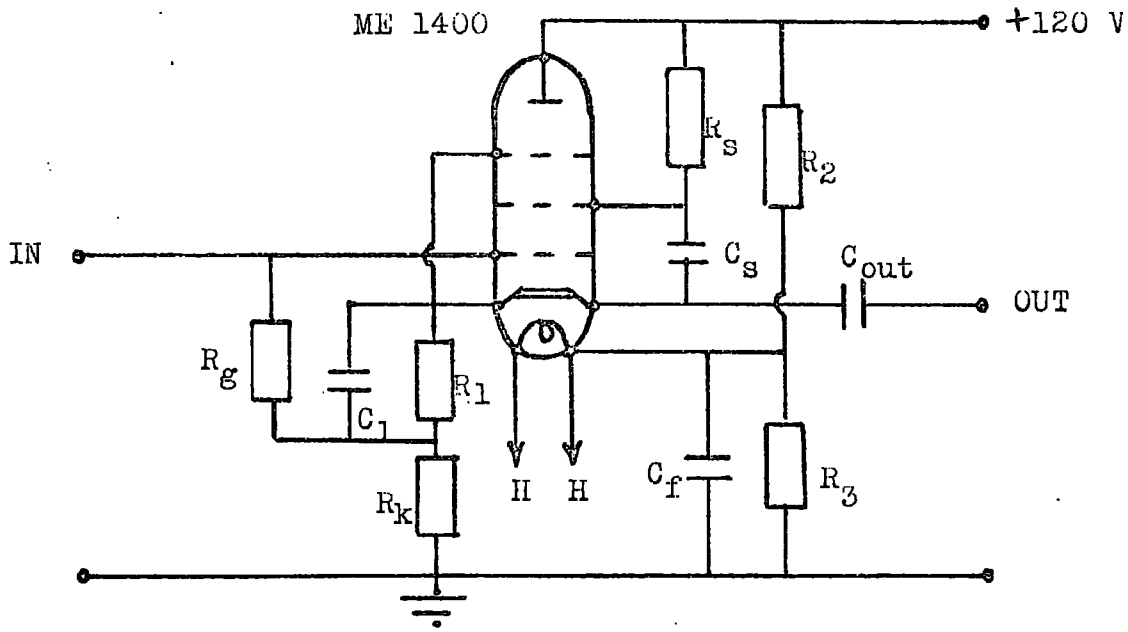

C_1	1000 μF	R_1	3·9 KΩ
C_{out}	8 μF	R_2	200 KΩ
C_s	8 μF	R_3	240 KΩ
C_f	32 μF	R_g	10^9 Ω
		R_k	150 KΩ
HH	4·4 V(D.C)	R_s	120 KΩ

Figure (3.6). Circuit diagram of the impedance-matching amplifier.

The main requirements of such a stage were an input resistance, R_{in}, of at least $10^{10}\Omega$ and an output resistance, R_{out}, of less than $10^{6}\Omega$. In addition the input capacitance was required to be small, and the frequency range of the device sufficient to avoid distortion of the signal for values of between 1 sec. and 1 msec.

3.3.2. The impedance-matching stage

The impedance-matching stage consisted of the cathode-follower circuit shown in figure (3.6). The input and output resistances of a cathode-follower are given by equations (3) and (4), where the amplification factor of the valve is $\mu_a \gg 1$, and the mutual conductance is g_m.

$$R_{in} = R_g(1 + g_m R_k) \qquad (3)$$

$$R_{out} = R_g/(1 + g_m R_k) \qquad (4)$$

The maximum value of R_g which may be employed depends on the grid-current, i_g, of the valve. For convential types the product $i_g . R_g$ becomes comparable with the grid-bias voltage for R_g $10^6 - 10^7\Omega$. Such a situation is undesirable in view of the non-linear and often time-dependent relationship between i_g and V_s. In order to increase R_g beyond $10^6\Omega$, an electrometer valve must be used. These valves are specifically designed to have low grid-currents, typically $\lesssim 10^{-11}$ A., and may therefore be operated with a grid-leak resistance of $\sim 10^9\Omega$.

The input capacitance of a cathode-follower is given by:

$$C_{in} = C_{ga} + C_{gc}/(1 + g_m R_k), \text{ for a pentode} \qquad (5)$$

$$C_{in} = C_{ga}(1 + 2g_m R_k)/(1 + g_m R_k) + C_{gc}, \text{ for a triode} \qquad (6)$$

where C_{ga} and C_{gc} are the grid-anode and grid-cathode capacitance respectively. Since $C_{gc} \gtrsim C_{ga}$, and $g_m R_k \gg 1$, it follows that the pentode version has the lower input capacitance.

The valve-type selected for the cathode-follower was a Mullard electrometer pentode, ME 1400. This valve has the grid-connection at the opposite end of the envelope from the base-pins, in order to facilitate the use of high value resistors. The valve was operated at an anode-cathode voltage of 60 V. and a current of 400 μA., with a grid-bias of - 2 V. Both the impedance-matching stage and the integrating circuit were enclosed in a metal case, from which stray light from the flash-source was carefully excluded.

The variation of gain, G, with frequency was determined between 10 c/s and 400 Kc/s, using a sine-wave generator and the 'Solartron' oscilloscope (see section 3.3.3). An order of magnitude value for the shortest detectable transit-time was given by the inherent rise-time t_r of the cathode-follower. This is related to the high-frequency cut-off (3db. reduction in voltage gain) by the expression:

$$t_r . f_h = 0.36 \qquad (7)$$

Figure (3.7) shows the frequency response of the device, from which a value for f_h of 40 - 50 Kc/s was deduced. The shortest detectable

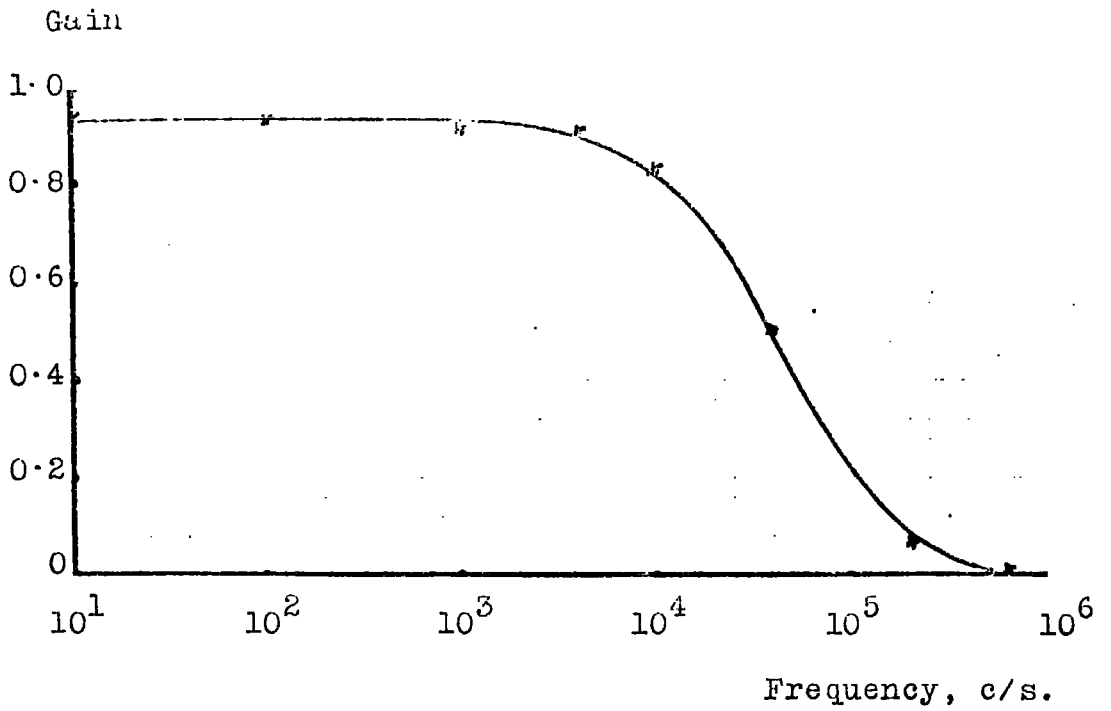

Figure (3.7). Frequency response of the impedance-matching amplifier.

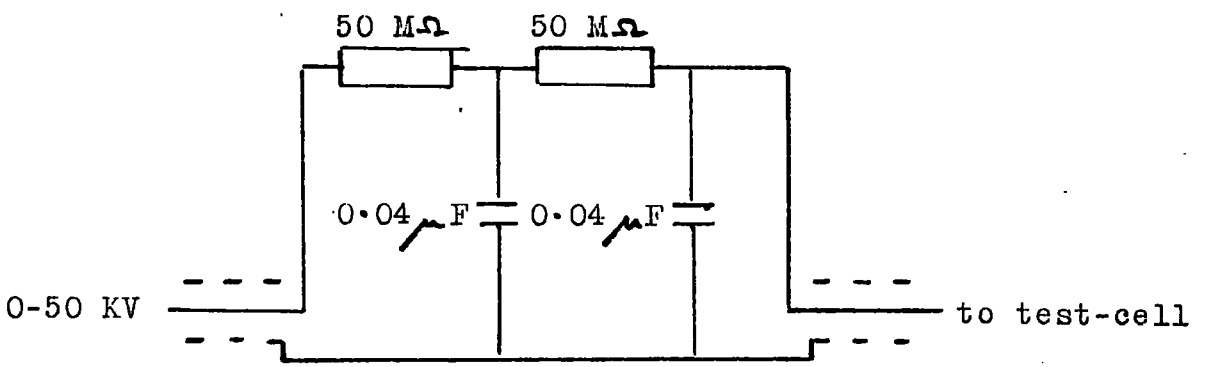

Figure (3.8). Filter circuit for 'Hursant' high-voltage supply.

transit-time was therefore in the range 1 - 10 μsec.

The maximum transit-time T which may be observed without major distortion was estimated by calculation of the percentage droop on a square wave of duration T. The loss of low-frequency components by the cathode-follower is due to division of the signal between the capacitance C_{out} - figure (3.6) - and the input resistance R_s of the DC-coupled oscilloscope. The percentage droop, D, is therefore given by:

$$0.01.D = 1 - \exp.\ (T/R_s.C_{out}). \qquad (8)$$

Substitution of the values $R_s = 10^6 \Omega$, $C_{out} = 8\ \mu F$ and D = 10%, yields the result T = 0.9 sec. An upper limit on the accurate determination of transit-time may therefore be set at $\sim$ 1 sec.

The experimental values of R_{in} and R_{out} were calculated from equations (3) and (4), using the relationship, valid for $\mu_a \gg 1$:

$$g_m R_k = 1/(1 - G) \qquad (9)$$

Taking the value of G from figure (3.7) as 0.93, the following results were obtained:

$$g_m R_k = 13.3\ ;\ R_{in} = 1.4.10^{10} \Omega\ ;\ R_{out} = 10\ K\Omega.$$

3.3.3. The oscilloscope

Two makes of oscilloscope were used to display the integrated current-transient. These were:

i) 'Tektronix' model 581 A, with a Type 82 Plug-in amplifier and

ii) 'Solartron' model CD 1443, with a CX 1442 Plug-in amplifier.

Both oscilloscopes had more than sufficient sensitivity and frequency range for this particular application and were therefore interchangeable with each other. The oscilloscope was d.c.-coupled to the output of the impedance-matching stage in order to maintain the low-frequency response of the transient detection system. The flash-source was used to trigger the oscilloscope, either by radiated electrical pick-up from the discharge, or from the light source itself by the use of a photocell.

Each oscilloscope was fitted with a camera taking $3\frac{1}{4}$" x $4\frac{1}{4}$" 3,000 A.S.A. Polaroid film, thus enabling actual-size records of the oscilloscope traces to be made. This facility was particularly useful in view of the need for detailed examination of each single-shot transient.

3.3.4. The high-voltage supply

Three types of high-voltage supply were used during the course of the investigation. They are listed below, together with their ranges and associated ripple amplitudes.

i) 'Dynatron' model N 103

Positive and negative voltages from 0.3 KV to 3.3 KV. Maximum ripple amplitude (peak to peak): 150 μV.

ii) 'Brandenburg' model S.0530/10

Positive voltages from 2.0 KV to 15 KV. Ripple amplitude: 5 mV.

iii) 'Hursant' model 50B

Positive and negative voltages from 0.5 KV to 50 KV. In addition to a ripple voltage of 0.1 %, pick-up from the R.F. oscillator and interference due to small corona discharges were found to be present under experimental conditions. The amplitude of these noise sources was reduced to an acceptable level (approximately 1 mV at 10 KV) by the use of the filter-circuit shown in figure (3.8). The connections between the high-voltage supply, the filter circuit and the test-cell were made with short lengths of 100 KV co-axial cable, with the outer conductor earthed.

3.4 REFERENCES

1. Kahan, E., and Morant, M.J.; Brit. J. Appl. Phys. 16, 943-945 (1965)

2. Pugh, D.R.; Ph.D. Thesis, Durham University (1968)

3. Potts, W.R.; J. Chem. Phys. 20, 5, 809-810 (1952)

4. Kahan, E.; Ph.D. Thesis, Durham University (1964)

5. Morant, M.J.; Nature 187, 4731, 48-49 (1960)

CHAPTER 4

PRELIMINARY MEASUREMENTS

This chapter deals with the development of the test-cell, described in Chapter 5, which was used to make accurate measurements of transit-time and signal magnitude as a function of electric field. Preliminary measurements of these quantities are included in the present chapter to illustrate the reasons for the various changes in test-cell design. For ease of reference, the cells are designated 'cell A', 'cell B' etc., and each is the subject of a section of the chapter.

4.1. CELL 'A'

The object of the measurements made in cell 'A' was to confirm (a) that an easily detectable signal could be obtained from the apparatus described in Chapter 3 and (b) that this signal was a result of photo-injection and not due to ionization or excitation processes. The cell was originally designed and used by Pugh (1) for his work on photo-injection from clean metal surfaces. It provided facilities for the high-vacuum evaporation of metals onto the electrodes, prior to filling the cell with de-gassed liquid. Although not primarily designed for the determination of carrier mobility, the cell was considered suitable for preliminary measurements of this quantity.

Figure (4.1) shows the basic features of cell 'A'. In order to

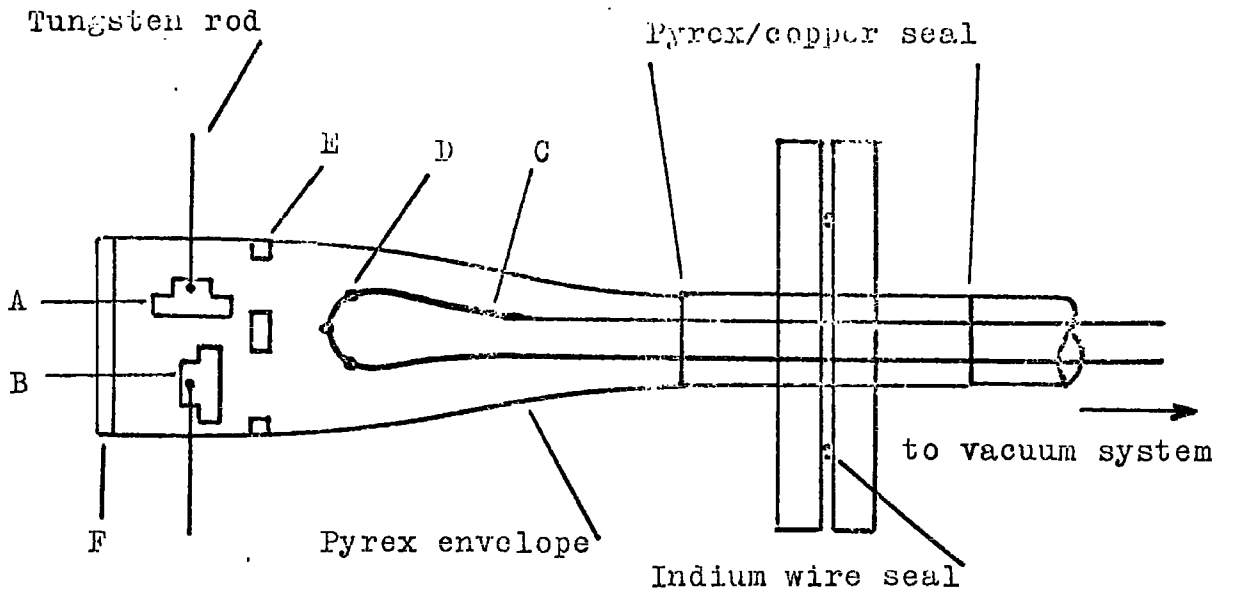

Figure (4.1). Basic features of cell 'A'.

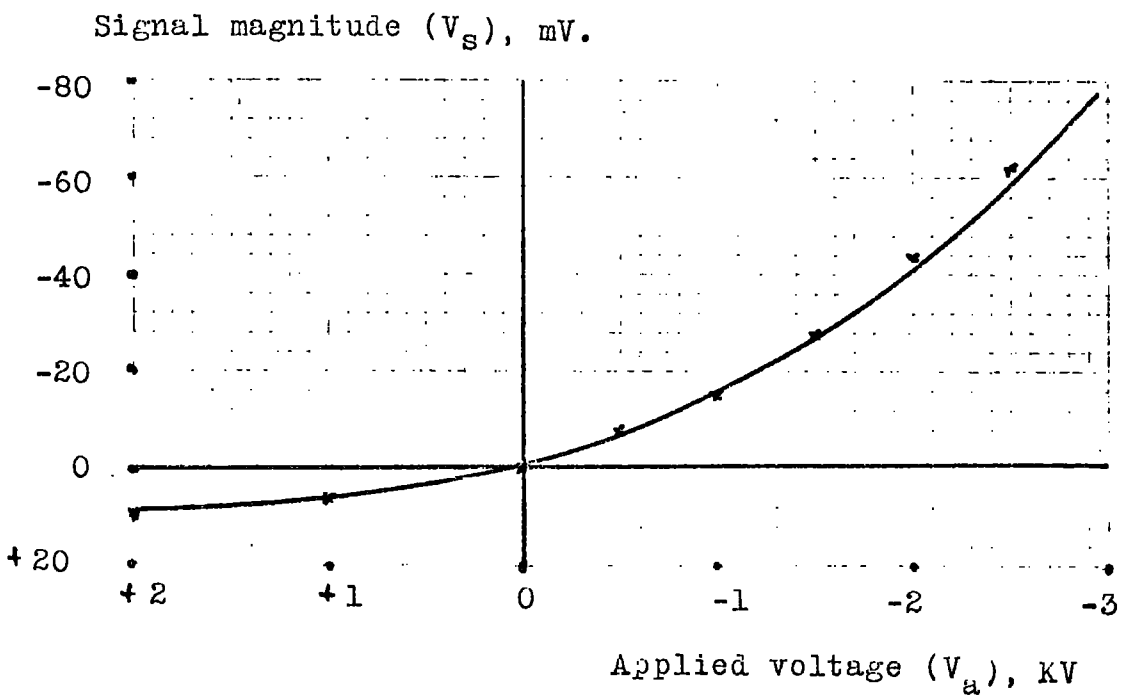

Figure (4.2). Signal magnitude versus applied voltage for the high-potential electrode of cell 'A'.

deposit a layer of aluminium onto the electrodes (A), the cell was inverted, causing them to rotate through 90° into the evaporating position (B). The tungsten filament (C) was then heated to vaporize the pre-formed aluminium beads (D). The nickel shield (E) prevented the formation of a reflecting layer on the silica disc (F) The evaporation process was carried out immediately before sealing-off the cell, while pumping with the mercury diffusion-pump - see section 3.1.2.

4.1.1. Photo-injection and photo-ionization

In order to determine the contributions of injection and ionization to the total signal, the ultra-violet source was directed towards one electrode only and the shape and size of the signal observed for both positive and negative applied voltages. Under these conditions, photo-injection produces a large signal in the forward direction and a considerably smaller signal, due to reflected or stray light, in the reverse direction. The signal magnitude due to ionization is, however, independent of polarity. Furthermore, the shape of a photo-injected signal should approximate closely to a ramp-function - see for example figure (2.4b) - whereas the formation of carriers throughout the liquid should give rise to a pronounced curvature of the rising portion of the transient, due to the distribution of transit-times.

Let the forward and reverse photo-injected signals be u_f and u_r, respectively, and the signal due to ionization be w. Then, denoting the total forward and reverse signals by v_f, v_r:

$$v_f = u_f + w$$
$$v_r = u_r + w \qquad (1)$$

The ratio of injected to ionized carriers, in the forward direction, is then given by:

$$u_f/w = (v_f - w)/(v_r - u_r) \qquad (2)$$

The exact determination of u_f/w requires that u_r be known or be negligible in comparison with v_r. In the latter case, when only one electrode is allowed to inject carriers:

$$u_f/w = v_f/v_r - 1 \qquad (3)$$

Since, in the test-cell described above, both electrodes are coated with freshly evaporated aluminium, the condition $u_r \ll v_r$ may not be satisfied. However, the above expression fixes the lower limit for u_f/w in that case.

4.1.2. Illumination of the high-potential electrode

The flash-source was positioned in such a way as to allow light to fall directly on the high-potential electrode only.

Figure (4.2) shows the variation of signal-magnitude V_s with applied voltage V_a, using a measuring capacitance of 1000 pF. The ratio v_f/v_r at 3.3 KV was 7.25, setting a lower limit for u_f/w of 6.25.

Figure (4.3) compares the shapes of the transients in the forward and reverse directions, for V_a = 3.3 KV. The pronounced curvature of

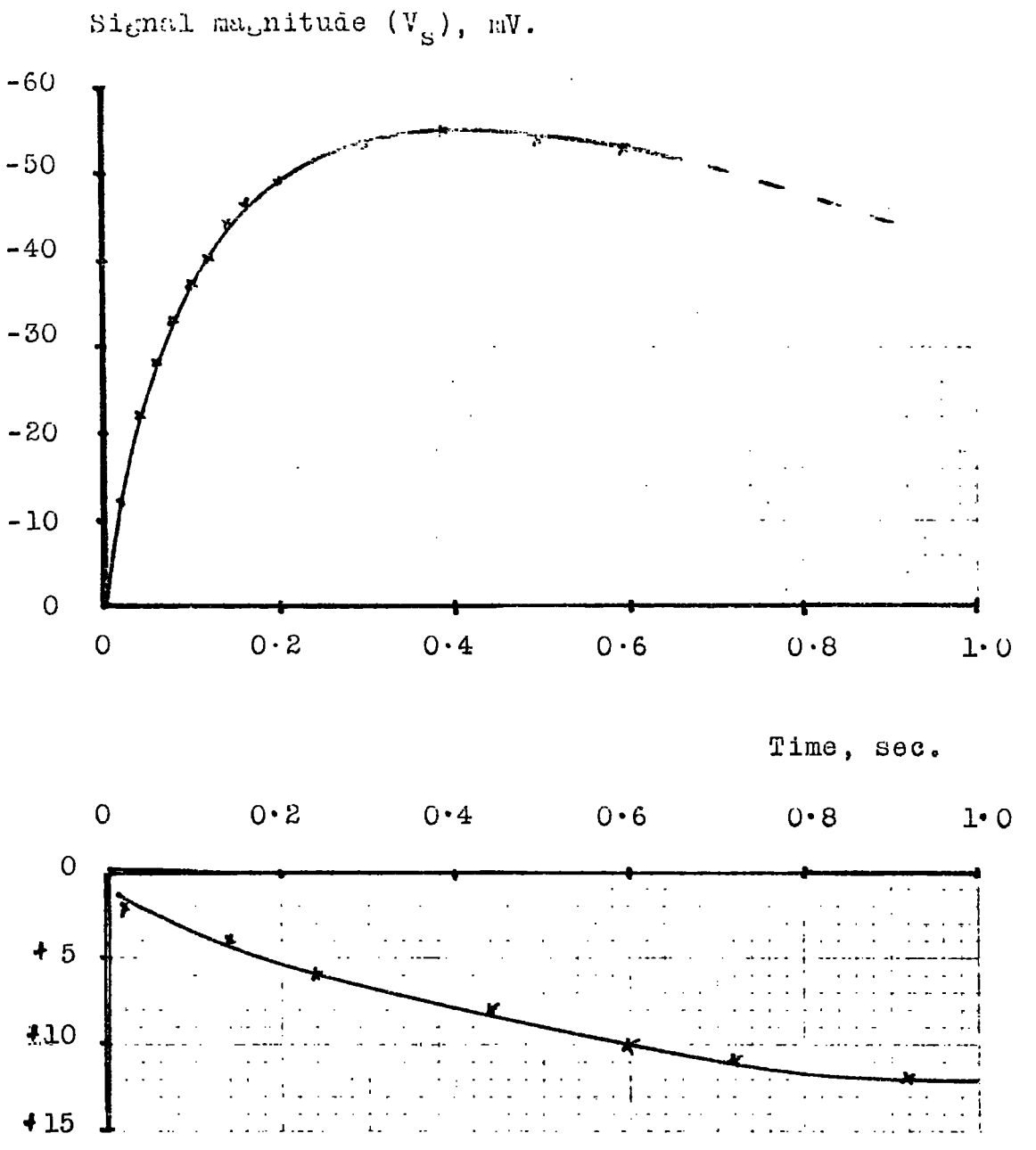

Figure (4.3). Shapes of the transients for cell 'A', with the high-potential electrode illuminated. Upper transient, forward direction; lower transient, reverse direction.

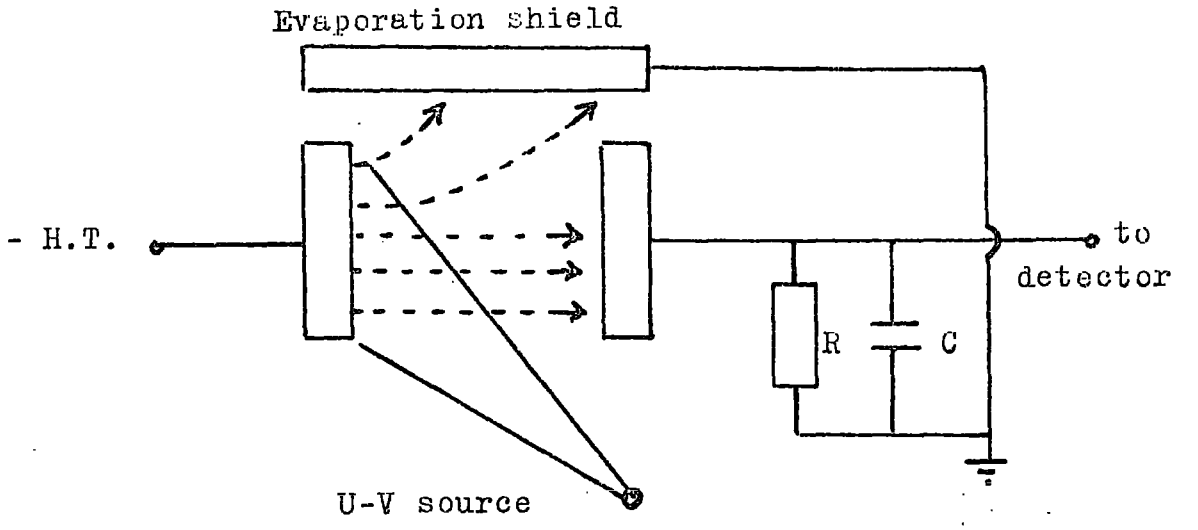

Figure (4.4a). Effect of the earthed evaporation shield in cell 'A'. High-potential electrode illuminated.

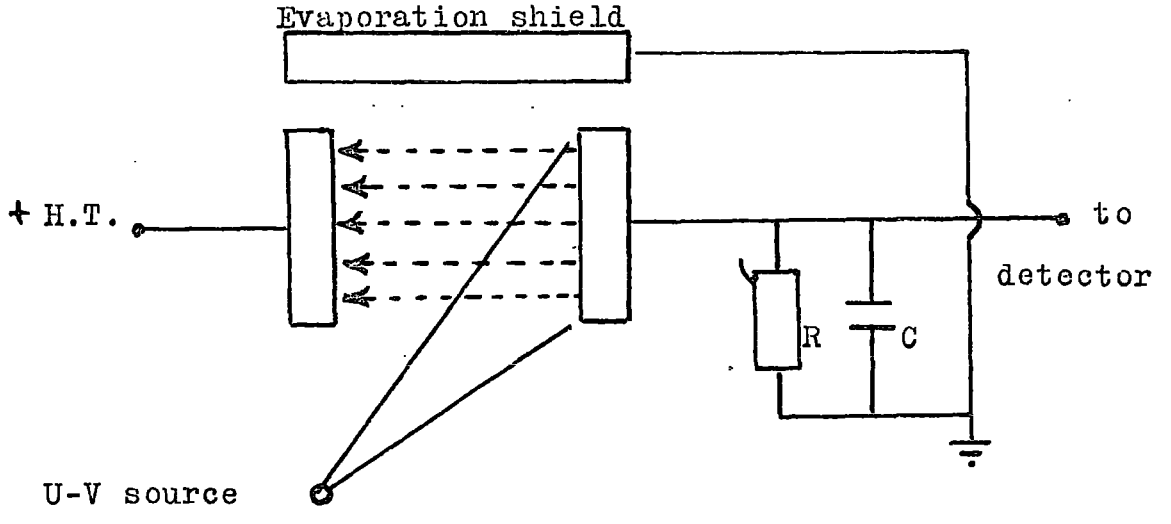

Figure (4.4b). Effect of the earthed evaporation shield in cell 'A'. Low potential electrode illuminated.

the forward transient is inconsistent with the high proportion of injected carriers indicated by figure (4.2). An explanation of this curvature, in terms other than of photo-ionization, was therefore sought, which would also allow for the considerably more linear trace-shape in the reverse direction. Among the postulated mechanisms was the collection of injected negative charge by the evaporation shield, which could have become electrically connected to the earthed vacuum flange - see figure (4.1) - during the evaporation process. The effect of such a situation would be to allow a proportion of the injected charge to by-pass the measuring circuit as the charge-layer moved towards the low-potential electrode. Charge-carriers moving in the opposite direction would not be affected to the same extent by the presence of the earthed conductor, as indicated schematically in figure (4.4). Evidence of the validity of the above explanation was obtained, as described in section 4.1.3. by illumination of the low-potential electrode.

4.1.3. Illumination of the low-potential electrode

Figure (4.5) illustrates the transient-shapes in the forward and reverse directions when the flash-source was placed in such a position as to illuminate the low-potential electrode. It is clear that, in the forward direction, the rising portion of the transient is considerably more linear than that of figure (4.3). Furthermore, the curvature of the trace has been transferred to the reverse direction, in agreement with the explanation put forward in section 4.1.2.

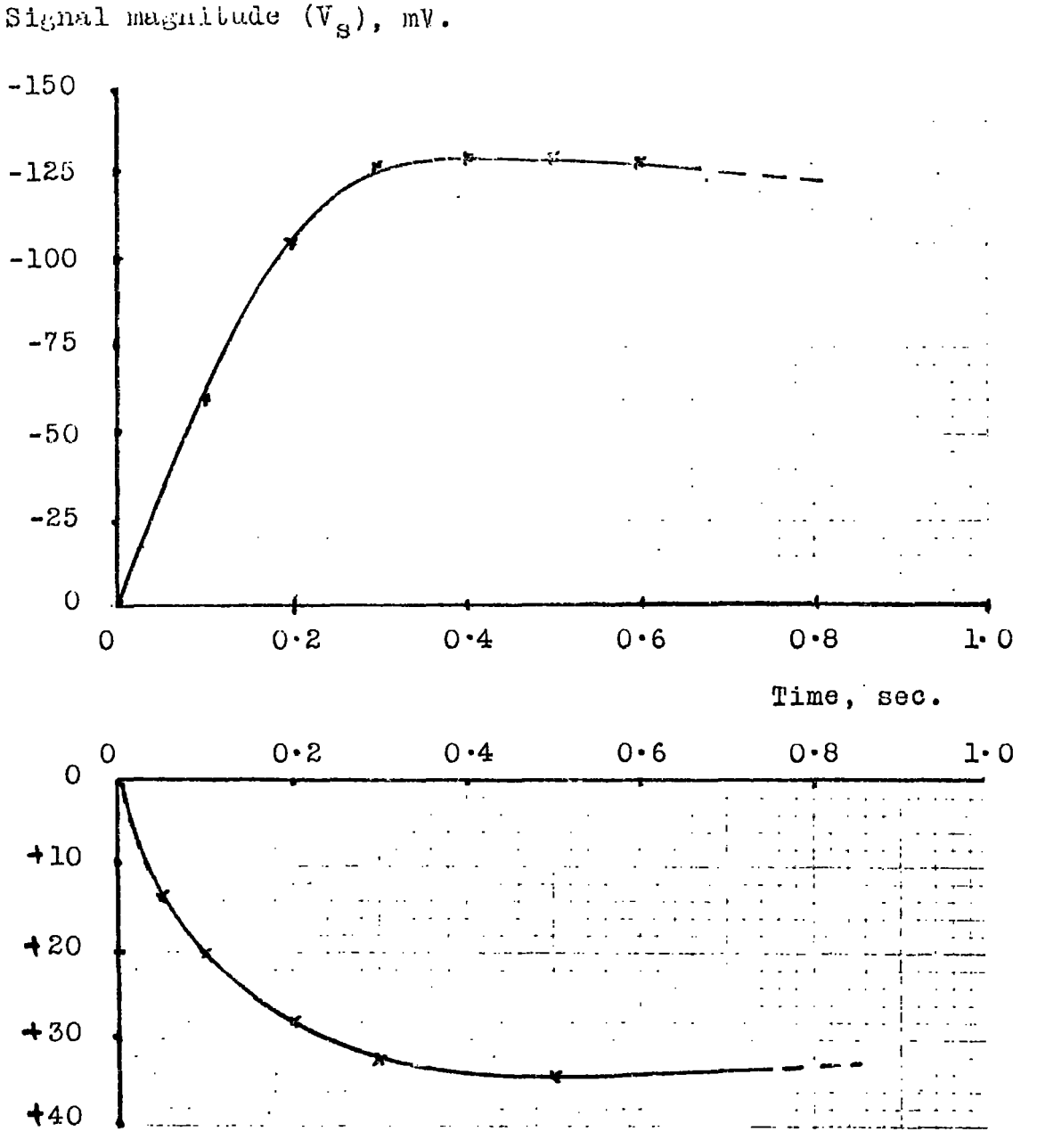

Figure (4.5). Shapes of the transients for cell 'A' with the low-potential electrode illuminated. Upper transient, forward direction; lower transient, reverse direction.

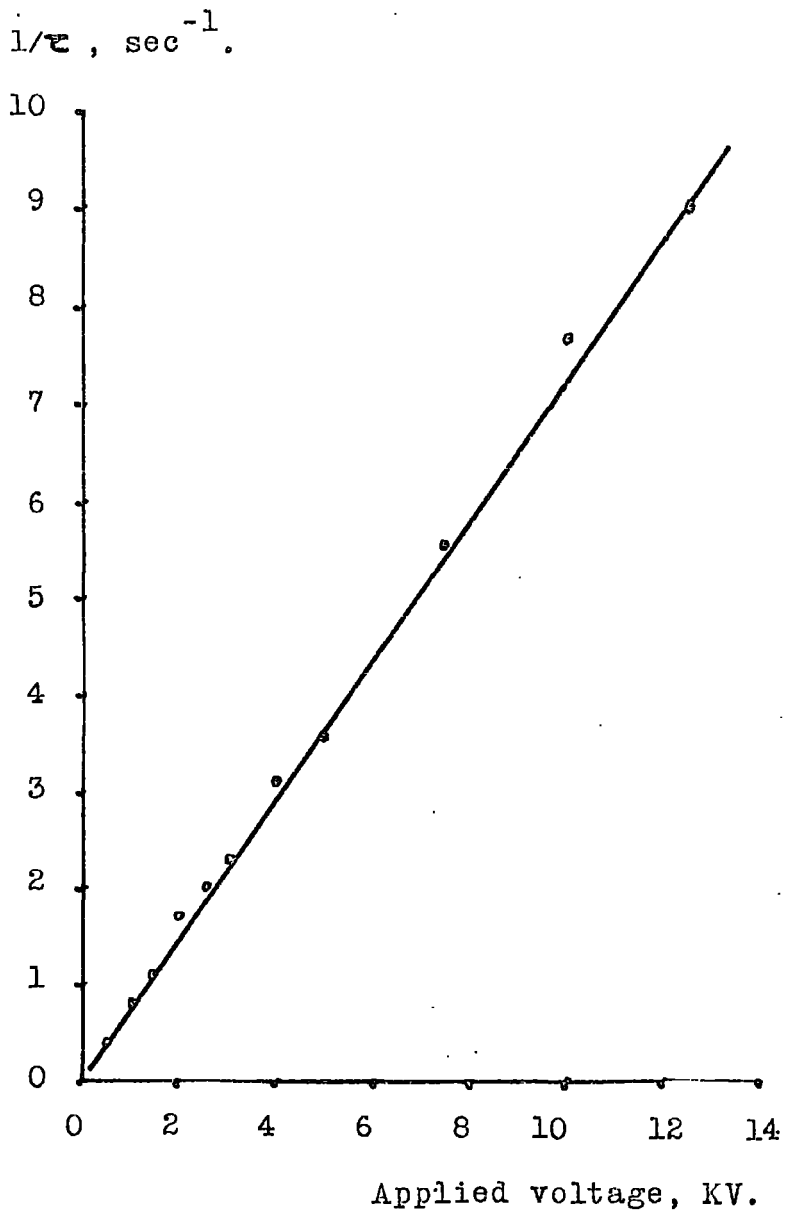

Figure (4.6). Variation of transit-time (τ) with applied voltage for cell 'A'. Low potential electrode illuminated.

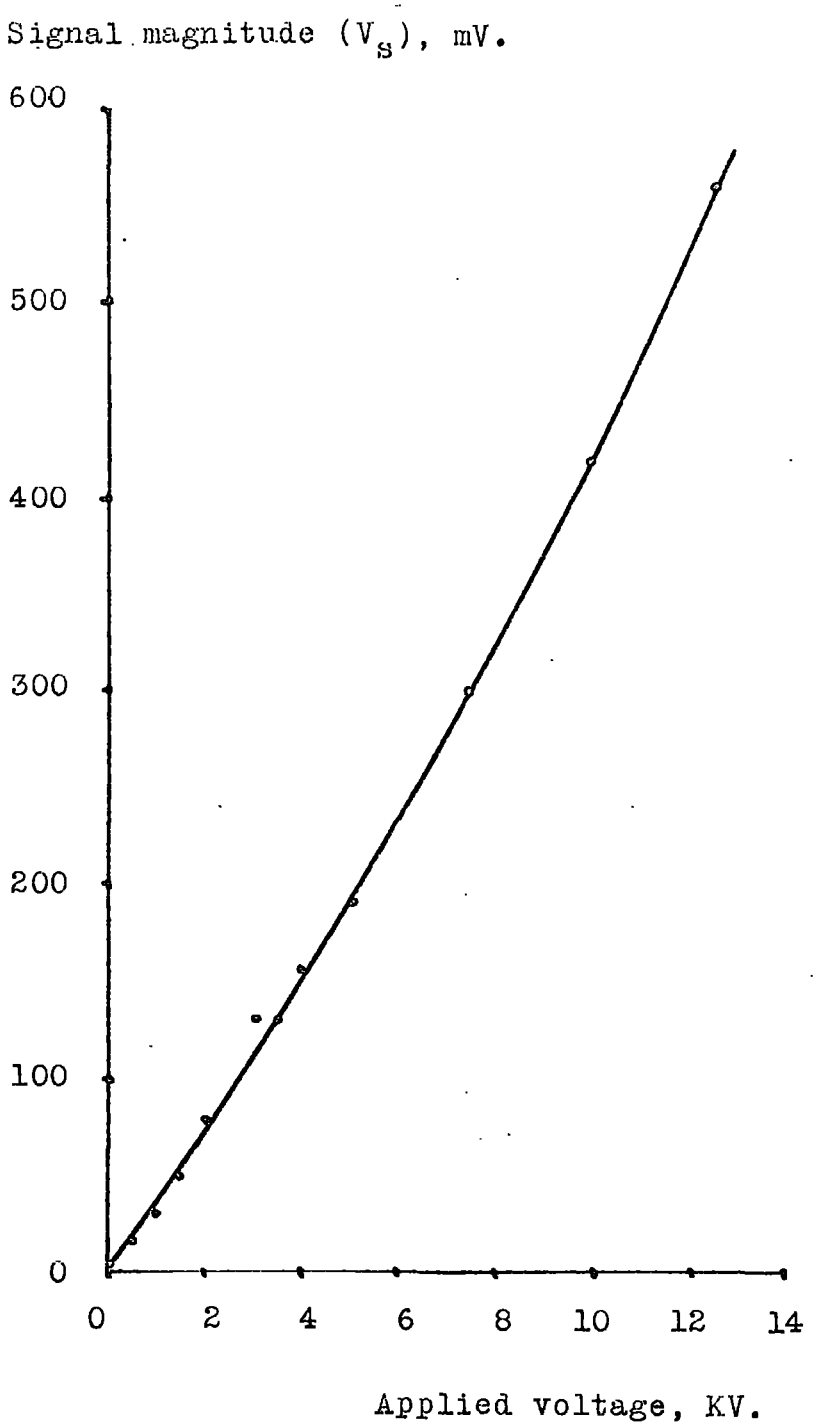

Figure (4.7). Variation of signal magnitude (V_s) with applied voltage for cell 'A'. Low potential electrode illuminated.

The shape of the transients in the forward direction was sufficiently close to the theoretical form for an estimate of the transit-time, τ, to be made in each case. Figure (4.6) shows the variation of $(1/\tau)$ with applied voltage V_a from 0.5 KV to 12.5 KV. From the relationship:

$$\mu = d^2 / V_a . \tau \qquad (4)$$

the gradient of this graph is μ/d^2, where μ is the carrier mobility and d the electrode separation. The value of d was determined by the use of a travelling microscope as (0.67 ± 0.02) cm., giving the mobility as (3.4 ± 0.2). 10^{-4} $cm^2/V.sec$.

The closely linear relationship between the (forward) signal magnitude V_s and applied voltage observed for the high-potential electrode was found to apply to the low-potential electrode up to 12.5 KV, as shown in figure (4.7).

A limitation to the maximum voltage which could be applied to the test-cell was encountered at approximately 14 KV. At this voltage the high-potential electrode was observed to rotate into the evaporating position, causing repeated breakdown of the liquid between the shield and the electrode. This phenomenon provided confirmation that the shield was connected electrically to the earthed vacuum flange.

4.1.4. Conclusions

The experimental results reported in the previous two sub-sections provided proof that photo-injection was achieved under the

proposed conditions for mobility measurement. The formation of other carriers, presumably due to ionization or excitation of the bulk of the liquid, was also observed, but their contribution to the total signal magnitude was small.

Curvature of the rising portion of the transient was present even when steps were taken to nullify the distorting effect of the evaporation shield. This made the accurate measurement of transit-time impossible. The value of mobility deduced from estimates of the transit-time (section 4.1.3) was considerably lower than that obtained under similar conditions by other workers (2, 3, 4). Two possible causes of this curvature were the poor alignment of the electrodes due to the necessity for free rotation into the evaporating position, and any residual effect of the shield. Further disadvantages of the test-cell, related to the evaporation process, were the fixed electrode separation and the limitation on the maximum applied voltage.

It was therefore decided to investigate alternative methods of producing a localized evaporated aluminium film on the cathode. The two types of cell resulting from this investigation are described in sections 4.2 and 4.3.

4.2 CELL 'B'

The basis of cell 'B' was a hollow, cylindrical anode containing the evaporating filament. An aluminium film was deposited on the cathode through a amall hole in the face of the anode. Figure

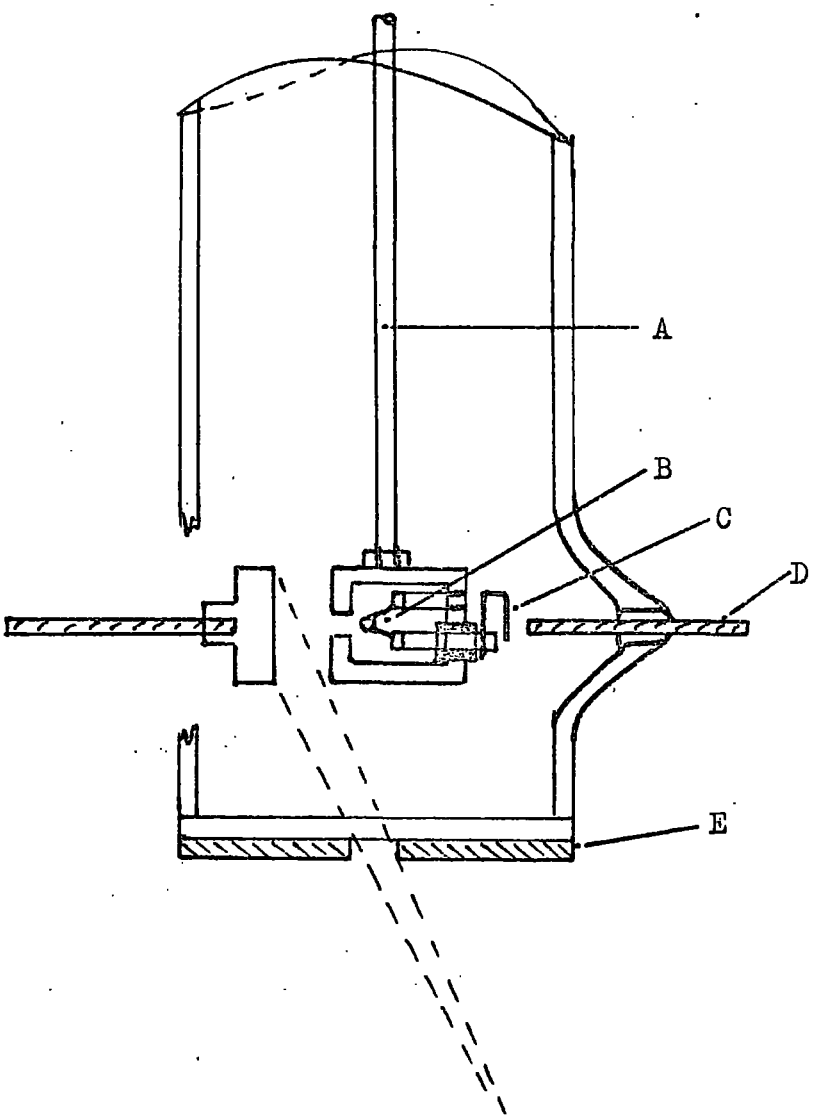

Figure (4.8). Part of cell 'B', showing the evaporating electrode.

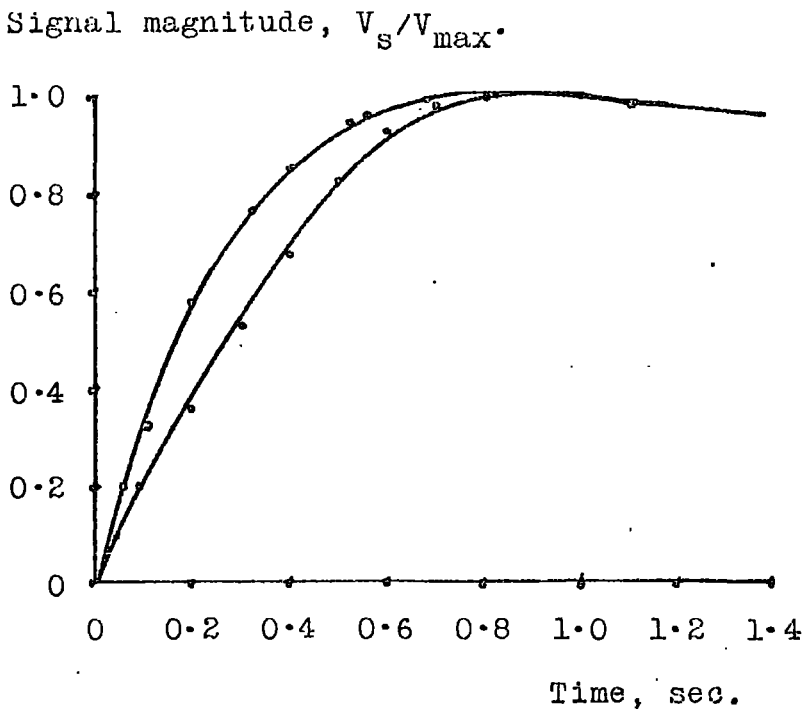

Figure (4.9a). Comparison of transients..Lower curve, cell '$\not{B}^{B}$'; upper curve, cell '$\not{B}^{A}$'.

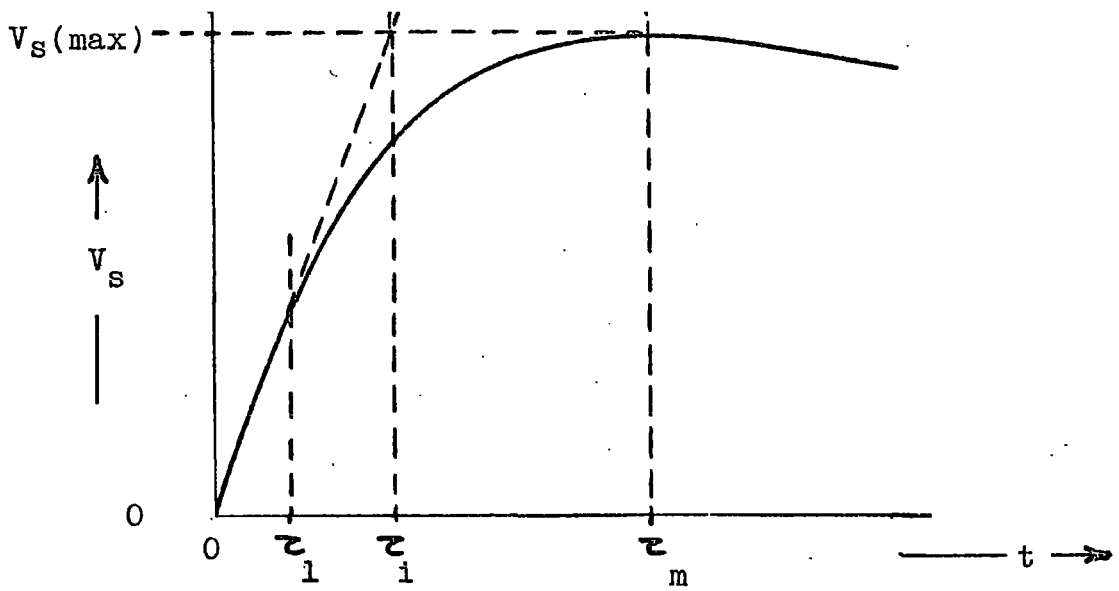

Figure (4.9b). Definition of the parameters τ_i, τ_1 and τ_m.

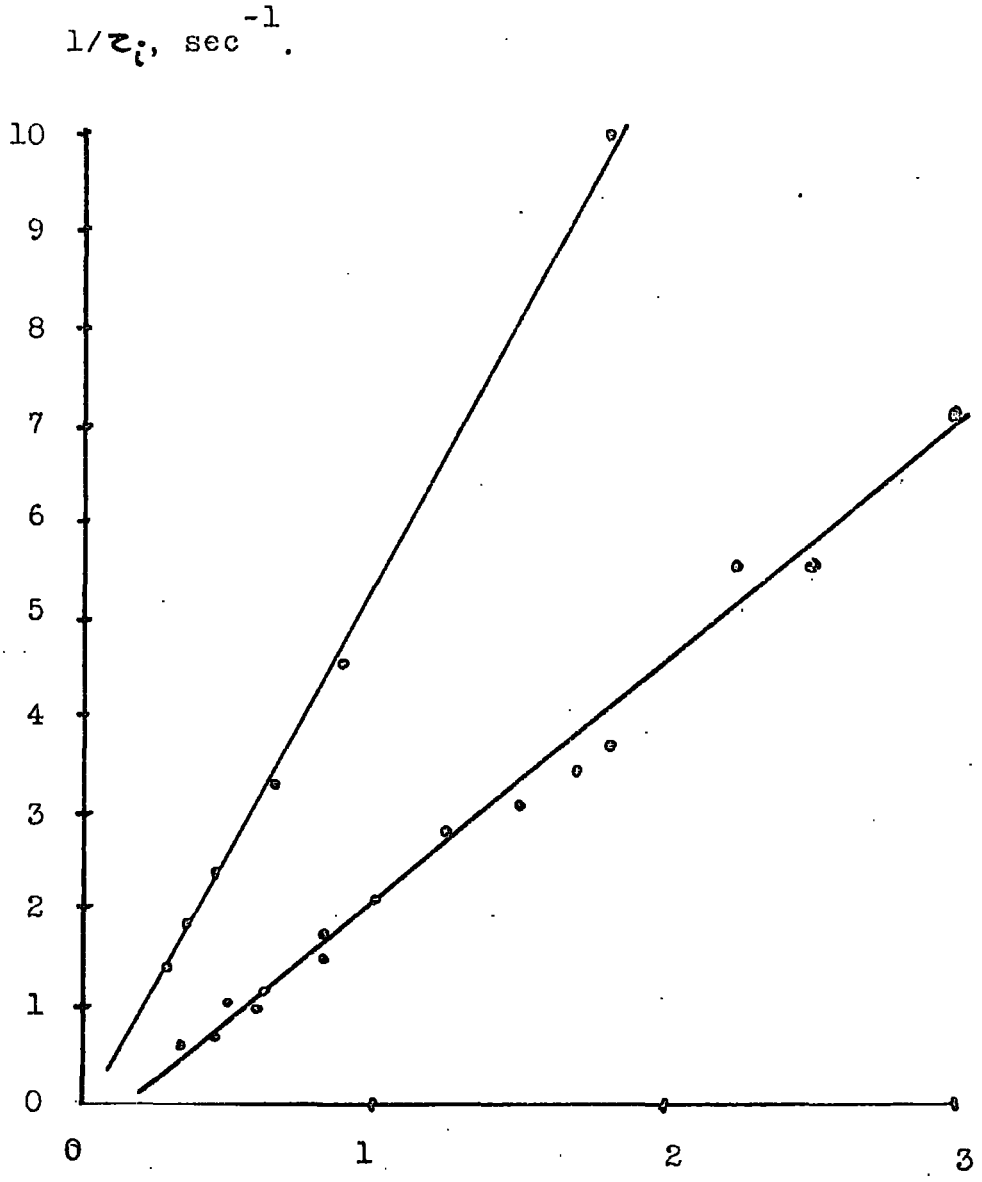

Figure (4.10). Variation of transit-time (τ_i) with applied voltage for cell 'B'.

Electrode separations: Upper curve, 0·46 cm.

Lower curve, 0·67 cm.

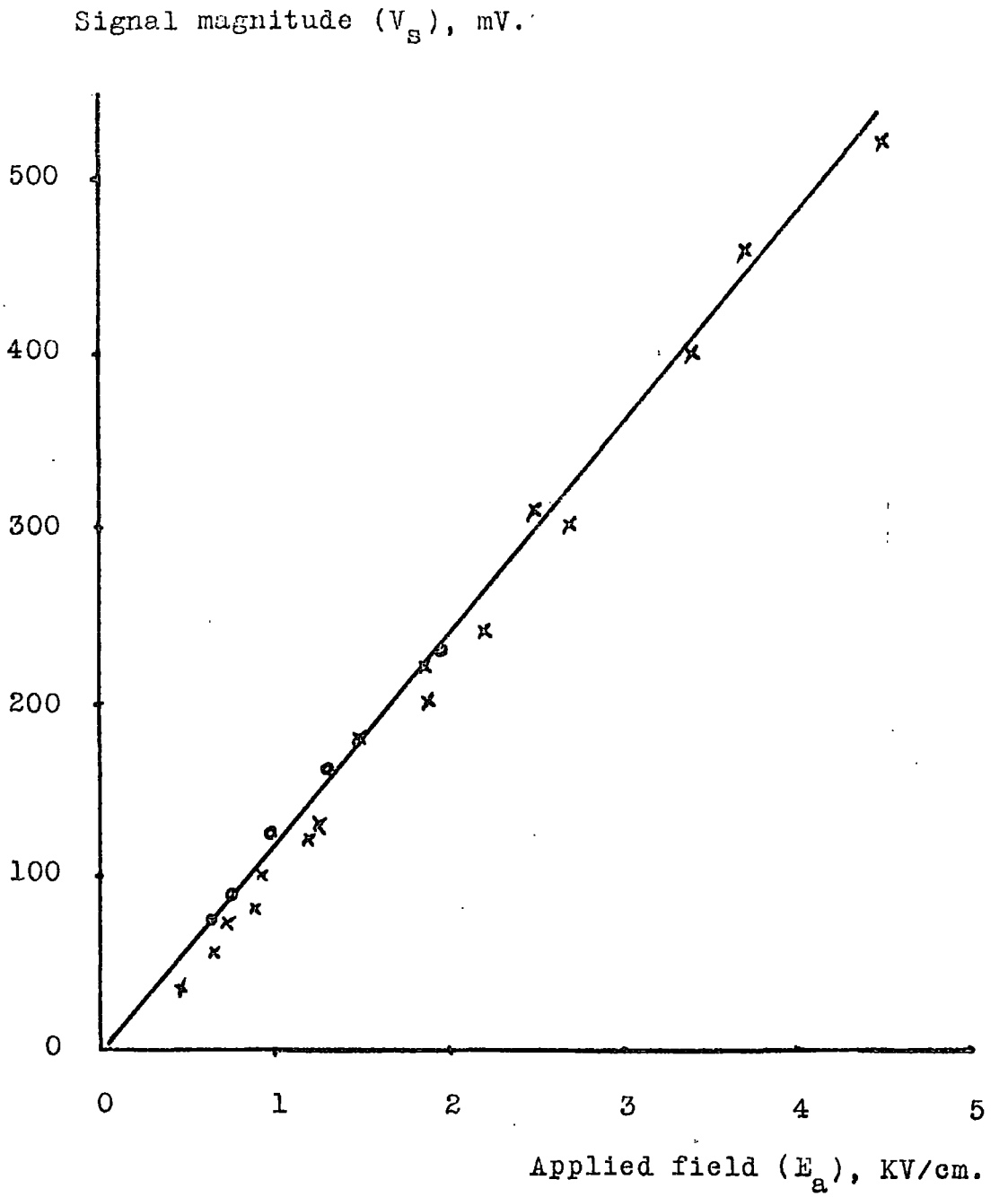

Figure (4.11). Variation of signal magnitude with applied field for cell 'B'.

Electrode separations: 0·46 cm. (o) and 0·67 cm. (×).

(4.8) shows the detailed construction of the evaporating electrode and the general features of the test-cell.

The anode was suspended, through a flexible vacuum seal, from a micrometer-driven carriage. The supporting rod (A) also served to carry the heating current to the filament (B). The filament circuit was completed by moving the anode away from the cathode until contact was made between the insulated terminal (C) and the tungsten rod (D). The flash-tube was positioned behind and below the anode, as indicated in the diagram, with its axis perpendicular to a line joining the electrode centres. In order to reduce injection from the edges of the cathode (a possible cause of trace-curvature), a mask (E) was placed on the silica disc in what was judged to be the correct position, and the flash-tube position adjusted slightly until the maximum signal was obtained.

4.2.1. Test-cell characteristics

A direct comparison of the transient-shape in this cell with that of cell 'A' was obtained by setting the electrode separation to 0.67 cm. Figure (4.9) shows the two transients, for V_a = 1.5 KV., plotted on the same time-scale with the signal magnitude normalized to unity. A considerable difference in shape is immediately apparent, the most noticeable feature being the linearity of the initial portion of the cell 'B' transient. This linearity was present to a lesser degree in the cell 'A' transient.

A certain amount of curvature was still present in the cell 'B' transient, however, rendering difficult the determination of transit-time

by inspection. A characteristic parameter of the transient was defined by extrapolation of the linear portion and of the line $V_s = V_s(\text{max.})$, as shown in figure (4.9b). The value of t determined by the intercept of these two lines is referred to subsequently as τ_i. Figure (4.10) shows the variation of $1/\tau_i$ with applied voltage for electrode separations of 0.67 cm. and 0.46 cm. The values of mobility calculated from the gradients of these straight lines were $(1.1 \pm 0.1).10^{-3}$ cm.^{2}/V.sec., and $(1.2 \pm 0.1).10^{-3}$ cm.^{2}/V.sec., in close agreement with the results of LeBlanc (2).

The signal magnitude obtained with this cell was some five times greater than that observed, with the same electrode separation, in cell 'A'. This was attributed to the increased electrode area and the reduced distance between the flash-source and the electrode surface. The ratio of forward to reverse voltage with the cathode illuminated was determined as $v_f/v_r = 9.3$, for $V_a = 3$ KV., and d = 0.67 cm. This was slightly greater than that for cell 'A' and places a lower limit on the injection/ionization ratio, u_f/w, of 8.3.

Figure (4.11) shows the signal magnitude V_s plotted against applied field E_a (= Va/d), for d = 0.67 cm. and 0.46 cm. The graph may be represented by a single straight line, indicating direct proportionality between the two quantities. Since V_s is related to the injected charge ne by:

$$V_s = ne/C \qquad (15, \text{Ch.}2)$$

where C is the measuring capacitor, we have the relation:

$$ne = A.V_a/d \qquad (5)$$

where A is a constant, depending on certain characteristics of the photo-cathode and the light-source.

4.2.2. Conclusions

Inspite of the attempt to restrict photo-injection to the centre of the cathode, it was considered possible that a major contribution to the curvature of the trace was due to long-path transits in the fringe-field of the electrodes. The basic difficulty in the use of collimating masks to counteract this phenomenon stemmed from the oblique incidence of the light on the cathode, and the necessity for movement of the anode. For small electrode separations in particular, the positioning of the mask became critical and had to be carefully re-adjusted for each new value of d.

In order to eliminate the contribution of this effect, it appeared imperative to arrange for the light to fall perpendicularly on to the cathode, and to place a mask as close as possible to the cathode surface. Under these conditions, any residual curvature of the trace could confidently be ascribed to some property of the conduction mechanism itself.

4.3. CELL 'C'

The photocathode for cell 'C' consisted of a semi-transparent aluminium film, deposited on a silica disc, and illuminated from the rear.

Figure (4.12) shows the main features of the design.

The anode (A) was an aluminium disc, 15 mm. in diameter, attached to the anode support (B) by three spring-loaded screws (C) equally spaced around its circumference. The anode was set parallel to the rim of the Pyrex envelope, and the required distance from it, by adjustment of these screws. By placing a depth-micrometer across the end of the test-cell, it was possible to carry out the alignment to within 0.001". After adjustment of the anode position, the circular evaporating filament (D), carrying the pre-formed aluminium beads, was located in the support-bushes (E) so that its plane coincided with the lower surface of the anode. Before sealing the silica disc (F) onto the cell, a substrate (G) was formed on one surface to provide electrical contact between the cathode and the exterior of the cell. The substrate consisted of an opaque layer of evaporated aluminium, covering the face of the disc except for a 10 mm. diameter area in the centre.

The semi-transparent cathode was formed, as usual, immediately before filling the evacuated cell with de-gassed hexane. The filament current source was connected to the tungsten rods (H). The change in transmission of the central area of the disc was observed closely during the formation of the film, the filament current being switched off just before the required degree of opacity was obtained. Although an optimum film-thickness must exist, it was found that an easily detectable signal could be produced so long as the film was

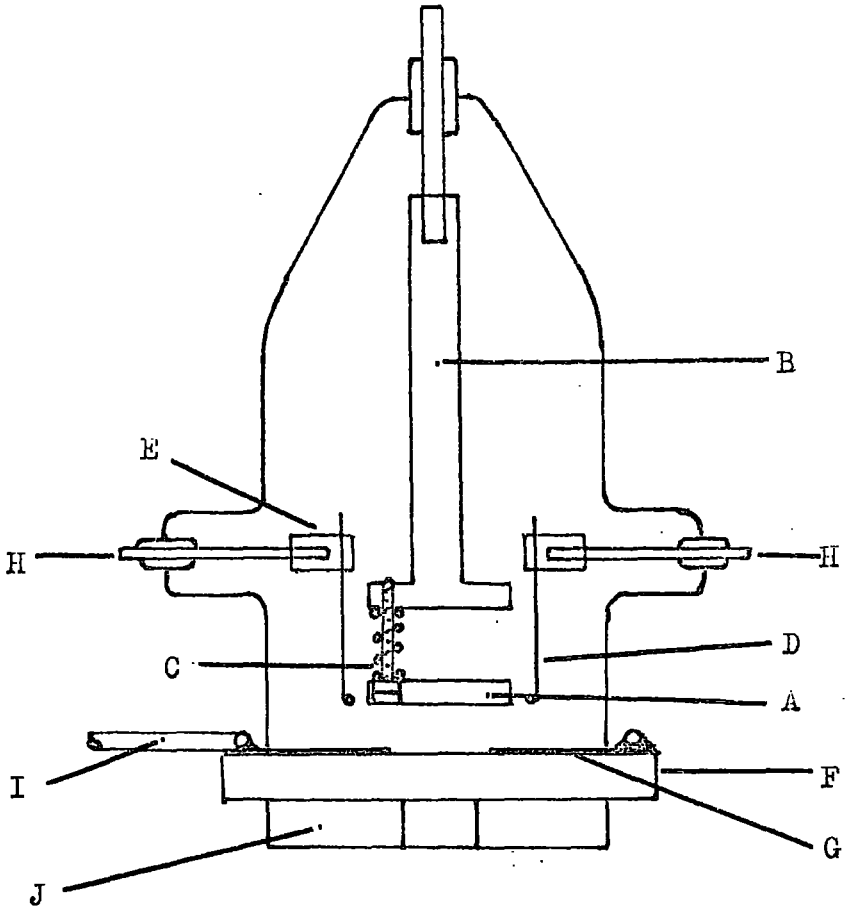

Figure (4.12). Main features of cell 'C'.

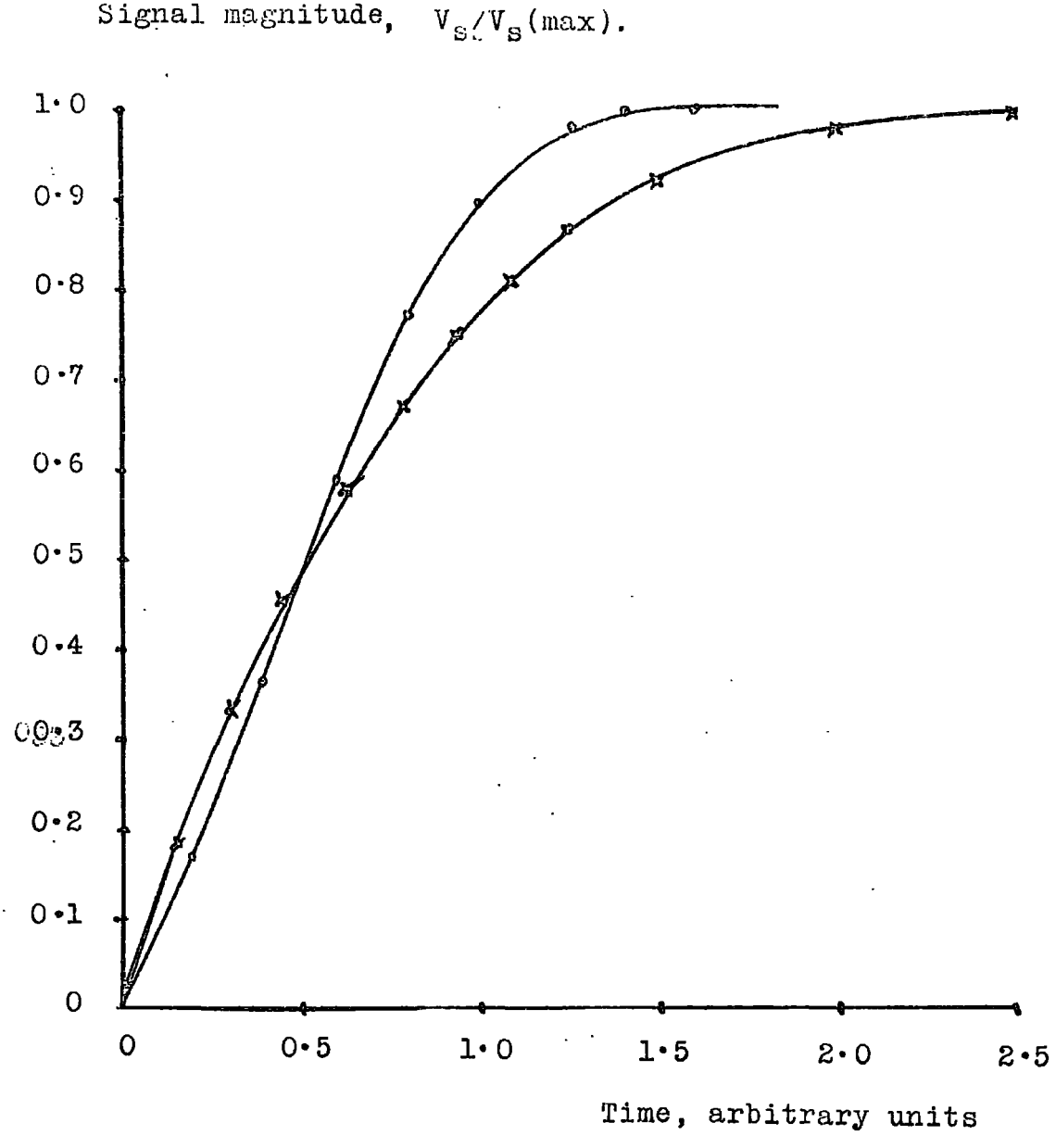

Figure (4.13). Comparison of transient shapes obtained with cell 'B' (✕) and cell 'C' (●).

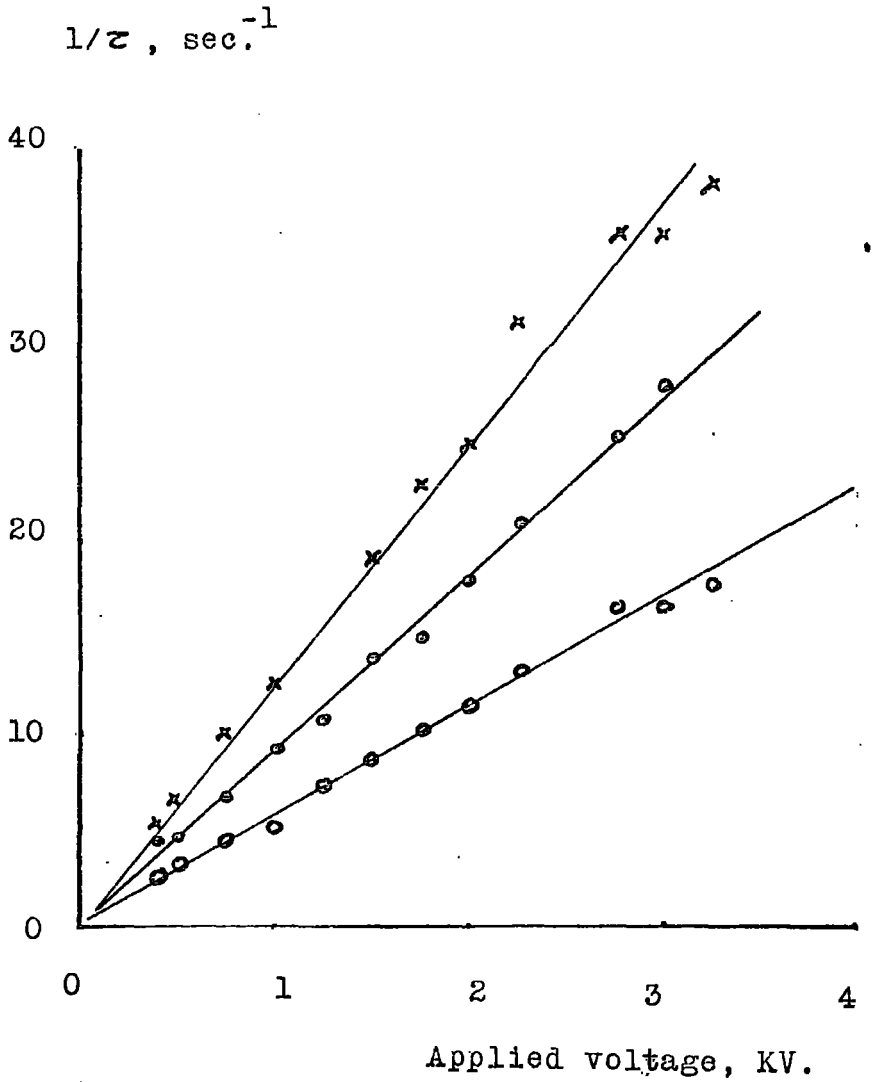

Figure (4.14). Variation of the three transit-times τ_l (×), τ_i (⊙) and τ_m (○) with applied voltage, for cell 'C'.

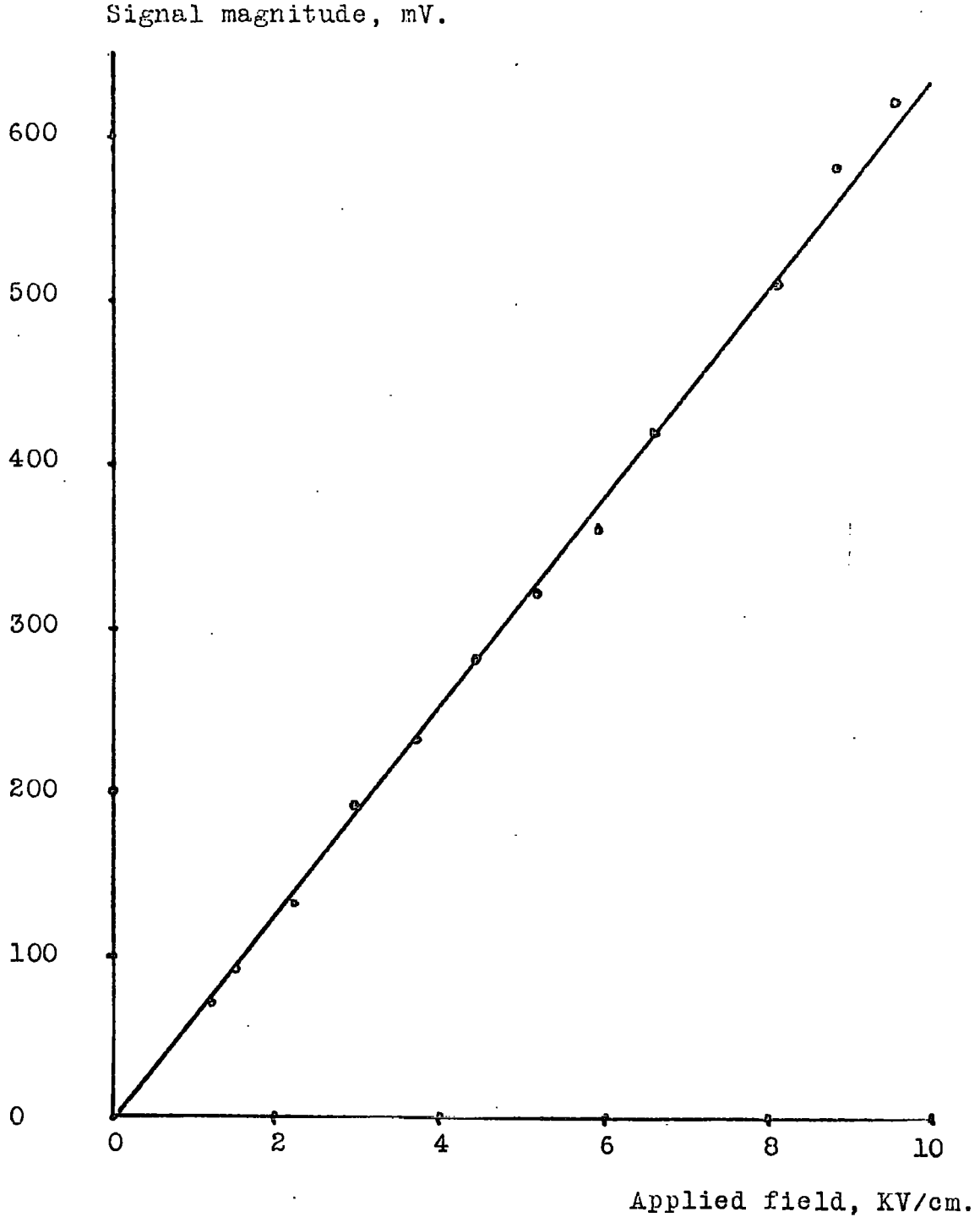

Figure (4.15). Variation of signal magnitude with applied field, for cell 'C'.

approximately semi-transparent in appearance, thus obviating the need for self-regulating control of the evaporation process.

Final additions to the test-cell were the attachment of the high-voltage lead (I) to the aluminium substrate, using a silver-suspension to ensure good contact; and the fixing of a mask (J) to the lower surface of the silica disc. The mask aperature was circular, and 6.3 mm. in diameter.

4.3.1. Test-cell characteristics

Figure (4.13) compares the shape of the transient with that observed using cell 'B'. Since the electrode separations were different in each case (0.27 cm. and 0.67 cm. respectively), the comparison is made for a comparable values of applied field (3 KV/cm. and 2.2 KV/cm. respectively) and the time-scale was plotted in terms of τ_i for each transient. In addition, the signal magnitude was normalized to unity. The further improvement in the linearity of the initial part of the transient was ascribed to the elimination of long-path transits, combined with an increase in the injection/ionization ratio. The reasons for the remaining curvature of the trace have direct bearing on the interpretation of transit-time measurements and the nature of the conduction mechanism, and will therefore be discussed in Chapter 6.

For the purposes of this preliminary investigation, however, the parameter τ_i, defined in section 4.2.1., was measured as a function of applied voltage. A mobility value of $(0.7 \pm 0.1).10^{-3}$ cm./V.sec. was

obtained from the graph of $1/\tau_i$ versus V_a . The fixed relationship of τ_i to other features of the transient was established by plotting the time to maximum height (τ_m) and the duration of the linear initial portion (τ_l) of the trace against applied voltage, in the same way. Figure (4.14) demonstrates that a good straight line plot was obtained in each case, yielding the three mobility values:

$$\mu_l = 1.0.10^{-3} \text{ cm}^2/\text{V.sec.}$$

$$\mu_i = 0.7.10^{-3} \text{ cm}^2/\text{Vsec.}$$

$$\mu_m = 0.5.10^{-3} \text{ cm}^2/\text{V.sec.}$$

The signal magnitude V_s was lower than that obtained from cell 'B' using the same applied field and measuring capacitor. This reduction by a factor of approximately 2 was due to the much smaller effective cathode area. Figure (4.15) shows the linear variation of V_s with applied field E_a between 0.9 KV./cm. and 9.5 KV./cm. The ratio v_f/v_r at 5 KV./cm. was 25, representing a considerable improvement over the previous test-cell.

4.3.2. Conclusions

In view of the favourable characteristics described above it was decided to construct a version of cell 'C' which would allow the continuous variation of the electrode separation. This facility would enable mobility measurements to be made over a wide range of electric fields, and would also permit the verification of equations (4)

and (5), relating transit-time and signal magnitude respectively, to field strength and electrode separation.

4.4. REFERENCES

1. Pugh, D.R.; Ph.D. Thesis, Durham University (1968)

2. LeBlanc, O.H.: J. Chem. Phys. 30, 6, 1443-1447 (1959)

3. Chong, P., and Inuishi, Y., J. Phys Soc Japan, 16, 1482. (1961)

4. Terlecki, J., Nature, 194, 4824, 172-3 (1962)

CHAPTER 5

MEASUREMENTS OF TRANSIT-TIME AND SIGNAL-MAGNITUDE

The preliminary measurements described in Chapter 4 established the basic design of a test-cell which introduced minimum distortion to the current transient. The test-cell, cell 'C', incorporated a semi-transparent aluminium cathode and was shown to be capable of providing a large signal, associated with a high ratio of forward to reverse current. In order to extend the preliminary measurements to a wider range of applied field and electrode separation, a variable gap version of cell 'C' was constructed. The basic features of this cell, referred subsequently as cell 'D1', are described in section 5.1.

Premature breakdown of cell 'D1' required the use of a surface oxide-layer on the cathode to withstand applied fields greater than 20KV/cm. The nature of the premature breakdown and the reasons for employing an oxidized cathode are discussed in section 5.3. In view of this development, the measurements of transit-time and signal magnitude are presented in sections 5.2. and 5.4., corresponding respectively to the use of (a) a non-oxidized cathode up to 20KV/cm., and (b) an oxidized cathode up to 140KV/cm. The modifications to the basic design required by the use of fields in excess of 20KV/cm are described in sub-section 5.4.2. The modified test-cell is referred to subsequently as cell 'D2'.

5.1. THE VARIABLE-GAP TEST-CELL (CELL 'D1')

Figure 5.1. shows the basic features of cell 'D1' in plan and elevation. Details of the electrode structure and the evaporating filament were identical with those of cell 'C' and are therefore omitted from this diagram for the sake of clarity. The extendable anode support (A), driven by a high-precision micro-meter screw (B), was mounted on the upper flange (C) of the vacuum connection. The Pyrex envelope (D) carrying the evaporation filament and the semi-transparent cathode was joined to the lower vacuum flange (E) by means of a Pyrex/copper feather-edge seal (F). Since the anode was electrically connected to the vacuum flanges and to the micrometer head, these components were insulated from the earthed supporting frame by means of four P.T.F.E. rods (G). In the absence of such insulation, the measuring resistor (R_m) would have been short-circuited. The entire test-cell was carefully screened from interference sources and capacitative charging by means of 16 gauge duralumin sheet attached to the supporting frame (H). The impedance-matching stage (I) was bolted to the screening cage and a direct connection made between the grid of the electrometer valve (J) and the anode support.

Figure (5.2) shows the construction of the extendable anode support, based on a design used by Morant (1) and Kahan (2). The anode levelling device (a) was identical to that described in section 4.3 and was joined to the brass tube (b) by the flexible brass bellows (c). Movement of the micrometer shaft (d) was transmitted to the anode by the steel rod (e),

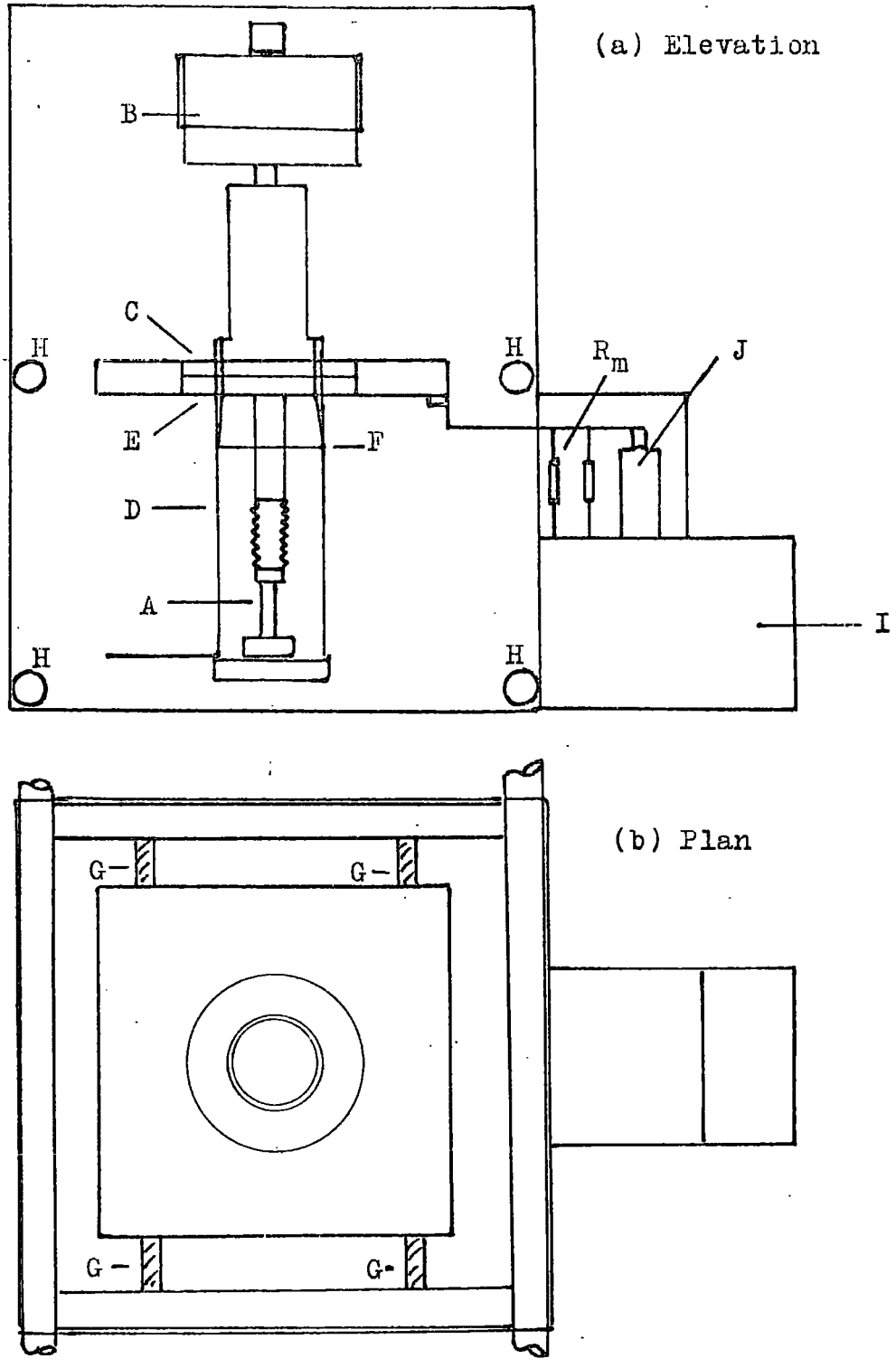

Figure (5.1). Basic features of cell 'D1'.

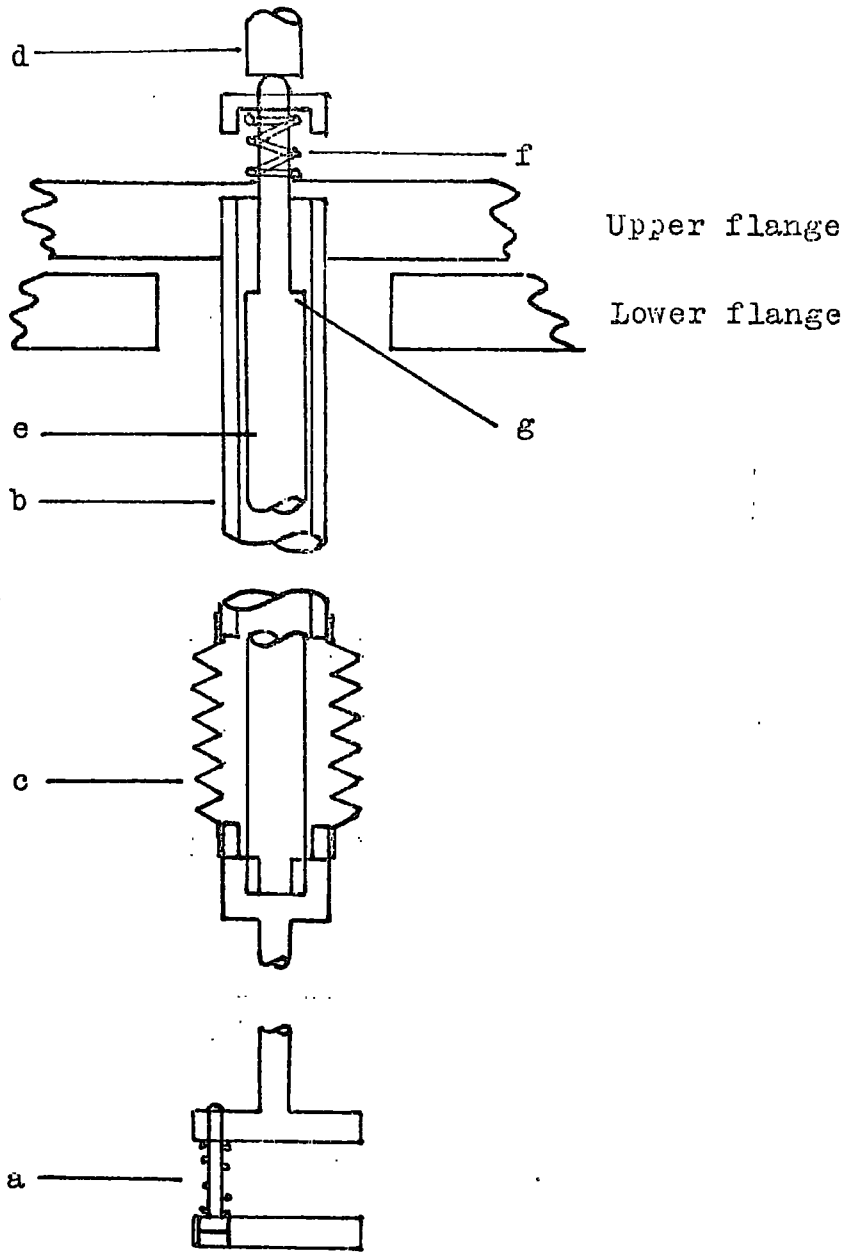

Figure (5.2). The extendable anode support of cell 'D1'.

causing extension or contraction of the bellows. The force due to atmospheric pressure, tending to extend the bellows, was balanced by a spring (f), the solid length of which was such as to prevent their extension beyond the elastic limit. The shoulder (g) on the rod served to prevent irreversible collapse of the bellows when the test-cell was not evacuated.

The alignment of the anode and cathode over the length of travel of the extendable anode support was checked by the method described in section 4.3. The anode was found to be parallel to the rim of the envelope to within 0.001 inch for all electrode separations.

5.2. THE NON-OXIDIZED CATHODE

The following measurements of transit-time and signal magnitude were obtained using a freshly evaporated semi-transparent cathode, formed as described in section 4.3. The integrated current transients were recorded for values of applied field (E_a) between 1 KV/cm. and 20 KV/cm using nominal electrode separations (d) of 4mm, 3mm, 2mm, and 1mm. The minimum transit-time anticipated under these conditions was calculated assuming a mobility of 10^{-3} $cm^2/V.sec$. For d = 1mm and E_a = 20 KV/cm, the calculated transit-time was 5 msec., indicating that use of the 'long' flash source (Duration $\doteq$ 0.5 msec.) was permissible throughout the stated range of applied field and electrode separation.

5.2.1. Measurements of transit-time

The parameter τ_i, defined in section 4.2.1., was measured for each recorded transient. The fixed relationship between τ_i and other basic features of the transient has been demonstrated for cell 'C' (see section 4.3.1.). The possibility of a simple fixed relationship between τ_i and the true transit-time is discussed further in Chapter 6, in connection with the shape of the transient.

Figures (5.3), (5.4), (5.5) and (5.6) show the variation of $1/\tau_i$ as a function of the applied voltage V_a, for each of the four values of electrode separation. Confidence in the use of the parameter τ_i was strengthened by the excellent linearity of these graphs, which enabled accurate values of the corresponding mobility μ_i to be determined from the gradients. Table (5.1) lists the values of mobility μ_i determined from each graph, together with the range of applied field involved and the nominal and actual values of electrode separation. The errors quoted in Table (5.1) arise from two sources: the error in estimating the gradient of the graph, and the error in measuring the electrode separation. The latter contribution became increasingly important as d was reduced, resulting in a slight decrease in accuracy for the highest range of applied field.

The difference between the values of mobility for the two extreme ranges of applied field (1 - 8 KV/cm and 4 - 20 KV/cm) is not statistically significant for a probability level of less than 0.001. Furthermore, no

significant difference was found between values of apparent mobility calculated from individual transients at 1 KV/cm. and 20 KV/cm.

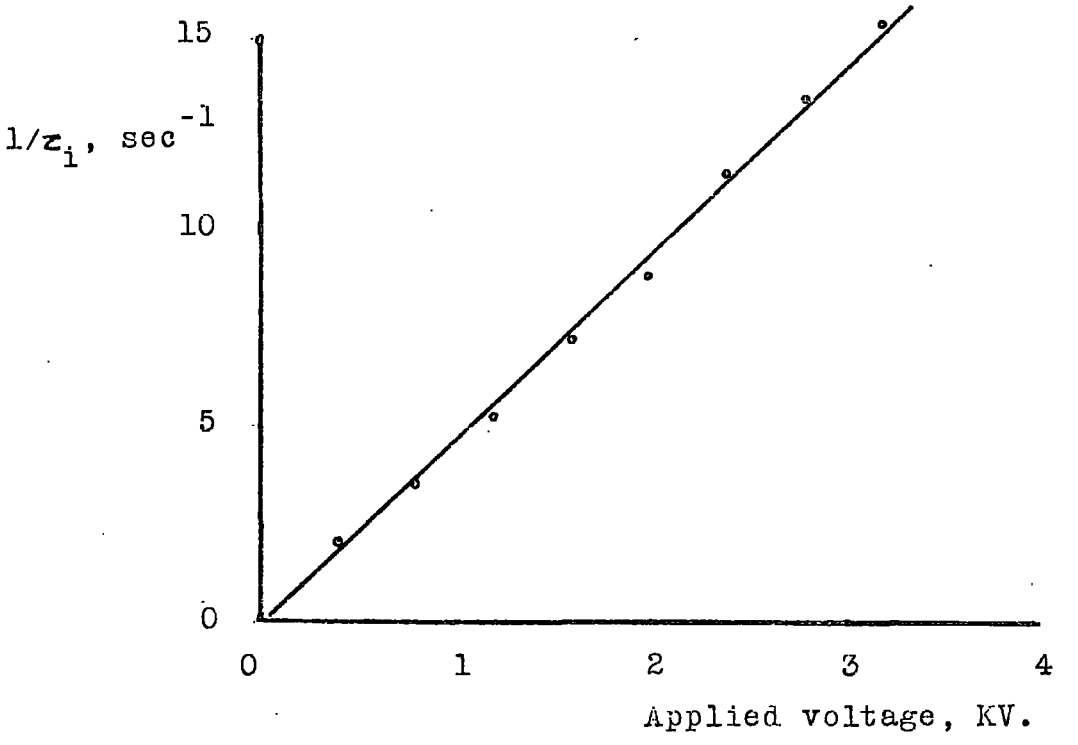

Figure (5.3). Variation of transit-time with applied voltage for cell 'D1'. Nominal electrode separation, 4 mm.

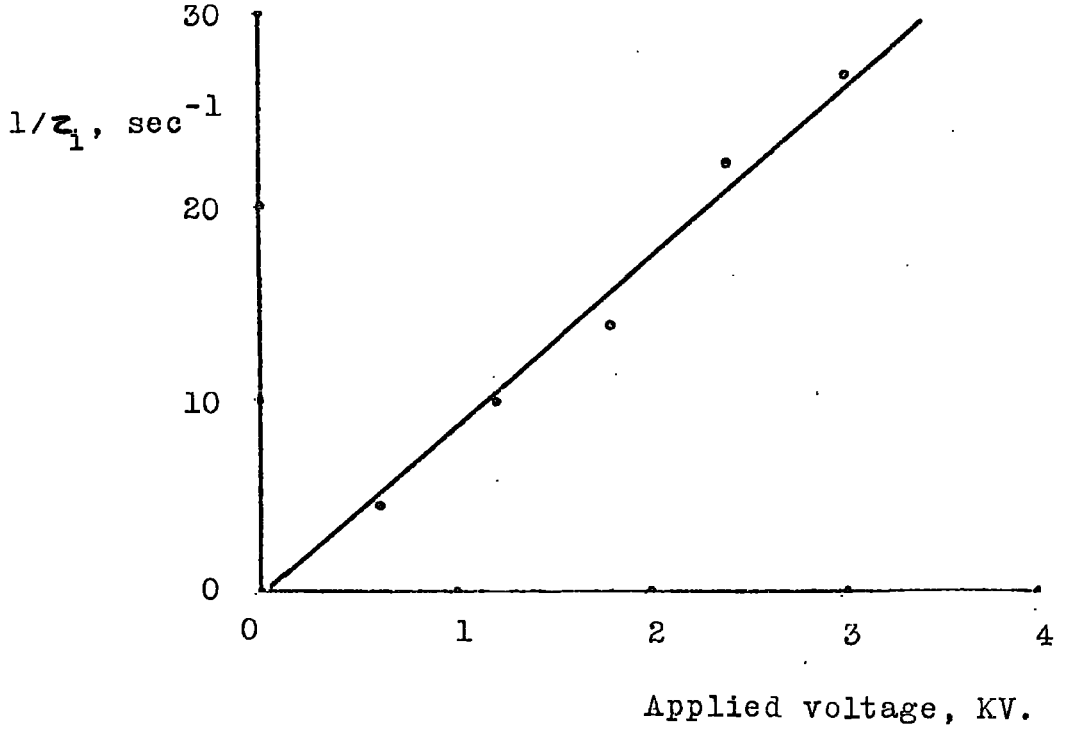

Figure (5.4). Variation of transit-time with applied voltage for cell 'D1'. Nominal electrode separation, 3 mm.

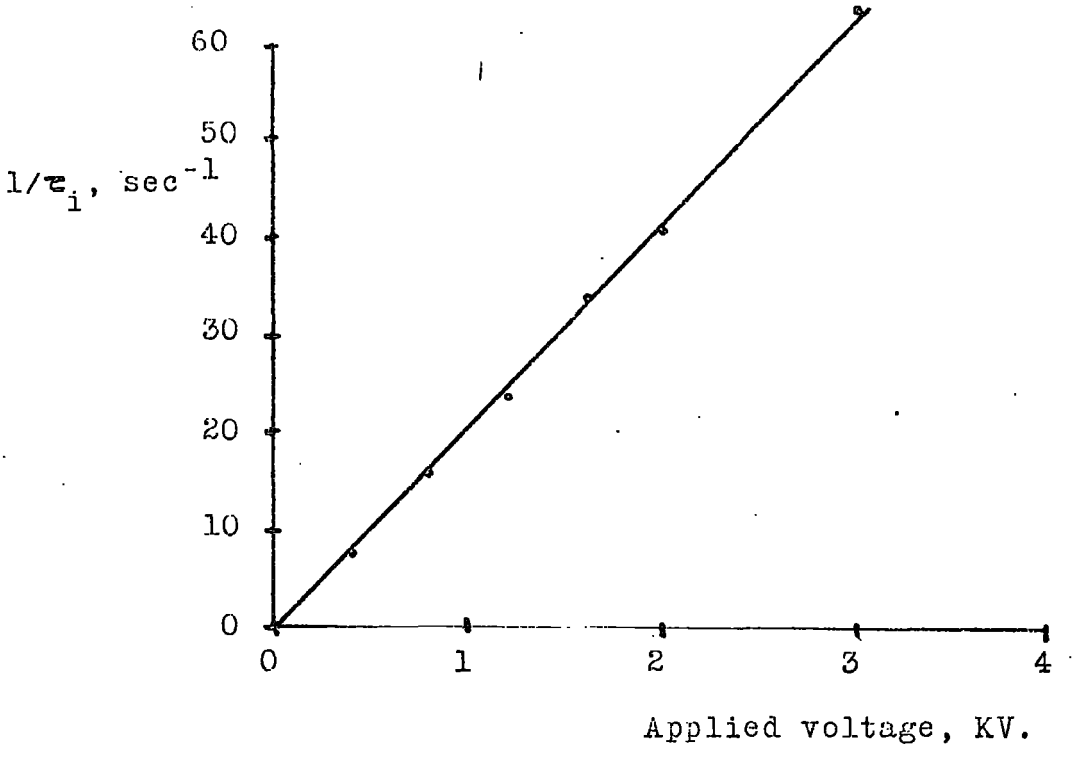

Figure, (5.5). Variation of transit-time with applied voltage for cell 'D1'. Nominal electrode separation, 2 mm.

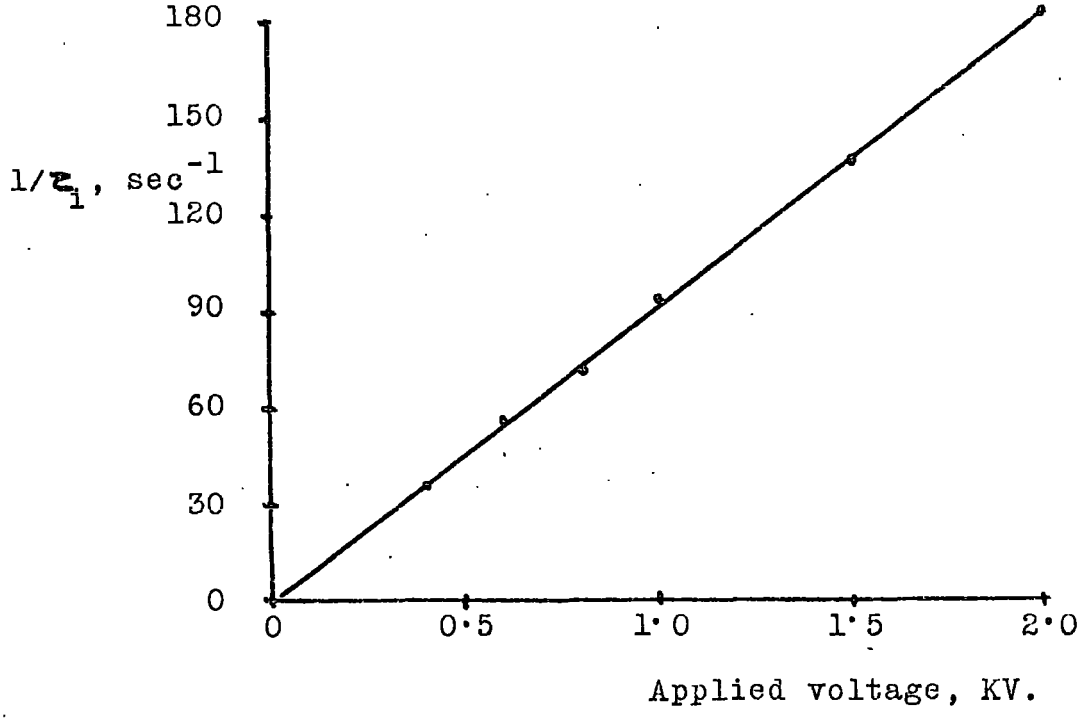

Figure (5.6). Variation of transit-time with applied voltage for cell 'D1'. Nominal electrode separation, 1 mm.

Figure	Electrode separation Nominal . (Actual)	Range of applied field, KV/cm.	Apparent mobility, μ_i, $cm.^2/V.sec. \times 10^3$
5.3.	4 mm. (3·96 ± 0·03)	1 - 8	(0·74 ± 0·02).
5.4.	3 mm. (2·96 ± 0·03)	1 - 10	(0·75 ± 0·02).
5.5.	2 mm. (1·95 ± 0·03)	2 - 15	(0·77 ± 0·02).
5.6.	1 mm. (0·92 ± 0·03)	4 - 20	(0·77 ± 0·03).

Table (5.1). Values of mobility, μ_i, determined using cell 'D1'.

5.2.2. Measurements of signal magnitude

The variation of signal magnitude with applied field was determined for each of the four selected values of electrode separation. The amplitude V_s of each recorded transient was measured, and the values plotted against applied field, as shown in figures (5.7), (5.8), (5.9) and (5.10). These graphs were used to verify the relationship, postulated in section 4.2.1., between the injected charge, ne, and the applied field E_a:

$$ne = A.E_a \quad \ldots\ldots\ldots\ldots\ldots\ldots\ldots \quad (5, \text{Ch.}4)$$

The measured signal V_s is given by:

$$V_s = G.ne/C \quad \ldots\ldots\ldots\ldots\ldots\ldots\ldots \quad (1)$$

where G is the gain of the impedance-matching stage, and

C is the measuring capacitance.

Thus;

$$V_s = A.G.E_a/C \quad \ldots\ldots\ldots\ldots\ldots\ldots\ldots \quad (2)$$

and the gradient, g_s, of figures (5.7) - (5.10) is constant and equal to A.G./C if equation (5, Ch.4) is valid.

Table (5.2) lists the values of g_s determined experimentally, together with the range of applied field involved and the nominal electrode separation in each case. The increased scatter in g_s at higher fields and lower values of d was due mainly to slow random variations in the

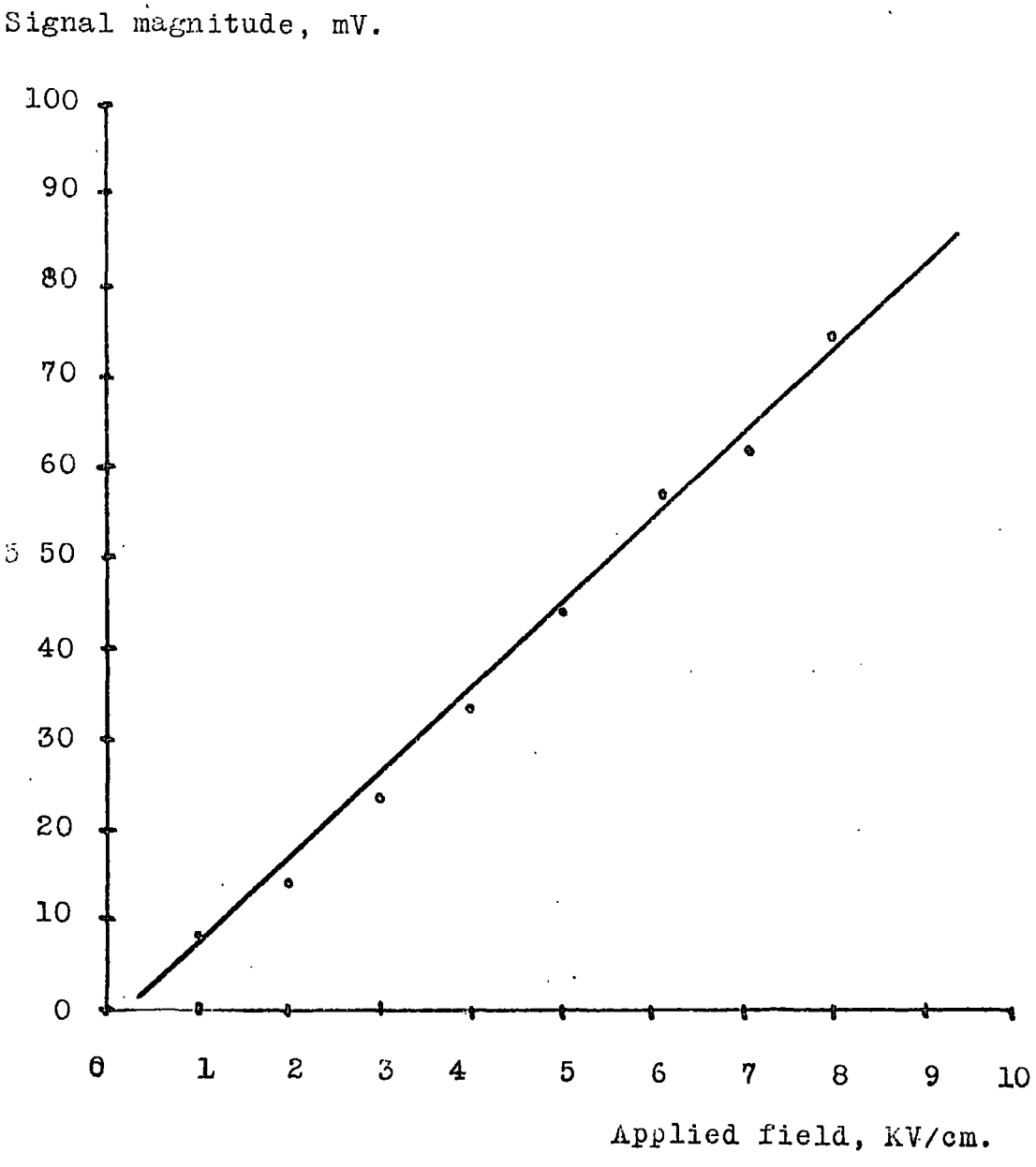

Figure (5.7). Variation of signal magnitude with applied field, for cell 'D1'. Nominal electrode separation, 4 mm.

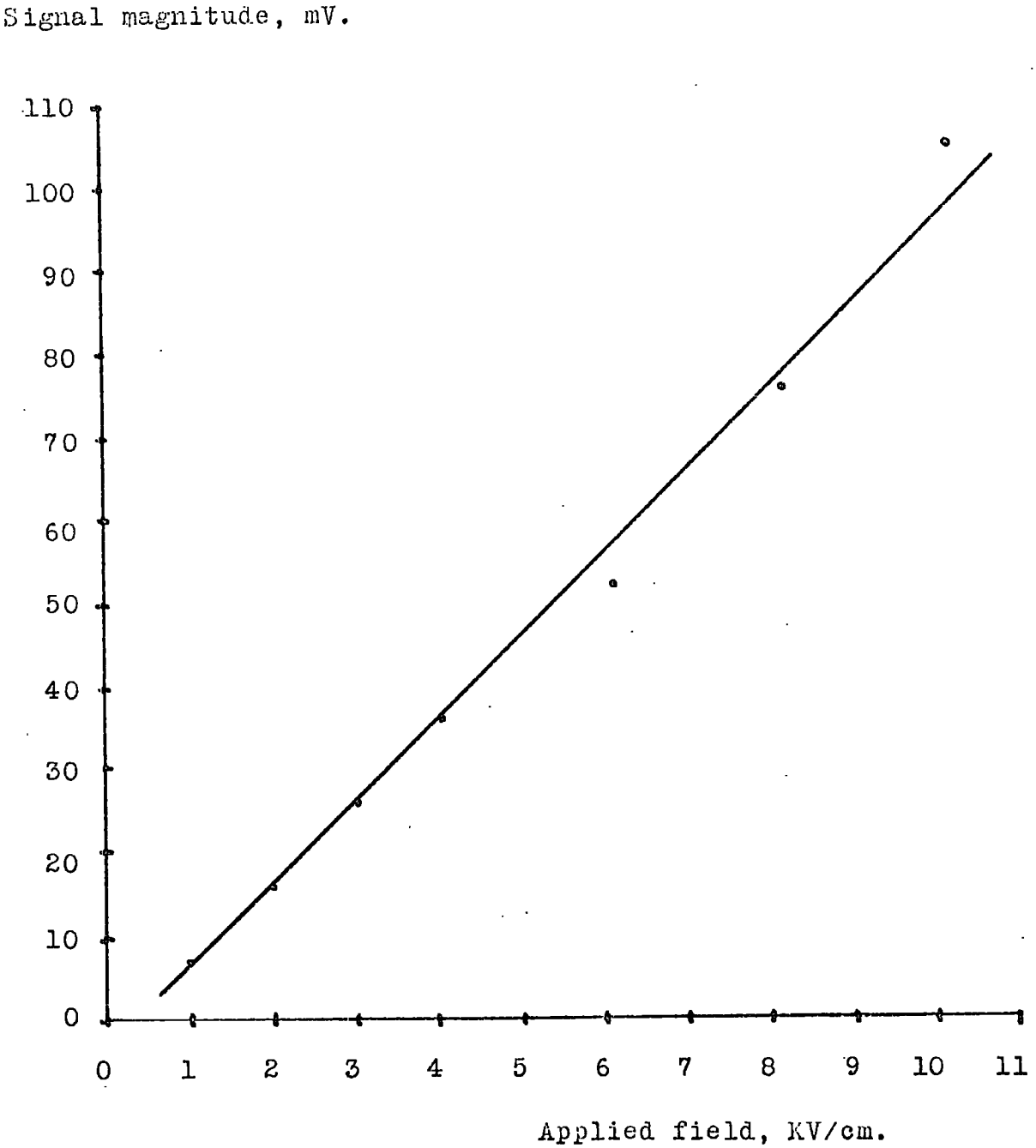

Figure (5.8). Variation of signal magnitude with applied field, for cell 'D1'. Nominal electrode separation, 3 mm.

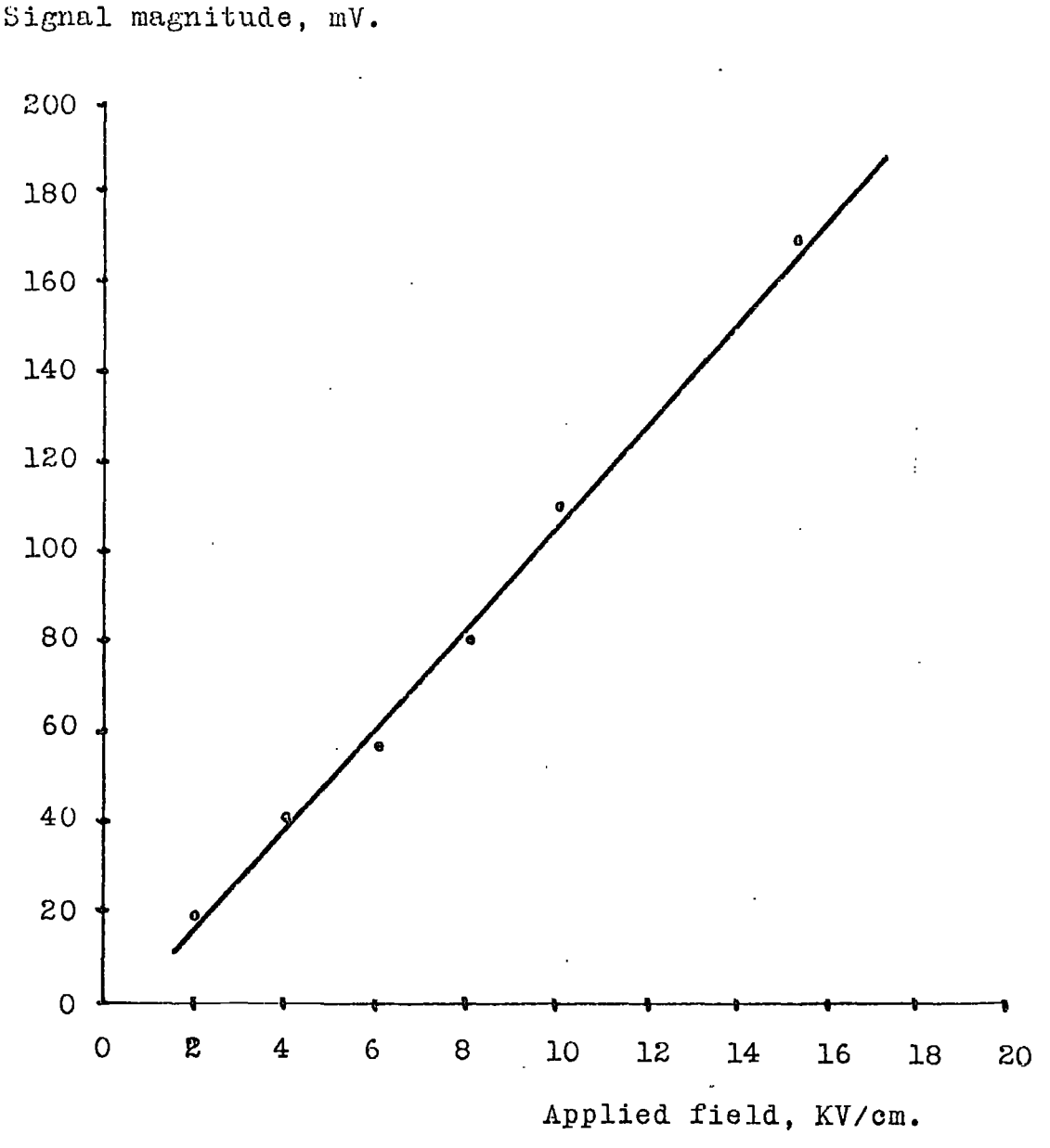

Figure (5.9). Variation of signal magnitude with applied field, for cell 'D1'. Nominal electrode separation, 2 mm.

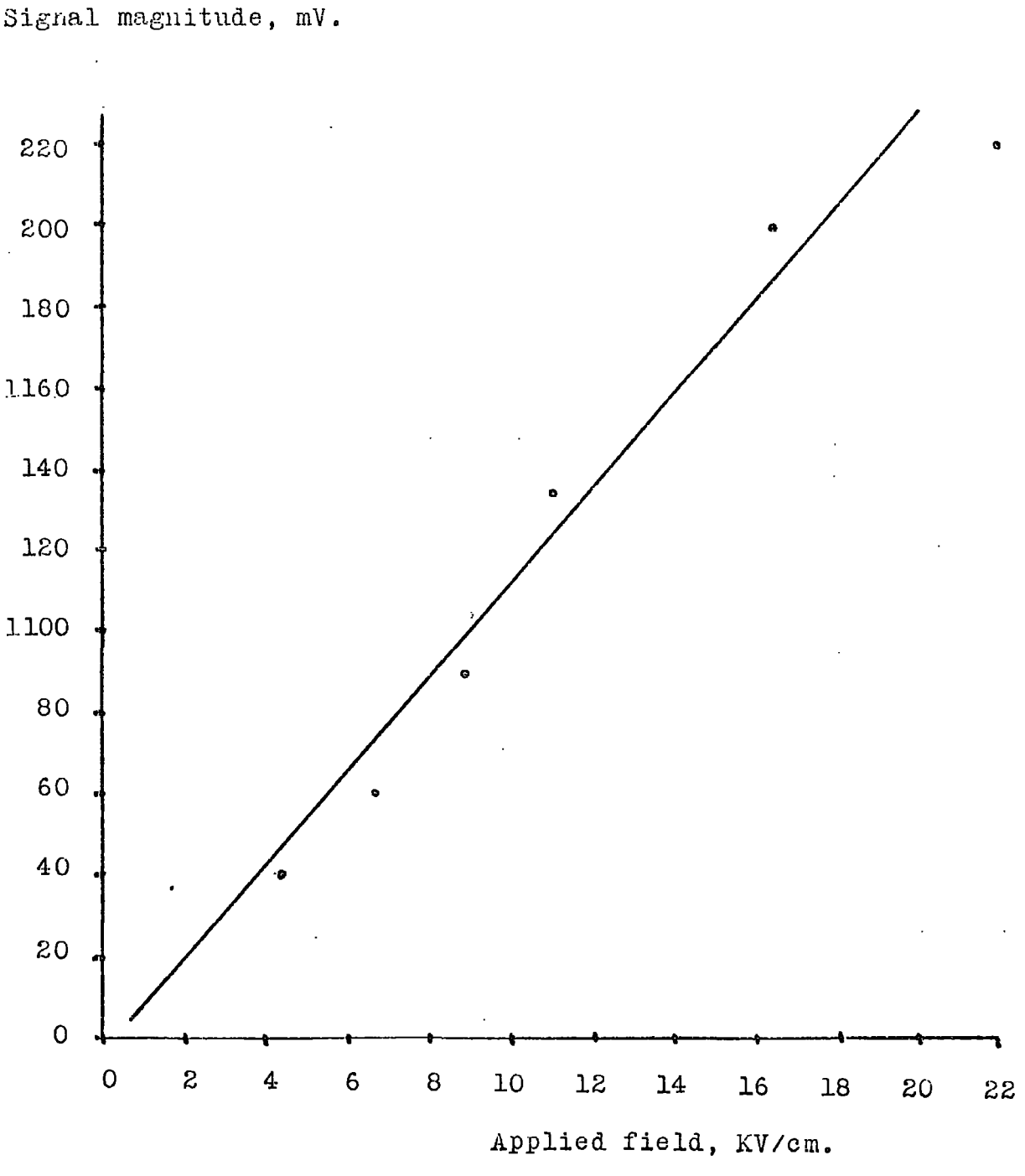

Figure (5.10). Variation of signal magnitude with applied field, for cell 'D1'. Nominal electrode separation, 1 mm.

Figure	Electrode separation (nominal)	Range of applied field, KV/cm.	Gradient, cm.
5.7.	4 mm.	1 - 8	$(8{\cdot}2 \pm 0{\cdot}3).10^{-6}$
5.8.	3 mm.	1 - 10	$(8{\cdot}6 \pm 0{\cdot}4).10^{-6}$
5.9.	2 mm.	2 - 15	$(9{\cdot}9 \pm 0{\cdot}5).10^{-6}$
5.10.	1 mm.	4 - 20	$(10{\cdot}5 \pm 0{\cdot}6).10^{-6}$

Table (5.2). The gradients of figures (5.7) - (5.10) inclusive.

D.C. level of the detection circuit. These variations occurred for applied fields of the order of or greater than 10 KV/cm and resulted in poor reproducibility of the high-field points on each graph. The apparent increase in gradient for decreasing values of electrode separation was found not to be statistically significant, particularly in view of the variation in scatter.

The postulated proportionality of injected charge to applied field was thus shown to be valid, within the limits of experimental error, over the stated range of values of applied field. The value of the constant of proportionality, A, was calculated from the expression:

$$g_s = A.G./C \quad \ldots\ldots\ldots\ldots\ldots\ldots\ldots\ldots \quad (3)$$

The values of G and C were taken as 0.92 (see section 3.3.2) and 1000 pF respectively, yielding the result:

$$A = (1.0 \pm 0.1).10^{-14} \text{ coul.cm./volt}$$

5.3. PREMATURE BREAKDOWN OF CELL 'D1'

5.3.1. Breakdown and pre-breakdown phenomena

The slow variation in d.c. level responsible for inaccuracies in the measurement of signal magnitude was accompanied, at field strengths greater than 10 KV/cm, by the appearance of fast, negative-going pulses. These pulses occurred singly and at irregular intervals of up to several minutes. Typical pulse activity, recorded at applied fields of 10 KV/cm

and 15 KV/cm, is shown in Figure (5.11), from which the main features of the phenomena are apparent. For a given applied field, the duration of the rising portion of the pulse (t_p) and the pulse amplitude (v_p) were both constant. On increasing the applied field, a decrease in t_p was observed, accompanied by an increase in v_p. The values of t_p measured from the recorded traces were of the order 10^{-4} sec., and the pulse amplitudes corresponded to a charge of about 10^{-12} coulomb.

A few minutes after raising the field strength from 15 KV/cm to 20 KV/cm, and recording the photo-injected transient at the latter value, breakdown was seen and heard to occur in the test-cell. Inspection of the electrode system revealed damage to the semi-transparent cathode. The silica disc was therefore carefully removed from the Pyrex envelope and the cathode examined more closely. No photograph of this particular cathode after breakdown was taken, but Figure (5.12) shows the type of effect observed. It was noted that, in addition to the damage apparently caused by the discharge itself (A), a number of small holes (B) approximately 0.1 mm in diameter had appeared in the aluminium layer directly below the anode. The number and size of these holes suggested a possible connection between cathode damage and the observed pre-breakdown pulses.

5.3.2. The connection between cathode damage and pre-breakdown pulses

A simple explanation, both of the cathode damage and the pre-breakdown pulses, is that the pulses were due to the transport of small aluminium particles between the electrodes. This hypothesis is well

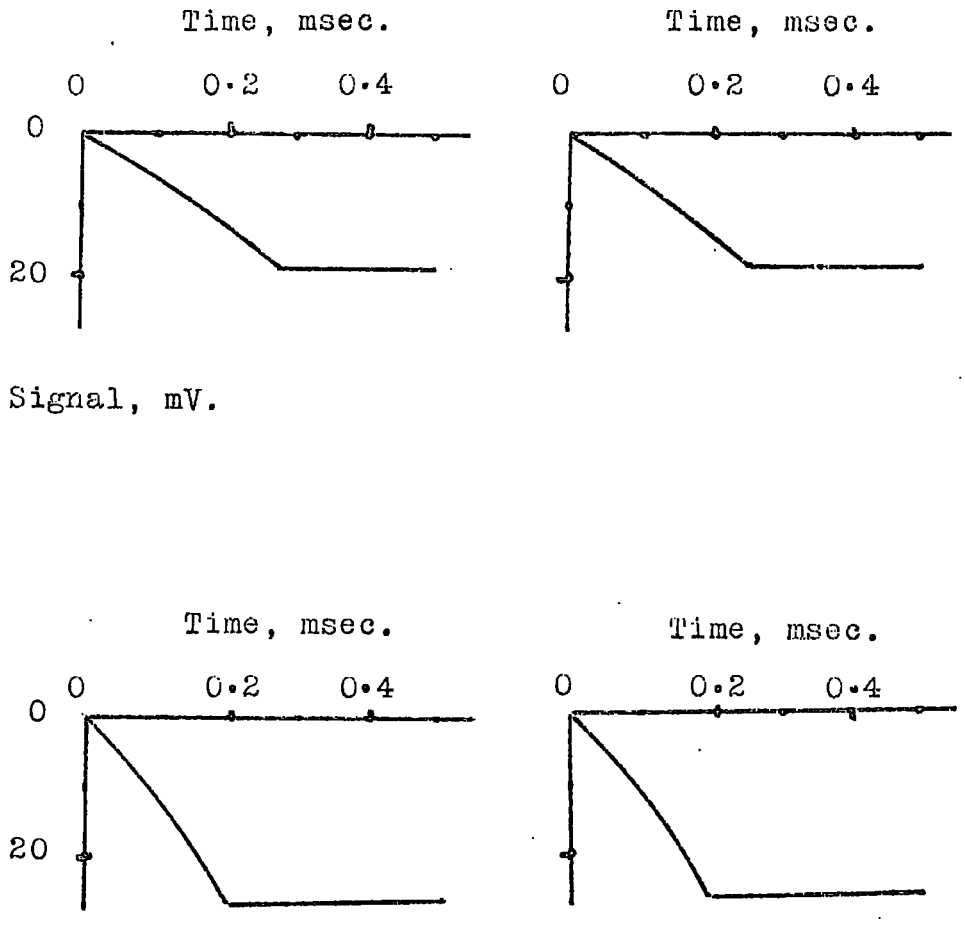

Figure (5.11). Typical pulses observed in cell 'D1'. Upper traces, 10 KV/cm.; lower traces, 15 KV/cm.

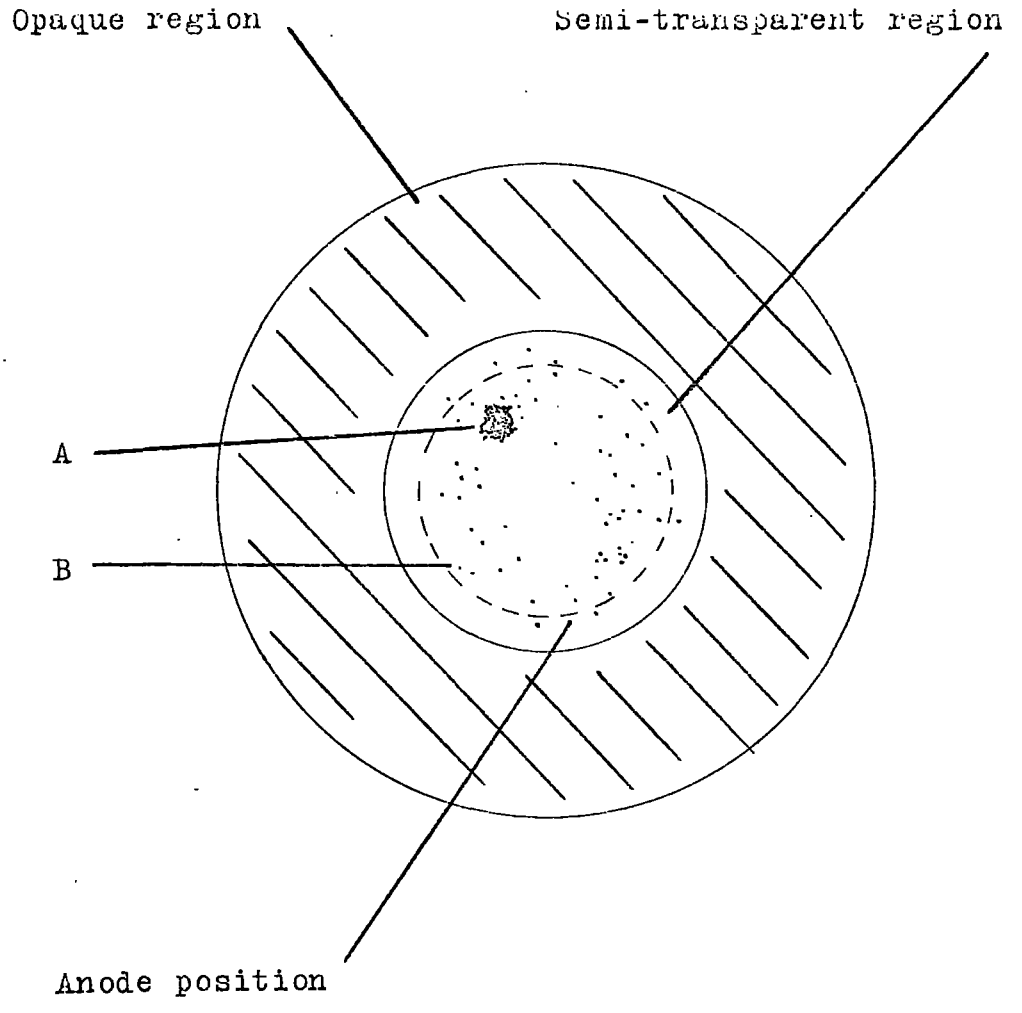

Figure (5.12). The cathode of cell 'D1' after breakdown.

supported by order-of-magnitude calculations of the size and duration of pulses produced by such a mechanism.

If it is assumed that a fragment of aluminium detached from the cathode retains the surface charge density of that electrode, then the charge, q, carried by a fragment of radius r is:

$$q = \pi r^2 \, E_a \, \kappa \varepsilon_o \qquad \ldots\ldots\ldots\ldots\ldots\ldots \quad (4)$$

where κ is the dielectric constant of n-hexane and

E_a is the applied field.

Substitution of the approximate values: $r \doteq 10^{-4}$ m.

$E_a \doteq 10^{6}$ V/m

$\kappa \varepsilon_o \doteq 10^{-11}$ F/m

gives an order-of-magnitude estimate for q of 10^{-13} coulomb, which is in reasonable agreement with the observed value of 10^{-12} coulomb.

Since the instantaneous current is proportional to the carrier velocity, the increasing gradient of the integrated pulses indicates acceleration of the carrier across the inter-electrode space. Under these circumstances the viscous forces may be ignored for the purposes of an approximate calculation of the transit-time t_p. The expression for t_p then becomes:

$$t_p \doteq (1/E_a).(2dh\rho/\kappa\varepsilon_o)^{\frac{1}{2}} \qquad \ldots\ldots\ldots\ldots\ldots\ldots \quad (5)$$

where d is the electrode separation,

h is the thickness of the aluminium film, and

ρ is the density of aluminium.

The value of h was estimated, from the observed light transmission and the published value of the optical attenuation coefficient for aluminium (3) as $\doteq 0.05$ micron. Substitution of the approximate values: d $\doteq$ 1 mm, $\rho \doteq 3.10^3$ Kg/m^3, yields the result $t_p \doteq 0.05$ msec. Bearing in mind that viscous forces have been neglected, this figure is in reasonable agreement with the observed values of $\doteq 0.\overset{2}{1}$ msec.

Further support of the hypothesis is provided by expressions (4) and (5). These correctly predict the following characteristics of the pulse activity:

(a) the general increase in signal size with applied field, for a given range of fragment radii;

(b) the decrease in transit time with increasing field;

and (c) the lack of dependence of the transit time on fragment radius.

5.3.3. The stability of the cathode

Two methods may be put forward by which the removal of aluminium from the cathode could have resulted in breakdown of the test-cell. The first of these is simply the detachment and rotation, about an axis in its plane, of a fragment of greater diameter than the electrode separation. The second method is discussed in a recent paper by Krasucki (4). This author has demonstrated that the presence of small conducting particles in a stressed dielectric liquid can result in the growth and formation of vapour bubbles, leading to premature breakdown. No attempt

was made in the present investigation to attribute the cause of breakdown to one or other of the above mechanisms, since both are basically dependent on the same factors: the stability of the cathode film and its adhesion to the silica disc.

In order to increase the breakdown strength of the test-cell, it was evidently necessary to improve the mechanical properties of the film. The usual causes of poor adhesion of evaporated layers are insufficient cleanliness of the substrate, or too high a gas pressure during evaporation (5). Since careful attention had been paid to both these factors as part of the general experimental conditions, it was considered that the film adhesion was as good as could reasonably be expected.

Reference is often made in the literature (5) to the transparent surface film of oxide which forms on vacuum- deposited aluminium exposed to the atmosphere. The protection of the metal surface from physical and chemical damage by this oxide layer is a well known phenomenon. It was considered possible, therefore, that surface oxidation of the aluminium cathode would also improve its mechanical stability and adhesion to the substrate. From measurements of forward and reverse signal magnitude in test-cells with one non-evaporated electrode (cells 'B' and 'C') it was deduced that photo-injection is possible from an oxidized aluminium surface, although the efficiency of the process is considerably less than for a non-oxidized cathode. Bearing in mind the proportionality of injected charge to applied field, it was considered that a reduction in signal due to oxidation

of the cathode could be accepted in order to extend the measurements beyond 20 KV/cm. Further, the decrease in transit-time at higher fields would allow the use of a smaller measuring capacitor, resulting in a larger signal for a given quantity of injected charge.

Section 5.4. shows that the reasoning of the previous paragraphs was substantially correct, in that the use of an oxidized aluminium cathode allowed the measurement of transit-time and injected charge for field strengths up to 140 KV/cm.

5.4. THE OXIDIZED CATHODE

5.4.1. Preliminary tests of an oxidized cathode

Preliminary tests made on an oxidized, semi-transparent cathode immersed in de-gassed n-hexane showed that, for a given field strength, the signal magnitude was approximately ten times less than that obtained from a non-oxidized cathode under the same conditions of illumination. This reduction in signal was not sufficient to prevent the accurate measurement of transit-time from the recorded transient.

It was necessary, however, to ascertain whether the observed signal was due to photo-injected charge, or to carriers formed in the bulk of the liquid. The experimental determination of the ratio of injected to ionized carriers has been discussed in section 4.1.1. For the particular case when the reverse photo-injected charge (u_r) is negligible, the expression:

$$u_f/w \doteq v_f/v_r - 1 \quad \ldots\ldots\ldots\ldots\ldots\ldots \quad (6)$$

was deduced, where u_f is the forward injection charge,

w is charge due to ionization,

and v_f , v_r are the total charge detected in the forward and reverse directions respectively. The above approximation is valid for cells 'A' and 'B', where only one electrode was directly illuminated, and also for cells 'C' and 'D1' where although both electrodes were illuminated, one electrode was considerably more photosensitive than the other. For the present cell (D2), however, equation (6) places a lower limit on u_f/w but does not provide a realistic indication of the injection-ionization ratio because of the condition:

$$u_f \sim u_r \sim w \qquad \ldots\ldots\ldots\ldots\ldots\ldots\ldots (7)$$

In order to determine the ratio u_f/w more accurately, the ratio $u_f/u_r = p$ must be known, whence:

$$\begin{aligned} w &= (p.v_r - v_f)/(p - 1) \\ u_f &= v_f - w \end{aligned} \qquad \ldots\ldots\ldots\ldots\ldots (8)$$

A value for p was obtained by comparing the forward and reverse photo-injected signals in the evacuated test-cell at saturation. The value of p so determined was 3.8 and the corresponding values of v_f and v_r in the same cell filled with hexane were 75 mV and 30 mV respectively. The latter measurements were made at an applied field of 10 KV/cm, using a 100 pF measuring capacitor. Substitution of these values of p, v_f, and v_r in equation (8) yielded the following result:

u_f = 61 mV ; w = 14 mV ; u_r = 16 mV.

The ratio of u_f to w in the oxidized-cathode cell was thus considerably lower than for cell 'C', in which u_f/w was $\doteq$ 20 at 5 KV/cm. However, the major portion of the signal from the oxidized cathode was evidently due to photo-injection, and no increase was detected in the curvature of the transient. The use of the cathode at fields in excess of 20 KV/cm was expected to improve the value of u_f/w, provided that the proportionality of injected charge to applied field were maintained.

In view of the favourable results of these preliminary tests, the following experimental programme was adopted:

i) determine the dependence of injected charge on applied field for field strengths greater than 10 KV/cm and ascertain the breakdown voltage of an oxidized cathode cell with a fixed electrode separation;

ii) using a second cell of the same basic design, measure transit-time and signal magnitude for several values of electrode separation and for applied fields up to breakdown.

The two stages of the programme are described in sections 5.4.3. and 5.4.4. respectively.

5.4.2. Modifications to cell 'D1'.

The use of applied fields greater than 20 KV/cm in conjunction with an oxidized cathode required certain minor modifications to cell 'D1' (described in section 5.1.). The modified test-cell is referred to subsequently as cell 'D2' and the changes in design are listed below:

i) The anode. In order to reduce the possibility of breakdown outside the active cathode area, the anode was fitted with an aluminium cap to increase the edge-radius, as shown in figure (5.13). The cap was screwed onto the anode after aligning the latter as described in section 4.3. The rim (A) was machined parallel to the face of the cap and the dimension (B) was known accurately. As a further check, however, the alignment and electrode separation were re-measured after the addition of the cap. The hole (C) allowed the rapid escape of air from the volume between anode and cap, on evacuating the cell.

ii) The cathode. The opaque aluminium substrate was extended to cover the rim of the silica disc. This was achieved by the use of a circular evaporating filament of a larger diameter than the disc, situated as shown in figure (5.14). The semi-transparent cathode film was formed, before mounting the silica disc on the test-cell, in the same vacuum coating unit as the substrate. The evaporating filament was U-shaped and placed about 5 cm above the centre of the disc. After the anode had been aligned with the rim of the Pyrex envelope, the cathode was mounted on the latter, using an epoxy resin. The resin was cured at 150°C for 30-40 hours which ensured the formation of an oxide layer on the aluminium.

iii) The high-voltage connection. Preliminary tests showed that for applied voltages greater than 5 KV, using the Hursant E.H.T. supply (see section 3.3.4), some corona discharge was present in the high-voltage line. The discharges were removed by careful elimination of all small radii in the E.H.T. supply itself, the smoother circuit, and

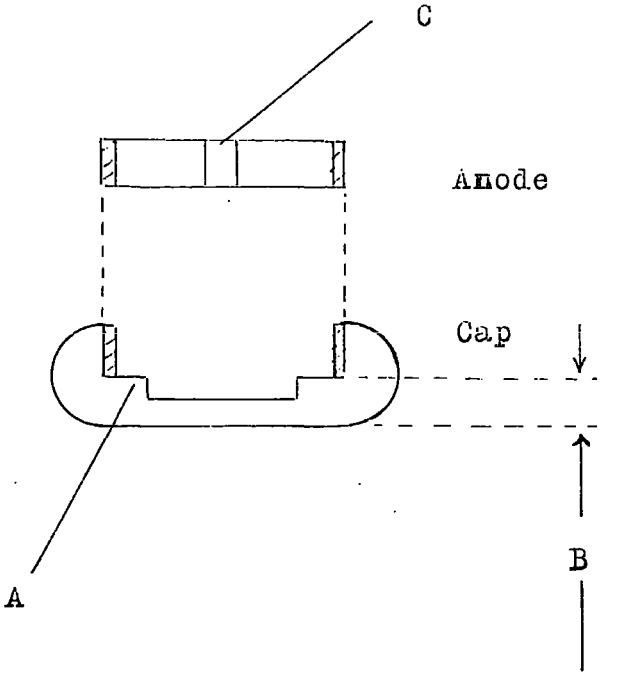

Figure (5.13). Anode and anode cap for cell 'D2'.

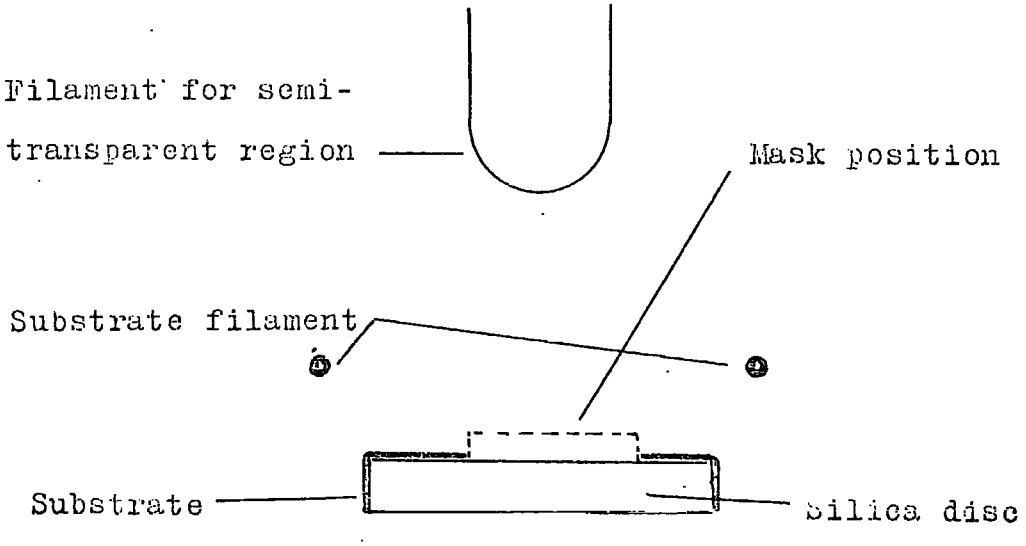

Figure (5.14). Evaporating filaments for the formation of cell 'D2' cathode.

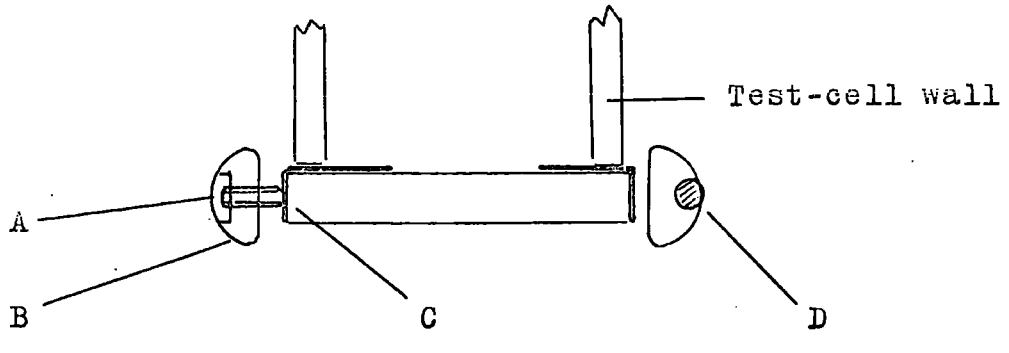

Figure (5.15). High-voltage connection to cell 'D2'.

the connections between these and the test-cell. The form of the connection to the cathode is shown in figure (5.15). Three small recessed Allen screws (A), spaced equally around the perimeter of the brass annulus (B), were adjusted to grip the aluminium layer on the rim of the silica disc (C). The centre conductor of the 100 KV co-axial cable (D) was soldered into a tangential recess in the annulus, leaving a smooth continuous surface.

iv) The Pyrex envelope. The tungsten rods, sealed through the glass, which carried the filament heating current in cell D1, were omitted. This modification decreased the fragility of the test-cell and eliminated a potential source of minor leakage which had previously been troublesome.

5.4.3. The determination of cathode sensitivity and breakdown strength.

With the cell filled with de-gassed hexane and the electrode separation set to a nominal 1 mm, the voltage applied to the cathode was raised, from an initial value of 1 KV, in steps of 1 KV. The photo-injected charge was measured at each stage, using the 'long'flash unit as the light source in order to be able to correlate the results with those already obtained for the non-oxidized cathode. Care was taken to ensure that the discharge voltage of the flash-tube was constant at 450 V for each determination of the signal magnitude.

Initially, a measuring capacitor (C_m) of 100 pF was chosen in conjunction with a measuring resistor (R_m) of $10^{10}\Omega$ and a grid-leak

resistor (R_g) of $10^9 \Omega$. The time-constant of this combination was 0.1 sec., compared with a theoretical transit-time at 1 KV of 10 msec. The reason for maintaining a high ratio of time-constant to transit-time, even though the latter was not measured, was to ensure that the full signal magnitude was recorded for each transient. For an applied voltage of 3 KV, the slow random variation of d.c. level in the detection circuit, encountered in cell 'D1' was again observed. The magnitude of the disturbance with 4 KV applied to the cell was of the order of 1 volt, compared with a signal magnitude of 400 mV. Direct measurement confirmed that the voltage developed across R_m by the leakage ('dark') current through the cell was responsible for the observed fluctuations. The effect of the leakage current was reduced to a negligible level, for an applied voltage of 3 KV, by reducing R_m to $10^8 \Omega$. In order to maintain the time-constant at $\sim$ 0.1 sec., the measuring capacitance was increased to 1000 pF. Measurements of the photo-injected signal were then continued, without major difficulty, at increasing fields up to breakdown.

Figure (5.16) shows that the variation of signal magnitude (V_s) with applied field (E_a) was found to be linear up to breakdown for a fixed electrode separation. The slope of the graph was $(1.0 \pm 0.1).10^{-6}$ cm compared with $(0.9 \pm 0.1).10^{-5}$ cm for the non-oxidized cathode at the same nominal electrode separation.

Breakdown eventually occurred several times in rapid succession

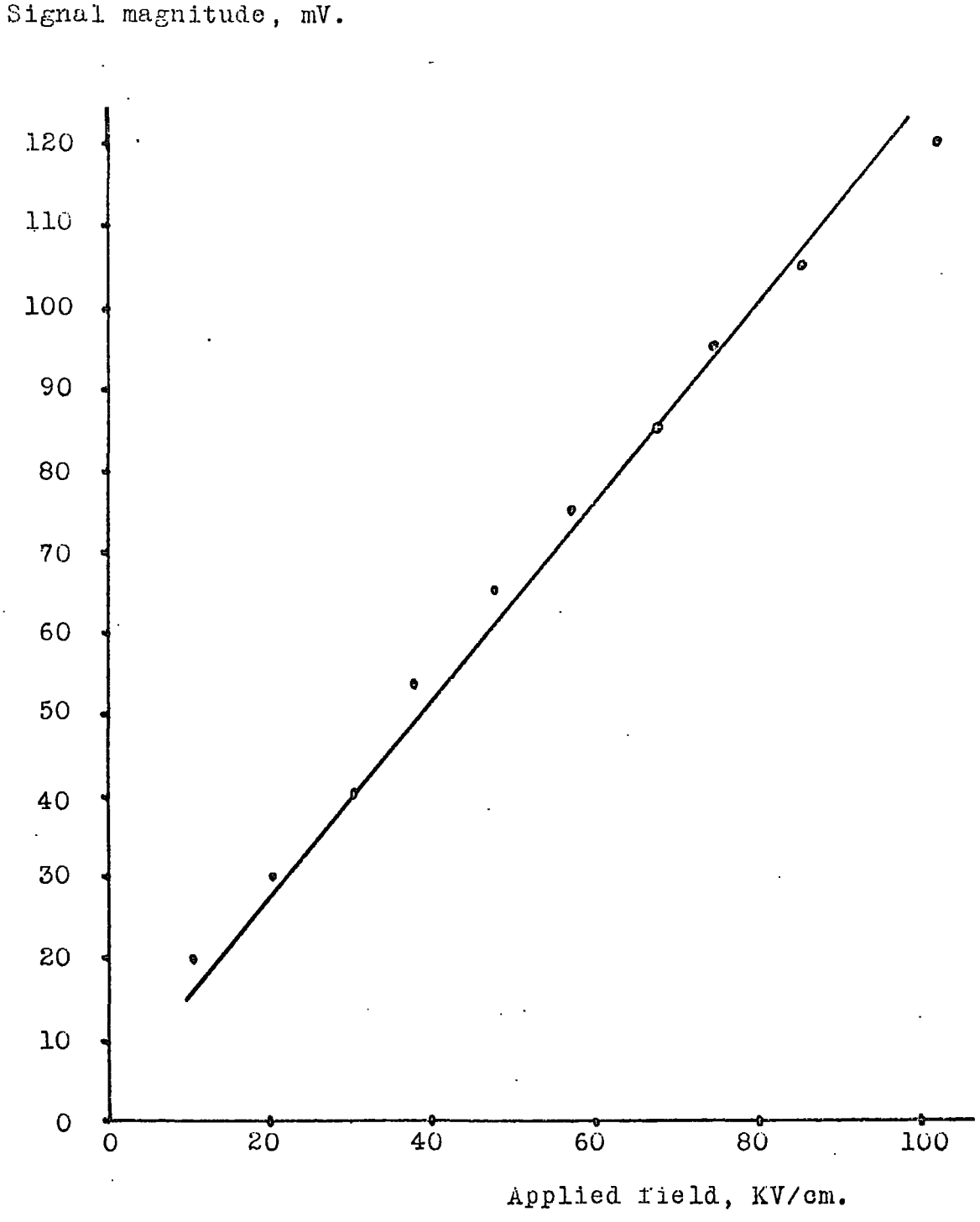

Figure (5.16). Variation of signal magnitude with applied field, for cell 'D2'. Nominal electrode separation, 1 mm.

after a voltage of 11 KV had been applied to the cell for a number of minutes. The damage to the cathode was almost identical with that sustained by the non-oxidized cathode. A large number of small holes had appeared in the aluminium film, corresponding to the pre-breakdown pulses which were observed. A relatively large area ($\sim$ 5 mm in diameter) of cathode damage was also apparent, the centre of which coincided with a small circular pit in the anode. The breakdown strength of this cell - 104 KV/cm - was a considerable improvement on the value of 22 KV/cm for the cell with a non-oxidized cathode.

5.4.4. Measurements of transit-time and signal magnitude

The investigation described in the previous section (5.4.3.) confirmed that the use of an oxidized aluminium cathode increased the breakdown strength of the test-cell, while allowing photo-injection of carriers into the liquid. The next stage in the programme outlined in section 5.4.1. was to make measurements of transit-time (τ_i) and signal magnitude (V_s) for a range of electrode separation (d) and applied voltage (V_a). The object of these measurements was basically to investigate the validity of the relationships between the above quantities for fields in excess of 20 KV/cm. The relationships in question have been verified for fields less than 20 KV/cm (sections 5.2.1. and 5.2.2.) and are:

$$\tau_i = d^2/\mu_i . V_a \quad \ldots\ldots\ldots\ldots\ldots\ldots \quad (9)$$

$$V_s = g_s V_a / d \quad \ldots\ldots\ldots\ldots\ldots\ldots\ldots \quad (10)$$

Three nominal values of electrode separation were chosen: 2 mm, 1 mm and 0.5 mm. Increasing fields up to 100 KV/cm were applied to these gaps in the order stated above and the injected transient recorded at each stage. The applied field was increased beyond 100 KV/cm (for $d \approx 0.5$ mm) only after a comprehensive set of data had been obtained in this way.

The theoretical transit-times for a carrier of mobility of 10^{-3} $cm^2/V.sec$ were in the approximate range 10 msec - 0.1 msec for the values of d and E_a employed. Since the duration of the 'long' flash source was $\sim$ 0.5 msec and therefore comparable with these values, the 'short' flash version, with a duration of $\sim$ 40 μsec (section 3.2.3.), was used throughout this series of measurements. The lower energy of the 'short' flash resulted in an overall reduction, by a factor of three, in the values of cathode sensitivity quoted in section 5.4.3. The associated decrease in signal/noise ratio complicated the measurement of signal magnitude from the recorded transients, but did not seriously affect the determination of transit-time.

The measuring resistance R_m was $10^8 \Omega$ for electrode separations of 2 mm and 1 mm, but the increased noise level for d = 0.5 mm, due to leakage current through the cell, made it necessary to reduce its value to $10^7 \Omega$. The consequent decrease in the time-constant of the integrating circuit was not sufficient to distort the transient, since the transit-times recorded for this value of d were all less than 2.5 msec.

Figures (5.17), (5.18) and (5.19) show the measured variation of $1/\tau_i$ with applied voltage, V_a, for each of the three electrode separations. The graphs are linear in each case, although the degree of scatter for each graph is greater than that observed using cell 'D1' (see figures (5.3.) - (5.6) inclusive). Table (5.3) lists the values of mobility, μ_i, calculated from the gradients of figures (5.17) - (5.19) inclusive, together with the appropriate values of electrode separation and applied field. A slight, but apparently systematic decrease in μ_i is evident in the three results, and although the differences are comparable with the experimental error, some significance must be attached to the decrease in view of the fact that all three values are lower than those obtained using cell 'D1'. A simple dependence of mobility on the electrode separation, d, may be eliminated from the possible explanations of the effect by comparing Table (5.3) with Table (5.1). It will be observed that the values of μ_i quoted for d = 2 mm and d = 1 mm in each table are consistently lower in the case of cell 'D2'. The possibility of a systematic variation in μ_i with applied field was investigated by plotting carrier velocity, u_i, against applied field, E_a, using all the experimental points obtained with cells 'D1' and 'D2'. The resulting graph is shown in figure (5.20). From equation (9), the theoretical form of figure (5.20) is given by;

$$\log_{10} u_i = \log_{10} \mu_i + \log_{10} E_a \quad \ldots\ldots\ldots\ldots (11)$$

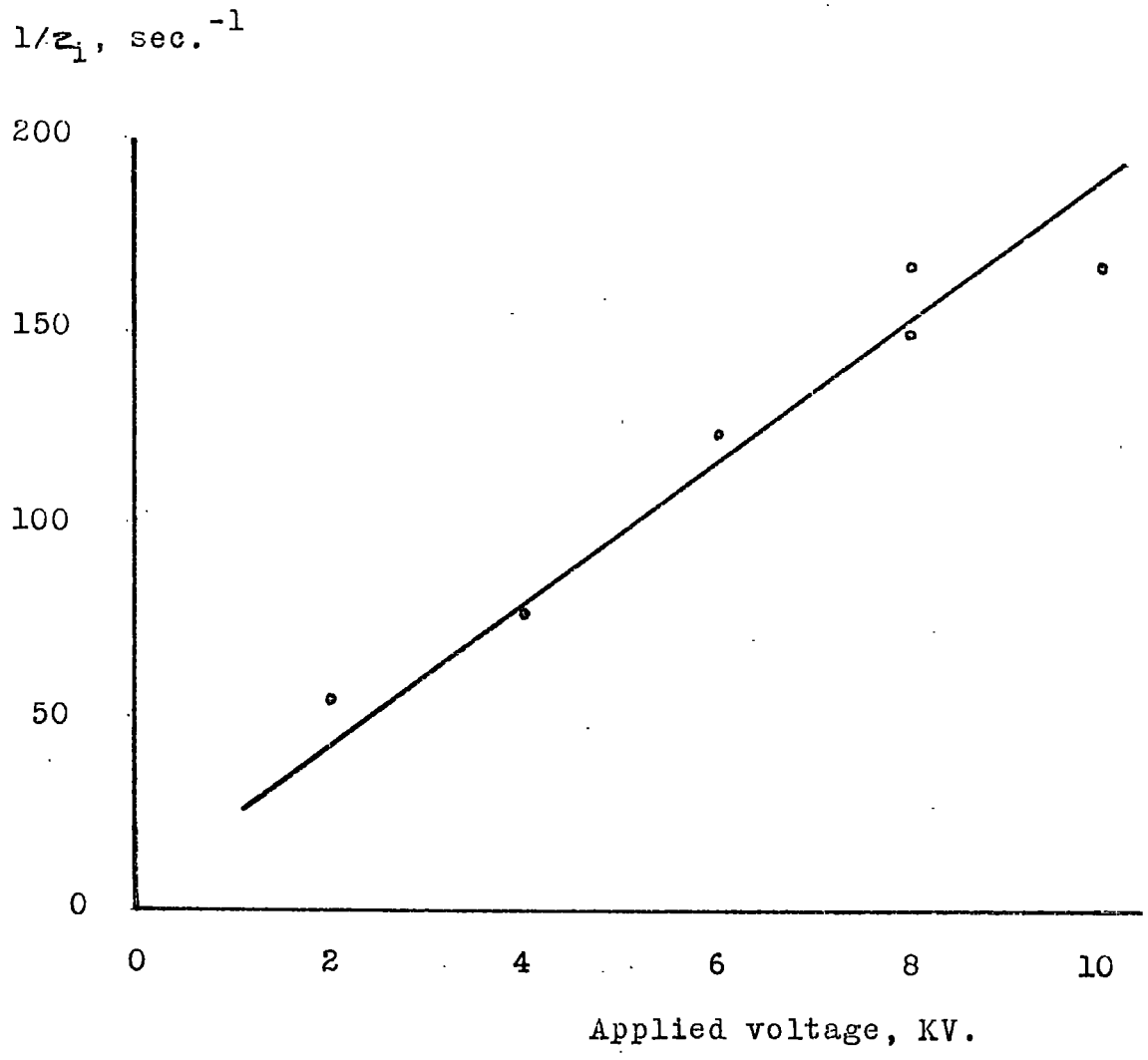

Figure (5.17). Variation of transit-time with applied voltage, for cell 'D2'. Nominal electrode separation, 2 mm.

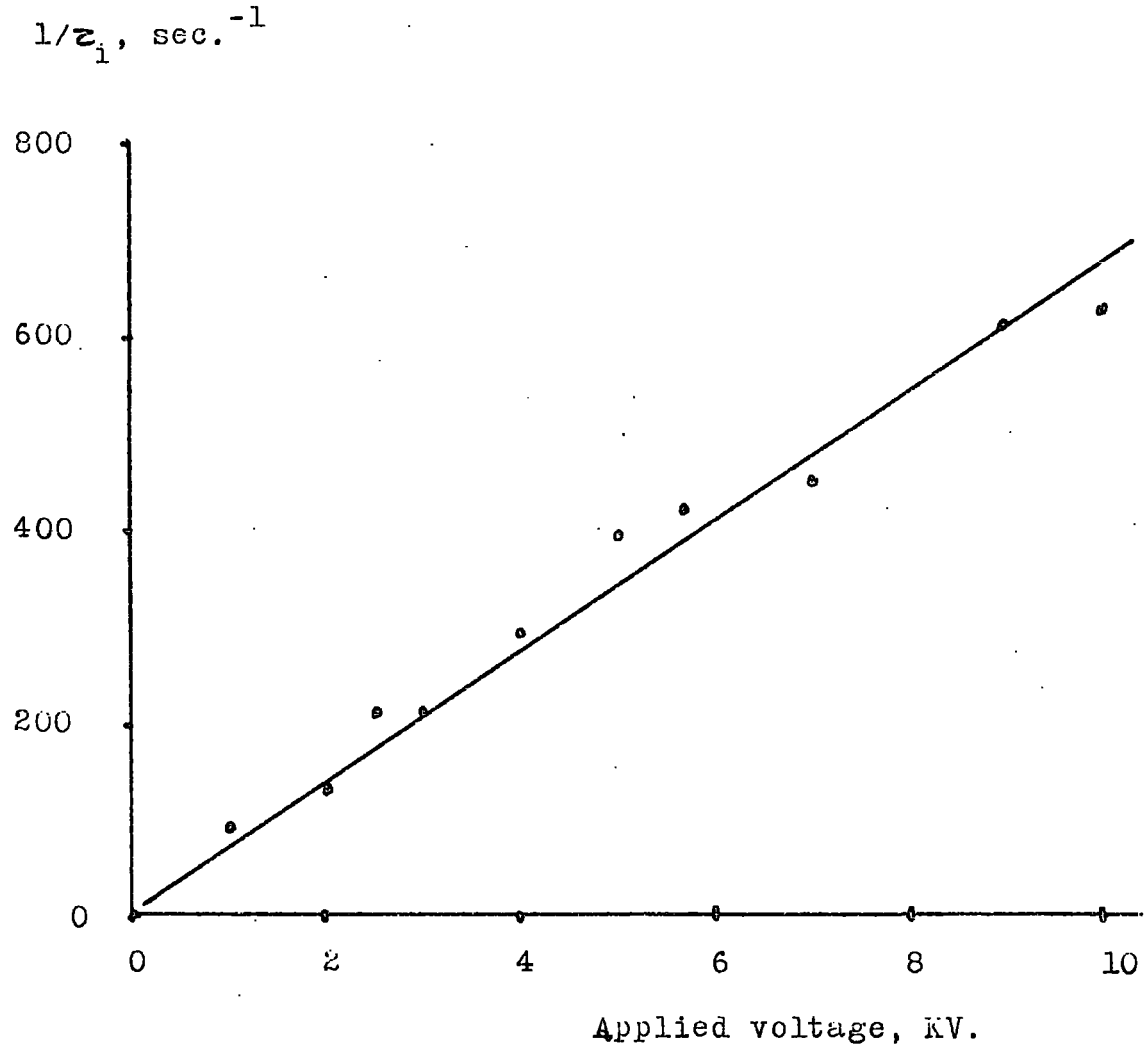

Figure (5.18). Variation of transit-time with applied voltage, for cell 'D2'. Nominal electrode separation, 1 mm.

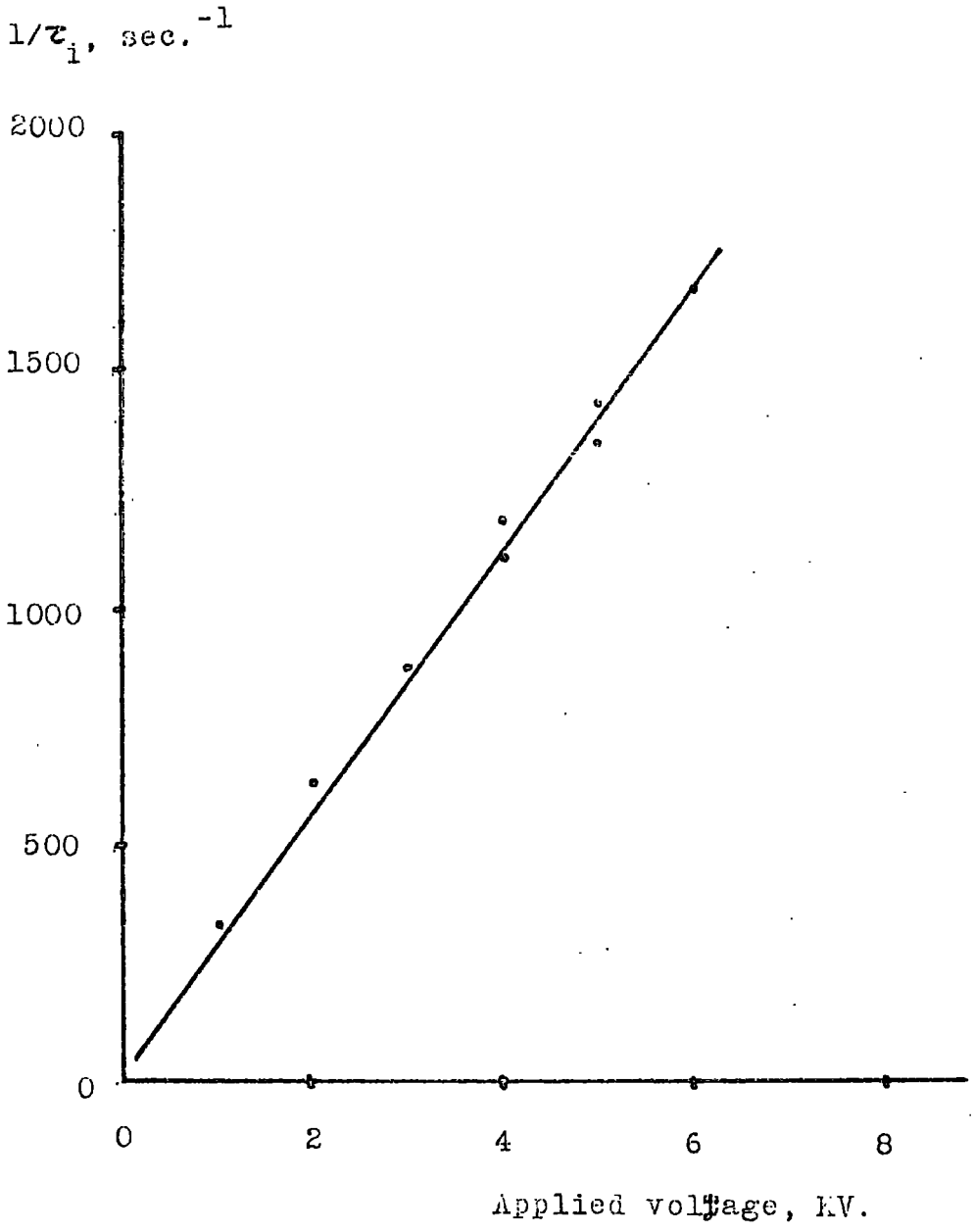

Figure (5.19). Variation of transit-time with applied voltage, for cell 'D2'. Nominal electrode separation, 0·5 mm.

Figure	Electrode separation Nominal (Actual)	Range of applied field, KV/cm.	Apparent mobility, μ_i. $cm.^2/V.sec. \times 10^3$
5.17.	2 mm. (1·92 ± 0·03)	10 - 50	(0·70 ± 0·05)
5.18.	1 mm. (0·94 ± 0·03)	10 - 100	(0·58 ± 0·05)
5.19.	0·5 mm. (0·43 ± 0·03)	23 - 140	(0·54 ± 0·05)

Table (5.3). Values of mobility, μ_i, determined using cell 'D2'.

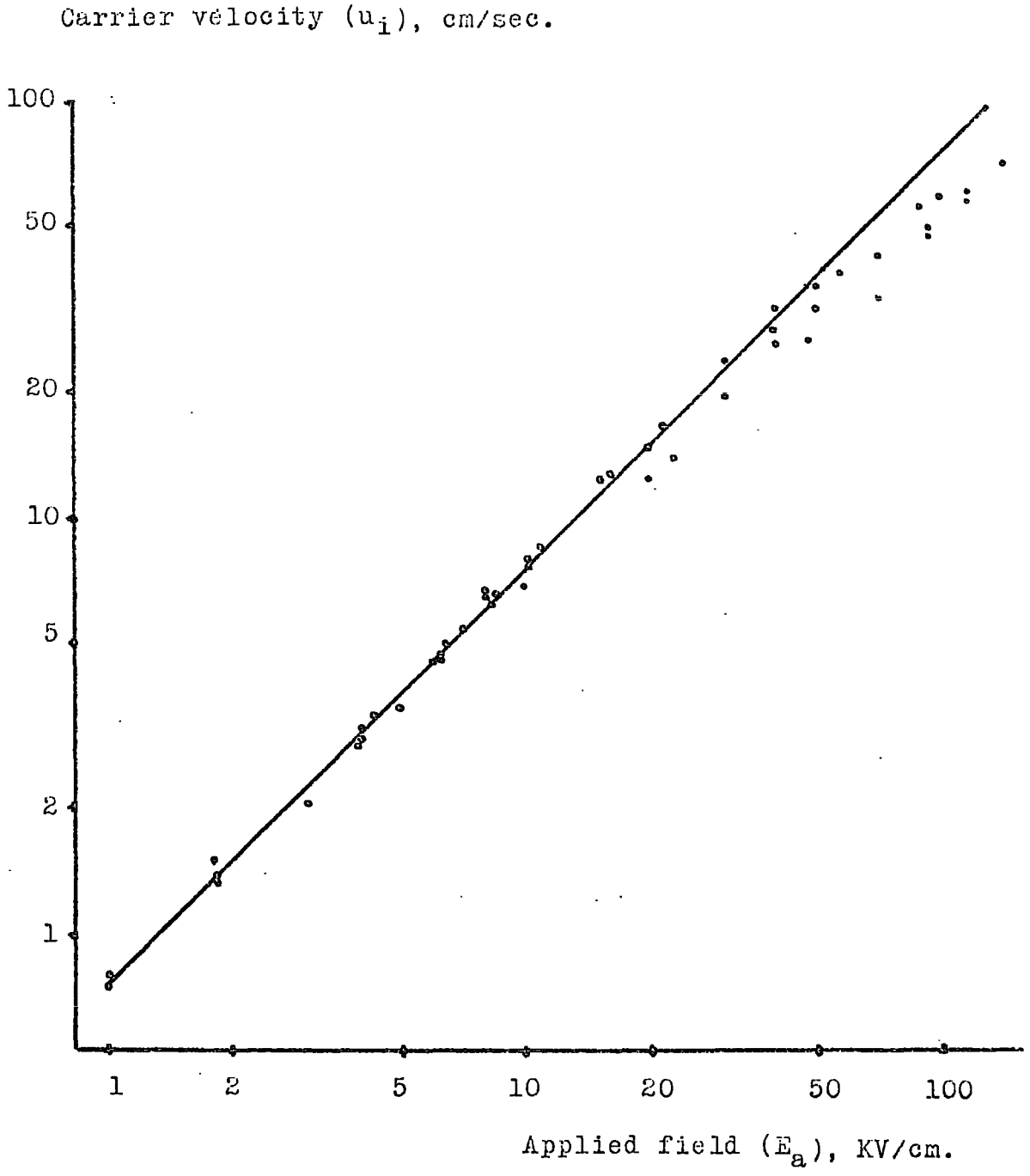

Figure (5.20). Variation of carrier velocity with applied field.

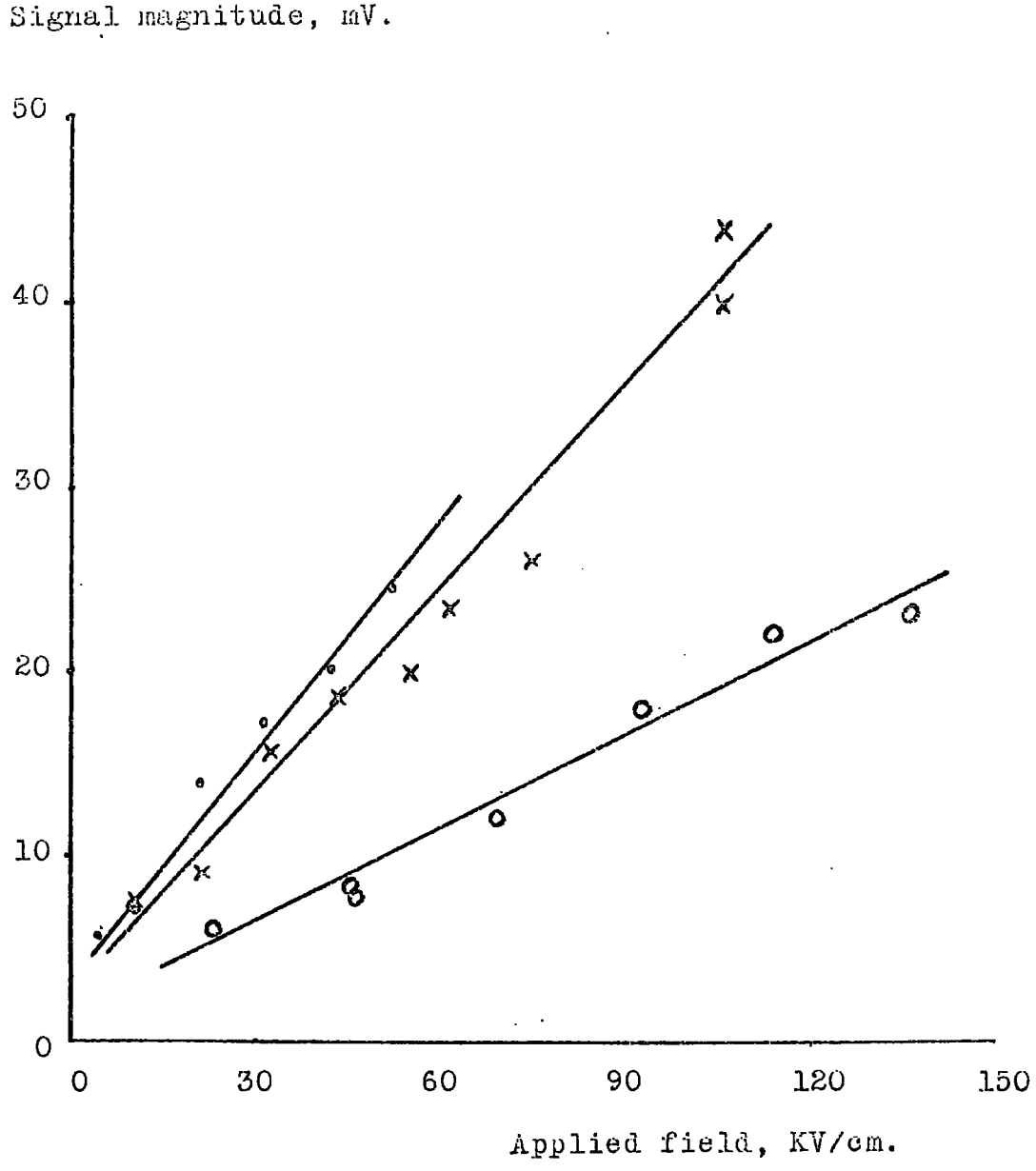

Figure (5.21). Variation of signal magnitude with applied field, for cell 'D2'. Nominal electrode separations : 2 mm. (•), 1 mm. (×), and 0·5 mm. (o).

where $u_i = d/\tau_i$. A line of unit gradient drawn on figure (5.20) is a good fit with most of the experimental points, thus confirming the general validity of equation (11) and hence of equation (9). The experimental points which do not lie on this line to within the estimated experimental error are those determined at high values of applied field and low values of electrode separation. It appears that extreme values of both electrode separation and applied field are necessary conditions for anomalous values of μ_i . However, the points not fitting the single straight line of figure (5.20) may themselves be fitted to a series of straight lines of unit gradient, one for each value of electrode separation. It may therefore be concluded that the anomalous values of mobility are associated with short transit-times, and that this condition does not necessarily involve violation of equation (9). The relationship between μ_i and the true carrier mobility, and the possible dependence of this relationship on the transit-time itself, are discussed in section 6.5. in connection with the shape of the integrated current-transient.

The linearity of figure (5.20) over the wide range of applied field investigated experimentally (1 KV/cm to 140 KV/cm) is of major importance to the present investigation. The lack of any detectable increase in mobility over this range of applied field eliminates one of the mechanisms postulated in Chapter 1 to explain the difference in conductivity between de-gassed and air-saturated hexane. An alternative explanation of the effect, also postulated in Chapter 1, is the existence of high-mobility

carriers in the de-gassed liquid. This explanation is not supported by the transit-time measurements described in this or previous sections. No recorded transient produced any evidence for the existence of carriers with a mobility greater than the maximum value quoted in Tables (5.1) and (5.3), even though the detection system was capable of resolving transit-times at least an order of magnitude less than the smallest observed value of τ_i.

The variation of signal magnitude with applied field for the oxidized cathode was determined from the transients recorded primarily for the measurement of transit-time. Figure (5.21) shows that, although the signal magnitude, V_s, increased in direct proportion to the applied field, E_a, for a given electrode separation, the slope of such plots decreased as the electrode separation was reduced. This result violates the expression:

$$V_s = g_s . E_a \quad \ldots\ldots\ldots\ldots\ldots\ldots\ldots\ldots (10)$$

which was previously established for non-oxidized cathodes. An explanation of the phenomenon in terms of the shape of the recorded transient is presented in section 6.5.

5.4.5. Breakdown of cell 'D2'

Breakdown of the test-cell occurred at a field strength of 140 KV/cm and a nominal electrode separation of 0.5 mm. The breakdown event, the pre-breakdown phenomena and the form of the electrode damage were essentially as described in sections 5.3. and 5.4. It may be

concluded that the breakdown strength quoted above was a property of the particular test-cell, rather than the hexane it contained.

Since no further attempts were made to increase the breakdown strength of the test-cell, this value of applied field was the maximum at which transit-time and signal magnitude determinations were made.

5.5. REFERENCES

1. Morant, M.J., Private Communication

2. Kahan, E., Ph.D. Thesis, Durham University (1964)

3. Handbook of Chemistry and Physics (Chemical Rubber Pub. Co., Cleveland, Ohio, 1958)

4. Krasucki, Z., E.R.A. Report 5157 (February 1966) and E.R.A. Report 5212 (June 1967)

5. Yarwood, J., High Vacuum Technique (Chapman and Hall, London, 1961).

CHAPTER 6

THE SHAPE OF THE CURRENT TRANSIENT

The shape of the integrated current transient is of major importance to the determination of mobility when as in the present case, it differs from the theoretical ramp-function. Two extraneous causes of trace-curvature, namely geometric distortion of the field and the generation of carriers in the bulk of the liquid, have been practically eliminated by the improvements in cell design recorded in Chapters 4 and 5. It must now be considered that the trace-curvature is connected with the conduction mechanism, or that under the present experimental conditions, the movement of the injected charge layer itself produces a distortion.

The following mechanisms are suggested as being potentially responsible for the trace-curvature:

i) axial and radial diffusion of carriers;

ii) formation of carriers in the bulk of the liquid;

iii) long term trapping of carriers in the liquid;

iv) a non-uniform field;

v) dynamic distortion of the injected charge layer.

Each of these mechanisms is the subject of a section of this chapter, where they are considered with the object of eliminating as many as possible from the discussion. In some cases it was necessary to obtain additional experimental data for comparison with the theoretical analysis

of a mechanism. Such experiments are described in the appropriate section.

6.1. RADIAL AND AXIAL DIFFUSION OF CARRIERS

Consider the injection of a disc-shaped charge-layer into cell 'D1' or 'D2'. The initial radius of the disc will be equal to that of the mask aperture, and the thickness of the injected layer will depend on the carrier velocity and the duration of the ultra-violet flash. During the transit time the shape of the charge-layer will change, due to diffusion, according to:

$$D.\nabla^2 n - \partial n/\partial t = 0 \qquad \ldots\ldots\ldots\ldots\ldots\ldots \quad (1)$$

where D is the diffusion constant.

Radial diffusion will not affect the shape of the current transient, provided that the effective radius of the disc is always less than that of the electrodes.

Axial diffusion, however, will result in an extended decay of the current transient for times greater than the transit-time of the leading edge of the disc. This will produce a curvature of the integrated transient.

In order to simplify the discussion of diffusion effects under the present experimental conditions, the radial and axial components will be considered separately, using one-dimensional models. Equation (1) then becomes:

$$D.\partial^2 n/\partial x^2 - \partial n/\partial t = 0 \quad \ldots\ldots\ldots\ldots\ldots (2)$$

For the initial condition:

$$n = 1, \quad |x| \leq x_o$$
$$n = 0, \quad |x| \geq x_o$$

the solution of equation (2) is:

$$n(x,t) = 0.5 \left[\phi(x_o + x)/2\sqrt{Dt} + \phi(x_o - x)/2\sqrt{Dt}\right] \ldots\ldots (3)$$

where $\phi(x)$ is the appropriate error integral:

$$(2/\sqrt{\pi}) \int_o^x e^{-\xi^2} .d\xi ,$$

and x_o is the initial radius (R_o) or half-thickness (W_o) of the disc. The parameter $\sqrt{Dt}$ is the diffusion length, which characterizes the extent to which diffusion has occurred during the interval t. The effects of diffusion may generally be ignored if $\sqrt{Dt}$ is small compared with x_o.

A value for the diffusion constant may be obtained from the Einstein Relationship:

$$D = \mu.kT/e \quad \ldots\ldots\ldots\ldots\ldots\ldots\ldots (4)$$

The validity of this relationship has been demonstrated for carriers in liquid saturated hydrocarbons, by Gazda (1, 2). Taking the mobility, μ, to be approximately 10^{-3} cm^2/volt.sec., the corresponding value of the diffusion constant is:

$$D \doteq 2.5. 10^{-5} \text{ cm}^2/\text{sec.}$$

6.1.1. Radial diffusion

The initial radius, R_o, of the injected charge-layer was normally between 0.3 cm and 0.4 cm. and the maximum transit-time recorded was 0.5 sec. The maximum diffusion length for radial diffusion was therefore approximately $3.5.10^{-3}$ cm., giving a minimum ratio $R_o/\sqrt{D\tau}$ of the order 10^2. The effect of radial diffusion must therefore be negligible, particularly since the anode radius of 0.8 cm. was at least twice that of the mask aperture.

6.1.2. Axial diffusion

Calculation of the degree of axial diffusion is complicated by the dependence of the initial width of the charge-layer on the applied field E and the duration t_f of the ultra-violet flash. The half-width of the layer, W_o, is given by:

$$W_o = \tfrac{1}{2}\mu E.t_f \qquad \ldots\ldots\ldots\ldots\ldots\ldots\ldots\ldots \quad (5)$$

The range of values of W_o and $\sqrt{D\tau}$ encountered during the experimental work is presented in fugures (6.1) and (6.2). Figure (6.1) refers to transients observed using the 'long' flash, the duration of which is taken to be 0.5 msec. For each electrode separation, d, the curve of $\sqrt{D\tau}$ versus E is shown only for the range of E actuallyused. The values of d quoted, and those used in the calculations, are the nominal values. Figure (6.2) refers to transients observed using the 'short' flash, for which a duration of 40 μsec. was assumed.

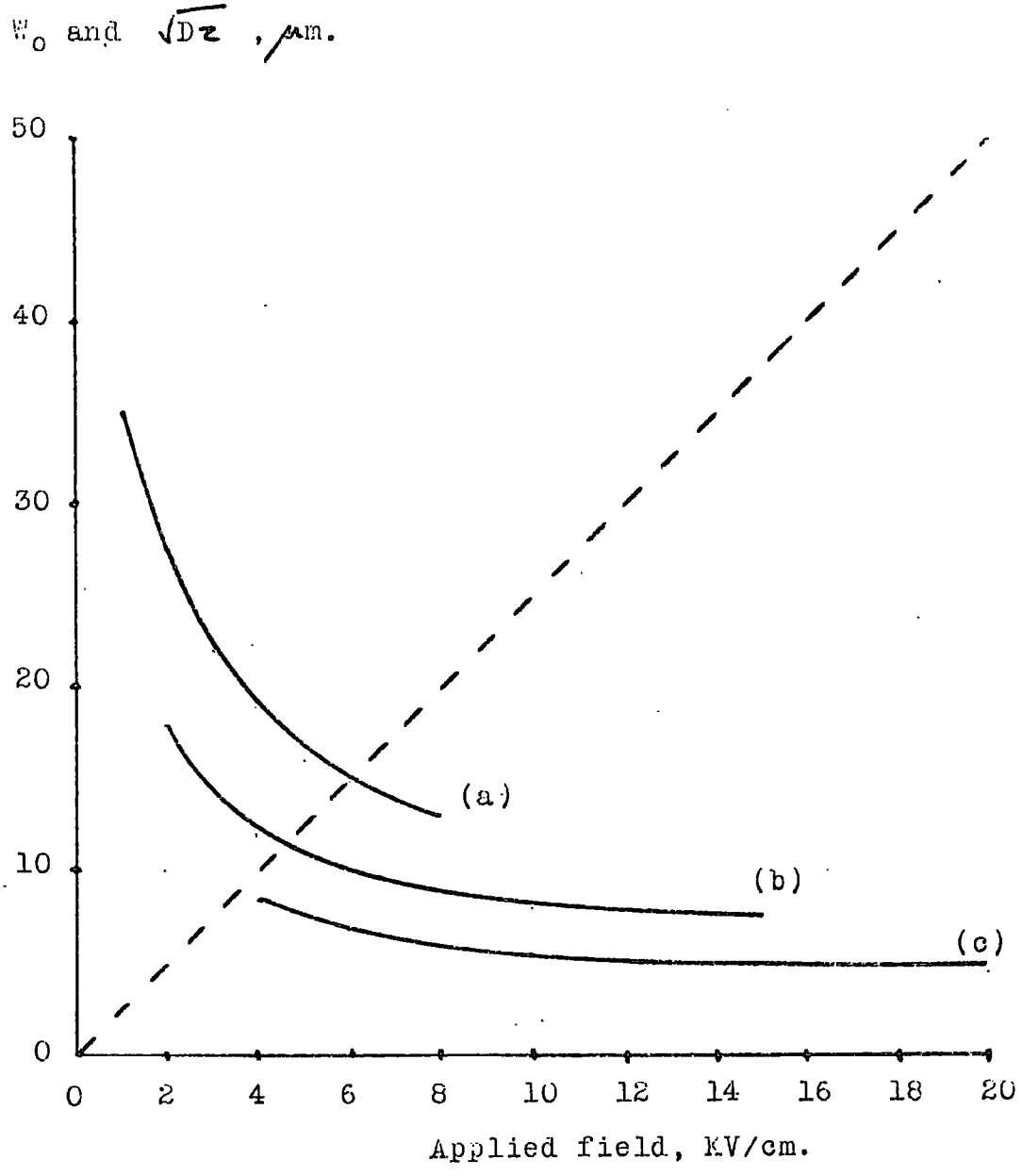

Figure (6.1). Variation of W_o (broken line) and $\sqrt{Dt}$ (full lines) with applied field, using the 'long' flash-source. Nominal electrode separations; (a) 4 mm.; (b) 2 mm.; (c) 1 mm.

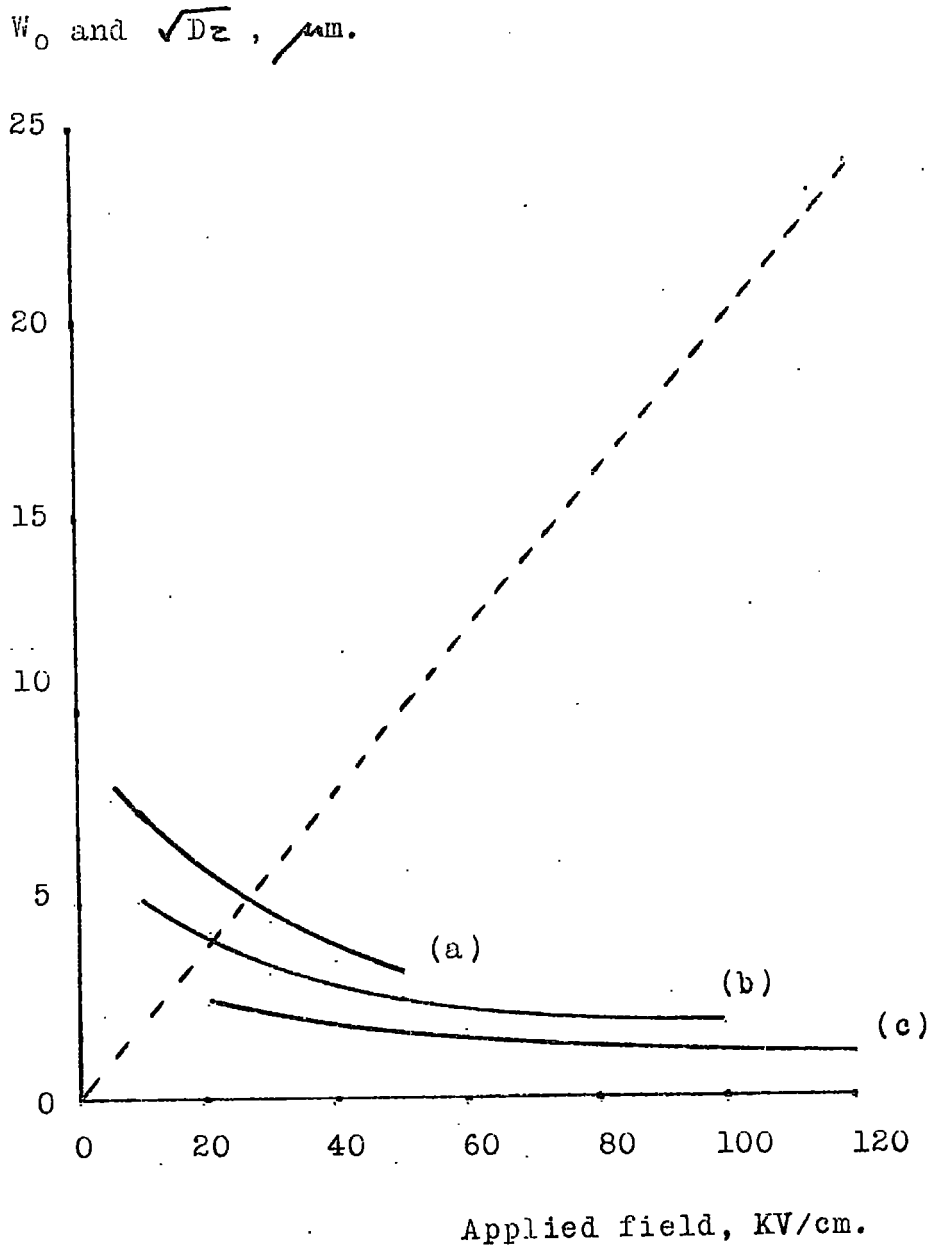

Figure (6.2). Variation of W_o (broken line) and $\sqrt{Dz}$ (full lines) with applied field, using the 'short' flash-source. Nominal electrode separations: (a) 2 mm.; (b) 1 mm.; (c) 0·5 mm.

It is evident from the two diagrams that, for high fields, the effect of diffusion on the final width of the disc is small, since the ratio $W_o/\sqrt{Dt}$ is of the order 10. For lower fields, $\sqrt{Dt}$ becomes comparable with, or up to 10 times greater than, W_o. Under these conditions the final width of the charge-layer is largely determined by the diffusion length. In spite of this, the effect of axial diffusion on the transient shape is negligible, for in no case does the diffusion length become comparable with the electrode separation.

Thus, for a given electrode separation, increasing the field increases the ratio $W_o/\sqrt{Dt}$ and reduces the degree of diffusion. Decreasing the field, on the other hand, although producing more extensive diffusion, reduces the initial width of the charge-layer. For the range of electrode separations and fields used in the present work, the effect of axial diffusion was therefore entirely negligible and it cannot reasonably be employed to explain the curvature of the integrated current transients.

6.2. THE FORMATION OF CARRIERS IN THE BULK OF THE LIQUID

The generation of charge-carriers in the bulk of the liquid, by short wavelength radiation from the flash-source, may be considered as a possible cause of the trace curvature. The primary objection to this explanation is the high ratio of photo-injected charge to bulk-generated charge achieved experimentally. This source of curvature may be discounted, therefore, unless it can be shown that a small amount of charge,

distributed throughout the inter-electrode space, could result in a signal capable of distorting the photo-injected signal. The following analysis evaluates the importance of bulk carriers to the trace shape under the present experimental conditions.

The electrode geometry of cells 'C', 'D1' and 'D2' ensured that any bulk effect of the ultra-violet radiation was restricted to a cylindrical volume of known dimensions. Since the liquid was highly transparent to ultra-violet light, it may be reasonably assumed that carriers were generated uniformly throughout this volume. In order to simplify the analysis, it is further assumed that the bulk-generated carriers have a single mobility, and that either (a) carriers of one sign only are formed, or (b) recombination between carriers of opposite sign may be ignored.

It may be shown (Appendix A) that the resulting variation of the integrated signal magnitude V_s with time is given by:

$$V_s = Q_u . (\pi r^2 d/C_m) . (t/T) . (1 + \log_e T/t) \quad \ldots\ldots\ldots (6)$$

where Q_u is the charge generated in unit volume of the liquid;

r is the radius of the mask aperture;

d is the electrode separation;

C_m is the integrating capacitance;

and T is the transit time of the bulk generated carrier.

The peak value of this transient occurs at t = T and is given by:

$$V_s(\max) = Q_u \cdot \pi r^2 d/C_m \quad \ldots\ldots\ldots\ldots\ldots \quad (7)$$

Figure (6.3) shows the normalized form of the transient, plotted in terms of $V_s/V_s(\max)$ and t/T. It is evident that the trace curvature observed experimentally is of the same form as that of Figure (6.3), and that given a low proportion of photo-injected charge in the total signal, the trace shape could well be ascribed to a photo-ionization process.

The determination of the ratio of injected to ionized carriers has been described in Chapters 4 and 5. Reference to these Chapters will show that the minimum value of this ratio (u_f/w) was obtained for cell 'D2' (oxidized cathode) at 10 KV/cm., when $u_f/w \doteq 4$. The non-oxidized cathodes gave ratios of $\gtrsim 20$ for lower fields than this. Using the above information, the effect of bulk carrier generation may be illustrated by the summation of the ideal photo-injected transient and the transient given by equation (6), for appropriate values of u_f/w. Figure (6.4) shows the result of such a summation for the case $u_f/w = 4$. The total signal, v_f, was normalized to unity and the time-scale to T. Inspection of the traces obtained experimentally indicated that the curvature extended to a point $t \doteq 2\tau_i$. The photo-injected signal was therefore plotted for a transit time of $\tau_i = T/2$.

It is evident from Figure (6.4) that even the maximum observed

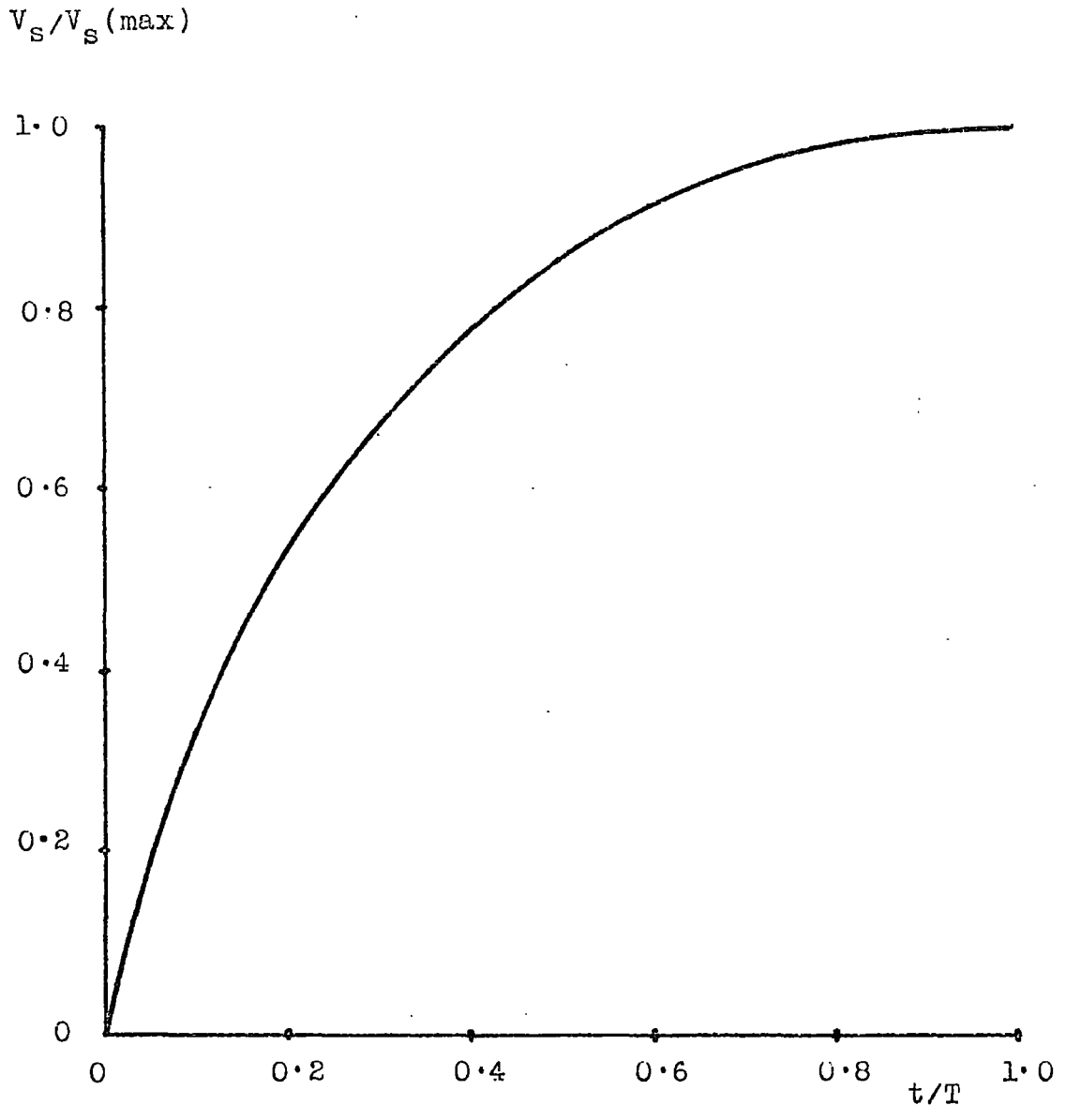

Figure (6.3). Theoretical form of the integrated current-transient due to uniform generation of carriers throughout the liquid.

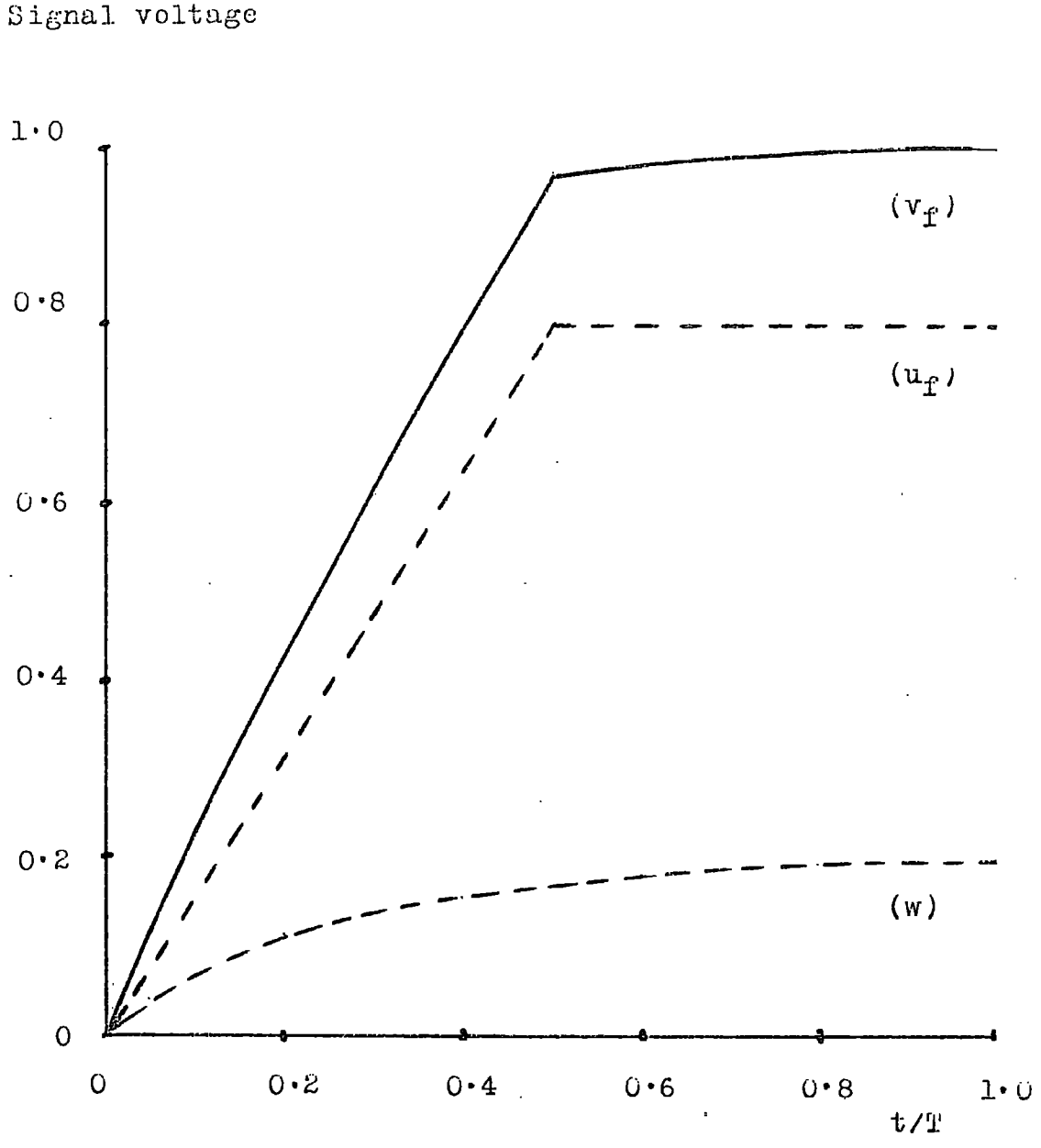

Figure (6.4). Theoretical form of the integrated transient (v_f) due to the combined effects of photo-injection (u_f) and photo-ionization (w), for $u_f/w = 4$.

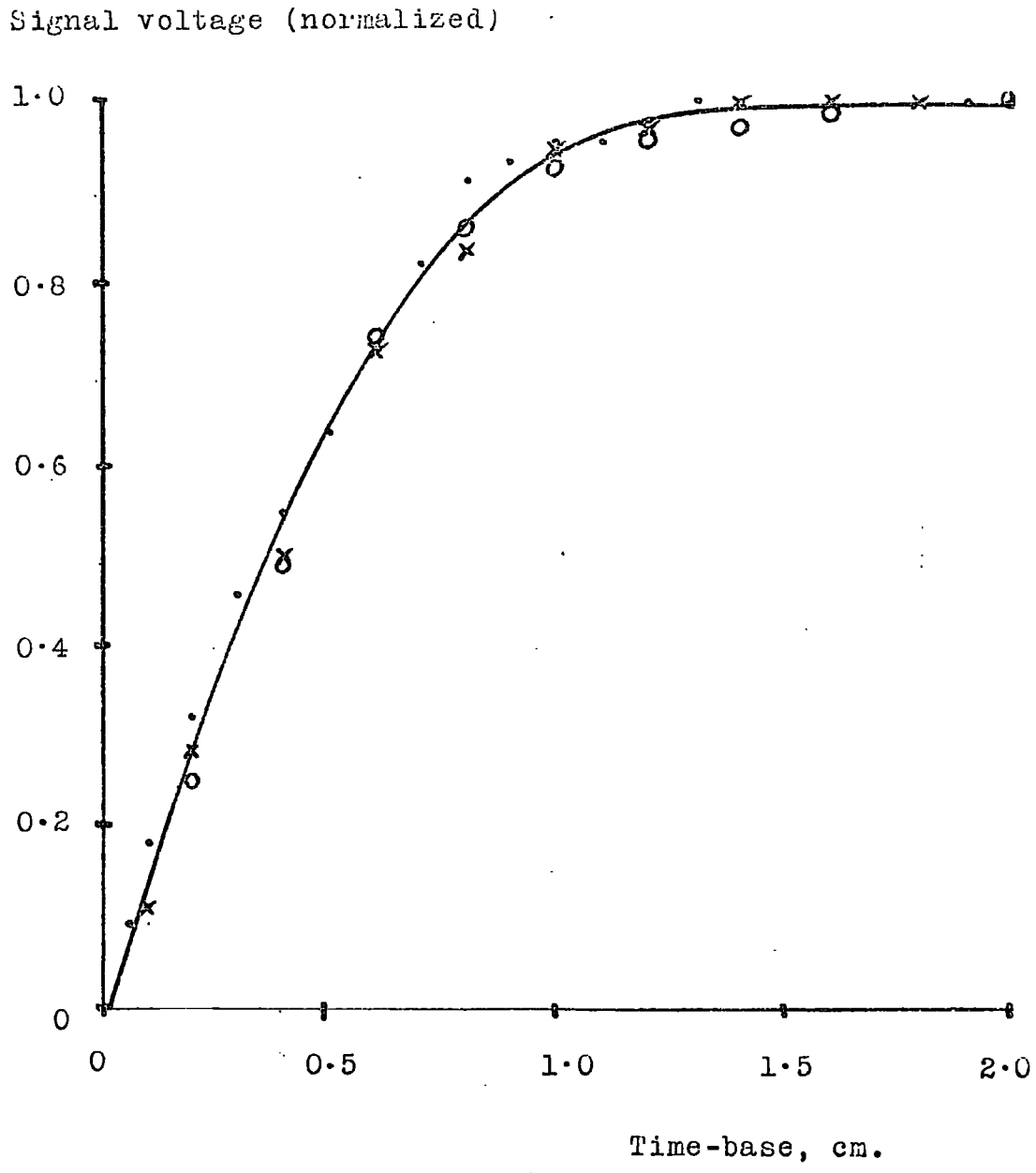

Figure (6.5). Integrated current-transients for an applied field of 10 KV/cm. Nominal electrode separations: 4 mm. (•); 2 mm. (×); and 1 mm.(o). Time-base scales: 40 msec/cm.; 20 msec/cm.; and 10 msec/cm. respectively.

value of u_f/w is not capable of masking the discontinuity in the photo-injected transient or of imparting detectable curvature to the total signal.

Direct experimental verification of the above conclusion was obtained by comparing transients recorded for three different electrode separations at constant field strength. Since the magnitude of the bulk effect signal is proportional to the electrode separation - equation (7) - and the photo-injected signal depends only on the applied field, the three transients illustrated the effect of changing u_f/w by known amounts. Figure (6.5) shows, superimposed, the three traces recorded for an applied field of 10 kV/cm. and electrode separations of 0.4 cm., 0.2 cm., and 0.1 cm. A common time-scale was chosen to take account of the three different transit-times. The figure clearly illustrates that the shape of the transient was not affected by a four-fold change in u_f/w. The slight curvature on the initial portion of the transient for d = 0.4 cm. may be ascribed to bulk effects, in view of the unusually low value of u_f/w ($\doteq 2$), but it will be noted that the major degree of curvature which occurs in the latter part of the transient is identical for each of the transients.

Theoretical and experimental evidence are thus consistent with the conclusion that, although photo-generation of carriers in the bulk of the liquid is known to take place, the magnitude of the signal so produced is not sufficent to affect the shape of the photo-injected transient in the manner, or to the extent, observed experimentally.

6.3. THE LONG-TERM TRAPPING OF CARRIERS IN THE LIQUID BY DISSOLVED OXYGEN

It has been postulated, as a basis for the present investigation (section 1.3) that the effect of dissolved oxygen on the conductivity of n-hexane could be explained by consequent variations in either the mobility or the concentration of the charge-carriers. Consideration of a simple model involving the trapping of carriers by dissolved oxygen, showed that a change in the oxygen content of the liquid would affect both the size and shape of a photo-injected transient. A mechanism offering explanations of the conductivity of degassed n-hexane and also of the trace-curvature observed under the present conditions of mobility measurement, obviously merited further investigation. The relevant theoretical considerations and predictions of such a model are set out in section 6.3.1., while section 6.3.2. compares these with the observed effects of admitting air to a mobility measurement cell containing de-gassed hexane.

6.3.1. Theoretical consideration of a simple trapping model

Consider the situation resulting from a uniform distribution of traps throughout the liquid. The traps are assumed to be closely associated with oxygen molecules, and capable of capturing photo-injected carriers to form a long-lived carrier having a mobility which is small compared with that of the photo-injected carrier.

The rate of trapping of injected carriers, dc_i/dt is equal to the rate of consumption of trapping centres, dc_t/dt. Both these rates

are proportional to the product of the two concentrations, such that:

$$dc_i/dt = dc_t/dt = -K_1 \cdot c_i \cdot c_t \quad \ldots\ldots\ldots\ldots\ldots (8)$$

The rate of removal of injected carriers is therefore;

$$dc_i/dt = K.c_i \quad \ldots\ldots\ldots\ldots\ldots\ldots\ldots\ldots (9)$$

where K is proportional to c_t and hence to the partial pressure of oxygen in equilibrium with the free surface of the liquid.

Let a number of carriers, n(0), be injected into the liquid at zero time. Equation (9) may then be written:

$$n(t) = n(0).\exp\left\{-Kt\right\} \quad \ldots\ldots\ldots\ldots\ldots\ldots (10)$$

The current observed in the external circuit is therefore:

$$\begin{aligned} i(t) &= n(t).e/\tau \quad \text{for } 0 \leq t \leq \tau \\ i(t) &= 0 \qquad\quad \text{for } t \geq \tau. \end{aligned} \quad \ldots\ldots\ldots\ldots (11)$$

The integrated current, expressed in terms of the signal voltage, $V_s(t)$, is given by:

$$\begin{aligned} V_s(t) &= \left[n(0).e/C_m.K.\tau\right]\left[1 - \exp(-K.t)\right] \quad \text{for } 0 \leq t \leq \tau \\ V_s(t) &= \left[n(0).e/C_m.K.\tau\right]\left[1 - \exp(-K.\tau)\right] \quad \text{for } t \geq \tau \end{aligned} \quad \ldots(12)$$

where C_m is the measuring capacitance

and τ is the transit time of the injected carriers.

It is assumed that the trapped carriers have a transit time which is large compared with τ, and comparable with the time constant of the integrating circuit. The contribution of these carriers to the signal magnitude would thus not be detected.

Figure (6.6) shows the variation of the normalized signal voltage V' with the parameter K.τ, over a wide range of the latter. The quantity V' is defined by:

$$V' = V_s(\tau).C_m/n(0).e \quad \ldots\ldots\ldots\ldots\ldots\ldots (13)$$

It is clear from the diagram that, for a fixed value of τ, there is a critical range of values for K within which a major change in V' occurs. Similarly, for a fixed value of K in the critical region, a decrease in the transit time at constant applied field would increase the signal magnitude, and vice versa.

Equation (12) also predicts departures from the ideal transient for large values of K.τ. The form of these departures is shown in figure (6.7.), for selected values of K.τ between 0.1 and 10. In each case the theoretical transients have been normalized to unit height and transit time. The relative heights of the transients may be deduced from figure (6.6.), whence it is evident that a reduction in signal magnitude, due to the proposed mechanism, would be accompanied by an increase in the curvature of the transient.

The oxygen partial pressure above the degassed liquid in the test-cell was of the order 10^{-5} torr (section 3.1.2.) whereas the

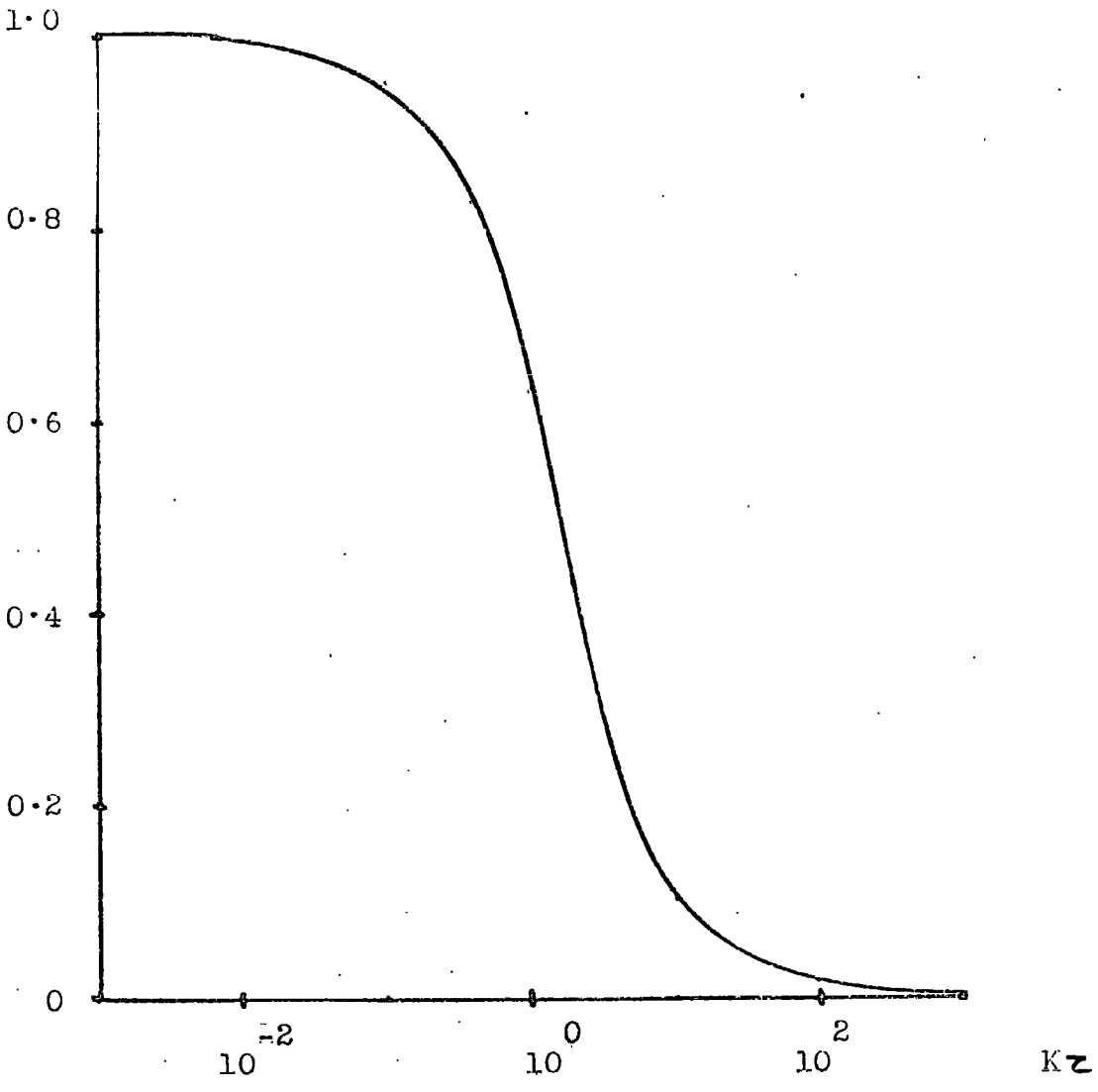

Figure (6.6). Theoretical variation of the signal voltage V' with the parameter $K\tau$.

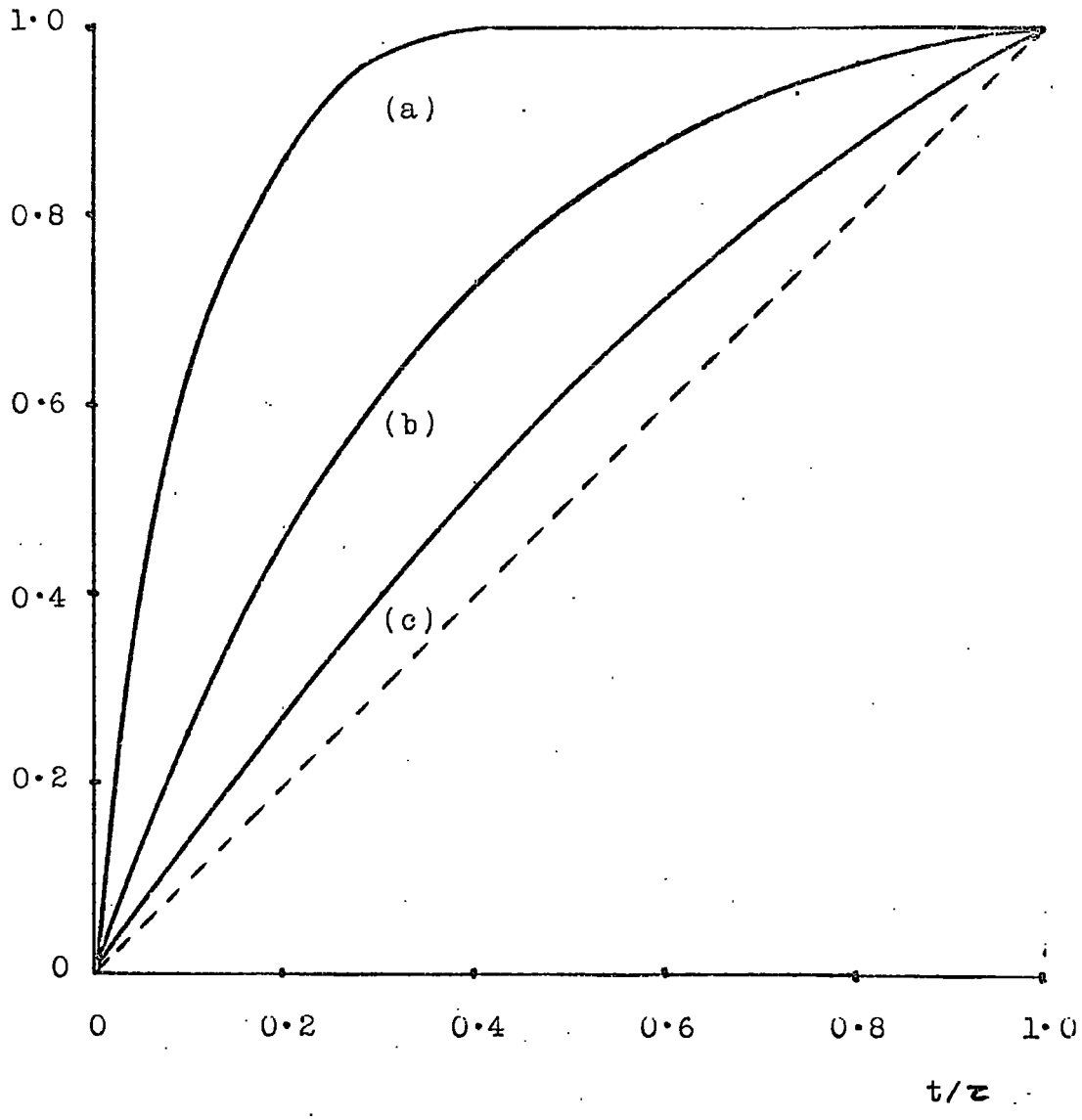

Figure (6.7). Form of the departure from the ideal transient (broken line) for various values of $K\tau$: (a) 10; (b) 1·0; (c) 0·1.

corresponding figure for air-saturated liquid is 10^{2} torr. The controlled admission of air to a volume of degassed liquid in the test-cell would therefore have the effect of varying the partial pressure of oxygen over a very wide range. The resulting variation in the concentration of dissolved oxygen would enable the phenomena described above to be observed, if the proposed model were valid.

6.3.2. Experimental determination of the effect of dissolved oxygen on the photo-injected signal.

It had been established previously that oxidation of a vacuum-deposited aluminium cathode by atmospheric oxygen reduces the photo-sensitivity by approximately 10 times. (section 5.4.1.). It was therefore necessary to distinguish between this surface effect and the postulated volume effect, when admitting air to the test-cell. The mobility measurements made using an oxidized aluminium photo-cathode showed that the reduction in signal magnitude was not associated with a change in the shape of the transient. The effects of dissolved oxygen on the photo-injected signal were therefore determined using the oxidized cathode cell (cell 'D2) described in Chapter 5.

Figure (6.8) is a block diagram showing the method of connecting the test-cell and its liquid reservoir to the distillation and de-gassing system. The only major difference between figure (6.8) and the description of the system given in section 3.1.2. is the substitution of a greaseless tap (B) for the sealing-off constriction.

Freshly de-gassed liquid was admitted to the test-cell, under vacuum, as described in section 3.2.2. and the taps (A), (B) were closed. An electrode separation of 0.2 cm and a field of 10 KV/cm were chosen as standard conditions, and the resultant photo-injected transient recorded for reference. With both pumps stopped, the pressure in the pumping system was adjusted to the required value by slowly admitting air through a phosphorus pentoxide drier. Tap (C) was then closed and tap (B) opened, and pressure equilibration allowed to take place between the two vessels. The photo-injected transient was recorded at intervals during this period.

It was found that equilibration with an air pressure of 200 torr, for approximately 16 hours, resulted in a reduction of the signal magnitude from 80 mV to a constant value of 20 mV. On subsequently connecting the test-cell to a pumping system pressure of 100 torr, the signal magnitude increased again, over a period of 5 hours, to 100 mV. Repetition of the de-gassing process, using the same sample of hexane, yielded an initial signal of 105 mV, falling to 100 mV during the 24 hours after closing tap (B).

No attempt was made to define the critical pressure region more accurately than indicated above (100 - 200 torr), in view of the shape of the signal recorded at a pressure of 200 torr. Figure (6.9) shows super-imposed, traces obtained using (a) freshly de-gassed hexane and (b) the same sample in equilibrium with an air pressure of 200 torr. The magnitudes of the signals (105 mV and 20 mV respectively) have been

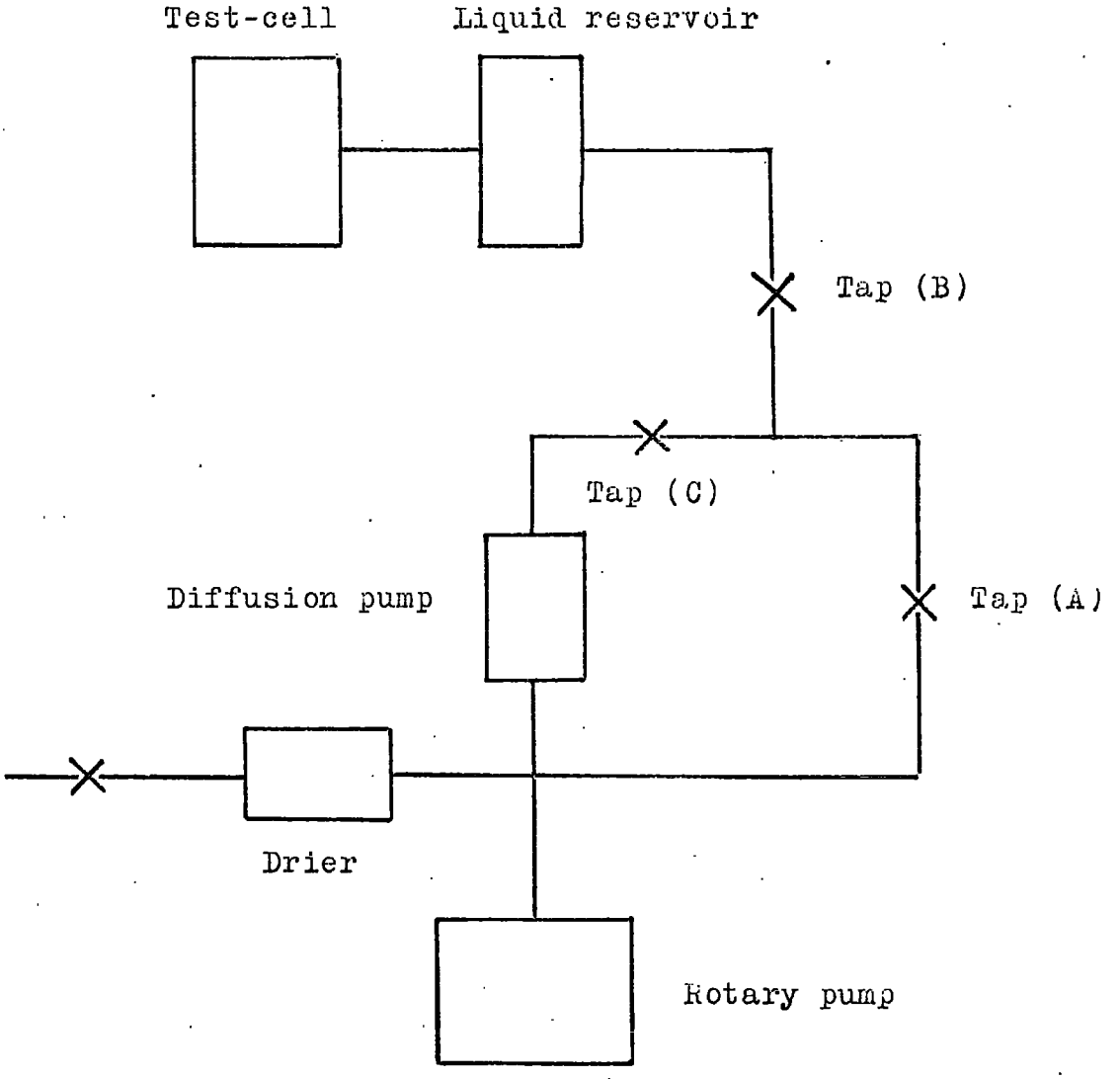

Figure (6.8). Block diagram of test-cell, liquid reservoir, and distillation/degassing system.

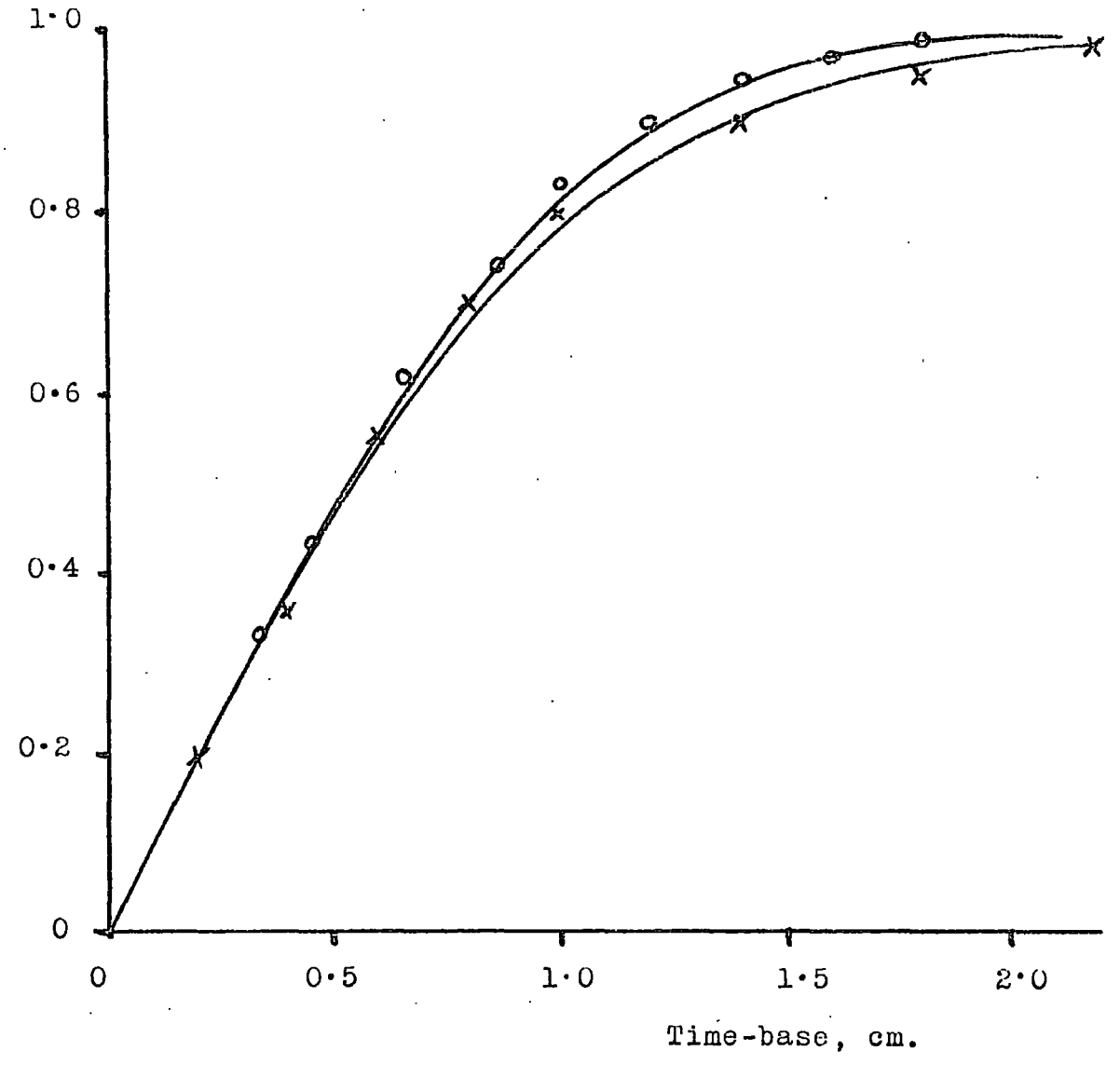

Figure(6.9). Transients observed using a) freshly degassed hexane (o) and b) the same sample in equilibrium with an air pressure of 200 torr (x).

normalized to unity. It is clear that there is no significant difference in the shapes of these transients, contrary to the predictions of the previous section (6.3.1.).

Further evidence against the mechanism proposed earlier was obtained when using a modification to the equilibration technique. On progressively reducing the equilibration pressure, it was found necessary to minimize the loss, by evaporation, of hexane into the pumping system. The method adopted was to reduce the reservoir temperature to - 80°C while tap (B) was open. This procedure involved the transfer of the entire liquid volume from the test-cell to the reservoir before opening tap (B). It was observed that, under these conditions, an equilibration time of 5 - 10 minutes at 100 torr was sufficient to reduce the signal size from 100 mV to 30 mV. Further, the original signal magnitude could only be regained by equilibration with pressures of 1 torr or less. The major difference between the two techniques, apart from liquid temperature, was that only the latter procedure involved the direct exposure of the electrode surfaces to the gaseous phase.

The work of Glendenning and Bedwell (3) on the absorption of gases by hexane indicates a slight increase in the Bunsen coefficient for temperatures below 20°C. In order to explain the phenomenon described above in terms of an increased oxygen content of the cooled hexane, it would be necessary to postulate a sharp discontinuity in the data of

reference (3), below - 30°C However, even if the Bunsen coefficient were substantially increased at - 80°C, considerable de-gassing of the liquid would occur during subsequent warming to room temperature and transfer to the test-cell. The results obtained using the modified equilibration technique are therefore not consistent with the long-term trapping of carriers by dissolved oxygen.

6.3.3. Conclusions

It is clear that the evidence presented in the previous section (6.3.2.) is more consistent with a surface effect of oxygen, than with the volume effect postulated earlier (section 6.3.1.). The former explanation of the reduction in signal magnitude due to the presence of oxygen is also supported by the observed reduction in photo-sensitivity caused by the oxidation of aluminium cathodes (section 5.4.1.).

The influence of surface effects on the signal magnitude is discussed further in section 7..2. Of more immediate importance, however, is the deduction to be made from the experimental evidence, that a volume oxygen-effect is not responsible for the curvature of the transient. A third mechanism may thus be eliminated from those listed at the commencement of this Chapter.

6.4. THE EFFECT OF A NON-UNIFORM FIELD

The possible effect of a non-uniform field on the calculation of mobility from transit-time measurements was recognized at an early stage in the present investigation (see section 2.3.3.). Appendix 'B'

discusses the errors introduced by non-uniform fields and also describes attempts made, as part of the present investigation, to determine the field-distribution in hexane using a physical voltage probe.

In addition to its effect on the total transit-time, a non-uniform field would be expected to result in departures from the simple transient shape deduced for a uniform field. It will be shown in section 6.4.2. that the experimental shape of the transient may, in the absence of other causes of distortion, be used to determine the actual field distribution. This technique, using the injected charge-layer as a moving electronic probe, will be applied to a typical transient (section 6.4.3.), for which the field distribution, potential profile, and relative space-charge density will be deduced. The implications of the results so obtained will be discussed in section 6.4.4., as will the implicit assumption that the shape of the transient is due solely to a non-uniform field.

Before proceeding with this exercise, however, the effect of the injected charge-layer on the uniformity of the applied field must first be considered. Section 6.4.1. shows that, under the present experimental conditions, the distortion of the transient due to the field of the injected charge-layer is small compared with the observed departures from the ideal trace-shape.

6.4.1. Distortion of the transient due to the field of the injected charge-layer

Consider a disc-shaped layer of injected charge, having

negligible thickness and area A, situated between the electrodes with its plane parallel to the electrode surfaces. The space-charge of the injected layer gives rise to a difference in field strength, ΔE, between the two faces of the charge-layer, as shown in figure (6.10). The difference in field, ΔE, is given by:

$$\Delta E = q/K.\varepsilon_o.A \quad \ldots\ldots\ldots\ldots\ldots\ldots \quad (14)$$

where q is the total injected charge

and $K.\varepsilon_o$ is the permittivity of the liquid.

Since the field at the leading face of the charge-layer is greater than that at the trailing face, there will be corresponding differences in velocity and transit-time for the two faces. The difference in transit-time $\Delta\tau$ is given by:

$$\Delta\tau/\tau = \Delta E/E_a \quad \ldots\ldots\ldots\ldots\ldots\ldots\ldots \quad (15)$$

provided that $(\Delta E)^2$ is small compared with E_a,

where E_a is the applied field

and τ is the mean transit-time of the charge-layer.

The magnitude of the effect may be estimated by substituting experimental values of q, K, A and E_a in equations (14) and (15). The calculated degrees of distortion for three particular experimental situations are expressed below in terms of the factor $\Delta\tau/\tau$:

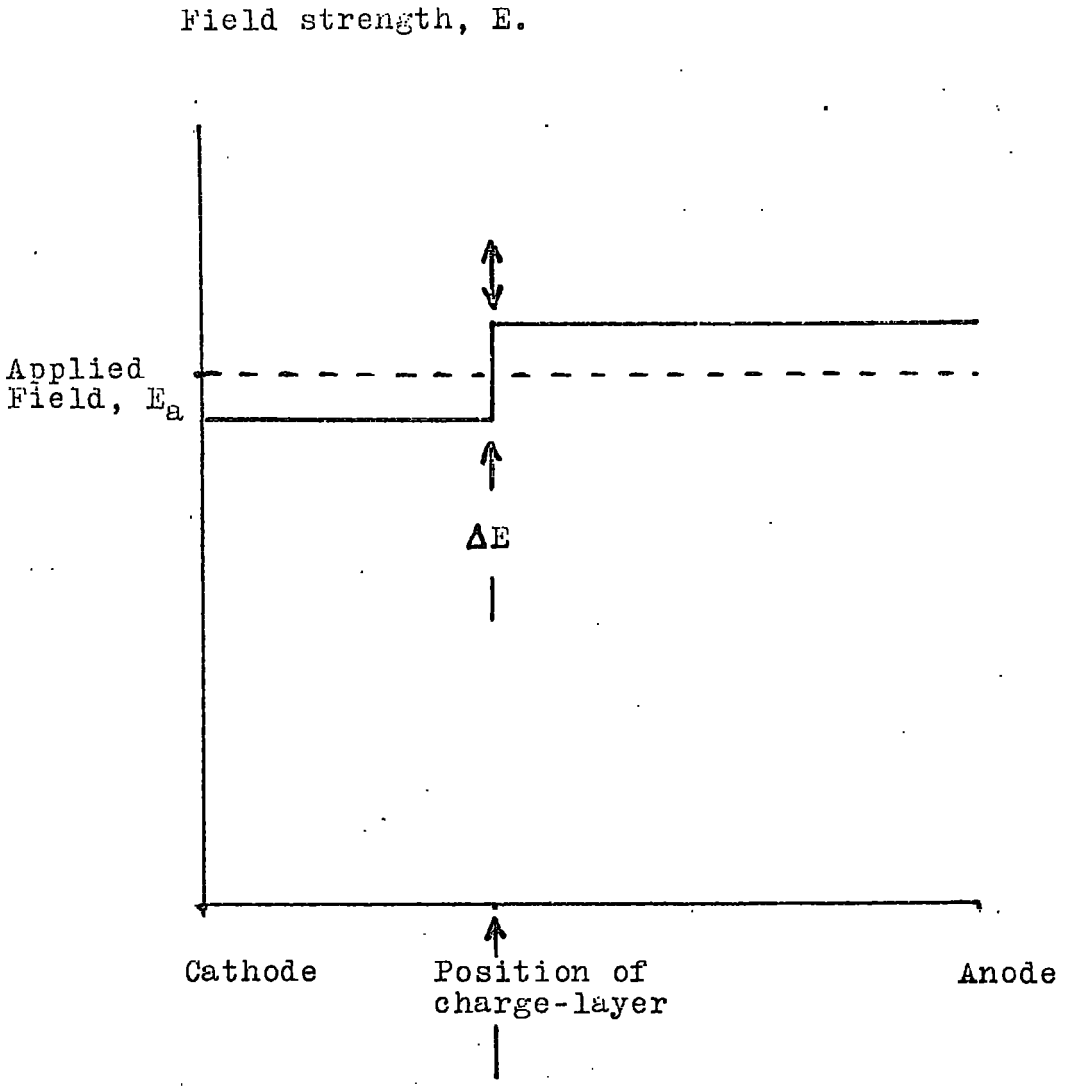

Figure (6.10). The electric field, ΔE, due to the injected charge-layer.

a) Cell 'D1' ('long' flash-source) : $\Delta\tau/\tau \doteq 0.2$

b) Cell 'D2' ('long' flash-source) : $\Delta\tau/\tau \doteq 0.02$

c) Cell 'D2' ('short' flash-source) : $\Delta\tau/\tau \doteq 0.007$

It is evident from these examples that the field of the injected charge-layer causes only slight distortion of the current-transient. Even for the case $\Delta\tau/\tau = 0.2$, the trace-curvature would be restricted to the region ($\tau \pm 0.1\tau$) which is small compared with the region of distortion exhibited by the typical transient shown in figure (6.11). The effect of the injected charge-layer on the shape of the current-transient will therefore be neglected in the discussion which follows.

6.4.2. The relationship between instantaneous current and local field strength.

Consider a negligibly thin negative charge layer situated, at time t, between two plane parellel electrodes, at a distance x from the cathode. Let the total charge of the layer be q and the local field strength be E(x). A small displacement δx of the charge layer towards the anode generates an instantaneous current i(t) in the external circuit. By equating the energy change in the external and internal circuits, we have:

$$q.E(x).\delta x = V_a.i(t).\delta t \quad \ldots\ldots\ldots\ldots\ldots (16)$$

where V_s is the applied voltage.

The instantaneous carrier velocity, $\mu.E(x)$, may then be written:

$$\mu E(x) = dx/dt = V_a \cdot i(t)/q \cdot E(x) \quad \ldots\ldots\ldots\ldots \quad (17)$$

where μ is the carrier mobility.

Re-arrangement of equation (17) provides the relationship:

$$E(x) = \left[V_a \cdot i(t)/\mu \cdot q \right]^{\frac{1}{2}} \quad \ldots\ldots\ldots\ldots\ldots\ldots \quad (18)$$

Thus a quantity E'(x), proportional to the local field, may be derived as a function of t from the instantaneous current i(t) in the external circuit. Since the carrier velocity dx/dt is itself proportional to E(x), graphical integration of the function $\left[i(t) \right]^{\frac{1}{2}}$, with respect to t, provides the relationship between x and t for the charge layer. With the aid of this information E' (x) may be plotted as a function of x. Integration of E'(x) with respect to x enables the constant of proportionality between E'(x) and E(x) to be calculated, since:

$$\int_0^d E'(x).dx = \int_0^d k_1 . E(x).dx = k_1 V_a \quad \ldots\ldots\ldots\ldots \quad (19)$$

Integration of E(x) then gives the potential profile V(x), while differentiation allows the charge distribution ρ (x) to be deduced, according to the following relationships:

$$V(x) = \int_0^x E(x).dx \quad \ldots\ldots\ldots\ldots\ldots\ldots \quad (20)$$

$$\rho(x) = -\frac{\varepsilon}{4\pi} \cdot \frac{dE(x)}{dx} \quad \ldots\ldots\ldots\ldots\ldots\ldots \quad (21)$$

Once E(x) is known, of course, the true carrier mobility may be determined by the method indicated in Appendix B.

The procedure involved in the conversion of the integrated current transient to the functions E(x), V(x), and $\rho(x)$ is illustrated in section 6.4.3., by its application to a particular oscilloscope trace.

6.4.3. Example of the interpretation of the trace-shape in terms of a non-uniform field distribution.

Figure (6.11) shows a typical oscilloscope trace obtained during the course of the measurements described in Chapter 5. The trace has been normalized to unit amplitude and unit transit time. The transit time chosen for normalization corresponds to the parameter τ_m, defined earlier (section 4.3.1.).

Differentiation of the trace with respect to the normalized time t' results in figure (6.12), which is a plot of $k_2 . i(t')$ versus t', where k_2 is a constant, depending on the parameters of the integrating circuit.

The quantity $\left[k_2 . i(t')\right]^{\frac{1}{2}}$, equal to E'(x) in equation (19), is plotted against t' in figure (6.13).

Integration of figure (6.13) with respect to t' provides the shape of the displacement versus time curve for the charge-layer, since the carrier velocity is proportional to $\left[k_2 i(t')\right]^{\frac{1}{2}}$. The integrated curve is shown in figure (6.14), with the ordinate normalized to the condition:

$$x' = x/d = 1, \text{ for } t' = 1 \quad \ldots\ldots\ldots\ldots\ldots \quad (22)$$

where d is the electrode separation.

With the aid of figure (14) the plot of $E'(x)$ versus t' - figure (6.13) - may be converted into a plot of $E'(x)$ versus x', as shown in figure (6.15). The area under figure (15) is used to calculate the constant k_1, which enables the ordinate to be re-calibrated in terms of $E(x')$.

Figures (6.16) and (6.17) show the integrated and differentiated forms of figure (6.15), representing respectively the potential profile, $V(x')/V_a$, and the space charge density $\rho(x')$.

The general conclusion to be drawn from figures (6.15) - (6.17) inclusive is that the curvature of the oscilloscope trace could be explained by the presence of a positive space-charge region extending into the liquid from the anode. The decreasing field experienced by the injected charge-layer in its motion towards the anode would then result in the observed decay of the current transient and the consequent curvature of the oscilloscope trace.

The calculation of the carrier mobility from the transit-time, corrected for the effect of the non-uniform field, may be approached as suggested in Appendix B, using the potential profile of figure (6.16). Alternatively, in this particular case, the field distribution of figure (6.15) may be used in conjunction with the oscilloscope trace to determine the carrier mobility in a region of constant field strength. The linear regions of figures (6.11) and (6.15) correspond to the movement of the charge-layer in the neighbourhood of the cathode, when both the

instantaneous current i(t) and the local field E(x) are constant. Substitution of the appropriate values of i(t-) and E(x) in equation (18) may be used to obtain the true value of μ :

$$\mu = V_a\, i(t)/q.E^2(x) \qquad \ldots\ldots\ldots\ldots\ldots\ldots \quad (18)$$

The oscilloscope trace of figure (6.11) is redrawn in figure (6.18) to illustrate the parameters $V_s(max)$, τ_i, and τ_m used in this and earlier chapters. Reference to this diagram shows that the initial value of i(t) is given by:

$$i(t) = C_{eff}.dV_s/dt = C_{eff}.V_s(max)/\tau_i \qquad \ldots\ldots\ldots\ldots \quad (23)$$

where C_{eff} is the effective integrating capacitance.

The value of E(x) corresponding to the initial current may be related to the applied field E_a by a constant k_3:

$$E(x) = k_3.E_a = k_3V_a/d \qquad \ldots\ldots\ldots\ldots\ldots\ldots \quad (24)$$

The total injected charge is simply:

$$q = C_{eff}.V_s(max) \qquad \ldots\ldots\ldots\ldots\ldots\ldots \quad (25)$$

Combining equations (18) and (23) - (25) inclusive, we have:

$$\mu = \mu_i/k_3^2 \qquad \ldots\ldots\ldots\ldots\ldots\ldots\ldots\ldots \quad (26)$$

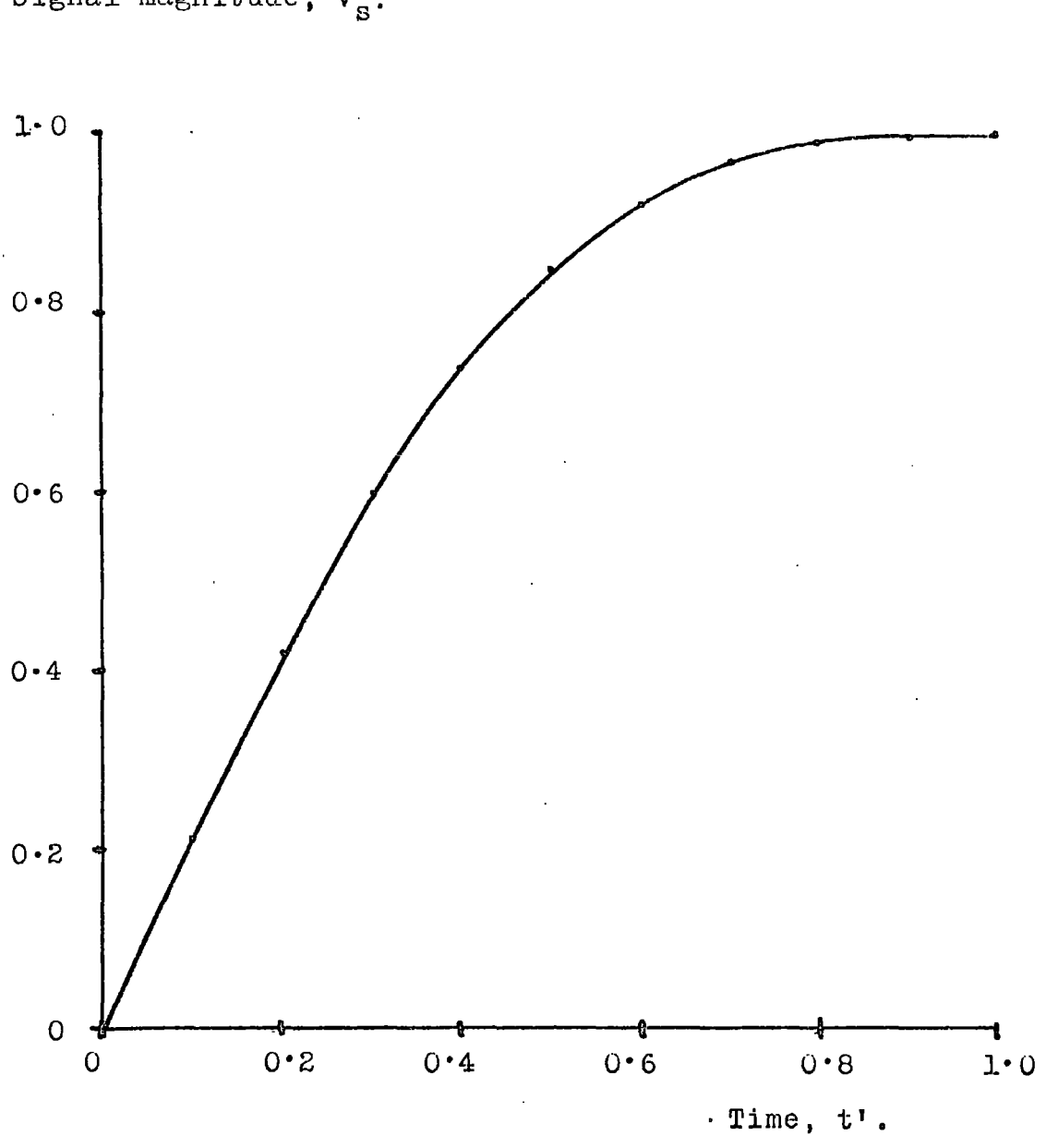

Figure (6.11). Typical transient, showing the extent of the region of distortion.

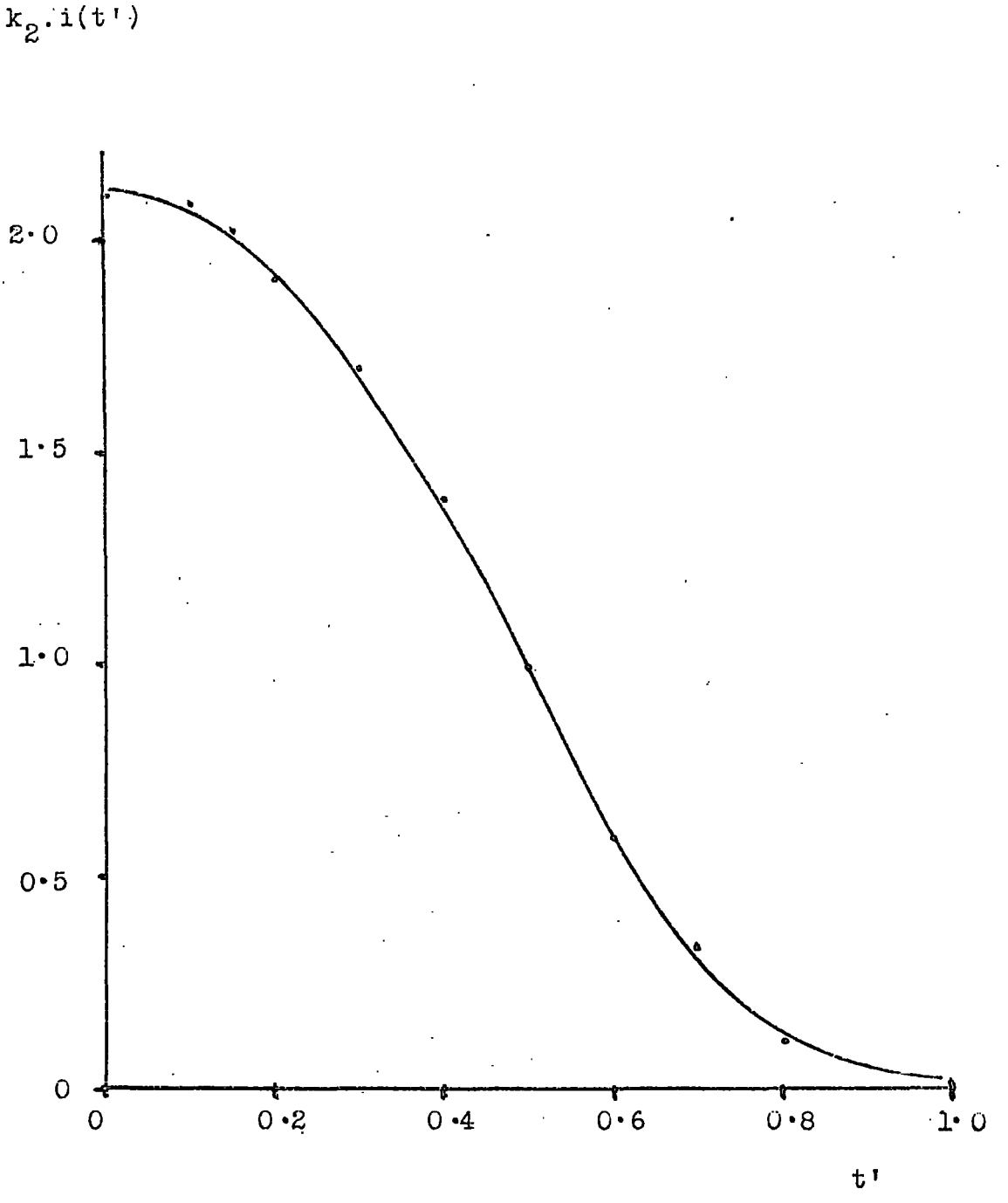

Figure (6.12) Differentiated form of figure (6.11).

$$E'(x) = \left[k_2.(t')\right]^{\frac{1}{2}}$$

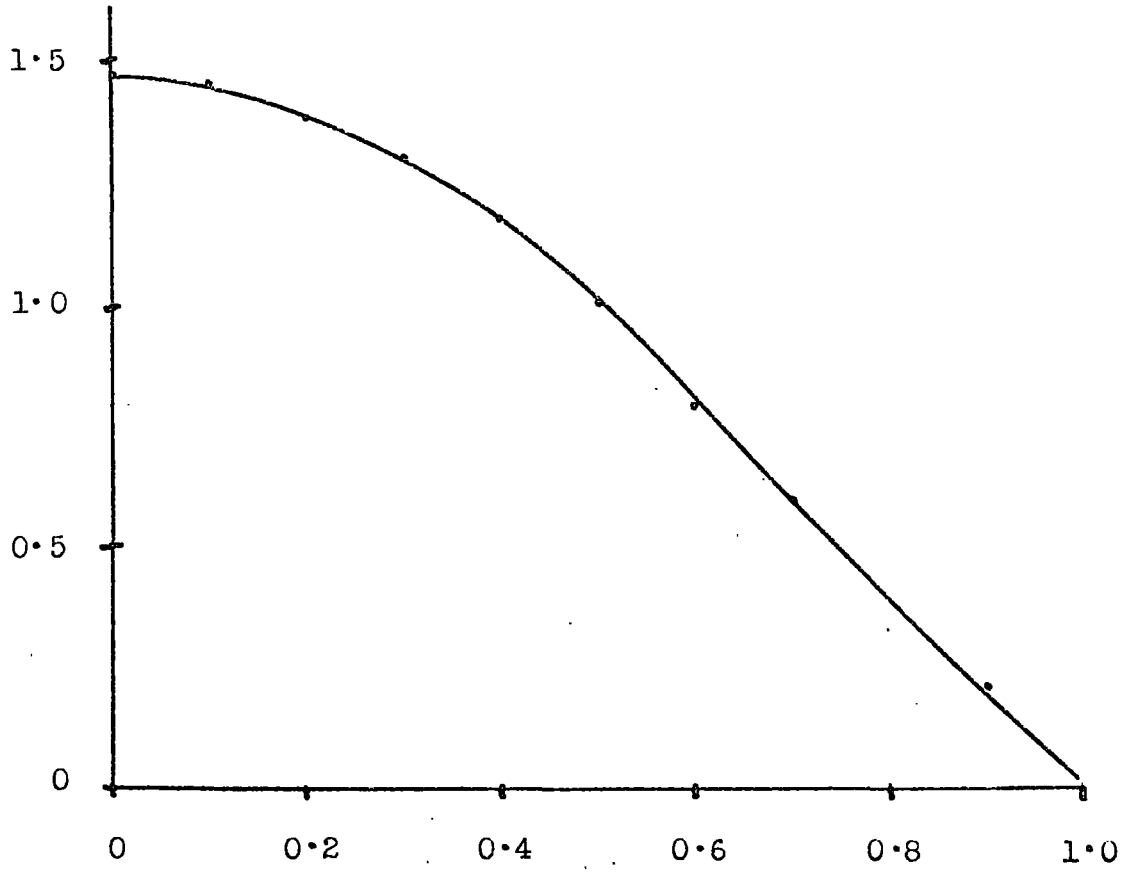

Figure (6.13). Variation of E'(x) with t', derived from figure (6.12).

$$\int_0^{t'} \left[k2.i(t')\right]^{\frac{1}{2}} .dt' \qquad x' = x/d$$

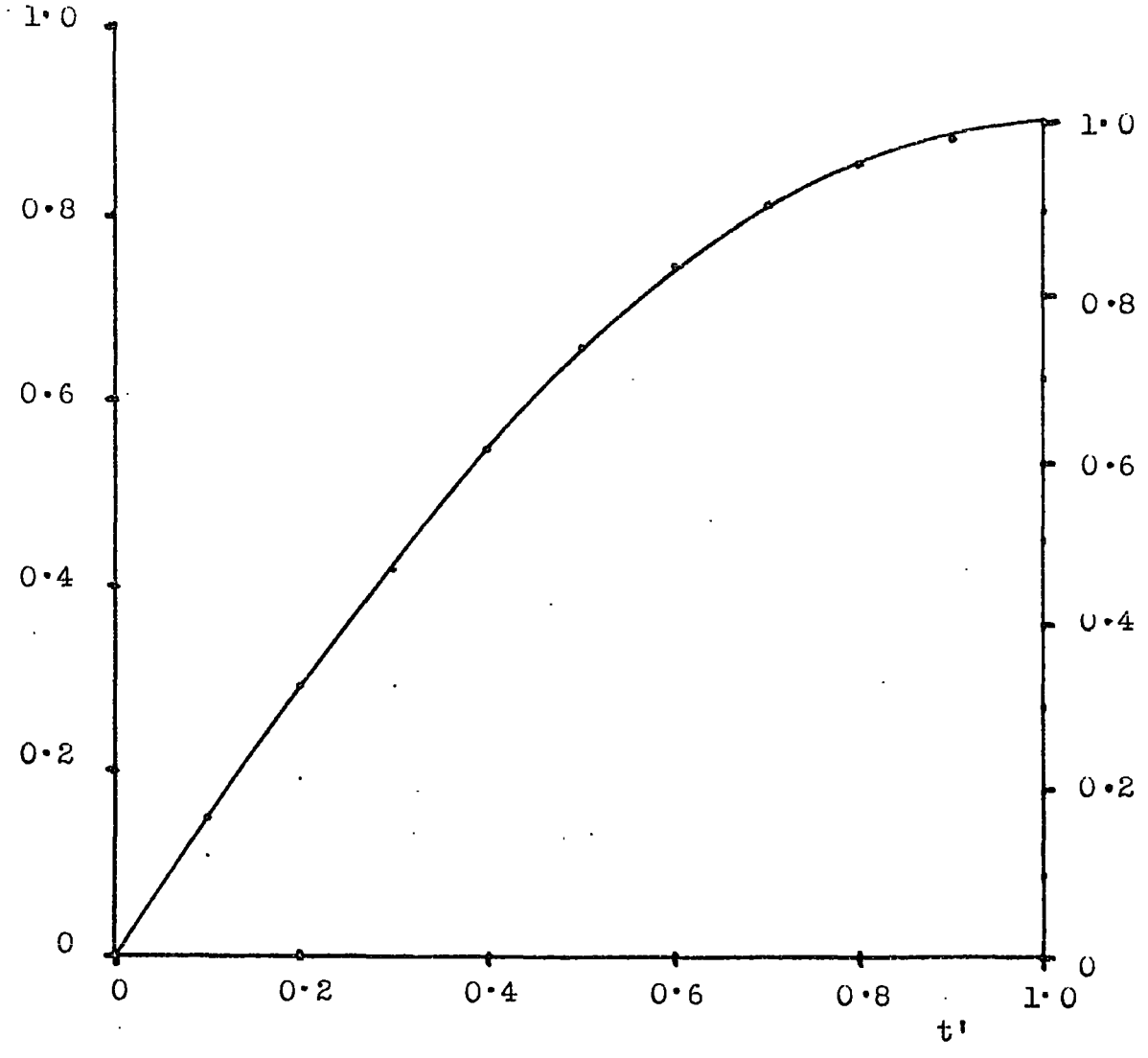

Figure (6.14). Integrated form of figure (6.13), providing the relationship between x' and t'.

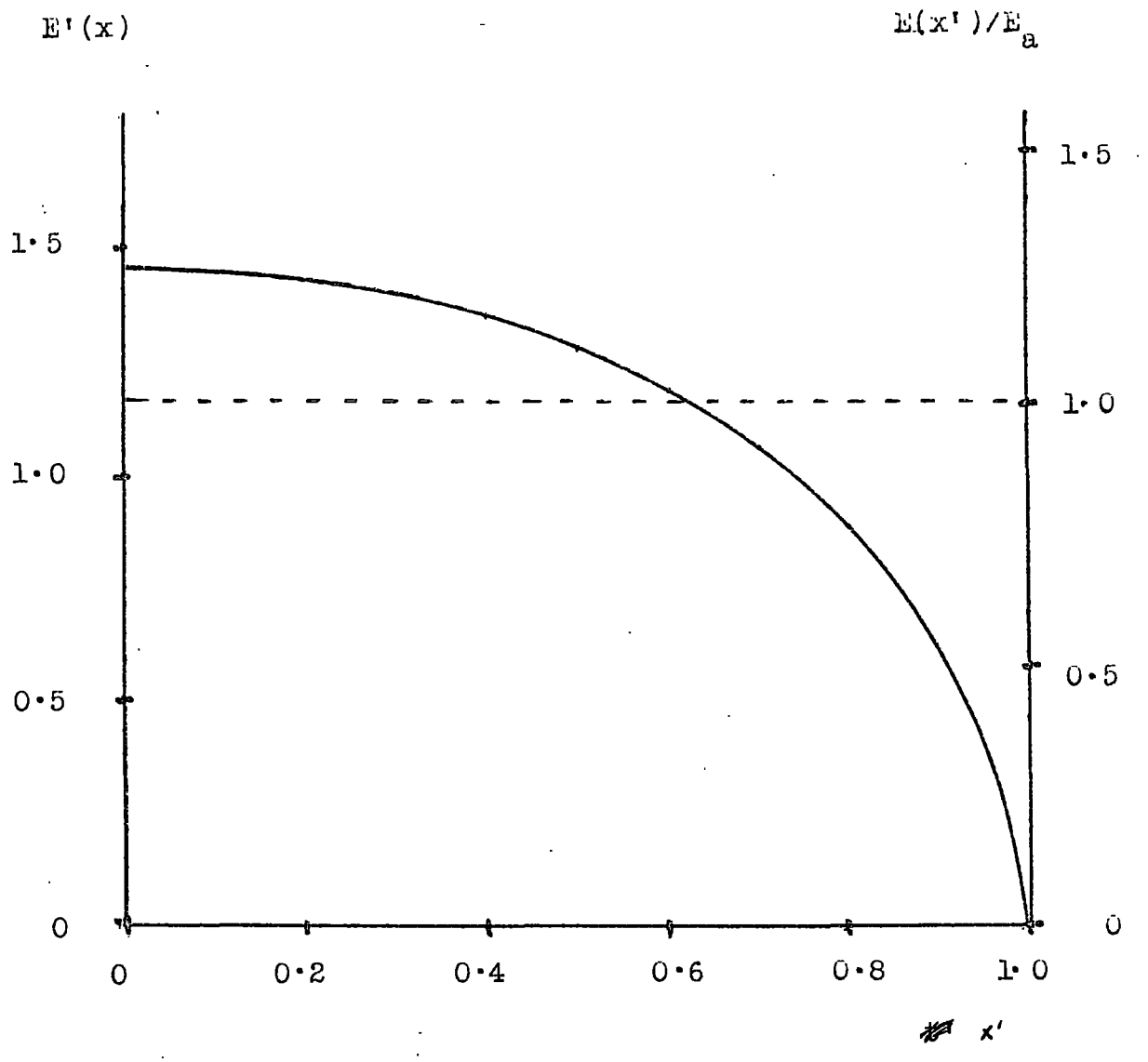

Figure (6.15). Variation of $E'(x)$ with x', derived from figures (6.13) and (6.14). The right-hand ordinate is calibrated in terms of the normalized local field, $E(x')/E_a$, where E_a is the applied field (broken line).

$\int_0^{x'} E(x').dx'$ $\qquad V' = V(x')/V_a$

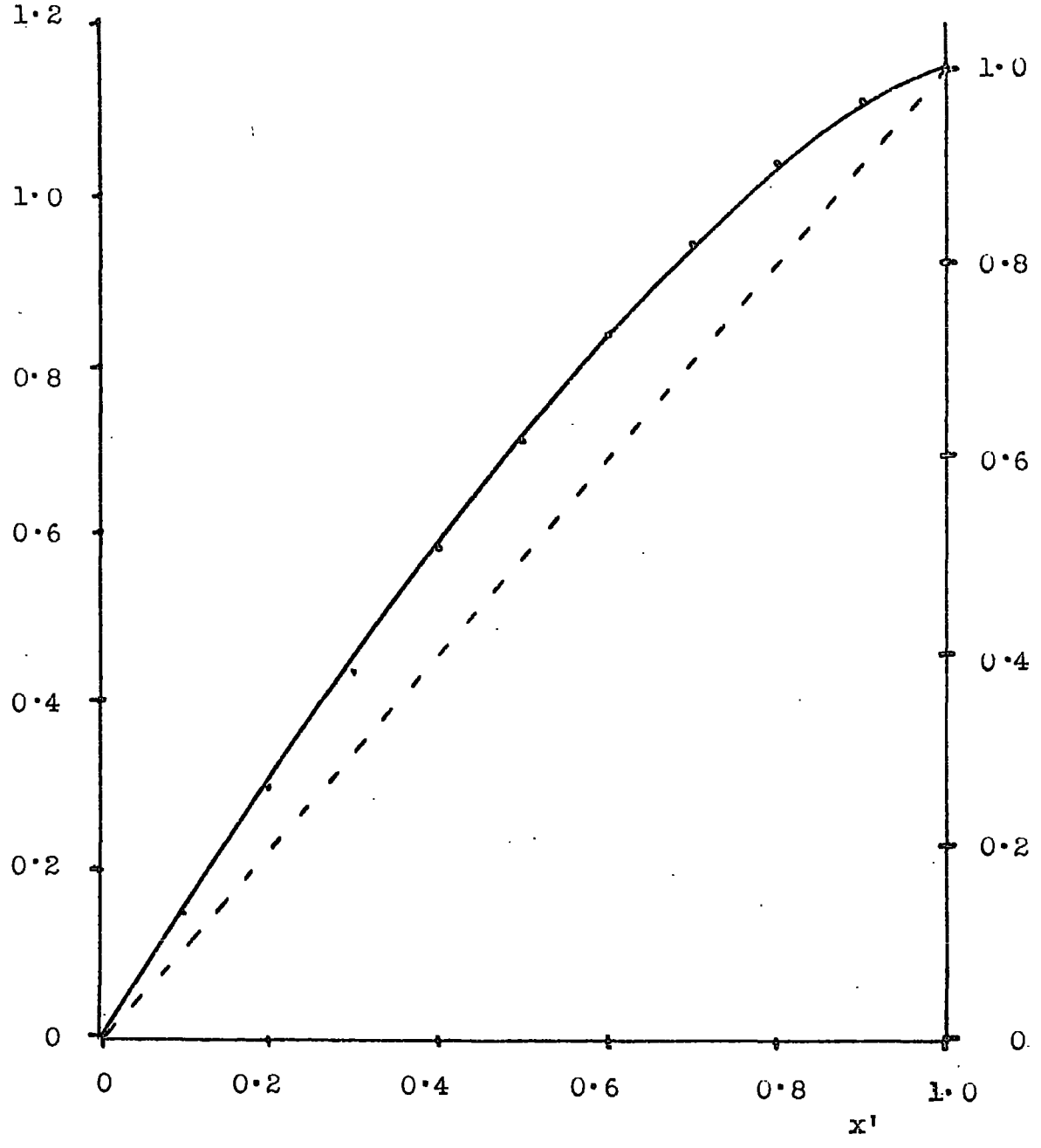

Figure (6.16). Integrated form of figure (6.15). The right-hand ordinate is calibrated in terms of the normalized local potential, $V(x')/V_a$. Broken line : uniform potential profile.

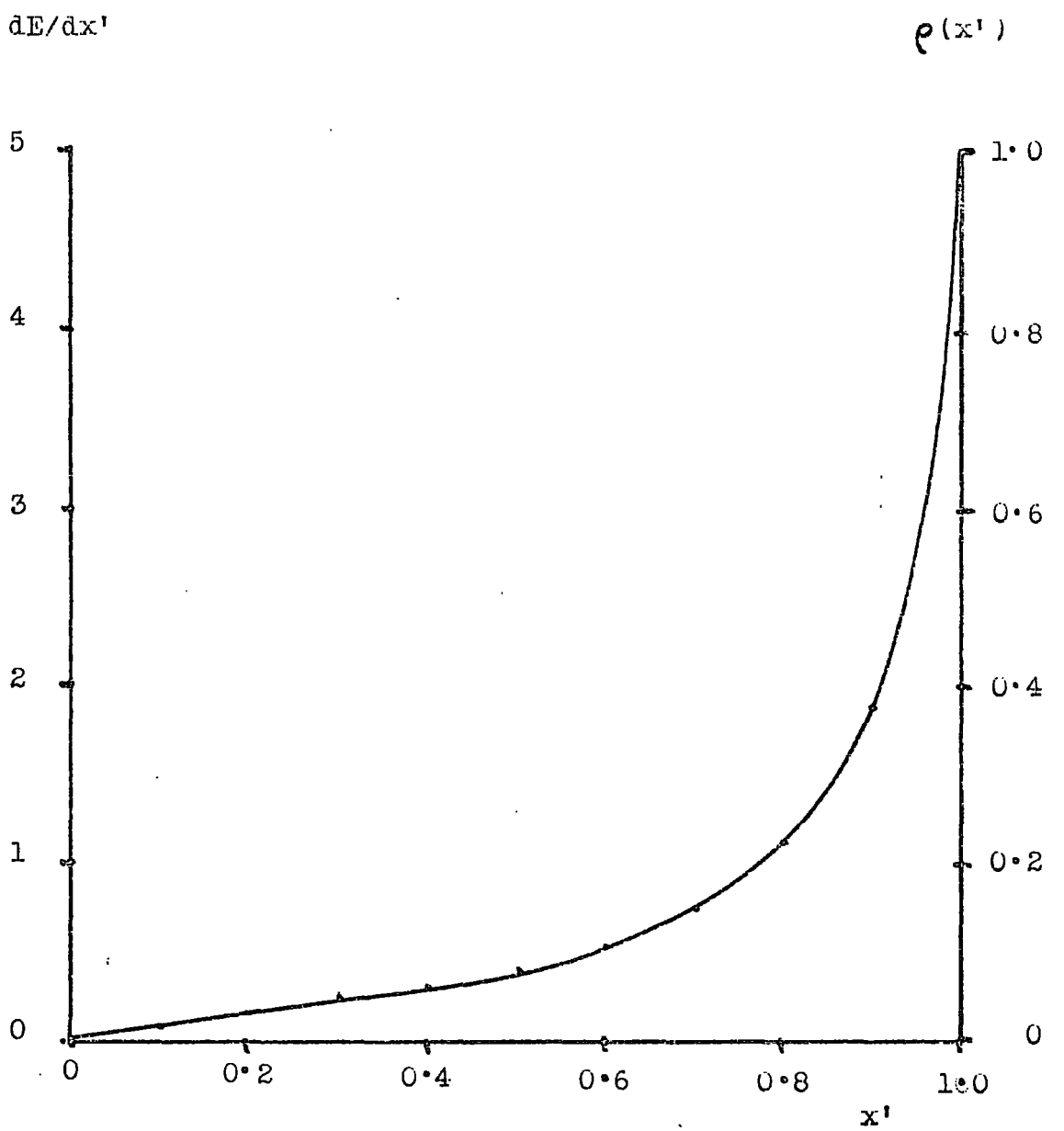

Figure (6.17). Integrated form of figure (6.16). The right-hand ordinate is calibrated in terms of the normalized space-charge density, $\rho(x')$.

Signal magnitude, V_s.

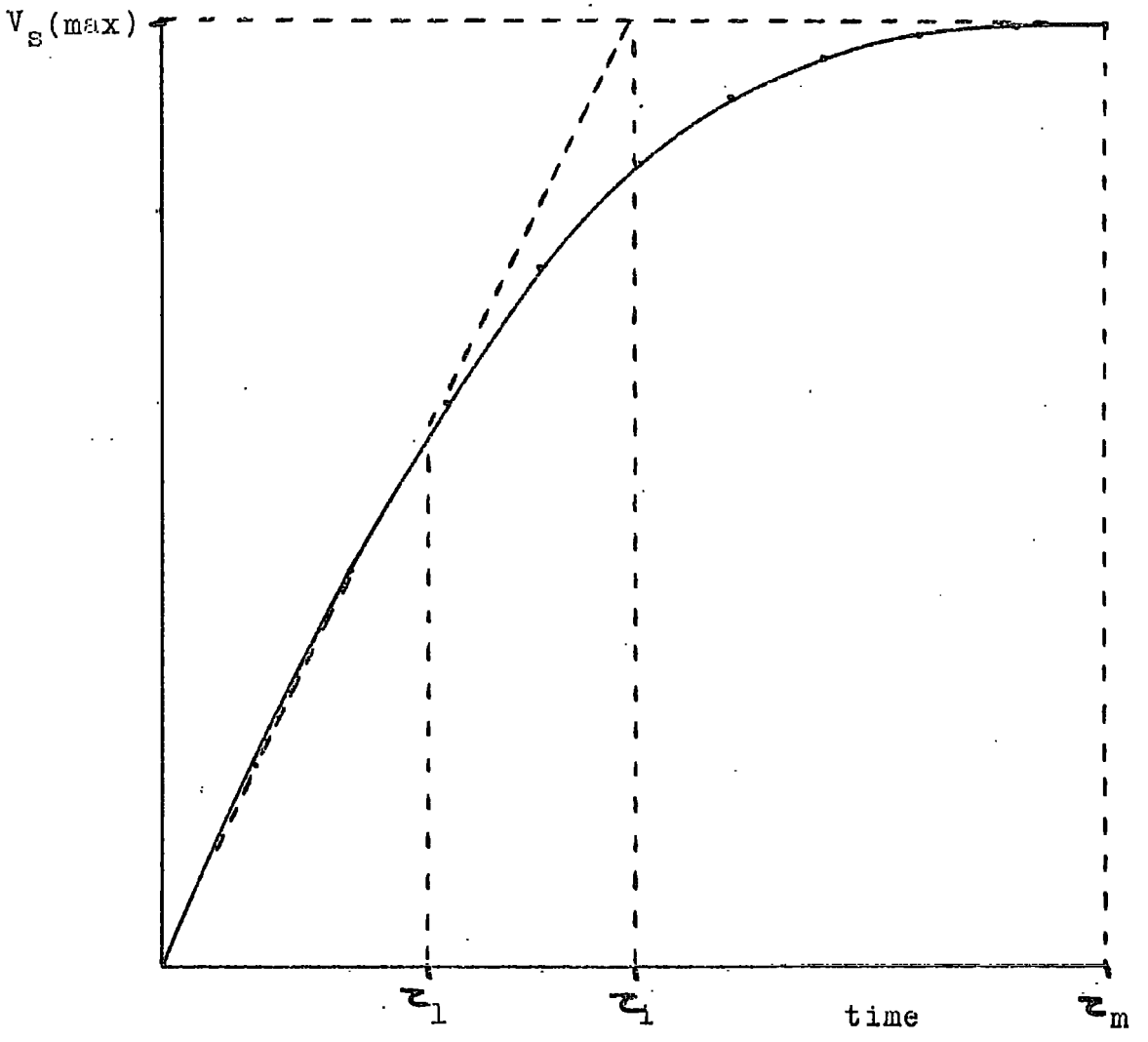

Figure (6.18). Illustration of the parameters V_s(max), τ_l, τ_i, and τ_m for a typical transient.

where μ_i is the apparent mobility deduced from the transit time τ_i, assuming a uniform field throughout the interelectrode region. The value of k_3^2 deduced from figures (6.15) and (6.16) was (1.59 ± 0.05). The assumption that the trace curvature is due to the presence of a positive space-charge near the anode thus leads to a value for the carrier mobility of:

$$\mu = (0.47 \pm 0.02).10^{-3} \text{ cm.}^2/\text{V.sec.}$$

This value is less than that determined from the parameter τ_i, but greater than the value resulting from the uncorrected use of τ_m as the transit time.

6.4.4. Conclusions

Having demonstrated that the curvature of the oscilloscope trace may be explained in terms of a non-uniform field, it is necessary to discuss the proposition that this phenomenon is in fact the cause of the curvature.

The positive space charge responsible for the decreased anode field must be ascribed to the 'dark' current in the test-cell. This deduction is a consequence of the negligible width of the charge-layer compared with the electrode separation (see section 6.1). Any transient space charge associated with the rate of extraction of photo-injected carriers from the liquid at the anode would only be apparent for a similarly insignificant proportion of the transit-time.

The exact mechanism by which a positive space charge could be generated by the 'dark' current is not clear. Two obvious possibilities are (a) the injection of low-mobility positive carriers at the anode, or (b) a rate of electron extraction at the anode which is considerably greater than the generation rate. Whatever the conduction mechanism of the 'dark' current, it would seem reasonable to conclude that a major increase in the latter due to an increased applied field would result in a change in the space charge distribution and hence in the shape of the transient. The parameter τ_i provides a useful indication of the shape of the transient, as may be seen from figure (6.17). The constant relationship of τ_i to the other major features of the transient has already been demonstrated (section 4.3.1.). The values of apparent mobility, μ_i, quoted in Chapter 5 were calculated from the expression $\mu_i = d^2/V_a.\tau_i$ and are therefore themselves strongly dependent on the shape of the transient. The work of Kahan and Morant (4) shows that, for de-gassed hexane, a major increase in the 'dark' conductivity occurs in the range of applied fields used in the present work. The relationship between conduction current and field strength determined by the above workers is shown in figure (1.1). That this increase occurs under the conditions of the present investigation was confirmed by the increase in the direct current level at high fields reported in sections 5.2.2. and 5.4.3. However, the apparent mobility, μ_i, was found to be constant, within the limits quoted in Chapter 5, over the range of applied field 1 - 120 KV/cm. This indicates that the transient shape

and hence the space charge distribution is independent of the magnitude of the 'dark' current.

If the original assumption, that the trace curvature is due to a non-uniform field, is to be maintained, then any associated theory of the 'dark' current mechanism must explain not only the positive space charge at the anode but also the invariance of its shape in a wide region of non-ohmic behaviour.

Alternatively, one may discard the above explanation of the trace curvature and ascribe the effect to some other cause.

6.5. THE EFFECTS OF LIQUID MOVEMENT

There is a considerable amount of published evidence to the effect that conduction processes in dielectric liquids induce movement of the bulk liquid. This 'pumping' phenomenon has attracted considerable attention in recent years, both from the theoretical and experimental standpoints (5). Two papers in particular (6), (7), provide direct evidence that the effect occurs in hexane when carriers are generated in the liquid either by ionization or electron injection. The possibility must therefore be considered that strong coupling between the carriers and the bulk liquid takes place under the present conditions. Given such a process, it is evident that distortion of the injected charge layer could occur due to the flow pattern in the test-cell, and that this distortion could affect the shape of the current transient. It is shown in the following sub-sections that not only does the above process offer a reasonable explanation

of the trace curvature, but it also accounts for two phenomena which cannot easily be explained in terms of any of the mechanisms discussed so far in this chapter.

Two distinct situations are considered in sections 6.5.1. and 6.5.2. These are respectively (a) an equilibrium flow pattern, set up either by the injected charge in a time short compared with the transit-time, or by the 'dark' current prior to the injection of charge; (b) a non-equilibrium flow pattern, set up by the injected charge, varying in form during the transit-time.

6.5.1. An equilibrium flow pattern

For the purposes of analysis, the liquid contained between the electrodes of the test-cell is considered to be flowing in a tube of radius r_o, the axis of which is that of the electrode system. The equilibrium velocity profile $u(r)$ is then given by:

$$u(r) = u(0).(1 - r^2/r_o^2) \quad \ldots\ldots\ldots\ldots\ldots\ldots (27)$$

It will be assumed that $u(0)$ in this case is the true carrier velocity, μE, and that r_o is determined by the cell geometry.

The effect of the velocity profile described by equation (27) is to distort the initially planar charge layer into a paraboloid form with its axis parallel to the direction of motion. Thus the carriers situated near the rim of the charge layer will reach the anode at a later time than those near the axis. It may be shown that the resultant shape of the current transient is described by equations (28) and (29), with the

aid of the parameters α and β:

$$i(t) = \frac{\pi N_a \cdot r_d^2}{\tau} \left(1 - 1/2\alpha\right) \text{ for } 0 \leq t \leq \tau \quad \ldots\ldots (28)$$

$$i(t) = \frac{\pi N_a \cdot r_d^2}{\tau} \left(1 - 1/2\alpha - \alpha\beta(1 - \beta/2)\right) \text{ for } t \geq \tau \ldots (29)$$

where $\alpha = r_o^2 / r_d^2$ ..... (30)

$$\beta = (1 - \tau/t) \ldots\ldots (31)$$

N_a is the charge per unit area of the charge layer;

r_d is the radius of the charge layer:

and τ is the transit time of those carriers for which $r = 0$.

Figures (6.19) and (6.20) show the normalized forms of the transients, together with the corresponding integrated signals, for selected values of α. It is evident that integrated signals for $\alpha = 1$ and $\alpha = 2$ are very similar to those observed experimentally, and that the transient shape is strongly dependent on α in this region. It was therefore decided to test the theory by using cathode masks of different apertures, thus varying α by changing r_d.

Figure (6.21) shows, superimposed, three traces obtained using masks of 8 mm., 4 mm., and 2 mm., diameter, but under otherwise identical conditions. According to the above theory, the variation in α by approximately 16 times should have had a pronounced effect on the trace shape. This was obviously not the case. The apparent value

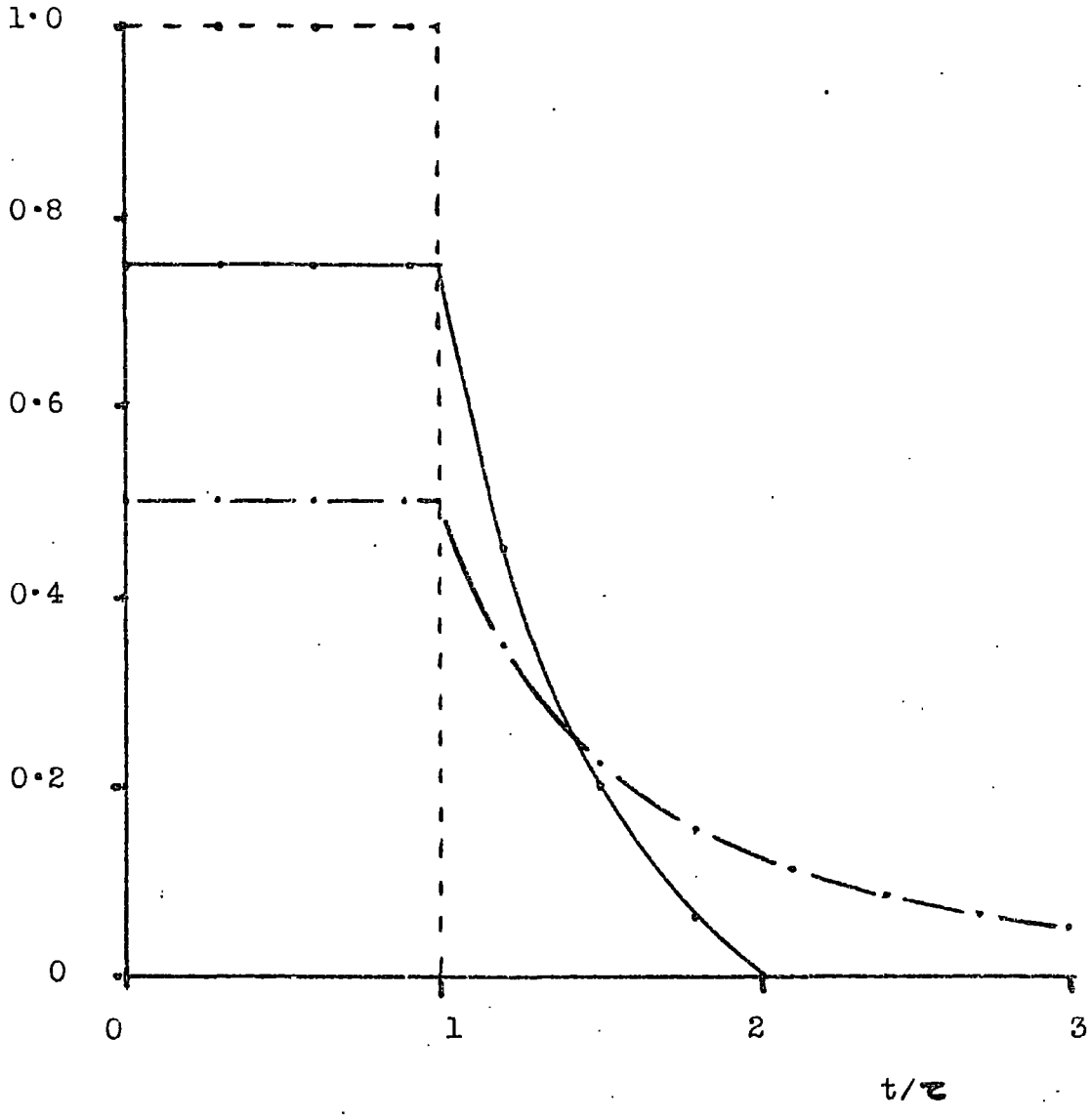

Figure (6.19)..Theoretical current transients for $\alpha \to \infty$ (-•- -•-); $\alpha = 2$ (•——•); and $\alpha = 1$ (•- •- •).

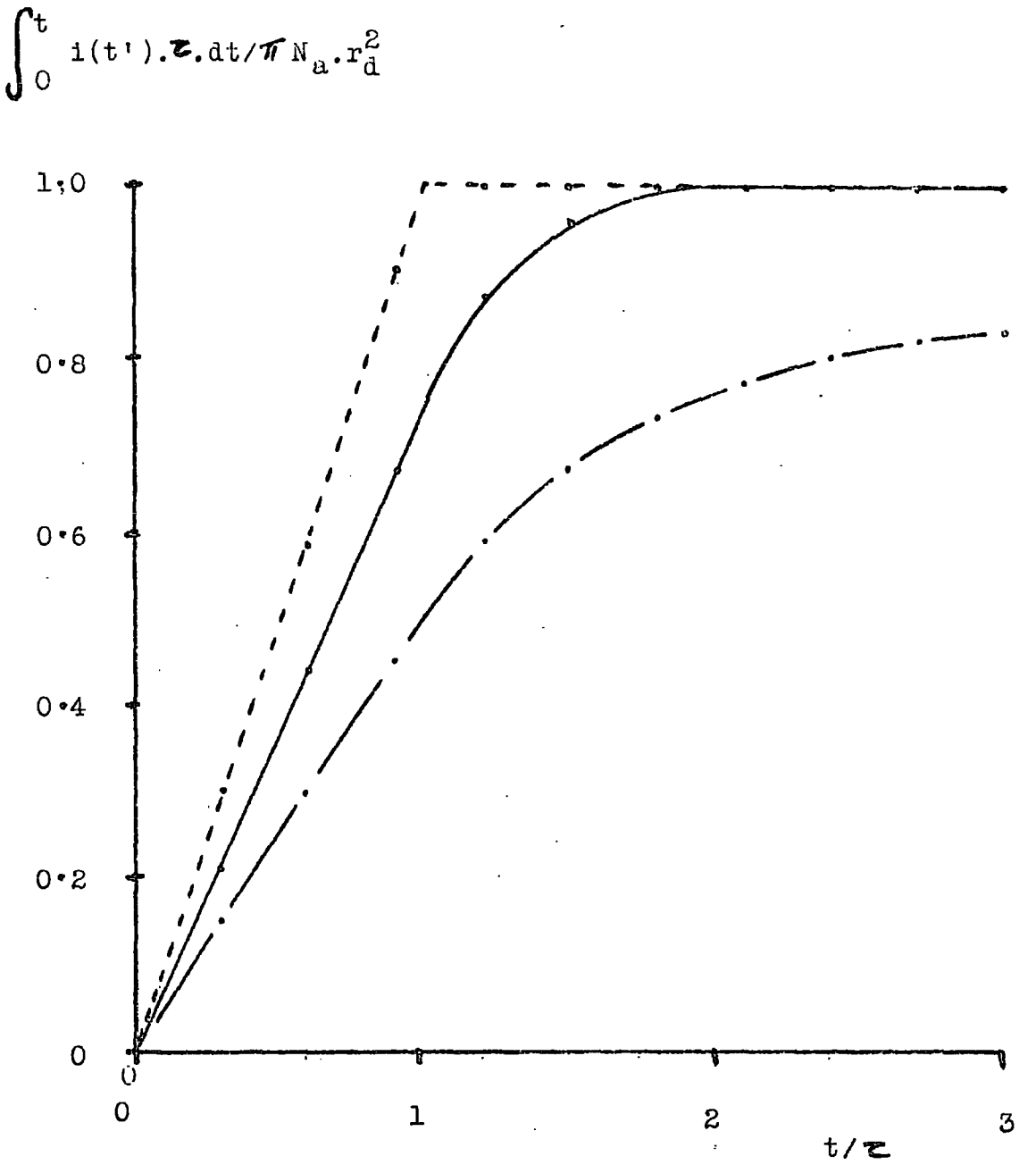

Figure (6.20). Integrated current transients (theoretical) for $\alpha \to \infty$ (- - -); $\alpha = 2$ (——); and $\alpha = 1$ (——).

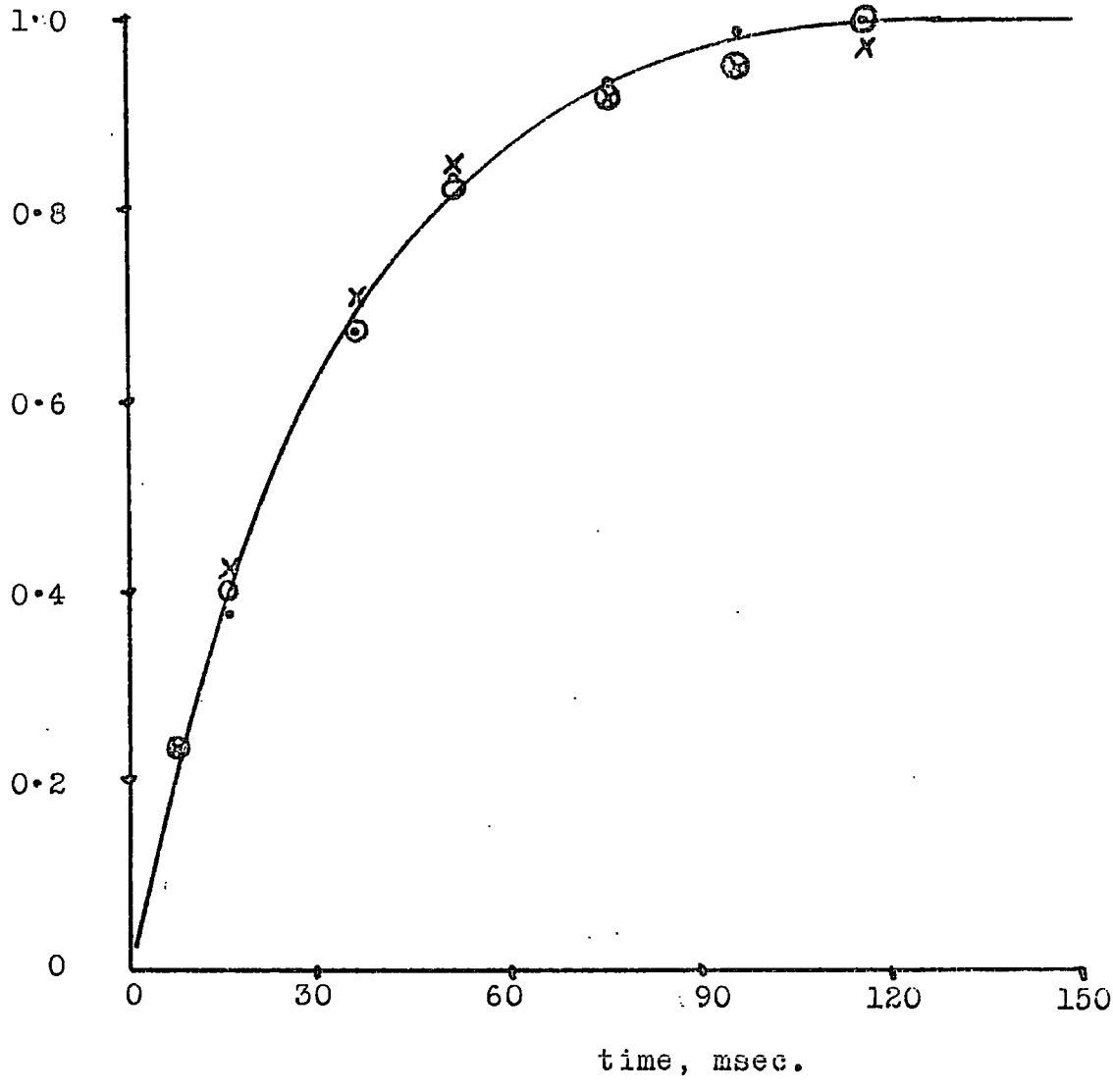

Figure (6.21). Effect of mask aperture diameter on the shape of the integrated transient. Aperture diameters : 8 mm (•); 4 mm (✕); and 2 mm (O).

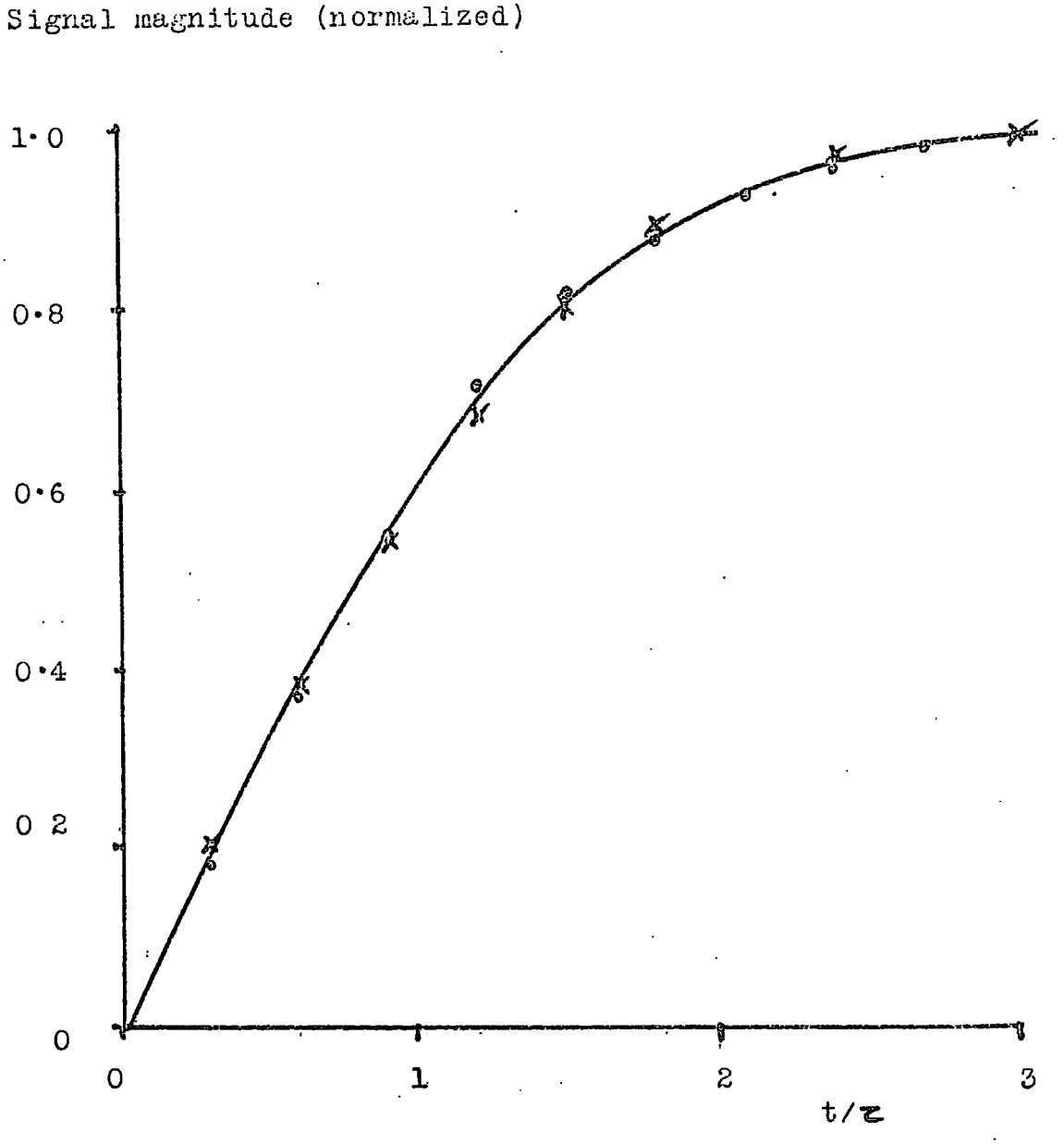

Figure (6.22). Comparison of an experimental transient (×) with the theoretical form, for $\alpha = 1{\cdot}2$ (∘).

of α, deduced from figure (6.21) was independent of r_d and equal to (1.2 ± 0.1). The mean curve of figure (6.21) is compared, in figure (6.22), with the trace shape obtained by substitution of the above value of α in equations (28) and (29). The agreement between the two curves is good, indicating that the general form of the trace curvature may be explained by a mechanism of the type proposed above. Some modification is required, however, to account for the lack of dependence of α upon r_d.

6.5.2. A non-equilibrium flow pattern

The argument set out in the previous sub-section assumed that the flow pattern responsible for the distortion of the signal was in equilibrium and therefore time-independent for the duration of the signal. The failure of the model to predict the variation of the trace shape with the mask diameter indicates that a non-equilibrium modification should be considered.

Consider the velocity profile in the test-cell at the instant of charge injection, neglecting any circulation induced by the dark current. Since only the charge carriers, and those molecules interacting closely with them, are subject to the electrostatic force, there will be a sharp discontiniuty in the velocity profile at $r = r_d$. The resulting viscous forces will tend to entrain and set in motion that part of the liquid defined by $r \geq r_d$. This process will also cause changes in the velocity profile for the region $r \leq r_d$, which will occur during the transit time of the injected carriers.

Assuming that a paraboloid from of the velocity profile is still applicable to the situation (even if only approximately), the redistribution of momentum in the liquid may be described as an increase in r_o with time, from an initial value equal to r_d. The parameter α would then be independent of r_d, but would vary with time, according to:

$$\alpha(t) = 1 + f(t) \quad \ldots\ldots\ldots\ldots\ldots\ldots\ldots\ldots \quad (32)$$

The derivation of f(t) in the above relationship presents a number of difficulties. The most fundamental of these is the lack of detailed information available on the nature of the charge carrier and its interaction with the neutral liquid molecules. It is of course information of this type that determinations of mobility and other carrier properties seek to elucidate. A number of simplifying assumptions may be made to assist in the derivation of f(t), but resulting calculations of the trace shape are tedious and relatively inconclusive, in that the derivation of a curve closely resembling those obtained experimentally does not constitute proof of the theory. This maxim has already been demonstrated in the present chapter (section 6.2). Moreover, it has already been shown that the simple equilibrium flow pattern theory may be fitted easily to the observed traces by using time-independent values of α close to unity. A qualitative analysis of the theory would therefore appear to be more rewarding than a quantitative approach.

The partial success of the equilibrium flow pattern theory suggests that the rate of variation of α is small in relation to the range

of transit times encountered in the present investigation. Thus a mean value of α can be ascribed to a particular trace, which, when substituted in equations (28), (29), agrees well with experimental results. Further, the value of α so determined must be fractionally greater than unity if the rate of increase of α is small. The major effect of the viscous drag will only be apparent in the latter part of the transient.

The effective increase in α during the initial part of the transient would also be expected to produce a slight concave curvature on the rising part of the integrated transient. This corresponds to the slight increase in current as the initially slow-moving peripheral regions of the charge layer are able to increase their velocity due to the changing flow pattern. This effect was not generally observed due to the presence of competing mechanisms such as bulk ionization (section 6.2) which tend to produce a convex curvature during the intitial part of the integrated signal. The effect was, however, observed when using a particularly sensitive photocathode. It is considered that the high charge density so achieved increased the resistance to flow of the bulk liquid through the injected charge layer and therefore increased the rate of change of α. In addition, the particularly high ratio of injected charge to bulk ionization would have helped to eliminate the tendency towards a convex curvature. An example of the type of trace observed under these conditions is reproduced in figure (6.23).

Further experimental evidence, which tends to support the theory under consideration, concerns the variation of injected signal

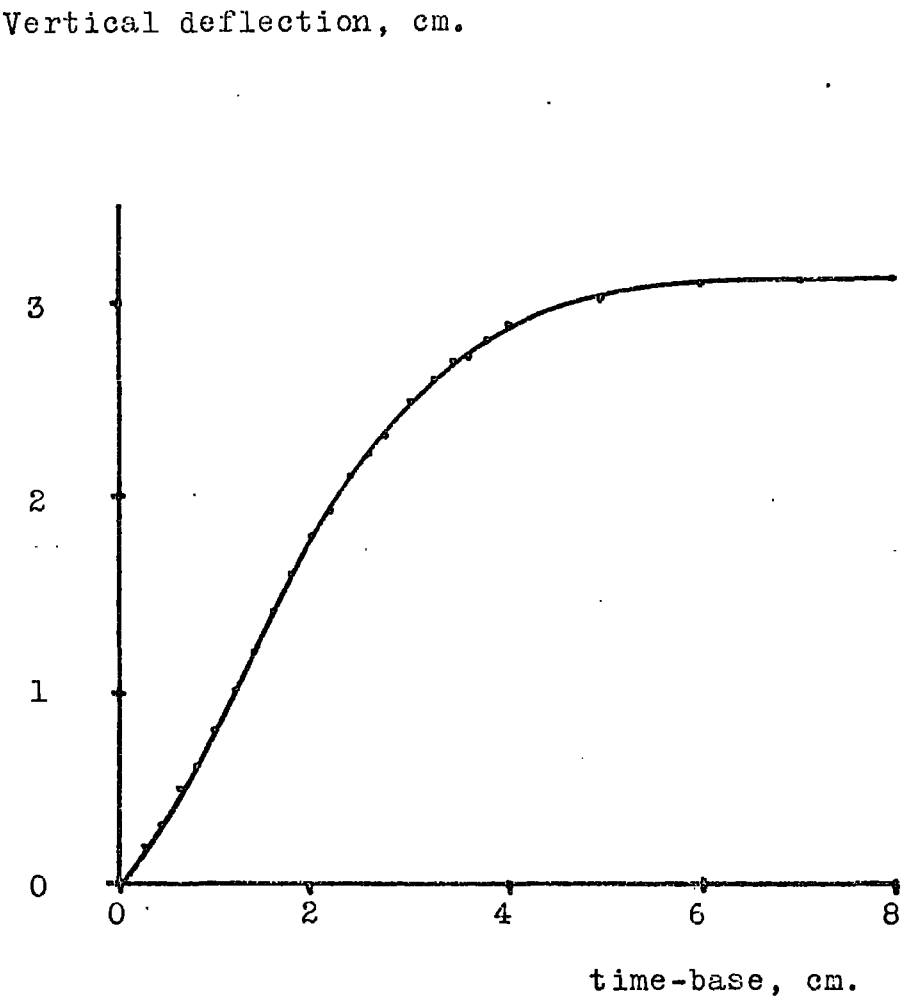

Figure (6.23). Transient exhibiting concave curvature.

magnitude, V_s, with the applied field E_a. It will be recalled that the proportionality between these two quantities was apparently violated at higher fields (section 5.4. 4.). Reference to figure (5.21.) shows that, under the latter conditions, the proportionality of V_s to E_a was maintained for given values of electrode separation, d, but that the gradient $\Delta V_s / \Delta E_a$ decreased with d. This phenomenon was not fully explained by the proportionality of bulk ionization to the electrode separation, but may in fact be ascribed to the effects of viscous drag on the charge layer. The high fields achieved in cell D2 were due in part to the use of small electrode separations, with a consequent reduction in the transit time. In view of the slow variation in α, the mean value of this parameter which could be ascribed to such traces would tend to unity as the transit time was decreased. Examination of figure (6.20) shows that as α tends to unity the tail of the current transient becomes very long. The rate of rise of the integrated signal is correspondingly slow and is eventually nullified by the decay time-constant of the integrating circuit. Thus the full signal magnitude may never be achieved in such a case, or it may simply not be recorded, since the oscilloscope time-base would normally be adjusted to include only the range $0 \leq t \lesssim 4\tau_i$. The net result of decreasing the transit time by decreasing d would therefore be an apparent reduction in the signal magnitude. The effect would be most noticeable at high fields when, as in the present investigation, these were synonymous with short transit times.

To sum up: the viscous drag effect provides a good qualitative explanation of the trace curvature when allowance is made for a non-equilibrium flow pattern within the test-cell. The theory is strengthened considerably by its explanation of two apparently unrelated phenomena observed under extreme conditions.

6.5.3. The effect of viscous drag on the measurement of transit time and mobility

The conclusion reached in Chapter 5, that there was no detectable increase of carrier mobility with applied field, was based on a somewhat arbitrary method of determining the transit time from the integrated transient. The parameter τ_i was defined in section 4.3.1., as were two other features of the transient, τ_1 and τ_m. Figure (6.18) illustrates these definitions. The choice of τ_i as the measured quantity was originally due to the ease and accuracy with which it could be determined from the oscilloscope trace. The parameter was used exclusively in later measurements after a constant relationship between τ_i, τ_1 and τ_m had been established for fields up to 10 KV/cm. (section 4.3.1.).

Comparison of figure (6.18) with figure (6.19) shows that the arrival of the axial carriers at the anode causes a discontinuity at a point on the integrated transient previously defined by τ_1. Substitution of τ_1 in the relation:

$$\mu_1 = d^2/V_a \cdot \tau_1 \qquad \ldots\ldots\ldots\ldots\ldots\ldots\ldots (33)$$

therefore yields the mobility of these carriers.

Since the influence of the transient flow pattern on the axial carriers is assumed to be small, μ_1 must be regarded as the mobility of the charge carriers themselves.

It is therefore important, in view of the conclusions reached in Chapter 5, to consider the relationship between τ_1 and τ_i for fields in excess of 10 KV/cm.

Figure (6.24) illustrates the theoretical forms of the integrated transient for several time-independent values of α. The curves represent the approximate shapes of transients for values of α averaged over the duration of the transient. The transients have been normalized with respect to magnitude, and the time scale is in terms of the parameter τ_1. It is evident from the figure that as α decreases from ∞ to 1, the ratio τ_i/τ_1 increases from 1 to 2, provided that the full signal magnitude is always realized. However, as discussed in section 6.5.2. the full signal height may be masked or not recorded when short transit times are involved. Thus, as the transit time is progressively reduced, the ratio τ_i/τ_1 will at first increase in the range $1 < \tau_i/\tau_1 < 2$ due to the decrease in α. As α tends to unity, however, τ_i/τ_1 may appear to decrease again. Figure (6.25) shows the variation of τ_i/τ_1 with τ_i over the range of values observed experimentally. As predicted by the simplified model presented above, the values of τ_i/τ_1 all lie between 1 and 2. In fact over 90% of the experimental points lie within

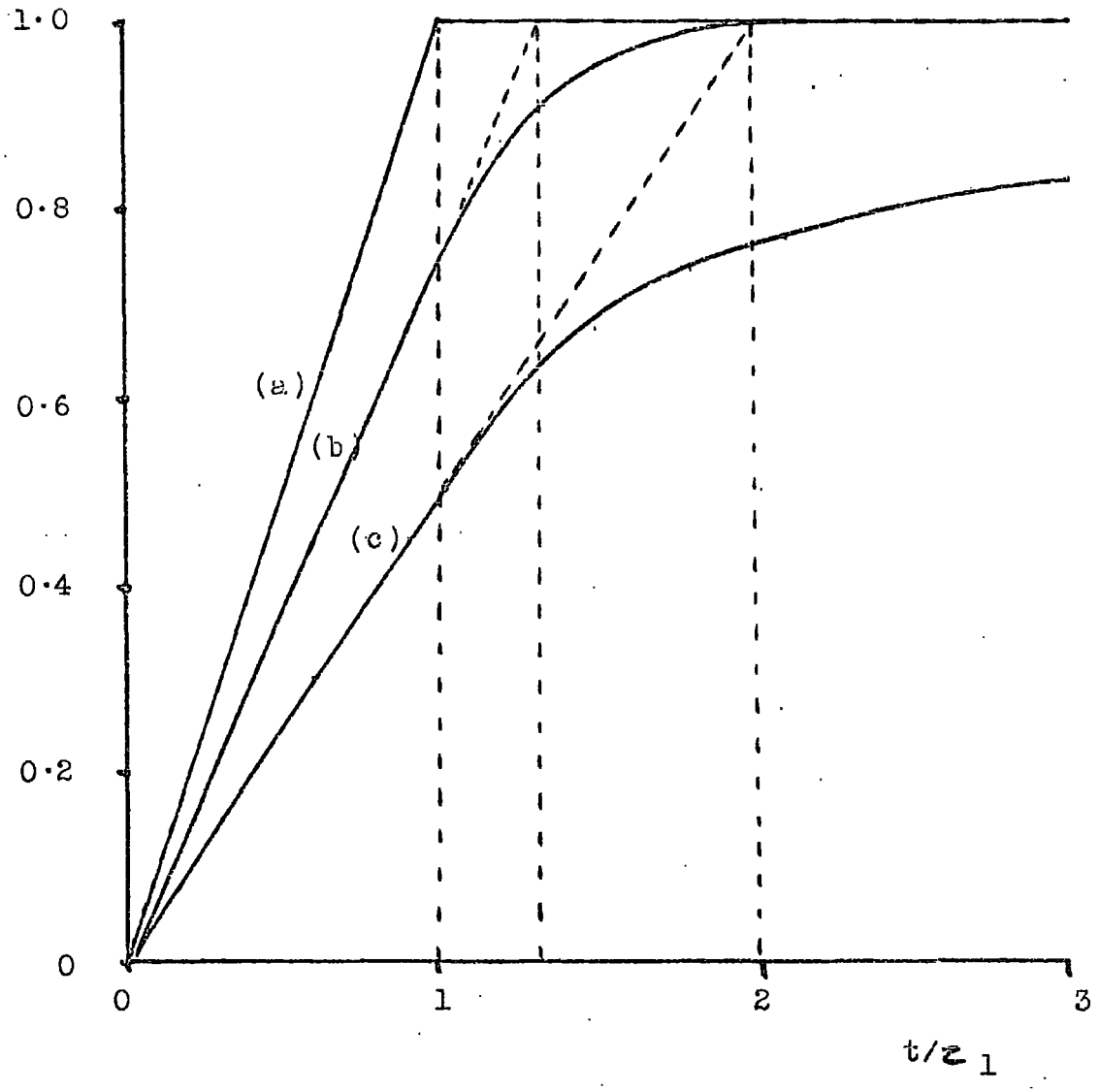

Figure (6.24). Integrated current transients (theoretical), for (a) $\alpha \to \infty$; (b) $\alpha = 2$; and (c) $\alpha = 1$, showing the variation of τ_i / τ_1 with α.

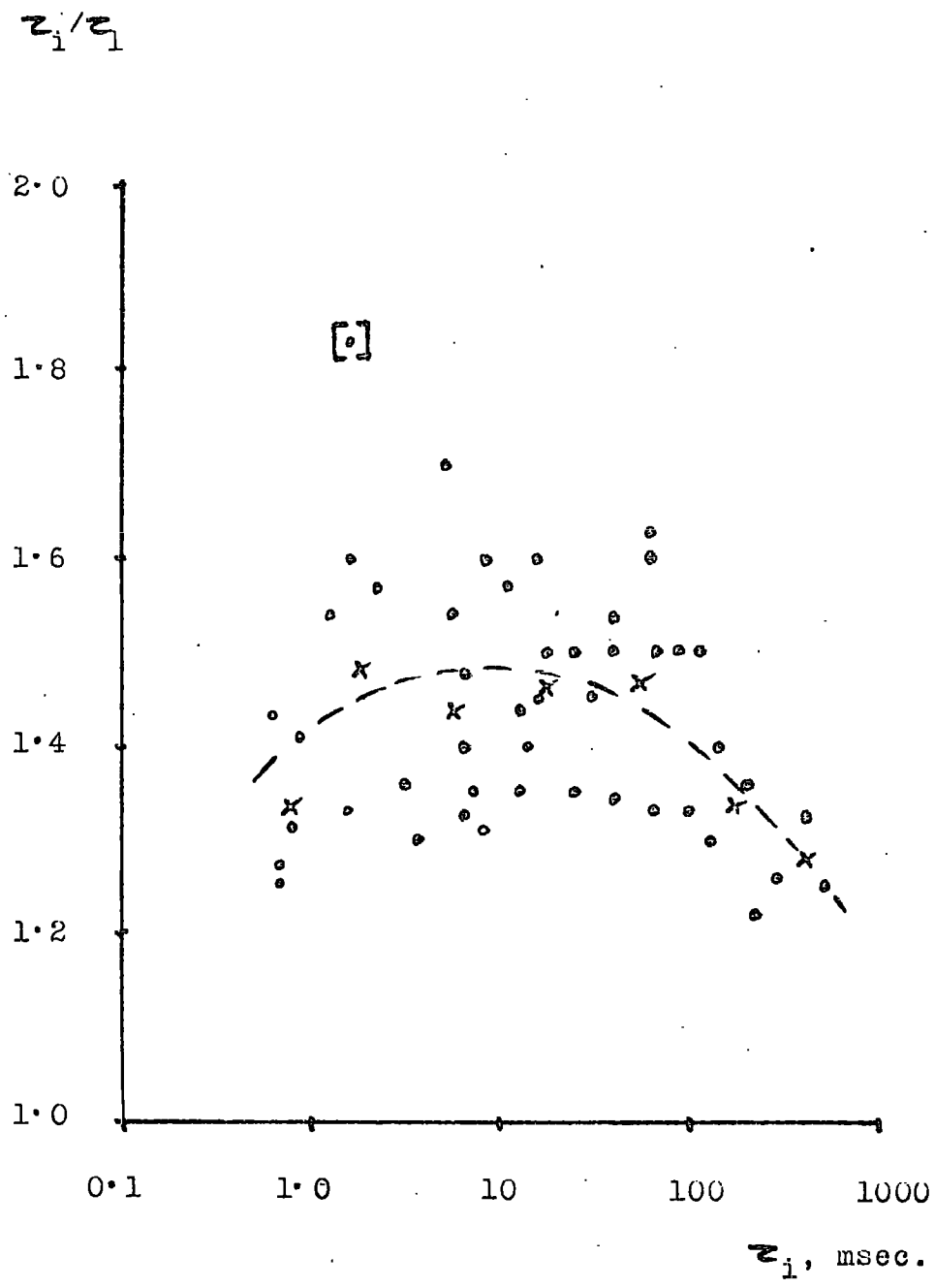

Figure (6.25). Variation of τ_i/τ_1 with τ_i, showing experimental points (•) and the approximate trend (x——x).

Figure	$\mu_l \times 10^3$ (cm^2/V.sec.)	$\mu_i \times 10^3$ (cm^2/V.sec.)	Range of τ_i, (msec.)
5.3	1·0 ± 0·1	0·74 ± 0·02	500 - 65
5.4	1·0 ± 0·1	0·75 ± 0·02	400 - 40
5.5	1·0 ± 0·1	0·77 ± 0·02	130 - 16
5.6	1·2 ± 0·1	0·77 ± 0·03	27 - 6
5.17	1·0 ± 0·1	0·70 ± 0·05	18 - 6
5.18	0·9 ± 0·1	0·58 ± 0·05	13 - 1·6
5.19	0·8 ± 0·1	0·54 ± 0·05	3 - 0·6

Table (6.1). Values of mobility, μ_l, determined by measurement of τ_l, compared with the values of μ_i.

the limits (1.4 ± 0.2). The large degree of scatter within these limits is due to the basic difficulty of measuring τ_1 from the integrated transient. This unfortunately makes it impossible to verify the predictions of the model more fully. The results are however consistent with an increase in τ_i / τ_1 as τ_i is decreased, and there is an indication that the ratio may begin to decrease again in the region of $\tau_i \lesssim 1$ msec. Thus the reduction of apparent mobility, μ_i, for short transit times (section 5.4.4.) may be ascribed to an increase in τ_i / τ_1, since:

$$\mu_1 = \mu_i \cdot \tau_i / \tau_1 \qquad \ldots\ldots\ldots\ldots\ldots\ldots\ldots \quad (34)$$

Table (6.1) lists the values of μ_1 determined directly from the oscilloscope traces by measurement of τ_1, together with the corresponding values of μ_i quoted in Chapter 5.

The mean value of μ_1 is: $\bar{\mu}_1 = (1.0 \pm 0{\cdot}1).10^{-3}$ cm.^{2}/V.sec. and is independent of applied field, within the limits of experimental error, over the range 1 KV/cm. - 140 KV/cm. Apart from a correction factor of (1.4 ± 0.1) to the mobility values quoted in Chapter 5, therefore, the application of the viscous drag theory to the experimental results does not change the conclusion, drawn earlier, that the mobility of the negative charge carrier in well degassed n-hexane is not field dependent.

6.6. REFERENCES

1. Gazda, E., Acta Phys. Polonica 28, 6, 881-892 (1965)

2. Gazda, E., Paper presented at Durham Conference on Electronic processes in Dielectric Liquids, April 1963. A summary of the conference was published; Morant, M.J. Brit. J. Appl. Phys. 14, 469-473 (1963)

3. Sletten, A.M., Appendix to Ph.D. Thesis, London (1960)

4. Kahan, E., Ph.D. Thesis, Durham University, (1964)

5. Pickard, W.F., J. Appl. Phys. 34, 246, (1963)

6. Gray, E. and Lewis, T.J., Brit. J. Appl. Phys. 16, 1049-1050 (1965)

7. Coe, G., Hughes, J.F. and Secker, P.E., Brit. J. Appl. Phys. 17, 885-890 (1966).

CHAPTER 7

CONCLUSIONS AND SUGGESTIONS FOR FURTHER WORK

The reasoning which led to the inception of the present work is presented in Chapter 1. In section 1.3. three mechanisms were postulated to explain the effect of oxygen on the breakdown strength and conductivity of n-hexane. It was suggested that the absence of dissolved oxygen in the liquid would allow (a) an increase in mobility of the carriers; (b) an increase in the number of available carriers; or (c) the existence of free electrons of high mobility, distinct from the normal carriers referred to in (a) above. It has also been proposed, by LeBlanc (1) after Crowe (2) for example, that the carrier mobility might be field-dependent at high fields. This was shown subsequently not to be the case in hexane containing dissolved oxygen (3), for fields up to 500 KV/cm. The high-field mobility of carriers in well de-gassed hexane was therefore considered to be of particular relevance to the understanding of the Oxygen Effect. The primary object of the investigation was, however, to test the mechanisms (a) and (c) above, by determining the carrier mobility in de-gassed hexane. The method adopted for the determination enabled mechanism (b) to be investigated simultaneously and under the same experimental conditions, and also allowed the use of moderately high fields.

As stated in Chapters 5 and 6, no experimental evidence was

found for a mobility increase due to de-gassing. Further, no field-dependence of the mobility in degassed liquid was observed for fields up to 140 KV/cm., nor was there any indication, under these conditions, of the existence of an additional 'fast' carrier. The implications of these results are discussed in section 7.1.

Section 7.2. deals with the measurements of injected charge made under the various conditions encountered during mobility determinations. From these observations, a mechanism is proposed which explains the Oxygen Effect in terms of a cathode surface phenomenon.

Finally, in section 7.3. the nature of the charge-carrier under investigation is discussed in terms of the conclusions of the preceding two sections, and in relation to other recent work. Suggestions for further work on the general topic of conduction in dielectric liquids are made where appropriate in each of the three sections.

7.1. THE CARRIER MOBILITY

The lack of any detectable increase in carrier mobility on de-gassing the liquid is of major significance to the explanation of the Oxygen Effect. Before completely discarding the idea that mobility variation is responsible for the effect however, other reasons for the failure to detect an increase must first be examined.

7.1.1. Field dependence

In spite of considerable work on the design and manufacture of the photocathodes used in the present work, the mobility values

obtained were limited to a maximum applied field of 140 KV/cm., i.e. about 30% - 40% of the breakdown strength for the degassed liquid. It could be suggested therefore that the mobility is field dependent and increases rapidly above (say) 150 KV/cm. An objection to this proposal is contained in the results of Kahan and Morant, summarized in figure (1.1). Reference to the figure shows that, although the major difference between the current levels in de-gassed and air-saturated liquid occurs at $\gtrsim$ 150 KV/cm., the rate of increase of current with applied field is greater for the de-gassed liquid even at 100 KV/cm. and is itself increasing very rapidly. Any increase in mobility with applied field should therefore be evident at fields below 150 KV/cm.

The extension of mobility measurements to higher fields in de-gassed hexane remains important, however, and it is suggested that the present method be utilized in a modified form for such determinations. Specifically, it will be necessary to develop methods of forming a semi-transparent photocathode on a silica window which will either (a) have surface adhesion properties equal or superior to the parent metal; or (b) be shielded electrostatically from the strong electrical forces encountered in a high-field test-cell. A further desirable improvement in test-cell design would be the reduction or elimination of the trace curvature. On the basis of the conclusions drawn in Chapter 6, this could be achieved by detecting only that part of the charge layer moving close to the axis of the electrodes. Thus a test-cell with a guarded anode,

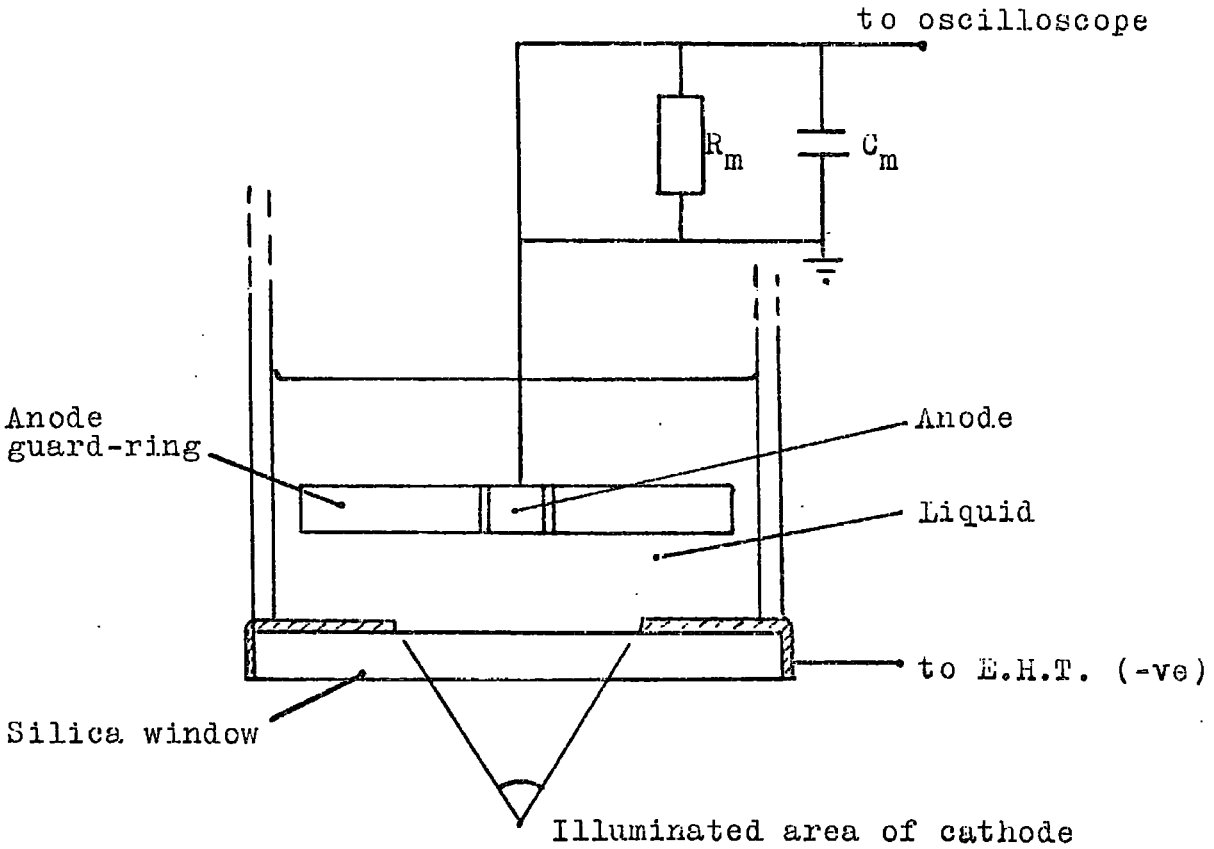

Figure (7.1). Suggested design of test-cell to reduce trace-curvature.

the active area of which is small compared with that of the charge layer, should result in an improved trace shape. The successful application of this type of cell, shown diagramatically in figure (7.1.) would provide additional confirmation of the viscous-drag theory proposed in Chapter 6.

7.1.2. Carrier identity

A further qualification to the conclusion that mobility variation is not the cause of the oxygen effect, is the consideration that the 'natural' or 'dark' conduction mechanism may be completely distinct from that operating under the present experimental conditions. However, given that the natural conduction process involves the transfer of electrons through the liquid, it becomes difficult to justify this criticism in the light of previous experimental work. Of the numerous methods by which carriers have been generated in the liquid saturated hydrocarbons, for the measurement of mobility, all have produced a negative carrier with a mobility of the order 10^{-3} cm.^{2}/V.sec. (4). This value has invariably been greater than that of the corresponding positive carrier, where produced. Both the artificially produced negative carrier and the natural conductivity can be shown, with reasonable certainty, to be non-ionic in character, at least under the conditions of the present investigation. This, together with the above tentative evidence for a unique negative carrier, may be used to counter the objection under discussion. The nature of the carrier in both the natural and artificial conduction mechanisms must, however, remain a possible qualification to the

conclusions reached in this section.

7.2. CATHODE SURFACE EFFECTS

Bearing in mind the considerations of the previous section, it may be concluded that a mechanism other than some form of mobility increase is responsible for the observed oxygen effect. The measurements of injected charge made in conjunction with the mobility determinations, provide a certain amount of evidence that the phenomenon is governed by processes occurring at the cathode surface.

It was established in Chapter 5 that the magnitude of the injected signal was a practically linear function of the applied field. An explanation of apparent departures from this law, for short transit-times, was proposed in Chapter 6 but, apart from this, the relationship was confirmed up to 100 KV/cm. The dependence of charge-injection on applied field rather than applied voltage is in itself a strong indication that the conduction mechanism is limited by a surface effect. Further support for such an effect is provided by (a) the decrease in photo-efficiency of an aluminium cathode on oxidation (section 5.4.); and (b) the fact that oxygen dissolved in the liquid reduces the photo-injected signal magnitude without changing the shape of the transient, pointing again to a surface effect (section 6.3.).

It is suggested that the dependence of injected charge on applied field is due to lowering of the surface potential barrier by the Schottky Effect. A simple form of the Schottky relationship applied to the present

situation is:

$$i = i_o . \exp \left\{ e.(e.E_a / \varepsilon)^{\frac{1}{2}} / kT \right\} \quad \ldots\ldots\ldots\ldots \quad (1)$$

where i is the transient current flowing through barrier;

and E_a is the applied field.

For a given duration of the ultra-violet flash, the current, i, will be proportional to the injected charge and hence to the signal magnitude, V_s.

A plot of $\log_{10} V_s$ against $E_a^{\frac{1}{2}}$ should therefore produce a straight line of gradient:

$$g = (e/\varepsilon)^{\frac{1}{2}} . (e/kT) . / 2.303 \quad \ldots\ldots\ldots\ldots\ldots \quad (2)$$

Substitution of the values: $e = 1 \cdot 6.10^{-19}$ coulomb

$\varepsilon = 1 \cdot 9 \times 8 \cdot 85.10^{-12}$ Farad/metre

$kT = 0 \cdot 025$ eV

yields the gradient $g = (1 \cdot 7.10^{-3})\ V^{\frac{1}{2}} . m^{-\frac{1}{2}}$.

The measurements of signal magnitude as a function of applied field, described in Chapters 5 and 6, are summarized in figure (7.2) in terms of a Schottky plot. In the case of the non-oxidized cathode, the plot is closely linear and has a minimum gradient of $(1.3 \pm 0.1).10^{-3}$ $V^{\frac{1}{2}} . m^{-\frac{1}{2}}$., which compares favourably with the theoretical value quoted above. The two plots for oxidized cathodes, using different flash lengths, are also practically linear and have gradients of $(0.35 \pm 0.04).10^{-3} V^{\frac{1}{2}} . m^{-\frac{1}{2}}$.

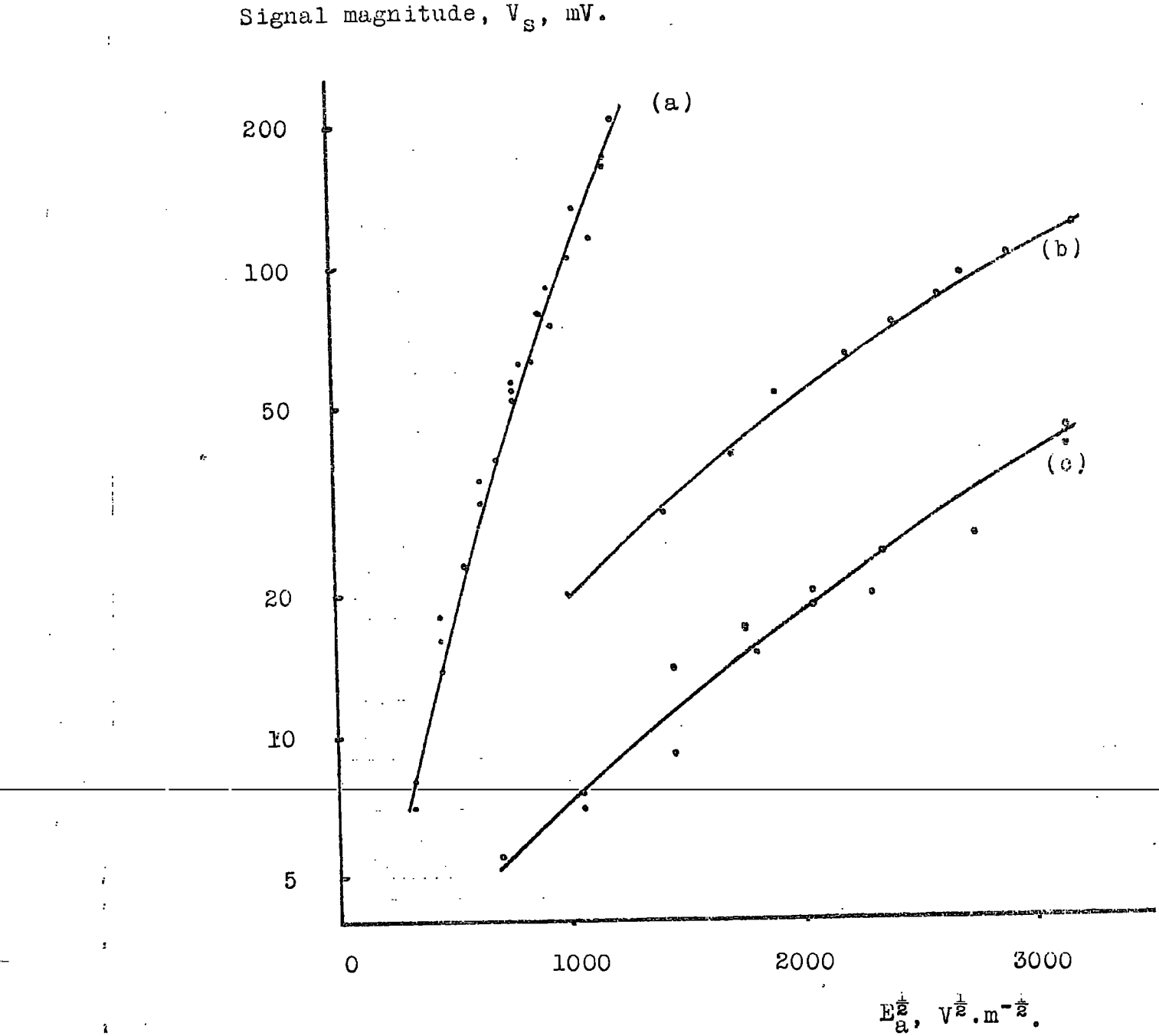

Figure (7.2) Schottky plot of signal magnitude results from cells 'D1' and 'D2'. (a): non-oxidized cathode, 'long' flash; (b): oxidized cathode, 'long' flash; (c): oxidized cathode, 'short' flash.

However, the curvature of the plots and the divergence of their gradients from the theoretical value are sufficient to cast doubts on the existence of a simple Schottky barrier at the cathode.

Despite these possible refinements, it may prove more profitable to devise a special barrier model, which would explain directly the observed proportionality of injected charge to applied field, than to attempt to fit such a relationship to a modified Schottky equation.

and $(0.34 \pm 0.04).10^{-3}\ V^{\frac{1}{2}}.m^{-\frac{1}{2}}$. for the 'long' and 'short' flashes respectively.

ADDITION OPPOSITE

It is difficult to predict, from a theoretical basis, the effect of an oxide layer on the Schottky gradient, under the present experimental conditons. From equation (2), however, it may be suggested that an increased dielectric constant or a decreased field in the surface layer would reduce the slope of the Schottky plot. The fact that such a reduction does occur may explain the difference between the theoretical and experimental slopes for the non-oxidized cathode in terms of slight oxidation of the evaporated metal. Thus evaporation at even lower pressures, preceded by rigourous de-gassing of the substrate, should increase the gradient of the plot to nearer the theoretical value.

ADDITION OPPOSITE

As detailed in the preceding paragraphs, there is considerable evidence to support the theory that the Oxygen Effect is a surface- rather than a volume-phenomenon. On this basis, the properties of the cathode surface barrier could account for the variation in 'dark' conductivity of hexane as a function of oxygen partial pressure, or at least that part of the conductivity which is due to electron emission from the cathode. Similarly, the limitation of electron emission by a surface barrier would increase the breakdown strength of the liquid for certain breakdown processes. The technique, described in Chapter 5, of mechanical stabilization of the cathode by an oxide layer indicates a further mechanism by which the presence of oxygen in the liquid may increase the breakdown strength. Evidence was presented in section

5.3. to the effect that for test-cells 'D1' and 'D2', both the pre-breakdown pulses and the breakdown event itself were caused by mechanical failure of the cathode surface. The relevance of this observation to breakdown strengths determined using other electrode materials is obvious. It is suggested that the tensile strength of the surface layer of an electrode may in some cases have a major effect on the apparent breakdown strength of the liquid. The phenomena of electrode 'conditioning' and of electrode damage prior to breakdown, reported by several workers (5), (6), may also be related to the mechanical properties of electrode surface and hence to its degree of oxidation.

7.3. THE NEGATIVE CHARGE-CARRIER

The exact nature of the negative carrier in n-hexane remains uncertain. It has been demonstrated in the present investigation that electrons may be injected into the liquid even in the presence of dissolved oxygen or of a surface oxide-layer. The electrons then traverse the inter-electrode space with a mobility higher than that expected of a hexane ion. It has further been shown, in the present work, that there is no detectable long-term trapping of the carriers in the liquid (section 6.3.); that there is strong coupling between the carriers and the neutral liquid molecules (section 6.5.); and that all the injected carriers are easily collected at the anode (section 6.4.).

The anomalous variation of mobility with liquid viscosity for negative carriers in saturated hydrocarbons, as determined by Gzowski

and Jachym (7), (8), indicates that the carrier is not ionic in the sense of a negatively charged molecule. This opinion is supported by Chong and Inuishi (9), (10), who have shown that the electron attachment coefficient for pure hexane is extremely low. The absence to date of evidence for a high-mobility carrier in hexane, or of an increase in mobility with applied field, casts doubts on theories involving the existence of the carrier, for short periods, as a free, highly mobile electron (1), (10). The concept of the shallow trap, in which the electron is supposed to be contained for the remaining periods of time, is however still tenable. It has been proposed by a number of authors (1), (2), (9), that such a trap could be formed by polarization of neighbouring liquid molecules due to the intense local field of the carrier-electron.

At this stage in the discussion a close analogy may be drawn between the situation in hexane and the experimental and theoretical work carried out in recent years on both liquid ammonia and water. It has been clearly demonstrated that electron solvation due to polarization occurs in the latter two liquids (11,12). The concentrations of solvated electrons can be sufficiently high, in the case of ammonia, to decrease the density of the liquid by a measurable amount. The trap depth and structure, for both liquids, is such as to produce optical absorption at red or near infra-red wavelengths.

Jortner (13) has presented calculations, which are confirmed experimentally, of the density change and optical absorption energy for solvated electrons in liquid ammonia. The calculations are based on a

spherical cavity model for the 'trapped' electron. The highly polar nature of both ammonia and water results in a large contribution to the solvation energy of the permanent dipole moment. Electron solvation thus occurs readily in these liquids. In calculating the size and depth of the 'trap', however, Jortner points out that the effect of the polarizability of the molecules must also be taken into account. The additional solvation energy due to this factor is, in the case of ammonia, of the same order as that due to the permanent dipole moment. It would appear reasonable therefore to expect shallow self-trapping of electrons even in an essentially non-polar liquid such as n-hexane.

The possibility of electron solvation in n-hexane is a topic which could well be investigated in future work on conduction in liquid hydrocarbons. The application of optical absorption techniques to samples of hexane containing photo-injected carriers could, in view of the evidence already available, provide the key to the identity of the negative charge-carrier.

In the context of the previous paragraph, it may prove useful to describe briefly an (unsuccessful) attempt made by the author to detect infra-red absorption due to a photo-current in de-gassed n-hexane. The test-cell consisted of two aluminium electrodes approximately 1.5 cm. in diameter and the same distance apart, mounted in a 'Pyrex' cylinder with silica windows at each end. A continuous ultra-violet source was focused on the negative electrode which was at a potential of 10 KV with

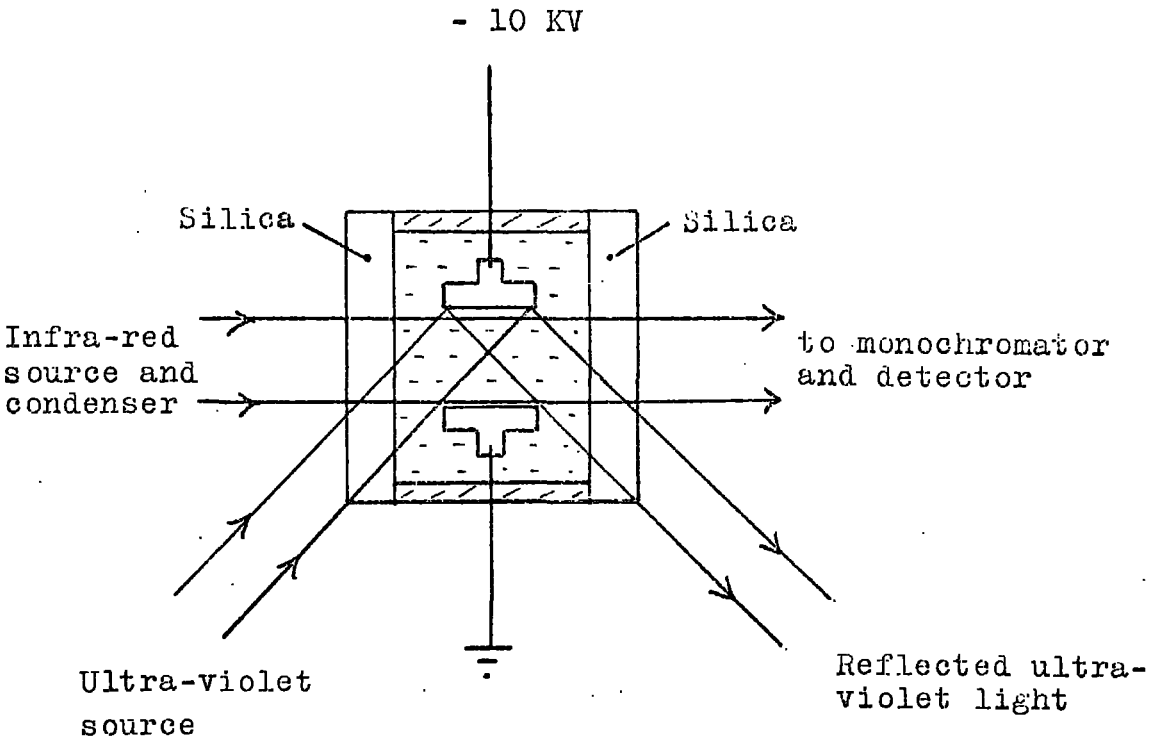

Figure (7.3). Schematic diagram of infra-red absorption cell.

respect to the anode. The optical path from the infra-red source to the spectro-photometer was perpendicular to the axis of the electrodes and to the planes of the silica windows, as indicated in figure (7.3). There was no detectable change in the absorption of the hexane between 0.8 and 2.5 microns wavelength when the photocurrent was initiated. It will be appreciated from previous Chapters that these experimental conditions were far from ideal. The negative result merely serves to indicate that the injected charge density must be optimized by the use of a clean aluminium cathode and high field strengths, combined with an intense source of ultra-violet radiation, if the experiment is to prove meaningful. Further, the concept of a very shallow trap implies that the optical absorption may well occur at wavelengths in excess of 2.5 microns, thus requiring the use of special cell-windows.

It has been demonstrated in the present work that high concentrations of carriers may be produced in hexane in a reproducible and controllable manner with minimal damage to the liquid itself. The experimental material is available in a highly purified state, and methods for further purification and the detection of trace impurities are well developed. On the theoretical side, a number of the factors affecting the injection of the carriers and their transport are reasonably well understood. It is therefore suggested that the question of the carrier identity is now amenable to investigation by techniques other than the basic electrical measurements previously employed. In view of the

considerations of the preceding paragraphs, it is further suggested that infra-red spectroscopy is such a technique which is both theoretically justifiable and experimentally applicable to the present situation.

7.4. RECENTLY PUBLISHED WORK ON THE IDENTITY OF THE NEGATIVE CHARGE-CARRIER.

Since the completion of the experimental aspect of this investigation, other workers have produced new evidence on the question of the carrier identity.

Minday, Schmidt and Davis (14) report negative carrier mobility values in n-hexane which are at least 50 times those determined in the present work. The existence of these fast carriers is ascribed to the use of barium getters to produce high vacuum ($\sim 10^{-8}$ torr). The barium films are presumed to remove residual electron scavengers such as oxygen from the liquid. The model proposed is that freeeelectrons in the liquid move with very high mobility between short-lived traps, the concentration of which limits the overall observed mobility. The implication of these results and the proposed model is that the mobility values determined in the present investigation, using a vacuum of 10^{-5}-10^{-6} torr, are minimum values corresponding essentially to the mobility of the negatively charged traps themselves.

Evidence for the existence of free electrons in other dielectric liquids is provided by the work of Schmidt and Allen (15) and Tewari and Freeman (16). These workers report the very rapid decays of conductivity in tetramethylsilane, neohexane (2.2 dimethyl propane) and neopentane, after a pulse of X-rays. High mobilities were deduced to be the cause of this decay

and the fast carriers disappeared when oxygen was admitted to the system. However, Tewari and Freeman showed that these effects do not apparently occur in n-hexane or n-pentane, which also differ from the former three liquids in having a much lower free-ion yield when subjected to X-rays.

The possibility of short-lived electron traps is supported in (14) by reference to the work of Cottrell and Walker (17) and Schulz (18). These workers report the interaction of electrons with polyatomic gases. Low energy electrons can apparently lose energy to the gas molecules, often by forming transient negative ions.

The main evidence for fast carriers in n-hexane, however, still rests with the work of Minday, Schmidt and Davis (14), since the supporting references (15-18) are concerned with the properties of other materials. Before the suggestion of impurity-conduction in carefully purified hexane, degassed to 10^{-5}-10^{-6} torr, can be accepted therefore, the experimental facts and the conclusions drawn from them must be carefully considered. Three points in particular require further investigation:

(a) The effect of liquid motion on the mobility determinations is not discussed in the publication. It has been demonstrated by several workers, (19) for example, that induced liquid velocities can be high and of the same order as the carrier drift velocities when as in this case, continuous currents are generated. The power levels required to produce significant liquid motion are usually lower than those encountered in these mobility measurements. Although the drift velocity is reported to be independent of current the relevant range of current-levels and the variation in drift velocity are not quoted. The fact that no liquid motion effects were apparently observed suggests either a test-cell with

a high flow-impedance or one with a low flow-impedance in which the liquid velocity reached a maximum for current-levels below the explored region. An example of this form of drift-velocity dependence on current-level is given in (19).

(b) The lack of reproducibility of mobility values using different hexane samples is taken as evidence that short-lived impurities are responsible for limiting the observed mobility. This deduction requires more quantitative evidence. The impurity (or impurities) concerned must be identified and both fast and slow carriers must be observed by varying the impurity concentration. If the main impurity concerned is a gas, then adjustment of the ambient gas pressure should produce a reversible change in carrier mobility. The mobility results shown for "negative ions in hexane" in the publication are those of Le Blanc (1). No attempt seems to have been made to observe these lower mobility carriers in the liquid prior to the use of barrium getters. If the principle impurity proves not to be a gas, then detailed analysis of the liquid composition both before and after the purification and de-gassing processes will be neccessary in order to establish what these operations remove from the liquid. The possibility of a high-mobility electron scavenging impurity being added by the purification process cannot be discounted.

(c) The variation of signal magnitude with impurity concentration is not reported in the publication. Such a study would provide valuable information on the nature of the carrier and the lifetime of the traps. Repetition of the experiment described in section

7.4. REFERENCES

1. LeBlanc, O.H., J. Chem. Phys. 30, 6, 1443-1447 (1959)
2. Crowe, R.W., J. Appl. Phys. 27, 156, (1956)
3. Chong, P., Inuishi, Y., J. Phys. Soc. Japan 16, 1482, (1961)
4. Adamczewski, I., Brit. J. Appl. Phys. 16, 759 (1965)
5. Swan, D.W., Brit. J. Appl. Phys. 13, 208 (1962)
6. Lewis, T.J., Progress in Dielectrics 1, 99 (Heywood, London, 1959)
7. Gzowski, O., Nature 194, 4824, 173 (1962)
8. Jachym, B., Acta Physica Polonica 29, 21-27, (1966)
9. Chong, P., Inuishi, Y., J.I.E.E. Japan 1112-1116 (1962)
10. Morant, M.J., J. Electrochem. Soc. 107, 671 (1960)
11. Douthit, R.C., Dye, J.L., J. Am. Chem. Soc. 82 4472 (1960)
12. Hart, E.J., Boag, J.W., J. Am. Chem. Soc. 84 4090 (1962)
13. Jortner, J., J. Chem. Phys. 30, 839-846 (1959)
14. Minday, R.M., Schmidt, L.D. and Davis, H.T., J. Chem. Phys., 50, 3, 1473 - 4 (1969).
15. Schmidt, W.F. and Allen, A.O., J. Chem. Phys., 50, 11, 5037 (1969).
16. Tewari, P.H., and Freeman, G.R., J. Chem. Phys., 49, 4394 (1968).
18. Schulz, G.J., Phys. Rev., 116, 1141, (1959); 125, 2291, (1962); and 135, A988 (1964).
17. Cottrell, T.L., and Walker, I.C., Trans, Far. Soc., 61, 1585 (1965).
19. Secker, P.E., and Lewis, T.J., Brit. J. Appl. Phys., 16, 1649 (1965).

APPENDIX A

THE SIGNAL RESULTING FROM INSTANTANEOUS GENERATION OF CARRIERS THROUGHOUT THE INTERELECTRODE VOLUME

Let a total charge, Q coulomb, be formed instantaneously at $t = 0$ throughout the cylindrical volume defined by two plane, parallel, circular electrodes of radius r. A thin disc of carriers, situated initially at a distance $x(0)$ from the collecting electrode will carry a charge $\delta Q = Q.\delta x/d$, where δx is the thickness of the disc, and d the distance between the electrodes.

At a time t, each such disc will have moved a distance $\mu.E.t$ towards the collecting electrode, where μ is the carrier mobility and E the applied field, assumed to be uniform. The discs for which $x(0)$ was less than $\mu.E.t$ will each have contributed their total charge δQ to the measured signal in the external circuit. The number of such discs will be $\mu.E.t/\delta x$, and their combined charge contribution is therefore:

$$Q_1 = (\mu.E.t/\delta x).(Q.\delta x/d) = Q.t/T \quad \ldots\ldots(1)$$

where T is the transit time of a carrier across the total inter-electrode space.

In addition to the quantity Q_1, each of the remaining uncollected discs may be considered as having contributed a fraction $\mu.E.t/x(0)$ of its charge to the measured signal. This contribution, Q_2, is given by :

$$Q_2 = \int_{x(0)=\mu.E.t}^{x(0)=d} (\mu.E.t/x(0)).(Q.\delta x/d) \quad \ldots\ldots\ldots\ldots \quad (2)$$

By letting the disc thickness become vanishingly small, and using the relationship $T = d/\mu.E$, equation (2) may be re-written:

$$Q_2 = (Q.t/T).\log_e T/t \quad \ldots\ldots\ldots\ldots\ldots\ldots \quad (3)$$

Thus, at a time t after the generation of the charges, the total charge recorded by the external circuit is:

$$q(t) = Q_1 + Q_2 = (Q.t/T).(1 + \log_e T/t) \quad \ldots\ldots \quad (4)$$

If the charge generated in unit volume of the liquid is Q', and the signal voltage developed across the integrating capacitor C_m is denoted by V_s, then equation (4) becomes:

$$V_s = (Q' . \pi r^2 d/C_m).(t/T).(1 + \log_e T/t) \quad \ldots\ldots\ldots\ldots \quad (5)$$

APPENDIX B

PROBE STUDIES OF THE POTENTIAL DISTRIBUTION

Reference has already been made (section 2.3.1. and section 6.4.) to a preliminary investigation into the measurement of the potential distribution in hexane. The investigation was undertaken primarily in order to determine the effect of any non-uniformity in the potential distribution on the measurement of mobility by the transit-time method. However, the importance of the space-charge distribution, which may be deduced from the potential distribution, has been recognized by many workers. This topic has been extensively reviewed recently by Croitoru (1), who emphasises the incompleteness of the experimental evidence on space-charges in liquids.

Direct measurement of the potential distribution has previously involved the use of either a physical voltage probe or of an electro-optical technique. For non-polar liquids at low fields, however, the latter method is insufficiently sensitive. It was therefore decided to examine the use of voltage probes in hexane, to compare the various measuring circuits available, and to determine their reliability for giving the true potential distribution. Croitoru's review has subsequently concluded that there is a need for such critical experimental studies of the probe method.

The effect of a non-uniform field, or potential distribution, on the measurement of mobility by the transit-time method, may be illustrated

by considering the simple mobility equation:

$$\mu_a = d/E.\tau . \qquad \ldots\ldots\ldots\ldots\ldots\ldots\ldots \quad (1)$$

where μ_a is the apparent mobility calculated from the observed transit-time, τ, and the electrode separation, d. The field, E, is here assumed to be uniform, that is independent of the co-ordinate x, defined by the electrodes at x = 0 (emitter) and x = d (collector). In the more general case, however, where the field is a function E(x) of x, the true mobility is given by:

$$\mu_t = 1/\tau . \int_0^d (1/E(x)) \, dx \qquad \ldots\ldots\ldots\ldots \quad (2)$$

Equations (1) and (2) are related by the voltage V_a applied to the electrodes:

$$V_a = E.d = \int_0^d E(x) \, dx \qquad \ldots\ldots\ldots\ldots\ldots\ldots \quad (3)$$

It can be shown that the true mobility μ_t is always greater than or equal to the apparent mobility μ_a, for real situations. Physically, this is due to the predominant effect of the reduced carrier velocity in the regions where the local field is less than the average value. Thus the effect of space-charge concentrations near the electrodes would be to reduce the field in the major part of the inter-electrode space, resulting in an erroneously low value for the apparent mobility. It is therefore important, when using the transit-time method for

mobility measurement, to know the potential distribution in the cell at the time of measurement.

B.1. EXPERIMENTAL METHODS AND RESULTS FOR HEXANE

Earlier probe measurements on a variety of dielectric liquids make use of one of three basic measuring circuits, and it is these three which were compared in the present investigation. Two of the circuits require the use of a high impedance voltmeter and at the onset a study was made of all commercially available instruments in order to choose one with the maximum possible input resistance. For potential measurements from 1 volt to 10 Kv, the instrument chosen was the Model 1170 electronic voltmeter produced by the B.K. Sweeney Mfg. Co., Denver, Colorado, U.S.A. The instrument has an input resistance greater than $10^{13}\,\Omega$ on all ranges, which appears to be far higher than any other currently available voltmeter, over this voltage range.

The test-cell constructed for the work is shown in figure (B.1.). The cell was designed for use at high vacuum, filled with de-gassed liquid, but was normally used at atmospheric pressure for the work described here. The 1.6 cm. diameter plane electrodes were mounted on tungsten rods sealed through the glass walls. The platinum probe was mounted on a highly insulating glass seal and could be

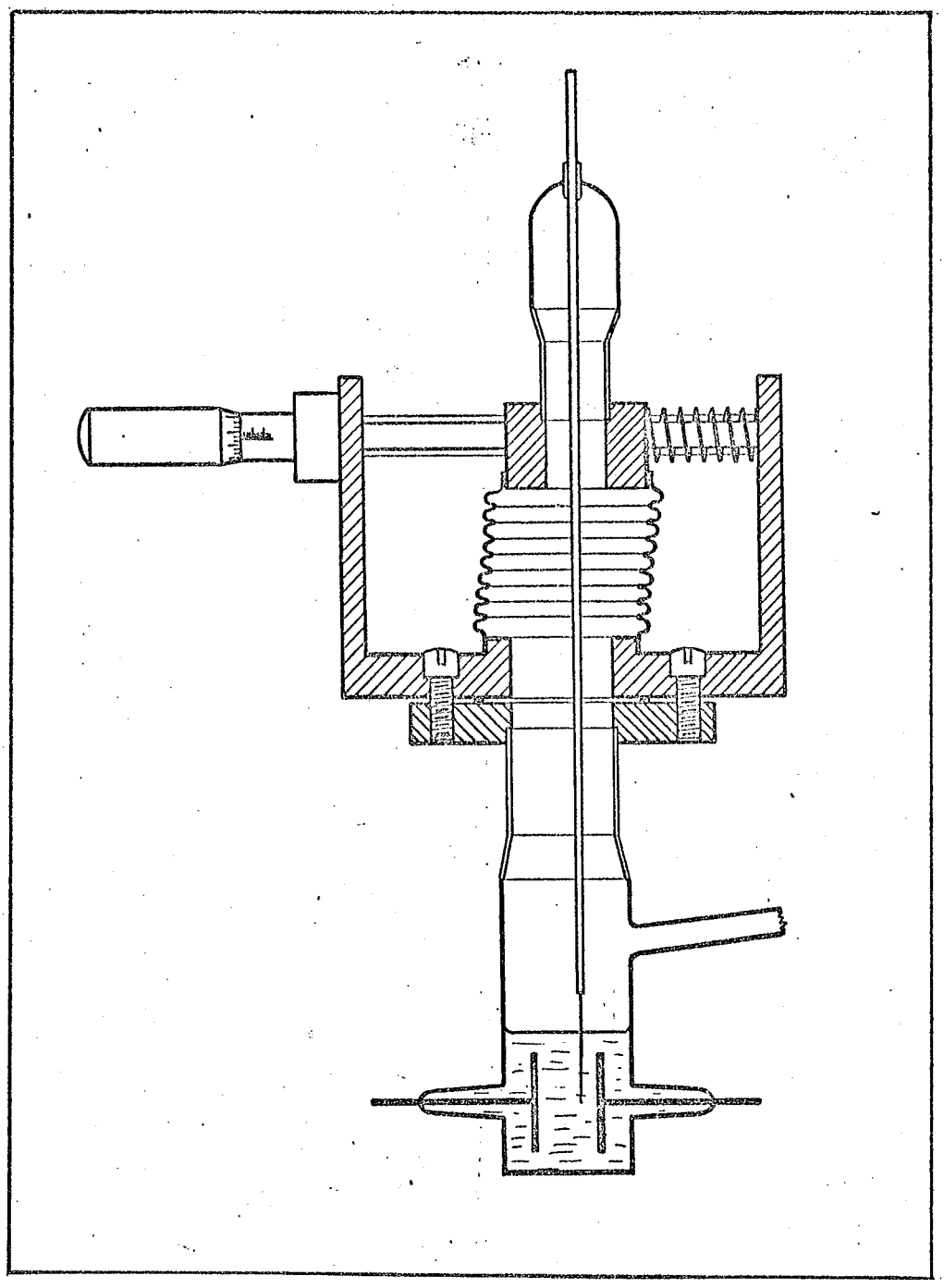

Figure (B.1). The probe test-cell.

traversed by means of a micrometer carriage, the vacuum seal being maintained by the lateral distortion of a metal bellows.

In this exploratory work air-saturated hexane was used as the test-liquid and the applied fields were generally below 1 KV/cm. Measurements were later made, however, on well de-gassed hexane at fields of up to 5 KV/cm., with very similar results to those quoted below. A subsequent section (B.2) describes the application of the three basic circuits to the above test-cell filled with benzene.

B 1.1. The direct probe method

The simplest method of attempting to determine the potential distribution in the liquid is to measure directly the potential taken up by the probe relative to one electrode, normally the earthed one. In practice this is often impossible, since the time constant for charging the voltmeter capacitance through the high resistivity liquid is prohibitively long. It is even difficult to extrapolate the potential-versus-time curves to their ultimate values, since they are not strictly exponential in form over long periods.

The difficulty was overcome by using the circuit shown in figure (B.2), which was first used by Whitehead and Marvin (2). The voltmeter and probe were initially charged to a known potential from the potential divider. On isolating the probe and voltmeter from the potential divider, a small positive or negative rate of change of voltmeter reading could be detected, indicating that the initial potential

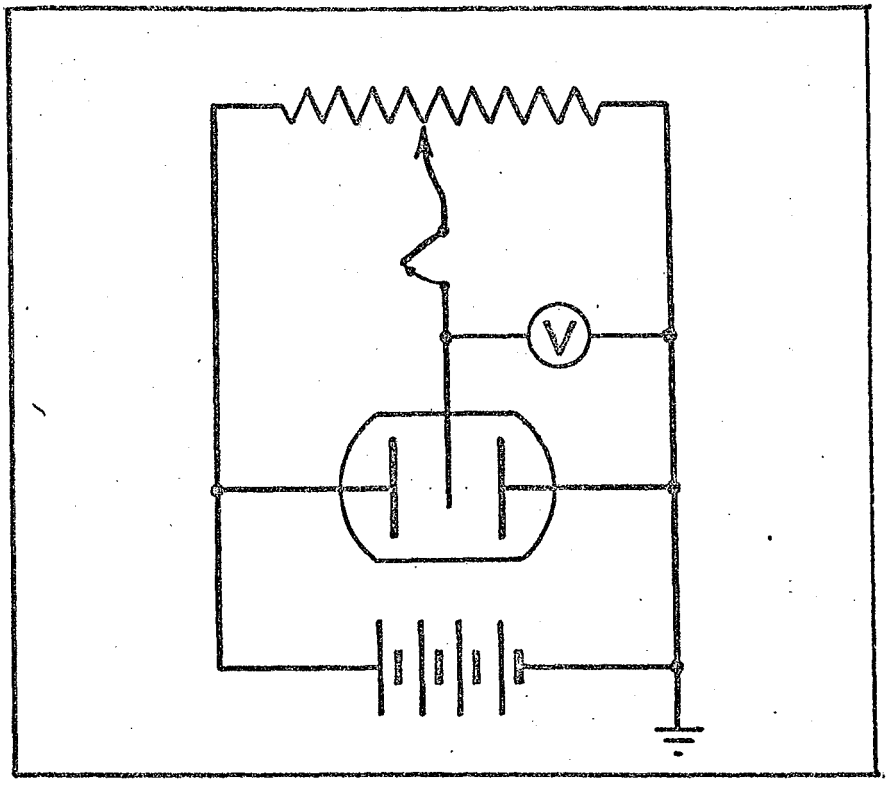

Figure (B.2). Circuit for direct measurement of the probe potential.

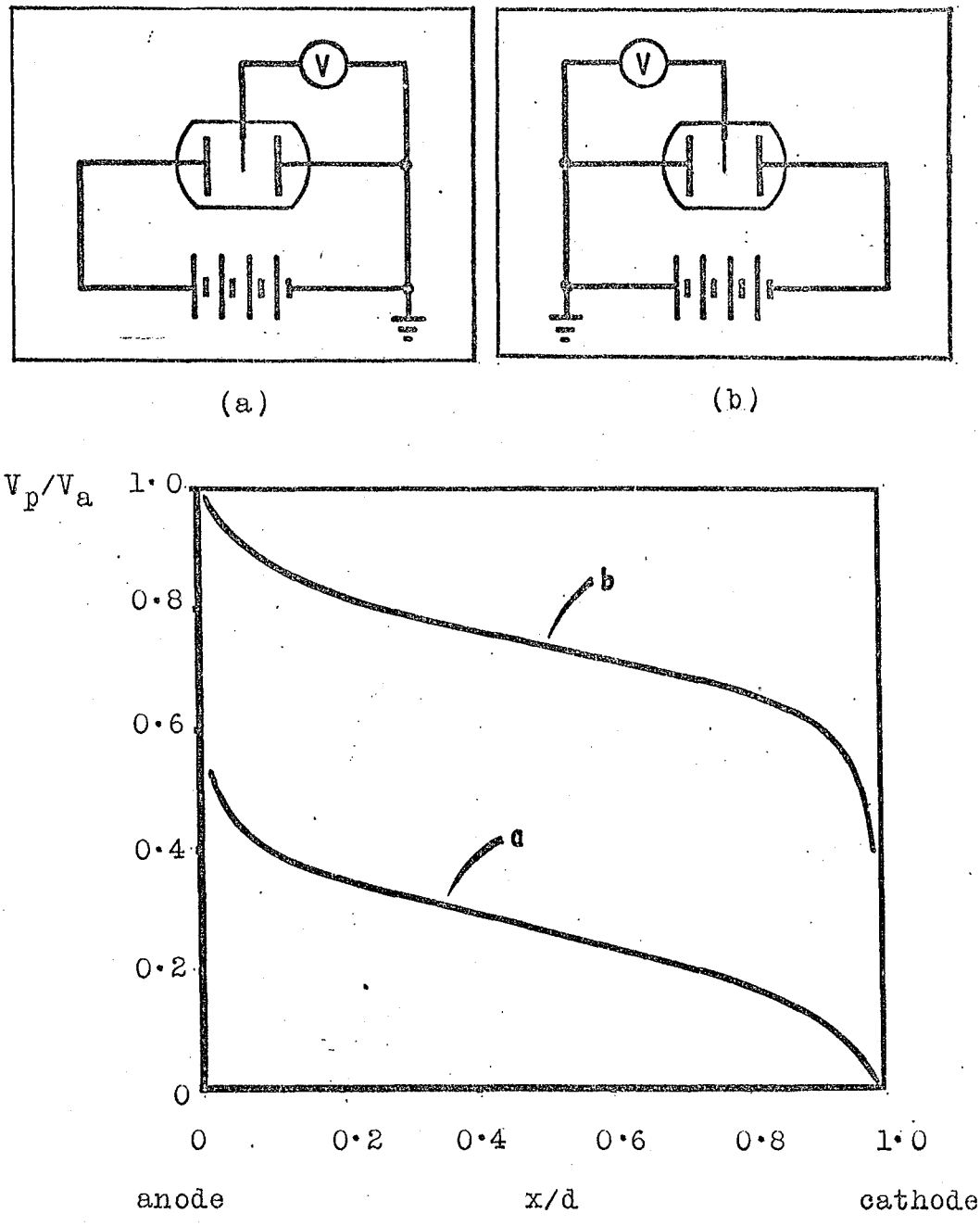

Figure (B.3). Apparent potential distributions measured in hexane, using circuits (a) and (b).

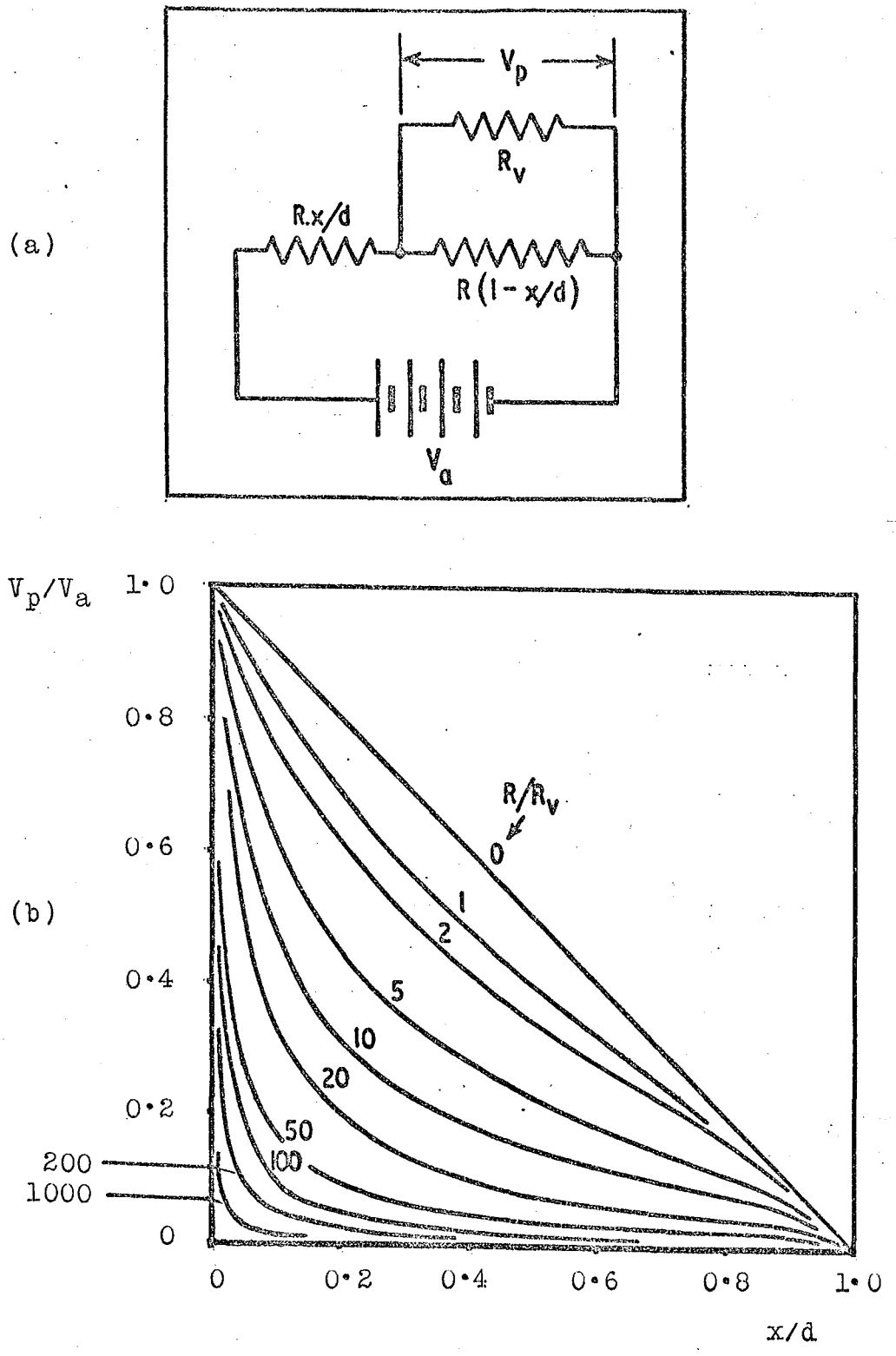

Figure (B.4). Basic equivalent circuit (a) and resulting potential distribution (b) for various values of R/R_v.

was either too high or too low. Appropriate adjustment of the trial probe potential and repetition of the procedure usually enabled the equilibrium potential at a point to be determined to within $\pm$ 5%, in a few minutes. A complete potential distribution could therefore be measured in approximately 30 minutes, a fraction of the time-constant for charging the voltmeter through the liquid.

For the method to be reliable, it is essential that the current taken by the probe should be much less than that passing between the electrodes. As pointed out by Croitoru, a simple check for this is to measure the apparent potential distribution with the voltmeter connected to each electrode in turn. Figure (B.3) shows typical results for the hexane-filled cell using each of the two resulting circuits. It is evident from the figure that the apparent distributions are largely determined by the current taken by the probe. The reason for the shape of the apparent distribution can be appreciated by reference to figure (B.4). The simple equivalent circuit shown in figure (B.4a) represents the electrical path between each electrode and the probe as ohmic reistances of total value R, and the voltmeter resistance as R_v. The probe potential V_p is then given by:

$$V_p = V_a / \left[(d/d - x) + (x.R/d.R_v)\right] \quad \ldots\ldots\ldots (4)$$

where x is the distance between the probe and the non-earthed electrode;

d is the inter-electrode spacing;

and V_a is the applied voltage.

The apparent potential distributions, derived from equation (4) for various values of R/R_v, are shown in figure (B.4b).

Comparison of the curves of figure (B.4b) with the experimental results shows that, although they are of the same general form, they never coincide for any value of R/R_v. This indicates that either the experimental curves are determined partially by a non-uniform potential distribution or the simple linear model is incorrect. Attempts were therefore made to correct the experimental curves for the current taken by the probe.

To derive the correction factor, the true potential distribution is represented in the circuit of figure (B.4a) by the dependence of the electrode/probe resistances on the probe position x. Thus the derivation assumes that the cell resistance is still ohmic, while allowing for a distribution of resistivity in the liquid due to space-charge. The true potential V_p' of a point in the liquid is related to the measured potential V_p by the expression:

$$V_p' = V_p/2. \left\{(1 - R_v.V_a/R.V_p) + \left[(1 - R_v.V_a/R.V_p) + 4R_v/R\right]^{\frac{1}{2}}\right\} \quad \ldots\ldots\ldots (5)$$

Figure (B.5.) shows the corrected versions of an experimental curve, for various values if R/R_v. It will be noted that none of the corrected versions approach a uniform field, so that the experiment appears to show that the potential distribution is in fact non-uniform, although the value of R/R_v is required in order to select the correct curve from

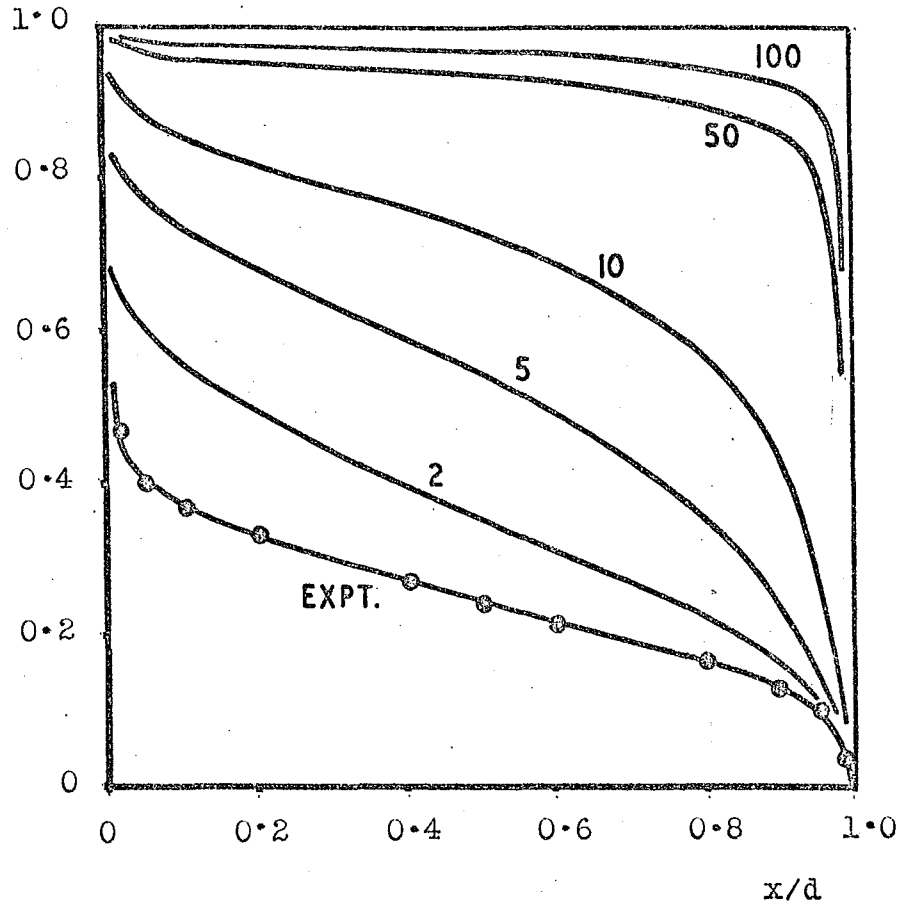

Figure (B.5). Typical potential distribution measured directly in hexane, with corrections for various values of R/R_v.

figure (B.5.), for example. Attempts have been made to measure R/R_V but these have not proved particularly successful because of the very high resistances involved. The voltmeter resistance R_V has however been measured satisfactorily and found to be between 10^{13} and 10^{14} chms, in agreement with the manufacturers' specification. The cell resistance is much higher than this and it has not been possible to determine it accurately. The most that can be said is that the ratio R/R_V is greater than 10, indicating a high degree of distortion of the true potential distribution. Emptying the cell has shown that even this very high resistance is largely due to parallel leakage paths over the cell walls. There are also indications that the leakage resistance of the probe – support to earth has some effect on the value of R_V and therefore contributes to the distortion of the measured potential profile.

In addition to the interpretation difficulty, this method of measuring probe potentials is still subject to experimental problems due to slow variations of current and voltage. There is evidence that either the potential distribution or the current through the cell (or both these factors) may change during the determination of the potential profile. Thus the values of R/R_V may vary for different points on the profile and the correction factor will not be constant.

All these difficulties show that direct measurements of probe potentials in liquids with resistivities as high as that of hexane cannot be made reliably with apparatus and method under discussion.

B.1.2. The capacitor method

The errors due to the voltmeter resistance may in principle, be eliminated by a method first used by Guizonnier (3). In this method a low leakage capacitor is connected to the probe in place of the voltmeter, as shown in figure (B.6a). In this circuit, the capacitor is first charged to the trial potential with switch S1 closed and S2 connected to point B. The capacitor is then isolated, with the probe, by moving the switch S2 to point A. After a certain time the capacitor voltage is read by reconnecting it to the isolated voltmeter and the change in potential ΔV is determined. The process is repeated for different trial potentials until $\Delta V \rightarrow 0$.

The main advantage of the method is that the leakage resistances of the cell, capacitor, and voltmeter can be determined from the time-constants for the discharge of the capacitor through the various leakage paths.

In practice, however, it was not possible to construct a capacitor to suit the circuit and test-cell with a leakage resistance of much greater than 10^{13} ohms. Measurements made in hexane using such a capacitor indicated that the error due to leakage was greater than that using the voltmeter alone, as in the direct method described above.

B.1.3. The bridge method

The circuit arrangement, shown in figure (B.6b) was used by

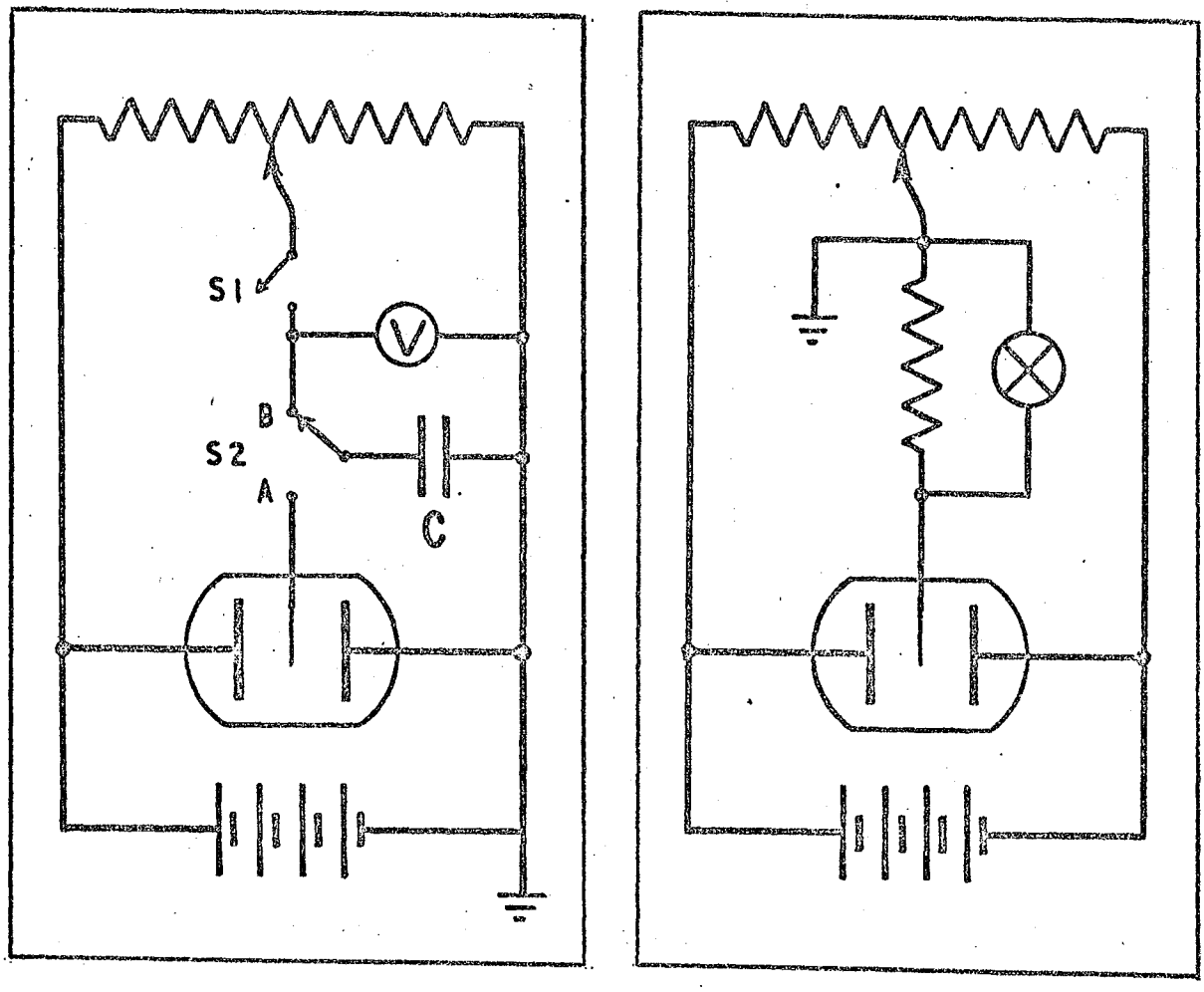

Figure (B.6). Circuits for probe measurements by (a) Capacitor- and (b) Bridge- methods.

Forster (4) for obtaining potential profiles in benzene. It was investigated here as a possible method for hexane, which has a considerably higher resistivity than benzene. The circuit is essentially a bridge with a sensitive electrometer as the detector. At balance, the circuit eliminates the distortion due current taken by the probe.

The detector used in the present investigation was a 'Vibron' Model B33C Electrometer (Electronic Instruments Ltd., Richmond, Surrey) which has a maximum sensitivity of 10^{-14} amp. full scale deflection. The disadvantage of this and similar instruments in this particular application is that one side of the measuring resistor is earthed, so that the potential of the remainder of the circuit varies with the potentiometer setting. This characteristic introduces major problems when using high voltages on the cell.

Unfortunately, the bridge method was not found to be successful for measurements in hexane under the present experimental conditions. The cell resistance was found to be too high to give sufficient probe-current to balance the bridge.

B.2. MEASUREMENTS IN BENZENE

The examination of the three basic circuits for potential distribution reported in the previous section showed that none of them can be regarded as reliable for liquids of very high resistivity, such as hexane. In order to present a more meaningful comparison of the three methods, it was decided to repeat the exercise using a liquid of lower

resistivity than hexane. Benzene was selected for this purpose as being a simple organic liquid with a resistivity of approximately 1,000 times less than hexane.

All three methods were found to function satisfactorily in benzene, although corrections were required for the direct and capacitor methods to allow for the current taken by the probe. The uncorrected profiles are compared, in figure (B. 7), with the distribution obtained by the bridge method. The difference between the direct and capacitor methods is due to the lower leakage resistance of the capacitor. Leakage corrections of the form presented earlier (equation (5)) cause the two curves to coincide, and raise them both towards the result for the bridge method. Comparison of the three curves after the application of the leakage corrections indicates, however, that the latter are complicated by non-ohmic behavior of the voltmeter resistance. This was confirmed by the fact that discharge curves of the voltmeter alone and in parallel with the capacitor were not strictly exponential in form. This factor accounts for the higher cathode field observed when using the direct and capacitor methods.

It is concluded that even in liquids of the same order of resistivity as benzene, the direct measurement of probe potential must be regarded as subject to errors due to the characteristics of the measuring instrument. Under these conditions, the bridge method is to be preferred.

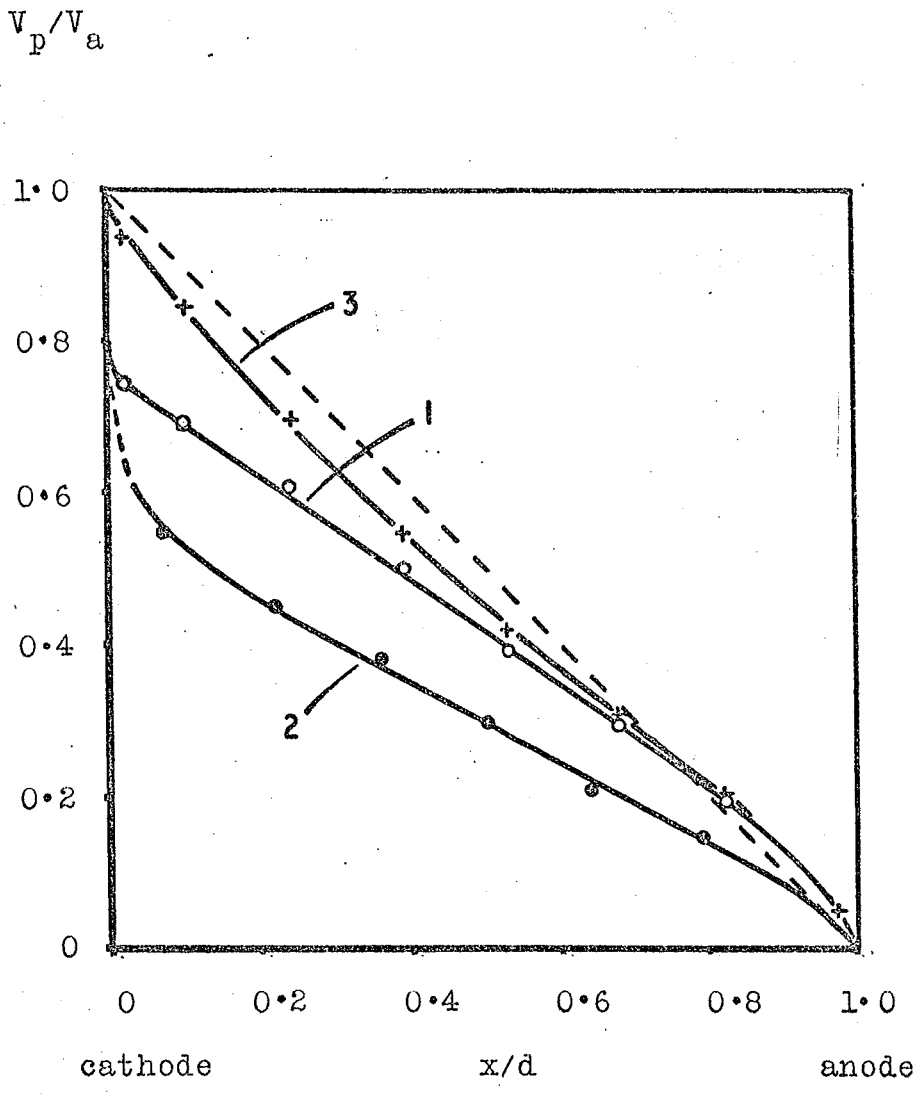

Figure (B.7). Potential distributions measured in benzene by the direct method (1); the capacitor method (2) ; and the bridge method (3).

B.3 REFERENCES

1. Croitoru, Z., Progress in Dielectrics 6, 103 (Heywood, London, 1965)

2. Whitehead, J.B., Marvin, R.M., Trans. Amer. Inst. Elect. Engrs. 49, 647 (1930)

3. Guizonnier, R., Gen. Elect. Rev. 63, 489 (1954)

4. Forster, E.O., J. Chem. Phys., 37, 1021 (1962)

ACKNOWLEDGEMENTS

Thanks are due to the Science Research Council for the award of a Research Studentship; to Dr. M.J. Morant for his supervision and encouragement and to the academic and technical staff of the Applied Physics Department, Durham University, for their advice and assistance.

COLLOQUES INTERNATIONAUX
DU
CENTRE NATIONAL DE LA RECHERCHE SCIENTIFIQUE

N° 179

PHÉNOMÈNES DE CONDUCTION DANS LES LIQUIDES ISOLANTS

Grenoble
17 - 19 Septembre 1968

EXTRAIT

ÉDITIONS DU CENTRE NATIONAL DE LA RECHERCHE SCIENTIFIQUE
15, quai Anatole-France — Paris - VII
1970

PROBE AND CHARGE TRANSIT STUDIES OF THE POTENTIAL DISTRIBUTION IN DIELECTRIC LIQUIDS

A. S. BLOOR* and M. J. MORANT

Department of Applied Physics, University of Durham, Durham, England

Abstract

Probe measurements can be used to determine the potential distribution between electrodes immersed in a liquid dielectric. Three circuit arrangements have been used in attempting to measure probe potentials in hexane. The apparent potential distribution is found to be determined largely by current taken by the probe even when this is reduced as much as possible. The effect of probe current can be explained qualitatively but it is not easy to correct the results quantitatively to obtain the true potential distribution. It is concluded that probe measurements are misleading in liquids of conductivity less than about 10^{-15} mho/cm. In benzene, which has a higher conductivity, the bridge method appears to give the most accurate potential distribution.

A new method is described for obtaining the potential distribution in hexane by analysing the current flow due to the transit of a pulse of injected charge from cathode to anode. This method appears to be reliable if certain experimental precautions are taken. Results show that the potential distribution in hexane is almost uniform up to applied fields of 120 kV/cm.

Résumé

La méthode de la sonde peut être utilisée pour déterminer la distribution du potentiel entre des électrodes plongées dans un diélectrique liquide. Trois dispositifs différents ont été utilisés pour mesurer les potentiels dans l'hexane par cette méthode. La distribution ainsi trouvée paraît dépendre considérablement du courant dérivé par la sonde quand bien même ce courant est réduit le plus possible. Cet effet peut être

* Present address : — Nelson Research Laboratories, English Electric Co. Ltd., Stafford, England.

expliqué qualitativement mais il n'est pas facile de déterminer une correction quantitative qui permette de trouver la distribution réelle de potentiel. On conclut que la méthode de la sonde est erronée quand la conductivité du liquide est inférieure à 10^{-15} mho/cm. Dans le benzène, qui a une plus grande conductivité, la méthode du pont semble donner les résultats les plus exacts.

Une nouvelle méthode est indiquée, qui permet de trouver la distribution de potentiel dans l'hexane en analysant le courant dû au transit d'un paquet de porteurs de charge, de la cathode à l'anode. La méthode paraît fiable si certaines précautions expérimentales sont respectées. Les résultats montrent qu'en dessous de 120 kV/cm le champ dans l'hexane est très sensiblement uniforme.

Introduction

The importance of space charge in controlling conduction processes in dielectrics has been recognized by many workers in the past. The topic has been well reviewed by Croitoru (1965) for all classes of dielectrics including liquids. It seems likely that space charge and the consequent field distortion are particularly important in highly purified insulating liquids and recent theoretical treatments of conduction in these materials (e.g. Silver, 1965) recognize this fact. The experimental evidence concerning space charge is, however, very incomplete as was emphasized by Croitoru. The slow current decay found after applying a potential step to an insulating liquid may be indirect evidence of space charge build up. Direct evidence can only be provided by measurements of the potential distribution using a voltage probe or optical techniques. For non-polar liquids at low field strengths the latter are insufficiently sensitive to detect even large space charge densities so that probe measurements appear to be the only way of investigating the topic further.

The present work was carried out as part of a continuing study of conduction processes in simple non-polar liquids, particularly highly purified *n*-hexane. It arose in considering possible errors in the determination of the mobility of negative carriers photo-injected from the cathode. In this method, used earlier by Le Blanc (1959), Chong, Sugimoto and Inuishi (1960) and Terlecki (1962), a pulse of carriers is formed by a flash of ultraviolet light falling on a specially prepared cathode. The carriers drift to the anode and their transit time is measured by observing the current in the external circuit. It has been found that the method may be subject to large errors due to doubts about the origin of the charges and the purity of the liquid, but, even when these are overcome, the observed mobility may be very different from the true mobility due to field distortion. Assuming

that the field is uniform the apparent mobility μ_a cm^2 volt^{-1} sec^{-1} deduced from a measured transit time τ sec is.

$$\mu_a = \frac{d}{E\tau}$$

where d cm is the electrode spacing and E volt cm^{-1} the applied filed. If the field, E_x, is a function of position x the true mobility μ_t will be given by

$$\mu_t = \frac{1}{\tau} \int_0^d \left(\frac{1}{E_x}\right) dx$$

With an applied voltage V_a we have

$$E.d = V_a = \int_0^d E_x \, dx$$

and in these conditions it can be shown that μ_t is always greater than μ_a. Physically this is due to the predominant effect of the reduced carrier velocity in the regions in which the field is less than the average value. With even a slightly non-uniform field the true mobility can be twice the apparent value, and increases considerably greater than this are feasible. Thus it is important to try to determine the field distribution at the same time as making mobility measurements.

For this reason it was decided to examine the use of probe measurements in very pure *n*-hexane, to compare the various measuring circuits and to determine their reliability for giving the true potential distribution. Croitoru's review has more recently concluded that there is a need for such critical experimental studies of the probe method. Our conclusion is that for pure non-polar liquids the probe method cannot always be used reliably even with the most advanced measuring techniques.

Experimental

All earlier probe measurements on a variety of dielectric liquids make use of one of three basic measuring circuits, and it is these which have been compared in the present investigation. Two of the circuits use a high impedance voltmeter and at the onset a study was made of all commercially available instruments in order to choose the one with the maximum possible input resistance. This is vitally important if probe measurements are to be made on liquids having very low residual conductivities. For potential measurements from 1 volt to 10 kV the instrument finally chosen was the

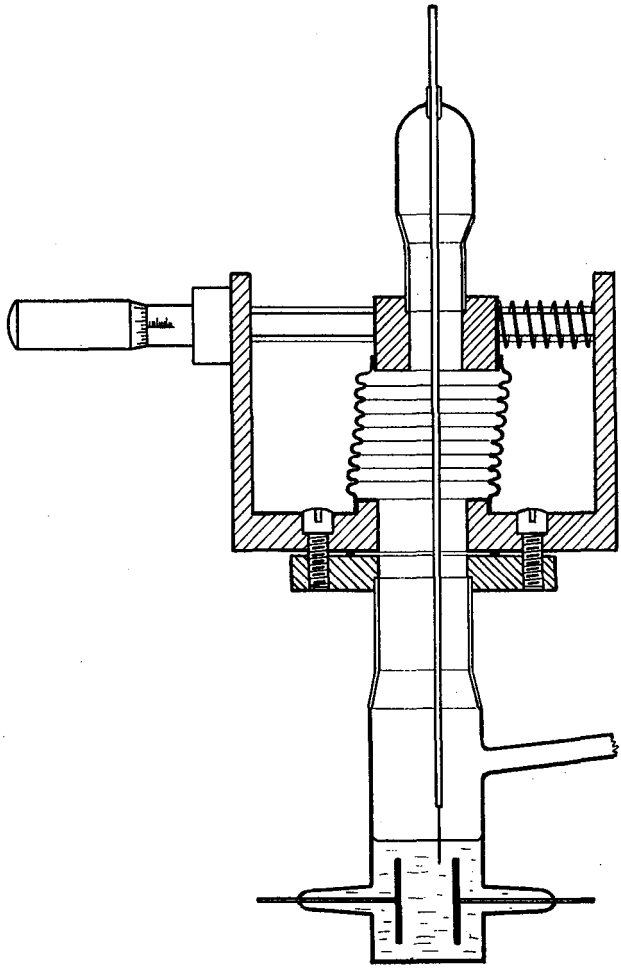

FIGURE 1
Probe test cell.

Model 1170 electronic voltmeter produced by the B. K. Sweeney Manufacturing Co., Denver, Colorado, U.S.A. This instrument has an input resistance greater than 10^{13} ohms on all ranges, which appears to be far higher than any other currently available voltmeter for this range of voltages.

The test cell constructed for the work is shown in Fig. 1. It is a vacuum cell intended for use with highly degassed liquid but it was normally used at atmospheric pressure. The 1.6 cm diameter plane electrodes are mounted on tugsten rods sealed through the glass walls. The platinum probe is mounted on a highly insulating glass seal on the top of the cell and it can be traversed by means of a micrometer carriage, the seal being maintained

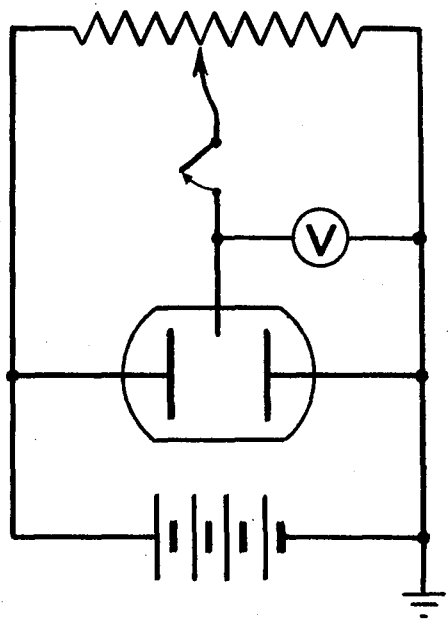

FIGURE 2
Circuit for direct measurement of probe potential.

by a flexible metal bellows which is distorted sideways. In this exploratory work only low field strengths up to 1 kV/cm were used.

The usual test liquid was *n*-hexane which has been extensively studied previously because it is the easiest of the simple non-polar liquids for experimental work. Purified hexane is probably one of the most highly insulating liquids and it is thus convenient for studying the limits of aplicability of probe measurements. A later section describes similar work on benzene.

Method 1. — Direct Probe Measurement

The simplest method of trying to obtain the potential distribution in a liquid is to measure directly the potential taken up by the probe relative to one electrode, normally the earthed one. In practice this is barely possible with a highly insulating liquid because of the extremely long time constant for charging the voltmeter capacitance through the liquid. It is difficult even to extrapolate the curves of potential against time because they are not exponentials over long periods. This is due to the changing

resistance of the liquid and possibly also to non-linearity of the voltmeter resistance. For this reason a direct voltmeter measurement is not practicable.

The difficulty is overcome in the circuit arrangement shown in Fig. 2 which was first used by Whitehead and Marvin (1930). The voltmeter is charged to a known potential from the potential divider and the change of reading when it is isolated with the probe is observed. The initial potential is adjusted and the process repeated until there is no change of reading on isolating the probe and voltmeter. When this occurs the probe is at its equilibrium potential in the liquid. Given sufficient voltmeter sensitivity a positive or negative rate of change of potential can be determined within a small fraction of the time constant for complete charging. In practice it takes about three minutes to determine the probe potential at one point to within $\pm$ 5 %, so that a complete profile can be measured approximately in 30 minutes. The method requires a very low leakage switch which is a liftable link between well isolated points of the circuit.

For the method to be reliable it is essential that the current taken by leakage from the probe should be much less than that between the electrodes, and, as pointed out by Croitoru, a simple check for this is to measure apparent potential distributions with the voltmeter connected to each electrode in turn. Fig. 3 shows typical results for the hexane filled cell using the two circuit arrangements. It is obvious from this that the apparent distributions are largely determined by the current taken by the voltmeter and not by the true, undisturbed, potential distribution. The reason for this can be seen by referring to the simple equivalent circuit of Fig. 4a in which the conduction between each electrode and the probe is represented by resistances assumed for simplicity to be ohmic and of total value R. R_v ohms is the voltmeter resistance. For this circuit the probe potential V_p relative to the applied potential V_a is given by

$$\frac{V_p}{V_a} = \left[\frac{d}{d-x} + \frac{x}{d} \frac{R}{R_v} \right]^{-1}$$

where x is the distance between the probe and the non-earthed electrode and d the interelectrode spacing. Apparent potential distributions, derived from this expression for various values of R/R_v, are shown in Fig. 4b.

Comparing the curves of Fig. 4b with experimental results such as those of Fig. 3, it has been found that, although they are of the same general form, they never coincide precisely for any value of R/R_v. This shows either that the simple linear model is incorrect or that the experimental curves are in fact affected by space charge in the liquid as well as by the current taken by the probe. Attempts have therefore been made to correct the experimental curves for the current taken by the probe in the

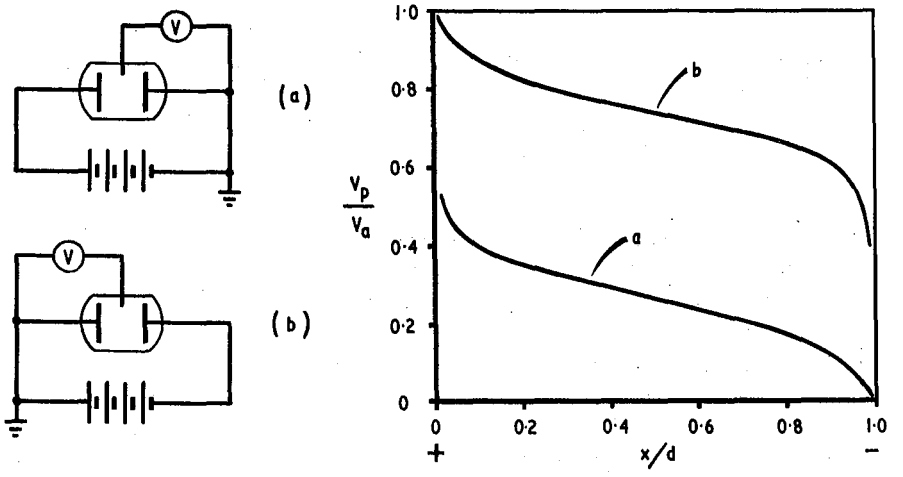

FIGURE 3
Apparent potential distributions measured in hexane with circuits *a* and *b*.

hope that a true potential distribution could be deduced in spite of the large error in the actual measurement. This appears to be the only way of proceeding in highly insulating liquids since we are already using what is believed to be the highest obtainable voltmeter resistance.

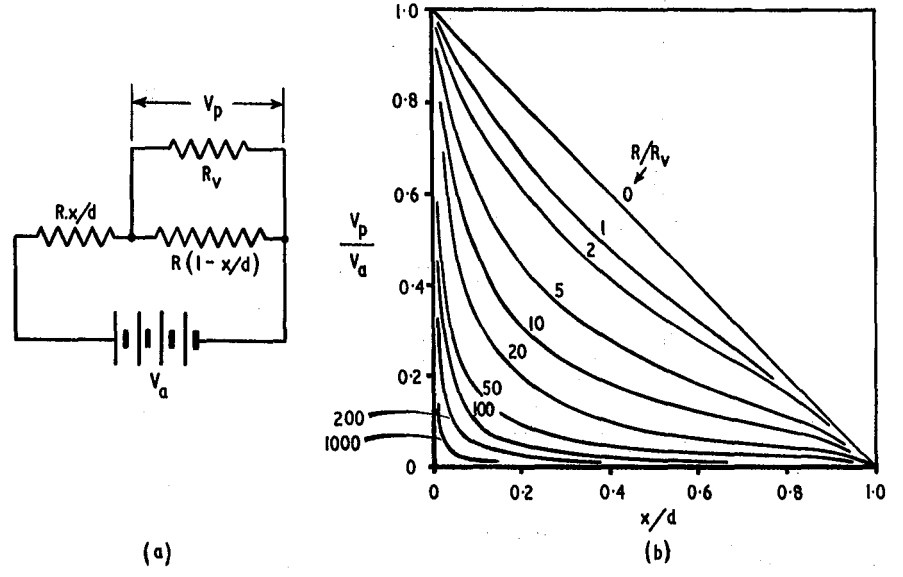

FIGURE 4
Basic equivalent circuit and resulting potential distribution for various values of R/R_v.

To derive the correction we use the fact that the true potential V_p' of a point in the undisturbed liquid is related to the measured potential V_p by the expression

$$\frac{V_p'}{V_p} = \frac{1}{2}\left[\left(1 - \frac{R_v}{R}\frac{V_a}{V_p}\right) + \left\{\left(1 - \frac{R_v}{R}\frac{V_a}{V_p}\right)^2 + 4\frac{R_v}{R}\right\}^{1/2}\right]$$

This equation assumes that the cell resistance is still ohmic although it allows for a distribution of resistivity in the liquid due to space charge. Fig. 5 shows the correction to one of the experimental curves for various values of R/R_v. It will be noted that none of them approach a uniform field so that the experiment appears to show that space charge *does* exist in the liquid although we require to know the value of R/R_v to determine which of the curves of Fig. 5 is the true one. Attempts to measure the value of R/R_v have not been successful because of the very high resistances involved. The voltmeter resistance, R_v, has been measured satisfactorily and found to be between 10^{13} and 10^{14} ohms in agreement with the manufacturer's specification. The cell resistance is, however, much higher

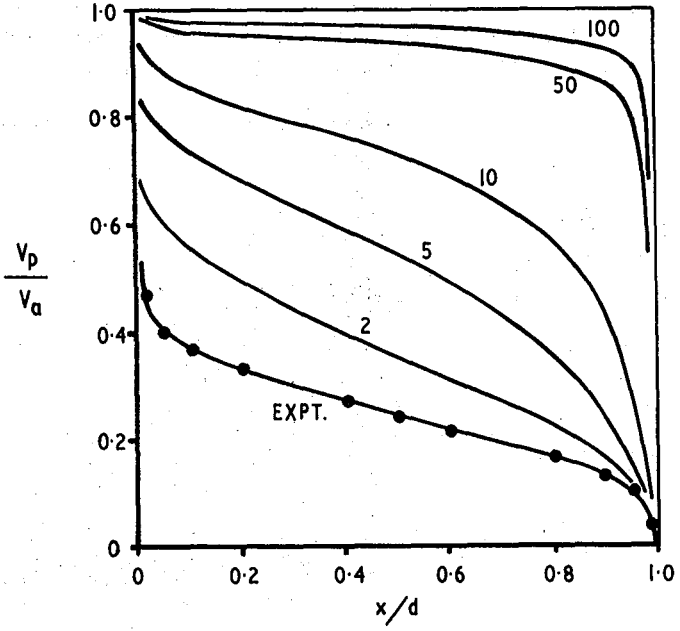

FIGURE 5
Typical potential distribution measured directly in hexane with corrections for various values of R/R_v.

than this with the large electrode spacings used and it has not been possible to measure it accurately. The best that can be said is that the ratio R/R_v must be much greater than 10, indicating a high degree of distortion of the true field. The method is not, therefore, capable of giving any more precise information than this.

In addition to the interpretation difficulty this method of measuring probe potentials is still subject to experimental problems due to slow time variations of current and voltage. Even within the 30 minutes required to obtain an approximate apparent potential distribution curve the current in the liquid will almost certainly have changed since slow current decays have been observed in hexane for many hours following a disturbance. Thus the values of R/R_v will vary for different points on the profile and the correction will not be constant. The same applies to profiles measured on one sample of liquid over long periods of time. These show considerable variation although once again one cannot be sure whether these are due to a change of the true potential distribution or of the liquid resistance or both. All these difficulties show that direct measurements of probe potentials in liquids as insulating as hexane cannot be made reliably.

Method 2. — Capacitor Method

The error due to the voltmeter resistance in probe measurements may be eliminated by isolating the voltmeter from the probe via a switched capacitor as done by GUIZONNIER (1954). We have used a slightly different circuit arrangement, Fig. 6a, which does not involve earthing the probe during measurement. In this circuit ,C is first charged to a potential V with S_1 closed and S_2 connected to B. The capacitor is then isolated and connected to the probe by switching S_2 to position A. After a certain time interval the capacitor is reconnected to the voltmeter which is isolated by opening S_1, and the change of capacitor voltage ΔV is measured. The process is repeated for different initial charging potentials until $\Delta V = 0$.

This method is very sensitive in principle and the measuring error may be greatly reduced since the capacitor leakage replaces that of the voltmeter as far as the probe is concerned. It is slightly slower than the first method because the increased capacitance reduces the rate of change of voltage. The greatest advantage in principle is that the leakage resistances of the cell, capacitor and voltmeter can be determined from the time constants for the discharge of the capacitor through the various paths. In practice a capacitor of about 15 pF is required and we have not been able to construct one of this value with a leakage resistance much greater than

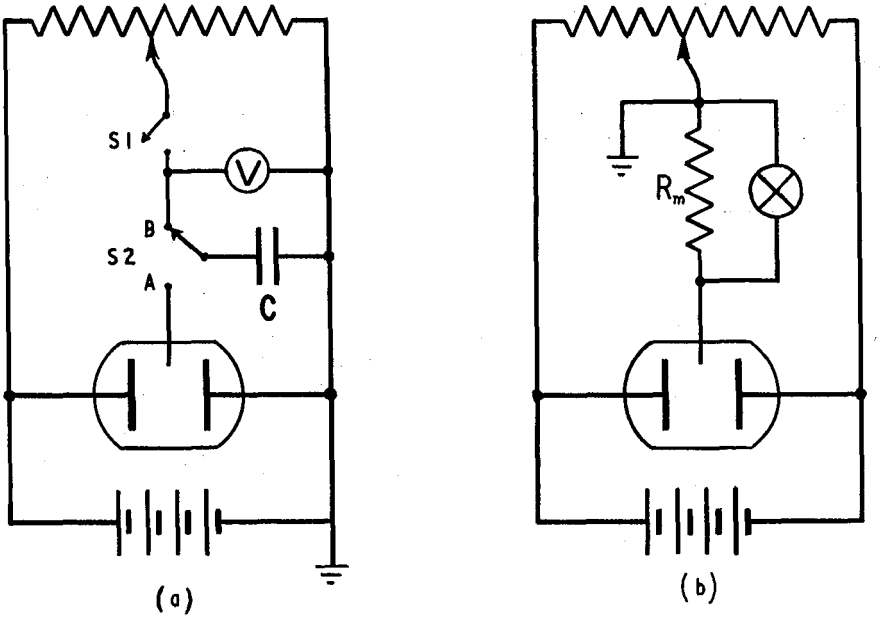

FIGURE 6
Circuits for probe measurements by (a) capacitor and (b) bridge methods.

10^{13} ohms. Measurements made in hexane using such a capacitor indicate that the error due to leakage is greater than that with the voltmeter alone. This emphasizes the exceptionally low leakage of the voltmeter used and shows that it will be difficult to improve on the first method for measurements on a very highly insulating liquid.

Method 3. — Bridge Method

The third circuit arrangement (Fig. 6b) has been used by Forster (1962) for obtaining potential profiles in benzene. It was investigated here to see whether it could be used for hexane which has a considerably lower conductivity than benzene.

The circuit is essentially a bridge with a sensitive electrometer as detector. At balance this arrangement entirely eliminates distortion due to current taken by the probe. The sensitivity is determined by the ratio of the measuring resistance to the cell resistance: if this is sufficiently high the method should enable the potential distribution to be determined more rapidly than by either of the previous methods.

Experimentally, the detector used was a Vibron Model B33C electrometer (Electronic Instruments Ltd., Richmond, Surrey, England) which uses a measuring resistor, R_m, of up to 10^{12} ohms giving a maximum sensitivity of 10^{-14} amp full scale deflection. The disadvantage of this and similar instruments in this particular circuit is that one side of the measuring resistor is earthed so that the potential of the remainder of the circuit varies with the potentiometer setting.

Unfortunately this method has not been successful for measurements in hexane. The cell resistance is once again too high to give sufficient probe current for balancing the bridge with this detector. This shows that the internal resistance of the cell, looking in from the probe, must be greater than 10^{15} ohms which is the practical limit for this method to be feasible. Emptying the cell has been found to make little difference, indicating that even this high resistance represents parallel leakage paths over the cell walls. The resistance of the liquid itself is therefore beyond the limit at which the method can be used.

Measurements in Benzene

The examination of the three circuit arrangements used for measuring the potential distribution showed that none of them is ever likely to be successful in hexane because of the extremely high resistivity of the liquid. It was therefore decided to compare the three methods using a more conducting liquid, and for this purpose laboratory benzene was used without further purification. The cell conduction current was then of the order of 10^{-12} amp at 100 volts.

All three methods were found to function satisfactorily in benzene although corrections were still required for the first two to allow for the current taken by the probe. The correction is not as easy as anticipated due to non-linearities in the cell resistance and probably also in the voltmeter resistance. This was shown by the fact that the discharge curves measured with the capacitor in the second method were seldom exponential. Apparent potential distributions obtained by the three methods are compared in Fig. 7 in which the direct probe measurements have not been corrected. The difference between the first and second methods is due to the lower resistance of the capacitor compared with the voltmeter. Leakage corrections would make the curves coincide and raise them both towards the curve for method 3. The exact correction cannot be determined because of the non-linearities and these probably also account for the larger apparent voltage drop indicated on the left hand side of the curves for

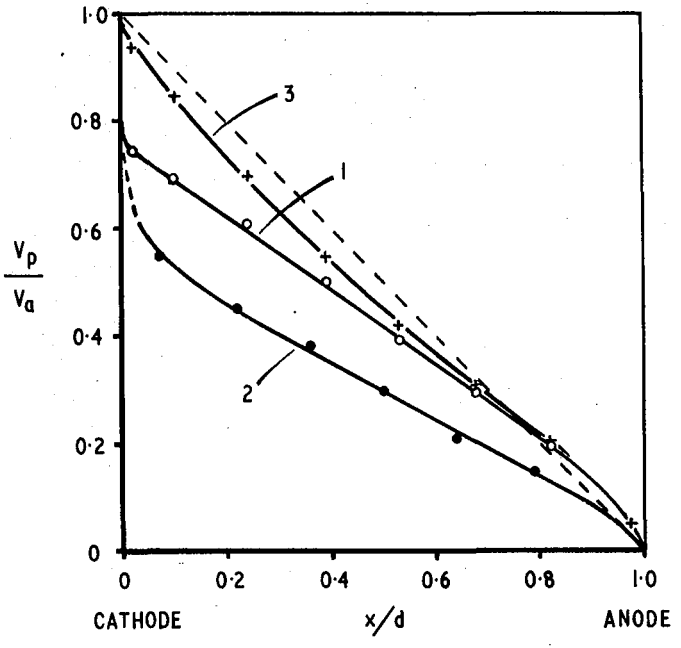

FIGURE 7
Potential distributions measured in benzene by the three methods.

methods 1 and 2. It is concluded that method 3 is the most reliable for potential measurements in a liquid such as benzene.

Potential Distribution using a 'Charge Probe'

It was shown in the introduction to this paper that the field distribution in the liquid greatly affects measurements of the mobility of negative charge carriers injected from the cathode. In view of the apparent failure of ordinary probe measurements in hexane it was decided to work backwards and try to use charge injection techniques to give information about the field distribution. In this experiment the pulse of injected carriers moves from cathode to anode with a velocity proportional to the localized field strenth. Analysis of the current transient in the external circuit enables the motion of the charge pulse, and thus the field, to be determined. The pulse of injected carriers can be thought of as charged 'probe' which is free to move in the liquid.

The sensitivity of the method is greatly increased by measuring the charge transferred between the electrodes rather than the current. This is done by using a measuring circuit which has a time constant very much greater than the charge transit time between the electrodes. If the pulse of negative carriers photoinjected from the cathode moves towards the anode at constant velocity the measured charge will increase linearly up to the transit time τ, after which it will remain constant. If the field is non-uniform there will be curvature on the rising part of the trace which can be analysed in terms of the field distribution as follows.

W consider the charge layer Q_i coulomb (assumed to be of negligible thickness) at a distance x cm from the cathode. The work done by the field E_x volt cm^{-1} in moving it a further distance dx is $Q_i E_x dx$ joules. The energy supplied by the external circuit in the corresponding time dt is $i_t V_a dt$ where i_t amps is the instantaneous current and V_a the applied voltage. Equating these we obtain

$$Q_i E_x \frac{dx}{dt} = i_t V_a$$

Also the carrier velocity is

$$\frac{dx}{dt} = \mu E_x$$

where μ cm^2 volt^{-1} sec^{-1} is the mobility. Thus

$$E_x = \left(\frac{V_a}{Q_i \mu}\right)^{1/2} i_t^{1/2}$$

The instantaneous current is obtained from the slope of the charge oscillogram as a function of time. The above expression enables us to deduce the field strength in the region through which the charge is moving also as a function of time. Since the carrier velocity is proportional to field the curve can be integrated graphically to give the charge position x versus time. By combining the last two curves we can then easily produce curves of field, and thus potential, against distance from the cathode. The final curves are normalized and it is not necessary to know the constants in the expression to obtain the relative field strengths. The largest error in the method is in the value of the transit time τ obtained from an oscillogram. An error in τ only affects the apparent shape of the field very close to the anode.

It is implicitly assumed in the above analysis that there is only one type of negative charge carrier involved and that its mobility is independent of field strength. There is evidence that both these assumptions are valid

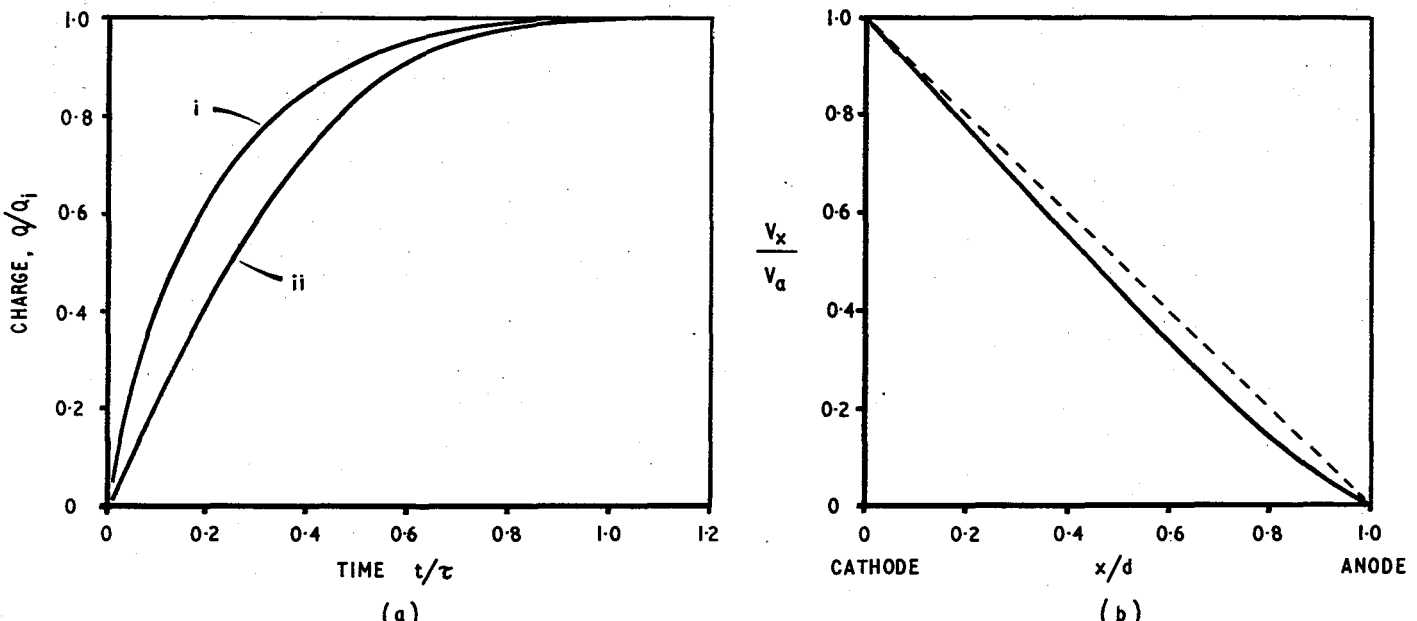

FIGURE 8
(a) Typical charge oscillograms with pulse injection (i) early test cell, (ii) final cell.
(b) Potential distribution derived from (ii).

in the experimental conditions used here. It can also be shown that carrier diffusion has a negligible effect in this experiment but it is necessary to assume that the natural space charge in the liquid is not affected by the injected charge.

Experimentally the method works well provided that the conditions are right for efficient photoinjection from the cathode. Thus the liquid must be of very high purity to eliminate bulk ionization due to the ultraviolet irradition and the cathode has to be suitably prepared. The liquid must also be well degassed and sealed in a vacuum tight cell. Further details of recent investigations of these effects will be published later.

Close examination of many charge oscillograms has shown that curvature of the rising part of the trace can be caused by a number of spurious effects as well as by a non-uniform field. Curvature is produced by liquid movement, by a long duration injecting pulse and by carrier movement in the non-uniform field near the edges of the electrodes. These effects account for most of the curvature of the trace shown at (i) in Fig. 8a which was an early result in the present investigation. Later work with an improved test cell geometry and limited injection gave reduced curvature as shown at (ii) in Fig. 8a. Assuming that the spurious effects have been eliminated this curve can be used to deduce the field distribution as shown in Fig. 8b. Even if this assumption is not correct the analysis does at least give an upper limit to the distortion of the field.

The results obtained by this method show that the field distortion is surprisingly small in hexane. The typical curve of Fig. 8b shows the main effect which is a slight *decrease* in field near the anode. Elsewhere the field is constant to within 10 % for 75 % of the gap width. The accuracy in deducing the field is worst near the anode and it is probable that the true field is even more uniform than indicated. Measurements have been made using this method with average fields up to 120 kV/cm with similar results.

Discussion and Conclusions

This paper shows that great care is needed in interpreting the results of probe measurements in highly insulating liquids. The validity of an apparent potential profile should always be checked by a number of simple tests including : —

a) Comparison of measurements made with different points of the circuit earthed.
b) Allowance for the effect of the voltmeter resistance in the circuit.

c) Comparison of measurements made with at least two different measuring circuits.

d) Comparison with measurements made with the cell empty.

These tests may not always have been applied to work reported previously.

By the use of careful technique it is possible to use all three methods of measurement on liquids such as benzene having a resistivity of approximately 3×10^{15} ohm cm. In the conditions used here the bridge method gives the best results without the need for correction. The measurements in benzene show slight field enhancement at both electrodes with positive space charge near the cathode and negative near the anode. This agrees with the more precise measurements made by Forster on benzene and by Guizonnier and others on a range of different liquids.

Carefully purified hexane has a resistivity probably greater than 10^{17} ohm cm and none of the methods using physical probes has been made to work accurately in this liquid in spite of the greatest possible precautions to minimize leakage etc. Corrections for the distortion due to the probe current cannot be made accurately without measuring the cell resistance and this is not feasible with such high values. The results do, however, appear to be consistent with a field distortion of the same general shape as is found in benzene. The experimental difficulty could be overcome by increasing the conductivity of the liquid by means of charge injection, for example by ultraviolet irradiation. This has not been done here because of fears that the potential distribution itself may be altered by the enhanced conduction.

The new method of field determination based on mobility measuring techniques overcomes the experimental difficulties with certain highly insulating liquids such as well degassed hexane. The probe is a pulse of injected charge and its movement is followed from the transient current in the external circuit. Mobility measurements will be reported in detail later but refined technique has already enabled the shape of the charge transient to be interpreted in terms of the potential distribution. The results show very little field distortion in these conditions right up to 120 kV/cm. The slight reduction of field found near the anode is consistent with positive space charge in the liquid at this point. This does not agree with the other observations although very little reliance can be placed on the latter in the case of hexane. The small amount of field distortion found by the new method will require further experimental confirmation and interpretation in terms of conduction processes in the liquid.

References

CHONG P., SUGIMOTO T. and INUISHI Y. — *J. Phys. Soc. Japan*, 1960, **15**, 1137.

CROITORU Z. — *Progress in Dielectrics*, **6**, p. 103 (Heywood, London, 1965).

FORSTER E. O. — *J. Chem. Phys.*, 1962, **37**, 1021.

GUIZONNIER R. — *Gen. Elect. Rev.*, 1954, **63**, 489.

LE BLANC O. H. — *J. Chem. Phys.*, 1959, **30**, 1443.

SILVER M. — *J. Chem. Phys.*, 1965, **42**, 1011.

TERLECKI J. — *Nature*, 1962, **194**, 172.

WHITEHEAD J. B. and MARVIN R. M. — *Trans. Amer. Inst. Elect. Engrs.*, 1930, **49**, 647.

Silver. — Dr Morant : did you check and see how much field distortion would be produced by the actual charge you measured by the light pulse and how much did that compare with the distortion in the field you represent ?

Morant. — No, we haven't done that. I did have one more slide. We got very nice results on mobility. This (Fig. 2) shows Bloor's results of drift velocity against field. Each of these points comes from one graph of time against distance. These results for mobility were taken on different occasions and they cover fields right up to 100 kV per centimetre. They show a constant mobility, and this we believe to be very good evidence that there is no bulk liquid motion. We've got none of the scatter which Lewis and Secker have reported, and we think that this is pretty good evidence that we are not having troubles of the type that you mention either. Now I haven't got any exact calculation on this...

Silver. — No, no, I was not concerned about that; I was concerned about the fractional change of the electric field by the amount of induced charge. For example, if one interjects 5 % of the *c d,* one should get a 5 % distortion because of the dispersion of the charge as it flows by.

Morant. — I haven't calculated it but we need to do so. There was another point I wanted to make on the mobility value. We believe it's about 1.0×10^{-3} cm²/volt. sec. when a small correction has been made to the values on the slide.

Guizonnier. — Je remercie le Dr Morant de s'intéresser à mes mesures. Mais je regrette que le circuit qu'il a analysé n'est pas celui que j'ai utilisé. C'est dommage, je m'en excuse; il l'a pris dans une première publication qui était assez longue; j'ai dit que j'ai employé un circuit avec capacité intermédiaire. Le Dr Morant très gentiment l'a imaginé, mais deux ans plus tard j'ai publié le circuit réel que j'ai utilisé qui est celui qui se trouve dans le fascicule qu'on a distribué. Je ne pense pas quand même que le circuit que j'ai utilisé ait les défauts que le Dr Morant a trouvé à celui qu'il a imaginé en mettant une capacité en service. Je le remercie d'avoir imaginé ce circuit pour m'être agréable mais il n'était pas exact. Il n'y a qu'à vous reporter aux figures faites il y a deux ou trois jours; je n'ai pas eu le temps de les exposer — je ne pense pas que le circuit qu'il utilise ait les défauts qui lui ont été prêtés. D'ailleurs...

Morant. — I didn't understand all that...

Bright, *Chairman.* — He was rather worried that the circuit which you ascribed to him was not exactly the circuit which he used.

Atten. — D'abord, Dr Morant, vous dites que la mesure du temps de transit

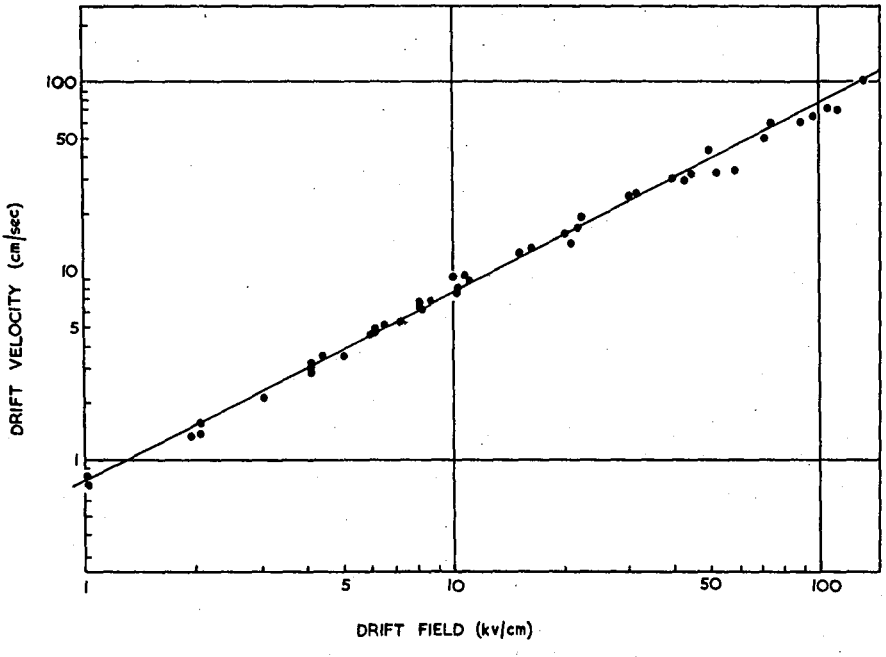

Drift velocity of photoinjected carriers in highly degassed *n*-hexane.

ne permet pas d'atteindre la mobilité de façon très précise. Je pense que ce n'est pas tout à fait exact; parce que si l'on prend d'abord la mesure du temps du premier transit lorsqu'on applique un échelon de tension et si on reprend la théorie de Many et Rakavy, on s'aperçoit que le rapport de la mobilité réelle sur la mobilité apparente est inférieur — ou égal au maximum — à $1/0{,}787 \simeq 1{,}27$. D'autre part, si on se place à l'état stationnaire dans le cas qui est le plus défavorable, c'est-à-dire dans le cas d'une limitation du courant par charge d'espace avec le champ nul à l'origine, on s'aperçoit à ce moment-là que le même rapport — mobilité réelle sur mobilité apparente, est égal en coordonnées réduites, à

$$\int_0^1 \frac{dx}{E(x)} = \int_0^1 \frac{dx}{\frac{3}{2}\sqrt{x}} = \frac{4}{3}$$

Et ce que je veux dire c'est que l'on a le cas le plus défavorable, pour l'état stationnaire, parce que, en présence de dissociation, le champ n'est plus nul à l'origine et la courbe du champ est beaucoup plus linéaire. Donc je pense que, lors des mesures du temps de transit, l'erreur que l'on fait est quand même relativement faible. Deuxièmement, il m'a semblé intéressant d'exposer un petit calcul concernant l'ordre de grandeur de la distorsion que l'on peut atteindre

dans un champ, par exemple dans l'hexane, avec les fortes résistivités que l'on a. En prenant les équations en l'absence de dissociation, l'on a :

$$j = \mathrm{K}q\mathrm{E}$$

$$\frac{d\mathrm{E}}{dx} = \frac{q}{\epsilon}$$

en intégrant et en faisant quelques calculs, on aboutit à la relation :

$$j = \frac{\mathrm{K}\epsilon}{2d}\left[\mathrm{E}^2(d) - \mathrm{E}^2(o)\right]$$

Ce calcul est fait dans le cas d'une injection unipolaire car, pour un courant donné, le maximum de distorsion de champ que l'on peut avoir à l'état stationnaire est donné par le champ unipolaire et je suppose évidemment que les électrodes ne sont pas bloquantes.

$j = \sigma\,\mathrm{E}$ (E : champ moyen) et en remplaçant dans l'équation précédente on obtient, en remarquant que $\mathrm{E}(d) + \mathrm{E}(o) \simeq 2\,\mathrm{E}$:

$$\mathrm{E}(d) - \mathrm{E}(o) = \frac{\sigma d}{\mathrm{K}\epsilon}$$

A partir de là, on peut mettre quelques valeurs numériques :

$$\mathrm{K} = 10^{-4}\ \mathrm{cm^2/V\text{-}s}\ ;$$

$$\epsilon = 2\epsilon_0 = \frac{10^{-9}}{18\pi}\ \mathrm{F/m}$$

(ordre de grandeur)

on a :

$$\mathrm{E}(d) - \mathrm{E}(o) \simeq 5.10^{16}\,\sigma d$$

(σ en mho/cm et d en cm).

Supposons que l'on ait de l'hexane de résistivité équivalente de l'ordre de $10^{15}\,\Omega \cdot$ cm et que d = 1 mm. En remplaçant ont voit facilement que l'on obtient une différence de l'ordre de 5 volts/cm entre le champ sur l'électrode injectrice. Donc, à partir du moment où le champ moyen est de 500 V/cm, par exemple, on aura une distorsion inférieure à 1 %, et plus le champ va augmenter, plus la distorsion sera faible. Donc, je me demande s'il est vraiment nécessaire de faire des mesures de champ dans les liquides extrêmement résistifs — dans la mesure évidemment où les électrodes sont ouvertes et où il n'y a pas de phénomène de blocage. J'ajoute que j'ai pris le cas le plus défavorable où on a une injection purement unipolaire. En fait, on n'a jamais une injection strictement unipolaire, ce qui fait que la distorsion du champ est encore plus faible.

Le troisième point concerne les méthodes de sonde ; je pense que l'utilisation des méthodes de sonde dans les liquides est très aléatoire, parce qu'on a déjà l'exemple des méthodes de sonde dans les gaz à la pression atmosphérique ou dans les plasmas où le potentiel que prend la sonde lorsque le courant est nul est différent du potentiel d'espace. Et dans un liquide très résistant on ne sait pas trop quel potentiel il va prendre. Je pense qu'il faut être très prudent.

Bright. — Mr Atten, I wouldn't to summarise that valuable communication : he's raised a number of points which I think Dr Morant and I would like to come back to. What I suggest now (I don't want to stifle discussion) : if you'd really like to, we can have perhaps one more question, but we could break now for tea. Those who are interested in Mr Atten's last contribution could talk to him and then we have almost as much time as you like for a general discussion, and we can discuss anything at 4.30.

Whalley. — I've got three very short questions to ask ... (laughter). Firstly, have you any information about the distortion of the field in the liquid under investigation ? Secondly, in what way does the viscosity vary with this field ? Finally, I notice that you have a degassing system connected to the test cell. Did you notice any effect of gas content on your measure of viscosity ?

Taylor. — To answer the first question, in common with other workers in the liquid dielectrics field, we have little information about local field strengths ; but our electrode gaps are relatively large. On the other hand we are measuring viscosity within a small region close to an electrode and if viscosity does vary with stress some of the effects of space charges in the vicinity of an electrode might become apparent.

Secondly, how does viscosity vary with field ?

For non polar liquids we have been unable to measure any changes ; but we think that we can detect effects too small to be measured, probably due to slight polar impurities. For polar liquids we find that " viscosity " ceases to be a really useful term, because we suspect from our provisional results that there is significant molecular alignment, and hence we must talk in terms of rheological behaviour. In fact we are fairly sure that the molecules do not completely follow a rapidly changing disturbance, and that the liquid exhibits a certain configurational rigidity in the presence of strong fields. This theory is borne out by the fact that the effect takes some time to die away when the field is switched off, and it looks as though the molecules have become ordered and this ordering then slowly breaks up.

What was your third question ?

Whalley. — Gas content ?

Taylor. — The only comment I can make about gas content is that breakdown values were often on the low side, but under these conditions there was little change in " viscosity ".

Stephenson. — I do not think that we have gas included in the form of

microbubbles : the apparatus and liquid were degassed to approximately 10^{-3} torr. We may have had some liquid impurities present, as to date we have only used relatively simple filtering and degassing techniques.

Bright. — Well, I must be absolutely heartless now in saying we'll close the discussion — or adjourn the discussion — and have tea and then come back for further questions. I would just like to thank all the speakers for adhering to the time...